รายงานวิจัยฉบับสมบูรณ์

โครงการ : เทคโนโลยี RNA interference เพื่อประสิทธิผลของการเพาะเลี้ยงกุ้งในประเทศไทย (ระยะที่ 2)

โดย

ศาสตราจารย์เกียรติคุณ ดร.สกล พันธุ์ยิ้ม และคณะ

25 พฤษภาคม 2563

สัญญาเลขที่ DBG6180011

รายงานวิจัยฉบับสมบูรณ์

โครงการ : เทคโนโลยี RNA interference เพื่อประสิทธิผลของการเพาะเลี้ยงกุ้งในประเทศไทย

คณะผู้วิจัย	สังกัด
1. นายสกล พันธุ์ยิ้ม, Ph.D.	ภาควิชาชีวเคมี คณะวิทยาศาสตร์และสถาบันชีววิทยาศาสตร์โมเลกุล มหาวิทยาลัยมหิดล
2. นางสาวพงโสภี อัตศาสตร์, Ph.D.	สถาบันชีววิทยาศาสตร์โมเลกุล มหาวิทยาลัยมหิดล
3. นางสาวเฉลิมพร องศ์วรโสภณ, Ph.D.	สถาบันชีววิทยาศาสตร์โมเลกุล มหาวิทยาลัยมหิดล
4. นายอภินันท์ อุดมกิจ, Ph.D.	สถาบันชีววิทยาศาสตร์โมเลกุล มหาวิทยาลัยมหิดล
5. นายวันชัย อัศวลาภสกุล, Ph.D.	ภาควิชาจุลชีววิทยา คณะวิทยาศาสตร์ จุฬาลงกรณ์มหาวิทยาลัย
6. นางสาวสุพัตรา ตรีรัตน์ตระกูล, Ph.D.	สถาบันชีววิทยาศาสตร์โมเลกุล มหาวิทยาลัยมหิดล

สนับสนุนโดยสำนักงานกองทุนสนับสนุนการวิจัย

สารบัญ

Abstract

RNA interference technology is developed and employed for efficient shrimp culture in Thailand. dsRNAs (~400pb) with the nucleotide sequence for yellow head virus (YHV) protease gene, and white spot syndrome virus (WSSV) Pro-rr2 were designed and synthesized in E.coli for knock-down of the cognate genes in shrimp. Similarly, dsRNA-GIH was produced in E.coli. Injection of dsRNA protease silenced YHV protease gene and prevented YHV infection. Injection for dsRNA Pro-rr2 protected YHV and WSSV infections and shrimp mortality. Injection of dsRNA-GIH produced from E.coli stimulated shrimp ovulation as good as eye-stock cutting which is considered cruel to the animals.

Such application of RNA interference technology in shrimp culture should lead to development of vaccine to prevent and to cure the virus infection in shrimp.

This research yielded six Q1 international publications and two manuscripts in-press.

บทคัดย่อ

งานวิจัยการใช้เทคโนโลยี RNA interference เพื่อการเพาะเลี้ยงกุ้งในประเทศไทย โดยการสร้างและใช้ dsRNA เพื่อพัฒนาวัคซีนป้องกันการติดเชื้อไวรัสในกุ้ง และเพื่อเพิ่มประสิทธิภาพการวางไข่ของกุ้งโดยการสร้าง dsRNA ประมาณ 400bp ซึ่งมีลำดับเบสตรงกับยีน protease ของไวรัสหัวเหลือง (YHV) และตรงกับยีน Pro-rr2 ของไวรัสตัวแดงดวงขาว (WSSV) เมื่อฉีด dsRNA ดังกล่าว พบสามารถป้องกันการติดเชื้อ YHV และ WSSV ในกุ้งได้ดี การใช้ dsRNA-GIH ผลิตจาก E.coli พบกุ้งวางไข่ได้ดีเท่าเทียม วิธีการตัดตาที่ใช้ในปัจจุบัน

ได้ศึกษาการทำ dsRNA เข้าสู่เซลล์กุ้ง พบการใช้กระบวนการ endocytosis ในการนำเข้า hepatopancreas แต่ไม่ใช้ในการนำเข้า gills

ได้ศึกษาการเข้าสู่เซลล์กุ้งของ YHV พบต้องใช้ early endosomal protein (PmEEA1) หาก knock-down ด้วย dsRNA พบ YHV ไม่สามารถ infect กุ้งได้ เป็นการป้องกันการติดเชื้อ YHV ได้

ได้ศึกษา Argonaut (Ago) protein ในการป้องกันการติดเชื้อไวรัส โดยในกุ้งมี Ago ถึง 4 ชนิด พบการใช้ dsRNA Ago1 และ Ago3 สามารถยับยั้งการตายของกุ้ง เมื่อติดเชื้อ YHV และพบ dsRNA ของ Ago3 เท่านั้นที่ยับยั้ง WSSV และลดการตายของกุ้งจากการติดเชื้อ WSSV ได้ การศึกษานี้ทำให้ทราบการลดการตายของกุ้งจากการติดเชื้อไวรัส ซึ่งจะนำไปสู่การพัฒนาวัคซีนป้องกันการติดเชื้อไวรัสในกุ้งในอนาคต

งานวิจัยนี้มีผลงานตีพิมพ์ในวารสารวิชาการนานาชาติ (Q1) จำนวน 6 ฉบับ และ manuscript พร้อมตีพิมพ์ จำนวน 2 ฉบับ

เนื้อหางานวิจัย

Research Outputs
(ทุนวิจัยพื้นฐานเชิงยุทธศาสตร์)

Involvement of endocytosis in cellular uptake of injected dsRNA into hepatopancreas but not in gill of *Litopenaeus vannamei*

RNA interference (RNAi)technology has been widely applied to shrimp research for functional genomics, as well as for investigation of its potential anti-viral applications. While the integral membrane protein SID-1 of *Litopenaeus vannamei* has been reported to participate in the uptake of injected dsRNA into shrimp cells, this may not be the only uptake mechanism. Therefore the possible involvement of endocytosis in the delivery of injected dsRNA into shrimp hepatopancreatic and gill cells was evaluated. Clathrin-mediated endocytosis was inhibited through the injection of shrimp with two pharmacological endocytosis inhibitors (chlorpromazine and bafilomycin-A1) before injection of long dsRNAs directed against STAT (dsSTAT) or Rab7 (dsRab7). Levels of STAT or Rab7 suppression in the treated shrimp as compared to the control shrimp reflect the capability of cells to take up dsRNAs (dsSTAT or dsRab7). Inhibition of clathrin-mediated endocytosis showed a reduction of specific mRNA suppression in the shrimp hepatopancreas. In contrast, neither chlorpromazine nor bafilomycin-A1 effectively blocked dsRNA mediated inhibition of STAT or Rab7 in gill tissue. These results support our conclusion that endocytosis is required in cellular uptake of injected dsRNA into shrimp hepatopancreas but is not participated in the process in gills. This is the first report of the involvement of different pathways of cellular dsRNA uptake into different tissues of shrimp.

Introduction

RNA interference (RNAi) technology is widely applied to shrimp research for functional genomics (Phetrungnapha et al., 2015; Sagi et al., 2013), but is additionally investigated for potential anti-viral applications (Assavalapsakul et al., 2014; Escobedo-Bonilla, 2011; Sagi et al., 2013; Shekhar and Lu, 2009). Injection of dsRNA into muscle or the haemocoel is routinely used for delivering dsRNA into shrimp (Labreuche et al., 2010; Sutthangkul et al., 2015), and while in the systemic circulation within the shrimp body cavity, dsRNA may be taken up by cells in different tissues. In invertebrates, at least two pathways for exogenous dsRNA uptake have been described so far, namely the systemic RNA interference defective (SID) transmembrane channel protein-mediated, and an endocytosis-mediated mechanism (Huvenne and Smagghe, 2010). Participation of SID-1 in dsRNA uptake has been demonstrated in *Caenorhabditis elegans* (C. elegans)(Feinberg and Hunter, 2003; Winston et al., 2002), Diabrotica virgifera (Miyata et al., 2014), *Leptinotarsa decemlineata* (Cappelle et al., 2016), *Nilaparvata lugens* (Xu et al., 2013) and *Apis mellifera* (Aronstein et al., 2006).

However, other studies have shown that endocytosis is a major pathway for cellular dsRNA uptake in some insects. For example, while *Tribolium castaneum* has three SID-1 homologues, they do not participate in dsRNA uptake, and clathrin-mediated endocytosis has been shown to be involved in the process (Tomoyasu et al., 2008; Xu and Han, 2008). Similarly, blocking endocytosis by specific inhibitors of clathrin-coated pit formation or of the vacuolar H+ ATPase (V-ATPase) required for endocytosis effectively inhibits the internalization of dsRNA in *Drosophila melanogaster* S2 cells (Ulvila et al., 2006; Winston et al., 2002), the red flour beetle (*Tribolium castaneum*)(Xiao et al., 2015) and desert locust (*Schistoceca gregaria*)(Luo

et al., 2012). However, the colorado potato beetle (*Leptinotarsa decemlineata*) uses both SID-1 and endocytosis for dsRNA uptake into midgut cells (Cappelle et al., 2016). Our previous study, the role of SID-1 of *Litopenaeus vannamei* (*Lv*SID-1) was evaluated in shrimp by monitoring the uptake efficiency of Cy3-labeled dsRNA as well as the silencing efficiency of target messages after increased expression of *Lv*SID-1 mRNA in a strategy utilizing sequential introduction of long dsRNAs (Maruekawong et al., 2018). The results showed that *Lv*SID-1 is involved in cellular uptake of injected dsRNA into shrimp gills and hemocytes. However, the *Lv*SID-1 may not be the only mechanism involved in this process. For this reason the possible involvement of endocytosis on the uptake of injected dsRNA into shrimp cells in the hepatopancreas and gill was evaluated. Shrimp were injected with either chlorpromazine (Cpz) to block clathrin-coated pit formation (Wang et al., 1993; Yao et al., 2002), or with bafilomycin-A1 (BafA) to block vacuolar acidification by V-ATPase (Yamamoto et al., 1998), and the treatedshrimpweretheninjected withdsRNAs specifictoshrimpsignal transduction and transcription protein (STAT) mRNA (dsSTAT) or shrimp small GTP-binding protein (Rab7) mRNA (dsRab7). Levels of STAT or Rab7 suppression in the treated shrimp as compared to the control shrimp reflect the capability of cells to take up dsSTAT/dsRab7.

Materials and methods

Shrimp specimens

Post larval (Pl15-Pl20) white leg shrimp (*L. vannamei*) were purchased from Chuchai farm in Chonburi province, Thailand and were maintained in 10ppt seawater with aeration in a 500L tank. A commercial diet (CP) was used to feed shrimp until they reached a juvenile stage of roughly 200– 300mg of body weight. During experiments, shrimp were kept in individual cages in the same tank to avoid cannibalism.

Production of dsRNA

A previously described plasmid (Maruekawong et al., 2018) containing an expression cassette of dsRNA targeting to the shrimp STAT mRNA (dsSTAT (406bp)) (Attasart et al., 2013) or Rab7 mRNA (dsRab7 (393bp)) (Ongvarrasopone et al., 2008) was transformed into E. coli HT115 (an RNase III defective strain). Expression of dsRNA was undertaken following the protocol of Ongvarrasopone and colleagues (Ongvarrasopone et al., 2007). Briefly, a single colony was inoculated in LB medium containing 100μg/ml ampicillin and 12.5μg/ml tetracycline and grown overnight at 37°C. This overnight starter culture (0.5 OD) was inoculated into 15ml of new medium and grown until OD600 reached 0.4. Expression of dsRNA was induced with 0.4mM of isopropyl-β-dthiogalactopyranoside (IPTG) for4h. Following the protocol of Posiri and colleagues (Posiri et al., 2013), one OD of bacterial cells was collected by centrifugation at 8,000×g at 4°C for 5min and resuspended in 100μl 75% ethanol in phosphate buffer saline (PBS) and incubated at room temperature for 5min. The treated cells were collected by centrifugation at 8000×g for 5min at 4°C before resuspending in 100μl of 150mM NaCl and incubation at room temperature for 1h. The cell suspension was centrifuged at 12000×g at 4°C for 5min to generate a cell-free supernatant. The dsRNA in the supernatant was diluted before loading onto agarose gels to estimate the concentration by comparing with a standard marker.

Evaluation of inhibition of endocytosis on dsRNA uptake

As suppression of clathrin heavy chain (CHC) by dsRNA is lethal to shrimp (Posiri et al., 2015), clathrin-mediated endocytosis was blocked by injection with specific inhibitors, namely chlorpromazine (SigmaAldrich) an inhibitor of clathrin-coated pit formation, and bafilomycinA1 (Abcam) an inhibitor of v-ATPase. To ensure endocytosis was inhibited, different amounts of the inhibitors (1.8 and 9.0μg of Cpz and 1.8 and 3.0μg of BafA per shrimp body weight (g)) were injected into eachshrimp. Twelve hours following injection of the inhibitors, dsSTAT or dsRab7 was administered. Targeted mRNAs (STAT or Rab7) expression in shrimp tissues (hepatopancreas and gill) was determined at 10–12h post dsRNAs injection.

Injection of dsRNA into shrimp

The dsRNA solution was diluted in 150mM NaCl to make 15ng/μl before injection. Twenty microliters of dsRNA solution (approximately 200–300ng) was injected into the shrimp haemocoel using a 0.5ml syringe with 29G needle.

Shrimp RNA extraction and cDNA synthesis

Hepatopancreas and gill tissues (approximately 10mg each) were dissected from *L. vannamei* using scissors and forceps. Total RNA was extracted using RiboZol™ (Amresco) following the manufacturer's instruction. The extracted RNA (1–2μg) was heated at 70°C for5minina reaction tube containing 2μM of random primers and RNase-free sterile distilled water and subsequently quickly cooled on ice. The primers were then allowed to anneal with the RNA at 25°C for 5min. The following components, 1× ImProm-II™ reaction buffer, 0.5mM dNTPs, 30mM MaCl2, 1μl of ImProm-II™ reverse transcriptase and RNase-free sterile distilled water were added into the reaction. The cDNA was synthesized at 42°C for 60min before termination at 70°C for 15min.

Semi-quantitative RT-PCR

The 25μl PCR reaction was composed of 2μl of cDNA template, 1× PCR buffer (75mM Tris-HCl (pH8.8 at 25°C), 20mM (NH4)2SO4 and 0.01% Tween 20), 0.2mM dNTPs, 0.2μM of each primer, 2mM of MgCl2, 200μM of dNTPs mix, 1.25 unit (0.25μl) of Taq DNA polymerase (homemade or Aspalagen) and sterile distilled water. For optimal conditions, which did not give saturated amplified products, 1:4 ratio of actin gene primers (5′ GACTCGTACGTCGGGCGACGAGG 3′ and 5′ AGCAGCGGTGGTCATCTCCTGCTC 3′) to STAT gene primers (5′ ATGTCGTTGTGGAACAGAGC 3′ and 5′ GTTTGTTGCATGTGAAACACC TCC 3′) or 1:12 ratio of actin gene primers to Rab7 gene primers (5′ ATGGCATCTCGCAAGAAGATT 3′ and 5′ TTAGCAAGAGCATGCATC CTG 3′) was used. The PCR reactions were held at 94°C for 2min, followed by 25cycles of denaturation at 94°C for 10s, annealing at 55°C for 30s, and extension at 72°C for 1min. Lastly, the amplification was held at 72°C for 5min. PCR products were analyzed by agarose gel electrophoresis. Levels of PCR products were quantified using the Scion Image program.

Statistical analysis

Data are presented as mean ± standard error of mean (SEM) using the GraphPad Prism 5 program. A p-value below 0.05 ($p < .05$) of a nonparametric test (Mann-

Whitney test) or paired t-test comparing between treatment and control groups was considered as statistically significant.

Results

Effect of two endocytosis inhibitors on RNAi in shrimp hepatopancreas

The level of STAT mRNA suppression induced by injection of dsSTAT was used as a marker to determine whether endocytosis is involved in the cellular uptake of dsRNA into shrimp gill and hepatopancreatic cells. Shrimp were pre-injected with drug inhibitors (Cpz and BafA) to block clathrin coated pit endocytosis before injection of dsSTAT. Thereafter, expression of STAT mRNA in the hepatopancreas and gill tissues of the treated shrimp was monitored and compared with the expression levels of control shrimp (without drug treatment).

In the first experiment, two doses of drugs (1.8 and 9.0μg of Cpz and 1.8 and 3.0μg of BafA per one gram of shrimp body weight) were used to block shrimp clathrin-mediated endocytosis. The relative transcript of STAT in the hepatopancreas of the untreated shrimp was significantly suppressed by approximately 40% from the control levels (STAT mRNA level of shrimp injected with drug-dissolving solvents (NaCl for Cpz or EtOH for BafA, respectively) (Fig. 1a and b). However, suppression level of shrimp pre-treated with two doses of Cpz or BafA were significantly reduced to approximately 10% from the control levels (STAT mRNA level of shrimp injected with Cpz or BafA without dsSTAT). In another experiment, doses of 9μg/g of Cpz and 3.0μg/g of BafA were used, and shrimp were initially injected with NaCl or drugs before injection with NaCl or dsSTAT. Compared to the suppression control (Na-Na/Na-St and Et-Na/Et-St) in which the RNAi response was not affected, the STAT mRNA suppression of shrimp after blocking with Cpz (CpzeNa/ Cpz-St) or with BafA (Baf-Na/Baf-St) were approximately 18% and 29%, respectively (Fig.1c and d). However, the change of RNAi efficiency of STAT after treatment with Cpz was not statistically different. To confirm that endocytosis is required for cellular uptake of not only dsSTAT into shrimp hepatopancreas, the different dsRNA targeted another shrimp endogenous gene (Rab7), dsRab7 was used. Shrimp were initially injected with solvents (NaCl and EtOH) or drugs (1.8μg/g of Cpz and 3.0μg/g of BafA) before injection with NaCl or dsRab7. The Rab7 mRNA suppression of shrimp after blocking with BafA was significantly reduced (Fig. 3b). However, the change of RNAi efficiency of Rab7 after treatment with Cpz was not statistically different from the control (Fig. 3a). Taken together the results indicated that inhibition of clathrin-mediated endocytosis affected the dsSTAT/ dsRab7 uptake in shrimp hepatopancreas resulting in reduction of RNAi-mediated STAT/Rab7 suppression.

Effect of two endocytosis inhibitors on RNAi in shrimp gills

The effect of the two endocytosis inhibitors on STAT or Rab7 suppression was also determined in gill tissue of the same shrimp. In contrast to hepatopancreas, the results showed levels of STAT or Rab7 suppression after blocking with two drugs (Cpz and BafA) were not significantly reduced (Figs. 2a–d, 3c–d), indicating that inhibition of clathrin-mediated endocytosis did not affect the uptake of dsRNAs in shrimp gill tissue.

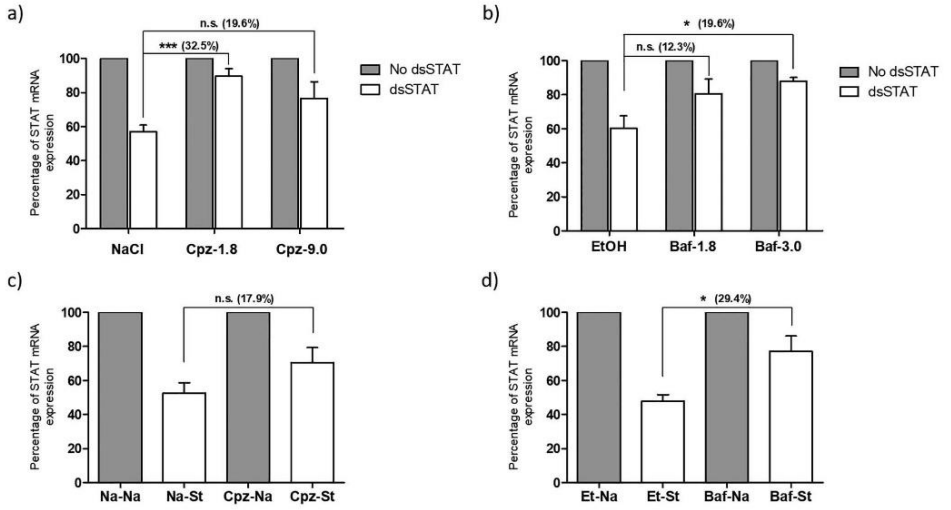

Fig. 1. Effect of inhibitors (chlorpromazine (Cpz) and bafilomycin A1 (Baf)) on endocytic uptake of injected dsSTAT into shrimp hepatopancreatic cells. Shrimp (n=3–9/group) were pre-injected with the solvents [NaCl (Na) or EtOH (Et)] or drug inhibitors [(a) Cpz (at 1.8 or 9 μg/g of shrimp) or (b) Baf (at 1.8 or 3 μg/g of shrimp)] before injection of NaCl (no dsSTAT) or dsSTAT (St). Twelve hours later, relative expression of STAT mRNA in the hepatopancreas of shrimp in each group was monitored by RT-PCR and plotted as mean±SEM. The percentage of STAT mRNA expression of the drug treated and untreated shrimp are presented. The statistical analysis was performed using the Mann-Whitney test at p-value<.05 (*) and<0.001 (***). Another set of experiments was performed (n=5–10/group) (c and d). The percentage of STAT mRNA expression of the treated (Cpz-St and Baf-St) and untreated (Na-St and Et-St) shrimp are presented. The statistical analysis was performed by a paired t-test at p-value<.05 (*).

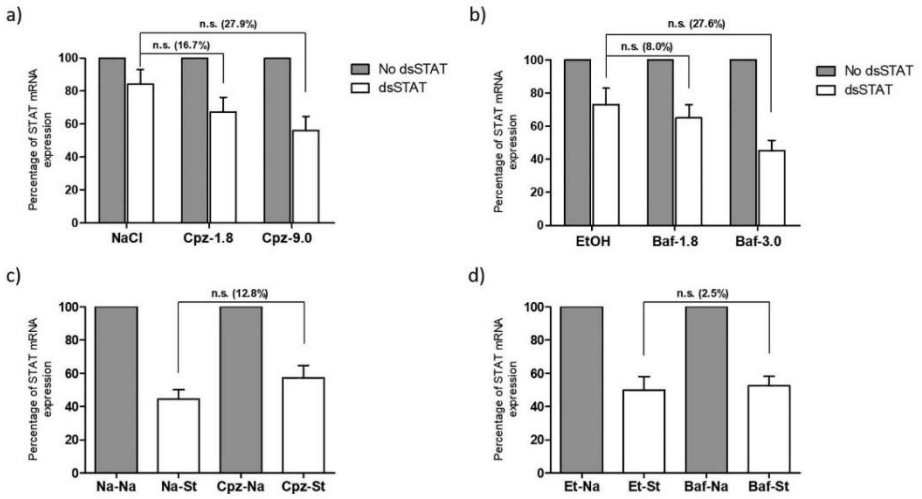

Fig. 2. Effect of inhibitors (chlorpromazine (Cpz) and bafilomycin A1 (Baf)) on endocytic uptake of injected dsSTAT into shrimp gill cells. Shrimp (n=3–9/group) were pre-injected with the solvents [NaCl (Na) or EtOH (Et)] or drug inhibitors [(a) Cpz (at 1.8 or 9 μg/g of shrimp) or (b) Baf (at 1.8 or 3 μg/g of shrimp)] before injection of NaCl (no dsSTAT) or dsSTAT (St). Twelve hours later, relative expression of STAT mRNA in hepatopancreas of shrimp in each group was monitored by RT-PCR and plotted as mean±SEM. The percentage of STAT mRNA expression of the drug treated and untreated shrimp are presented. The statistical analysis was performed using the Mann-Whitney test. Another set of experiments was performed (n=5–10/group) (c and d). The percentage of STAT mRNA expression of the drug treated (Cpz-St and Baf-St) and untreated (Na-St and Et-St) shrimp are presented. The statistical analysis was performed by a paired ttest.

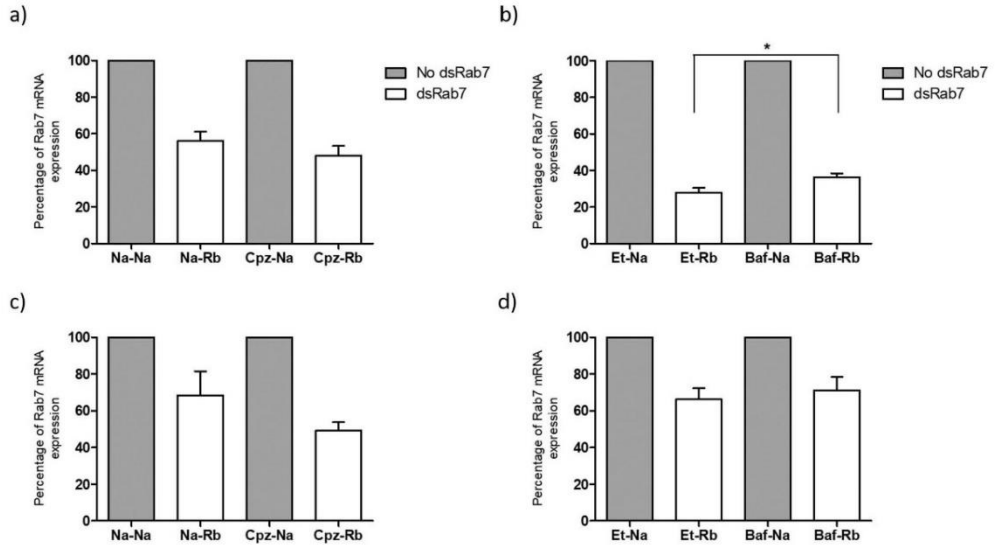

Fig. 3. Effect of inhibitors (chlorpromazine (Cpz) and bafilomycin A1 (Baf)) on endocytic uptake of injected dsRab7 into shrimp cells. Shrimp (n=3–10/group) were pre-injected with the solvents [NaCl (Na) or EtOH (Et)] or drug inhibitors [(a, c) Cpz (at 1.8 μg/g of shrimp) or (b, d) Baf (at 3 μg/g of shrimp)] before injection of NaCl (no dsRab7) or dsRab7 (Rb). Twelve hours later, relative expression of Rab7 mRNA in the hepatopancreas (a-b) or gill (c-d) of shrimp in each group was monitored by RT-PCR and plotted as mean±SEM. The percentage of Rab7 mRNA expression of the drug treated and untreated shrimp are presented. The statistical analysis was performed using the Mann-Whitney test at p-value<.05 (*).

discussion

Over the last few years, the role of endocytosis in the cellular uptake of dsRNA has been studied in several insects either using drug inhibitors (Cappelle et al., 2016; Saleh et al., 2006; Ulvila et al., 2006; Xiao et al., 2015) or RNAi dependent silencing of the key genes in the pathway (Cappelle et al., 2016; Ulvila et al., 2006; Xiao et al., 2015). In most insect species, either the SID-1 like transmembrane protein (Aronstein et al., 2006; Miyata et al., 2014) or endocytosis (Ulvila et al., 2006; Winston et al., 2002; Xiao et al., 2015) or both (Cappelle et al., 2016) are required for cellular importation of dsRNA. There is no consensus about which pathway is involved in dsRNA uptake for several insects.

Our previous study in shrimp (Maruekawong et al., 2018) showed that LvSID-1 is involved in cellular uptake of injected dsRNA into shrimp gills and hemocytes, and this study sought to investigate whether there was a role for endocytosis in dsRNA uptake. Using pharmacological inhibitors (Cpz and BafA) in conjunction with RNAi induced inhibition of STAT or Rab7 as a marker for dsRNA uptake, we observed that both drugs diminished STAT/Rab7 suppression in shrimp hepatopancreas. In contrast, the drugs showed no significant effect on the targeted mRNA silencing in gill tissue. This indicates that injected dsRNA is taken up into shrimp hepatopancreas through the clathrin mediated endocytosis pathway, while this pathway does not seem to play an important role in delivering dsRNA into shrimp gill. Combined with our previous study these results indicate that when dsRNA is circulating in the shrimp body cavity, the SID-1 mediated pathway is a major mechanism in the cellular uptake of dsRNA into gill and hemocyte cells (Maruekawong et al., 2018), while endocytosis is required for dsRNA uptake in hepatopancreatic cells. However, because dsRNA does not affect

LvSID-1 mRNA expression levels in the shrimp hepatopancreas, the requirement for LvSID-1 in the uptake of dsRNA in this tissue could not be evaluated (Maruekawong et al., 2018). Therefore, the possible combined involvement of LvSID-1 together with endocytosis in dsRNA uptake into the shrimp hepatopancreatic cells cannot be excluded. It is clear that factors such as species and the nature of specific cells have to be taken into account when elucidating the mechanisms of dsRNA uptake. For instance, two closely related species of coleopteran, *Tribolium castaneum* (Tomoyasu et al., 2008) and *Diabrotica virgifera* (Miyata et al., 2014) utilize different mechanisms for dsRNA uptake. The latter species uses SID-1 for this process, whereas the former species does not, and utilizes endocytic uptake. Uptake of injected dsRNA into shrim phepatopancreatic cell sutilized an endocytic pathway, while this pathway did not play an important role in dsRNA uptake into gill tissue (this study). Moreover, the introduction of dsRNA from different routes may promote different mechanisms of cellular dsRNA uptake. In this study, as in our previous study (Maruekawong et al., 2018) the dsRNA was introduced into shrimp by injection, and it was dsRNA that was being circulated in the shrimp body cavity in the hemolymph that was in contact with cells in the gill and hepatopancreas tissues that was being taken up. Other routes of dsRNA administration, such as feeding and soaking, may utilize different pathways, which needs to be investigated.

References

1. Aronstein, K., Pankiw, T., Saldivar, E., 2006. SID-I is implicated in systemic gene silencing in the honey bee. J. Apic. Res. 45, 20–24.

2. Assavalapsakul, W., Kiem, H.K.T., Smith, D.R., Panyim, S., 2014. Silencing of PmYPR65 receptor prevents yellow head virus infection in Penaeus monodon. Virus Res. 189, 133–135.

3. Attasart, P., Namramoon, O., Kongphom, U., Chimwai, C., Panyim, S., 2013. Ingestion of bacteria expressing dsRNA triggers specific RNA silencing in shrimp. Virus Res. 171, 252–256.

4. Cappelle, K., de Oliveira, C.F., Van Eynde, B., Christiaens, O., Smagghe, G., 2016. The involvement of clathrin-mediated endocytosis and two Sid-1-like transmembrane proteins in double-stranded RNA uptake in the Colorado potato beetle midgut. Insect Mol. Biol. 25, 315–323.

5. Escobedo-Bonilla, C.M., 2011. Application of RNA interference (RNAi) against viral infections in shrimp: a review. J. Antivir. Antiretrovir. S9. Feinberg, E.H., Hunter, C.P., 2003. Transport of dsRNA into cells by the transmembrane protein SID-1. Science 301, 1545–1547.

6. Huvenne, H., Smagghe, G., 2010. Mechanisms of dsRNA uptake in insects and potential of RNAi for pest control: a review. J. Insect Physiol. 56, 227–235.

7. Labreuche, Y., Veloso, A., de la Vega, E., Gross, P.S., Chapman, R.W., Browdy, C.L., Warr, G.W., 2010. Non-specific activation of antiviral immunity and induction of RNA interference may engage the same pathway in the Pacific white leg shrimp Litopenaeus vannamei. Dev. Comp. Immunol. 34, 1209–1218.

8. Luo, Y., Wang, X., Yu, D., Kang, L., 2012. The SID-1 double-stranded RNA transporter is not required for systemic RNAi in the migratory locust. RNA Biol. 9, 663–671.

9. Maruekawong, K., Tirasophon, W., Panyim, S., Attasart, P., 2018. Involvement of LvSID-1 in dsRNA uptake in Litopenaeus vannamei. Aquaculture 482, 65–72.

10. Miyata, K., Ramaseshadri, P., Zhang, Y., Segers, G., Bolognesi, R., Tomoyasu, Y., 2014. Establishing an in vivo assay system to identify components involved in environmental RNA interference in the western corn rootworm. PLoS One 9, e101661.

11. Ongvarrasopone, C., Roshorm, Y., Panyim, S., 2007. A simple and cost effective method to generate dsRNA for RNAi studies in invertebrates. ScienceAsia 33, 35–39.

12. Ongvarrasopone, C., Chanasakulniyom, M., Sritunyalucksana, K., Panyim, S., 2008. Suppression of PmRab7 by dsRNA Inhibits WSSV or YHV Infection in Shrimp. Mar. Biotechnol. 10, 374–381.

13. Phetrungnapha, A., Kondo, H., Hirono, I., Panyim, S., Ongvarrasopone, C., 2015. Molecular cloning and characterization of Mj-mov-10, a putative RNA helicase involved in RNAi of kuruma shrimp. Fish Shellfish Immunol. 44, 241–247.

14. Posiri, P., Ongvarrasopone, C., Panyim, S., 2013. A simple one-step method for producing dsRNA from E. coli to inhibit shrimp virus replication. J. Virol. Methods 188, 64–69.

15. Posiri, P., Kondo, H., Hirono, I., Panyim, S., Ongvarrasopone, C., 2015. Successful yellow head virus infection of Penaeus monodon requires clathrin heavy chain. Aquaculture 435, 480–487.

16. Sagi, A., Manor, R., Ventura, T., 2013. Gene silencing in crustaceans: from basic research to biotechnologies. Genes 4, 620–645.

17. Saleh, M.C., van Rij, R.P., Hekele, A., Gillis, A., Foley, E., O'Farrell, P.H., Andino, R., 2006. The endocytic pathway mediates cell entry of dsRNA to induce RNAi silencing. Nat. Cell Biol. 8, 793–802.

18. Shekhar, M.S., Lu, Y., 2009. Application of nucleic-acid-based therapeutics for viral infections in shrimp aquaculture. Mar. Biotechnol. 11, 1–9.

19. Sutthangkul, J., Amparyup, P., Charoensapsri, W., Senapin, S., Phiwsaiya, K., Tassanakajon, A., 2015. Suppression of shrimp melanization during white spot syndrome virus infection. J. Biol. Chem. 290, 6470–6481.

20. Tomoyasu, Y., Miller, S.C., Tomita, S., Schoppmeier, M., Grossmann, D., Bucher, G., 2008. Exploring systemic RNA interference in insects: a genome-wide survey for RNAi genes in Tribolium. Genome Biol. 9, R10.

21. Ulvila, J., Parikka, M., Kleino, A., Sormunen, R., Ezekowitz, R.A., Kocks, C., Ramet, M., 2006. Double-stranded RNA is internalized by scavenger receptor-mediated endocytosis in Drosophila S2 cells. J. Biol. Chem. 281, 14370–14375.

22. Wang, L.H., Rothberg, K.G., Anderson, R.G., 1993. Mis-assembly of clathrin lattices on endosomes reveals a regulatory switch for coated pit formation. J. Cell Biol. 123, 1107–1117.

23. Winston, W.M., Molodowitch, C., Hunter, C.P., 2002. Systemic RNAi in C. elegans requires the putative transmembrane protein SID-1. Science 295, 2456–2459.

24. Xiao, D., Gao, X., Xu, J., Liang, X., Li, Q., Yao, J., Zhu, K.Y., 2015. Clathrin-dependent endocytosis plays a predominant role in cellular uptake of double-stranded RNA in the red flour beetle. Insect Biochem. Mol. Biol. 60, 68–77.

25. Xu, W., Han, Z., 2008. Cloning and phylogenetic analysis of Sid-1-like genes from aphids. J. Insect Sci. 8, 30.

26. Xu, H.J., Chen, T., Ma, X.F., Xue, J., Pan, P.L., Zhang, X.C., Cheng, J.A., Zhang, C.X., 2013. Genome-wide screening for components of small interfering RNA (siRNA) and micro-RNA (miRNA) pathways in the brown planthopper, Nilaparvata lugens (Hemiptera: Delphacidae). Insect Mol. Biol. 22, 635–647.

27. Yamamoto, A., Tagawa, Y., Yoshimori, T., Moriyama, Y., Masaki, R., Tashiro, Y., 1998. Bafilomycin A₁prevents maturation of autophagic vacuoles by inhibiting fusion between autophagosomes and lysosomes in rat hepatoma cell line, H-4-II-E cells. Cell Struct. Funct. 23, 33–42.

28. Yao, D., Ehrlich, M., Henis, Y.I., Leof, E.B., 2002. Transforming growth factor-β receptors interact with AP2 by direct binding to β2 subunit. Mol. Biol. Cell 13, 4001–4012.

Suppression of argonautes compromises viral infection in *Penaeus monodon*

Argonaute (Ago) proteins, the catalytic component of an RNA-induced silencing complex (RISC) in RNA interference pathway, function in diverse processes, especially in antiviral defense and transposon regulation. So far, cDNAs encoding four members of Argonaute were found in Penaeus monodon (PmAgo1-4). Two PmAgo proteins, PmAgo1 and PmAgo3 shared high percentage of amino acid identity to Ago1 and Ago2, respectively in other Penaeid shrimps. Therefore, the possible roles of PmAgo1 and PmAgo3 upon viral infection in shrimp were characterized in this study. The level of PmAgo1 mRNA expression in shrimp hemolymph was stimulated upon YHV challenge, but not with dsRNA administration. Interestingly, silencing of either PmAgo1 or PmAgo3 using sequence-specific dsRNAs impaired the efficiency of PmRab7-dsRNA to knockdown shrimp endogenous PmRab7 expression. Inhibition of yellow head virus (YHV) replication and delayed mortality rate were also observed in both PmAgo1-and PmAgo3-knockdown shrimp. In addition, silencing of PmAgo3 transcript, but not PmAgo1, revealed partial inhibition of white spot syndrome virus (WSSV) infection and delayed mortality rate. Therefore, our study provides insights into PmAgo1and PmAgo3 functions that are involved in a dsRNA-mediated gene silencing pathway and play roles in YHV and WSSV replication in the shrimp.

Introduction

Multiple innate defenses including cellular and humoral immune reactions and RNA interference (RNAi) of invertebrates were wildly known as host defense mechanisms against microbial infection. In shrimp, discoveries of several molecules related to both cellular (encapsulation, coagulation, and melanization) and humoral (Toll, Immune deficiency (IMD) and JAK/STAT pathway) immune reactions reveal the existence of innate immune activities to fight against invading pathogens (Borregaard et al., 2000; Hoffmann et al., 1999). In addition, RNAi is also known as one of the potent antiviral immunities in many organisms such as mammals, plants, insects and shrimp (Robalino et al., 2004; Wang et al., 2006; Zambon et al., 2006). The RNAi pathway is triggered by different classes of small regulatory RNAs originating from either endogenous transcripts or exogenous dsRNAs such as small-interfering RNA (siRNA), microRNA (miRNA) and piwiinteracting RNA (piRNA). These small RNAs serve as guide sequences to direct the formation of an RNA-induced silencing complex (RISC), which contains an Argonaute (Ago) family protein as the catalytic core, to regulate viral replication by specific cleavage of the corresponding viral mRNA or translation inhibition (Aliyari et al., 2008).

Regarding their structural features, four domains are identified in a bilobate architecture of Ago proteins; one lobe with N and PAZ domains and the other lobe with MID and PIWI domains. Based on crystal structure analysis, the N domain takes part in unwinding of small RNA duplex (Kwak and Tomari, 2012), while a specific binding pocket on the PAZ domain binds to the 3′ end of small RNA duplex (Lingel et al., 2003; Ma et al., 2004). The 5′ phosphate of small RNAs is held onto the Ago protein by the MID domain (Kiriakidou et al., 2007; Till et al., 2007). A catalytic motif Asp-Asp-His

(DDH) in the PIWI domain is responsible for the endonucleolytic activity (Song et al., 2004; Wang et al., 2008).

Multiple members of the Argonaute family exist in a wide range of organisms and are highly conserved among species. Ago proteins can be separated according to their phylogenetic relationships into Ago and Piwi subfamilies (Chen and Meister, 2005; Hammond et al., 2000; Janowski et al., 2006; Leebonoi et al., 2014; Yigit et al., 2006). Members of the Ago subfamily mediate post-transcriptional gene regulation by associating with either miRNA or siRNA. Piwi subfamily proteins are germ cell specific Argonautes associating with piRNAs, which behave as a small RNA-based immune system to safeguard genome integrity against transposon movement in germ cells and to control spermatogenesis and germ cell differentiation (Kalmykova et al., 2005; Kuromochi et al., 2004). In addition, another class of Argonaute proteins, a worm-specific Argonaute (WAGO), was exclusively found in the nematodes where they play a role in RNAi pathway to mediate a variety of cellular processes (Yigit et al., 2006). Numbers of Argonaute genes are different among organisms, ranging from a single member in Schizosaccharomyces pombe to twenty-seven members in Caenorhabditis elegans (Hock and Meister, 2008). So far, Ago2 of Drosophila and human were demonstrated to possess slicer activity (Meister et al., 2004; Miyoshi et al., 2005) and mediate antiviral defense via RNAi cleavage mechanism (Chen et al., 2011a; Van et al., 2006).

To date, at least two Ago subfamily members were identified and characterized in Penaeid shrimps. In Litopenaues vannamei, two Argonaute genes, LvAgo1 and LvAgo2 were identified; only LvAgo2 was involved in siRNA mediated post-transcriptional gene silencing (Chen et al., 2011b; Labreuche et al., 2010). Likewise, MjAgo1 and MjAgo2 were found in Masupenaeus japonicus. MjAgo1 play important role in antiviral response in the shrimp (Huang and Zhang, 2012), while MjAgo2 acts as a key protein in viral siRNA biogenesis and function (Huang and Zhang, 2013). These studies suggest that Argonaute 2 proteins were essential for the functional siRNA-associated RISC and play a role in antiviral defense via siRNA-mediated viral mRNA degradation in the shrimp.

Interestingly, cDNAs encoding four types of the Ago subfamily proteins were reported in the black tiger shrimp, Penaeus monodon (PmAgo1-4). From phylogenetic analysis, PmAgo1 is clustered in the same group with LvAgo1 and MjAgo1, and was demonstrated for its important function in effective RNAi pathway in the primary culture of lymphoid cells (Dechklar et al., 2008). PmAgo3 was classified into the same group of Argonaute 2 proteins in penaeid shrimp i.e. LvAgo2 and MjAgo2, and was shown to be involved in the pathway of dsRNAmediated gene silencing (Phetrungnapha et al., 2013). In addition, PmAgo2 and PmAgo4 were classified in the same cluster, but located on a separate branch from PmAgo3. The expression of PmAgo2 was responsive to both viral and bacterial infections, and was also activated upon dsRNA and ssRNA administration (Yang et al., 2014). All members of PmAgos, except PmAgo4 are expressed ubiquitously in all shrimp tissues. Interestingly, PmAgo4 displays a gonad-specific expression similar to that of the Piwi subfamily. The gonad-specific PmAgo4 was suggested to be involved in the protection of shrimp genome against transposons invasion (Leebonoi et al., 2014). Although accumulating evidences have demonstrated that PmAgos could exhibit diverse-functions, no report has thus far indicated the actual function of Argonaute proteins for innate immunity in shrimp

compared to model organisms such as Drosophila. In this study, we reported the possible involvement of PmAgo1 and PmAgo3, homologs of DmAgo1 and DmAgo2, respectively in the mechanism of dsRNA-mediated gene silencing. Moreover, the involvement of PmAgo1 and PmAgo3 in viral infection was also characterized. Functional analysis of PmAgo1 and PmAgo3 in the RNAi mechanism during viral infection will provide a basis for further development of effective strategies to control viral diseases in the economically important Penaeid shrimp.

Materials and methods

Animals

Live adolescent black tiger shrimp (approximately 10–15 g body weight) were purchased from shrimp farms around the central area of Thailand. They were first screened for yellow head virus (YHV) and white spot syndrome virus (WSSV) infection by RT-PCR as previously described (Attasart et al., 2009; Yodmuang et al., 2006). The virus-free shrimp were used in all experiments. Shrimp were gradually acclimatized to the laboratory condition in 10 ppt (parts per thousand) sea water with aeration for 2 days. They were also fed with commercial shrimp feed (CP, Thailand) twice a day for a few days before setting the experiment.

Viral stock preparation

To obtain fresh viral stock of YHV and WSSV, crude viruses were injected into the healthy virus-free shrimps. After 48 h, the hemolymph was drawn from moribund shrimp, and the viruses were then purified and determined for viral titer (YHV stock; –2×106 virions ml–1, WSSV stock; –3×105 virions ml–1) as previously described by Assavalapsakul et al. (2003). Appropriate dilutions of the viral stock (100-fold and 10-fold for YHV and WSSV, respectively) that gave complete mortality within 3 days post-infection (dpi) were freshly prepared before use.

Detection of gene transcripts by reverse transcription-polymerase chain reaction (RT-PCR)

Gills were dissected from individual shrimp and homogenized in TRI-REAGENT® (Molecular Research Center), while hemolymph was collected and subsequently mixed with TRI-REAGENT®. Total RNA was isolated according to the manufacturer's protocol. The concentration and purity of the extracted total RNA was examined by Nanodrop® ND-1000 spectrophotometer (Nanodrop Technologies). First strand cDNA was reverse-transcribed from 1 to 2 μg of total RNA priming with PRToligo-dT16 primer by Impromp-II™ reverse transcriptase (Promega) using the following condition: 25 °C for 5 min, 42 °C for 60 min, and 70 °C for 15 min.

One microliter of the first strand cDNA was used as a template to examine mRNA expression. Multiplex-PCR with two primer pairs was applied to determine the expression of the mRNA of interest and β-actin mRNA (internal control) simultaneously. The reaction contains the standard components according to Tag DNA polymerase's protocol (Thermo scientific). PmAgo1 transcript was amplified with PmAgo1-F and PmAgo1-R primers using the following condition: 94 °C for 5 min, 2 cycles of 94 °C for 1 min, 60 °C for 1 min, 72 °C for 1 min and additional 30 cycles of 94 °C for 1 min, 55 °C for 1 min, 72 °C for 1 min (Phetrungnapha et al., 2013). The final extension was performed at 72 °C for 7 min. Amplification of PmAgo3, PmRab7,

YHV-helicase (YHVHel) and WSSV vp28 mRNAs were carried out with specific primer pairs and specific conditions as previously described (Attasart et al., 2009; Ongvarrasopone et al., 2008; Phetrungnapha et al., 2013; Yodmuang et al., 2006). In the experiment, two β-actin PCR products of either 550 bp or 350 bp were amplified with the same forward primers (Actin-F) and different reverse primers, Actin-R or Actin-R2, respectively. The oligonucleotide sequences of Actin primers and specific conditions are previously described by Posiri et al. (2013). The primers used in this study and their nucleotide sequences are shown in Table 1.

Table 1
List of Primers used in this study.

Primers	Sequence (5′ to 3′)	Experiment
Oligo-dT_{16} (PRT)	CCGGAATTCAAGCTTCTAGAGGATCCTTTTTTTTTTTTTTT	Reverse transcription
PmActin-F	GACTCGTACGTGGGCGACGAGG	Detection of Actin transcript
PmActin-R	AGCAGCGGTGGTCATCTCCTGCTC	
PmActin-R2	CGTAGATGGGCACGGTGTGGG	
PmAgo1-F	CAAGAATTTGGTCTGACGAT	Detection of PmAgo1 transcript
PmAgo1-R	AGTGTCACCCACACGCTTCAC	
PmAgo3-F	GGTGGAAGGATTTCCCACTT	Detection of PmAgo3 transcript
PmAgo3-R	CACTGGGGAGTGAGTTGCTT	
PmRab7-F	ATGGCATCTCGCAAGAAGATT	Detection of PmRab7 transcript
PmRab7-R	TTAGCAAGAGCATGCATCCTG	
YHV-Hel-F	CAAGGACCACCTGGTACCGGTAAAAC	Detection of YHV transcript
YHV-Hel-R	GCGGAAACGACTGACGGCTACATTCAC	
WSSV-Vp28-F	ATGAGAATGAACTCCAACTTTAA	Detection of WSSV transcript
WSSV-Vp28-R	CAGAGCCTAGTCTATCAATCAT	

Double-stranded RNA (dsRNA) production

The hair-pin dsRNA precursor was produced by in vivo bacterial expression system as described by Ongvarrasopone et al. (2007). The recombinant plasmids pET17b-st-PmAgo1 (previously construct in our laboratory), pET17b-st-PmAgo3 (Phetrungnapha et al., 2013), pET17bst-PmRab7 (Ongvarrasopone et al., 2008) and pET3a-st-GFP (kindly provided by Asst. Prof. Witoon Tirasophon) harboring the cassette for producing the hair-pin dsRNA of corresponding genes were used to transform ribonuclease III-deficient Escherichia coli strain HT115 (DE3). The expression of hair-pin dsRNAs were induced with 0.4mM IPTG for 4 h with shaking. The hair-pin dsRNAs were extracted by ethanol extraction method (Posiri et al., 2013) before dissolving in 150mM NaCl. The concentration and purity of the hair-pin dsRNAs were monitored by agarose gel electrophoresis and Nanodrop® ND-1000 spectrophotometer. The hair-pin dsRNAs were verified by RNase digestion assay as described previously (Posiri et al., 2013).

Analysis of PmAgo1 expression in response to dsRNA or virus injection

Alteration in PmAgo1 transcript level in shrimp hemolymph was investigated upon either dsRNA or viral injections. Shrimp, approximately 10 g body weight (b.w.) were injected with GFP-dsRNA at 2.5 μg g−1 b.w. or challenged with 50 μl of the 10−2 dilution of YHV stock. After that, the hemolymph was collected from individual shrimp from each group (n=5 and 10 for GFP-dsRNA and YHV injected group, respectively) at 0, 3, 6, 9, 12, 24, 36, 48 and 72 h post-injection (hpi) for determination of PmAgo1 mRNA expression by RT-PCR. Multiplex amplification of PmAgo1 and the internal control, β-actin transcripts was carried out by specific primers for each gene as described in 2.3, and the PCR products were subsequently analyzed by agarose gel electrophoresis. The Scion image analysis program was applied to quantify the band intensity of PmAgo1 PCR product normalized with that of β-actin, and presented as

mean ± standard error of mean (SEM) as relative expression levels of PmAgo1. The significant difference of relative PmAgo1 expression level ($p < 0.05$) between each time point was analyzed by sample T-Test.

Investigation of the effect of PmAgo1 and PmAgo3 knockdown on the efficiency of RNAi

P. monodon (approximately 10 g b.w.) were injected with PmAgo1- or PmAgo3-dsRNA at 2.5 μg g−1 b.w. Either 150mM NaCl or GFP-dsRNA was injected into shrimp as control groups. At 2 days-post injection, the hemolymph sample from shrimp in each group (n=5) was collected to determine the expression levels of PmAgo1 and PmAgo3. Subsequently, PmRab7-dsRNA was injected into PmAgo knocked-down shrimp at 0.63 μg g−1 b.w. to suppress PmRab7 mRNA expression. Expression of PmRab7 was determined by multiplex RT-PCR analysis as described in 2.3 at 0, 24, 48 and 72 h post PmRab7-dsRNA injection.

Biological assay for antiviral function of PmAgo1 and PmAgo3

Shrimps (approximately 10 g b.w.) were injected with 25 μg g−1 b.w of PmAgo1-, PmAgo3- or GFP-dsRNA (5–10 shrimp per group). The hemolymph was collected at 48 h post-dsRNA injection to determine the transcript levels of PmAgo1 and PmAgo3 as described in 2.3. The shrimp were subsequently injected with 50 μl of either the 100 fold diluted YHV or 10 fold diluted WSSV stock. Shrimp injected with 150mM NaCl following with viruses were used as positive control for YHV infection, and shrimp injected with unrelated GFP-dsRNA followed by YHV was used as a control for the effect of dsRNA on viral infection. Multiplex RT-PCR analysis of helicase gene of YHV (hel) or Vp28 gene of WSSV was performed to determine viral mRNA expression relative to that of actin in the shrimp at 0, 36, and 48 h post viral injection. PCR detection of WSSV genome was also performed to determine the level of WSSV genome. In addition, mortality of individual shrimp in each group was also recorded.

Results

Expression of Ago1 in P. monodon upon YHV and GFP-dsRNA administration

Because the two isoforms of Ago1 in P. monodon, PemAgo1 (Dechklar et al., 2008) and PmAgo1 (Unajak et al., 2006) contain the same coding sequences and cannot be differentiated by the RT-PCR detection, they were collectively referred to as PmAgo1 in this study. In order to determine whether PmAgo1 expression is correlated to its possible role in antiviral immunity and dsRNA mediated gene silencing as reported earlier, the expression of PmAgo1 in response to YHV injection or GFPdsRNA in the hemolymph of shrimp at various time points was determined by multiplex RT-PCR. Successful YHV infection was confirmed at 72 hpi by the detection of YHV helicase gene expression in the hemolymph of individual shrimp. The result in Fig. 1A revealed that the expression levels of PmAgo1 in YHV injected shrimp gradually increased from 0 hpi to the highest level of approximately 2-fold with significant difference ($p < 0.05$) at 9 hpi before continuously decreasing until 72 hpi. On the other hand, PmAgo1 expression in shrimp hemolymph at every time point post-GFP-dsRNA injection was rather constant throughout the course of the experiment

(Fig. 1B). These data demonstrated that PmAgo1 expression was activated by YHV, but not by dsRNA administration.

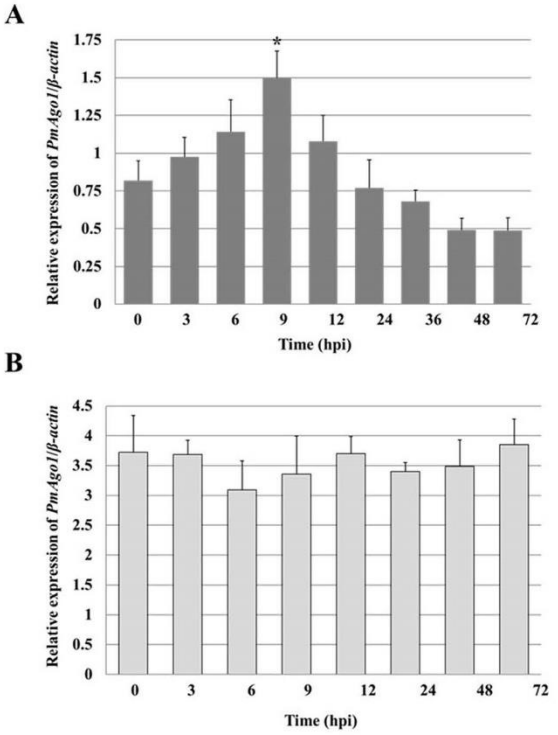

Fig. 1. PmAgo1 expression in response to yellow head virus (YHV) and GFPdsRNA administration Multiplex RT-PCR was used to determine the expression of PmAgo1 in the hemolymph of *P. monodon* at different time points after injected with either 50 μl of 100-fold dilution of purify YHV lysate (A; n=10) or GFP-dsRNA at 2.5 μg g−1 shrimp (B; n=5). The bar-graphs represent expression level of PmAgo1 normalized with that of β-actin as analyzed by Scion image analysis program. Each bar represents mean ± SEM. Asterisk indicates significant difference from 0 hpi ($p < 0.05$).

Silencing of PmAgo1 and PmAgo3 by specific dsRNAs

To study the function of PmAgo1 and PmAgo3, their expression was first suppressed by dsRNA-mediated gene silencing approach. The injection of PmAgo1-dsRNA significantly suppressed PmAgo1 transcript level ($p < 0.05$) approximately 60% and 50% on day 2 and day 4 postinjection, respectively. More than 95% suppression of PmAgo3 transcript was found in the hemolymph after one day post-PmAgo3-dsRNA injection, and this level of suppression lasted for at least 3 days (Figure S1). Moreover, PmAgo1-dsRNA did not have effect on PmAgo3 expression and vice versa (Fig. 2A and B). Therefore, these dsRNAs were able to efficiently and specifically suppress PmAgo1 and PmAgo3 expression, and thus could be used for further functional analysis of both PmAgos.

Impairment of RNAi-mediated PmRab7 repression in PmAgoknockdown shrimp

To investigate possible involvement of PmAgo1 and PmAgo3 in dsRNA-mediated RNAi pathway, the efficiency of PmRab7-dsRNA to repress shrimp endogenous PmRab7 mRNA expression was studied in PmAgo-knockdown shrimp. The silencing of PmAgo1 and PmAgo3 expression in shrimp hemolymph was confirmed on day 2 after injected with corresponding dsRNAs compared with that in the control shrimp injected with NaCl or an unrelated GFP-dsRNA (Figure S2), whereas the expression of PmRab7 among each group was not dramatically different (Fig. 3; Day0). Shrimp in each group were then injected with PmRab7-dsRNA, and PmRab7 expression was determined at 24 h interval after PmRab7-dsRNA injection. The result in Fig. 3 showed the complete suppression of PmRab7 mRNA expression in

both control groups (NaCl or GFP-dsRNA injection followed by PmRab7-dsRNA) at 24, 48 and 72 h post-PmRab7-dsRNA injection. Interestingly, the expression of PmRab7 could be detected in PmAgo1- and PmAgo3-knockdown shrimp to a certain extent, but significantly different ($p < 0.05$) from the control shrimp, at all time-points from 24 to 72 h after injected with PmRab7-dsRNA. These results indicated that dsRNA-mediated PmRab7 suppression in PmAgo-knockdown shrimp was not as efficient as that in the control shrimp. Moreover, PmRab7 expression PmAgo1-knockdown shrimp was noticeably higher than that in PmAgo3-knockdown shrimp at 72 h post-PmRab7-dsRNA injection, suggesting that both PmAgos contribute to the dsRNA-mediated gene silencing pathway in shrimp at different extent.

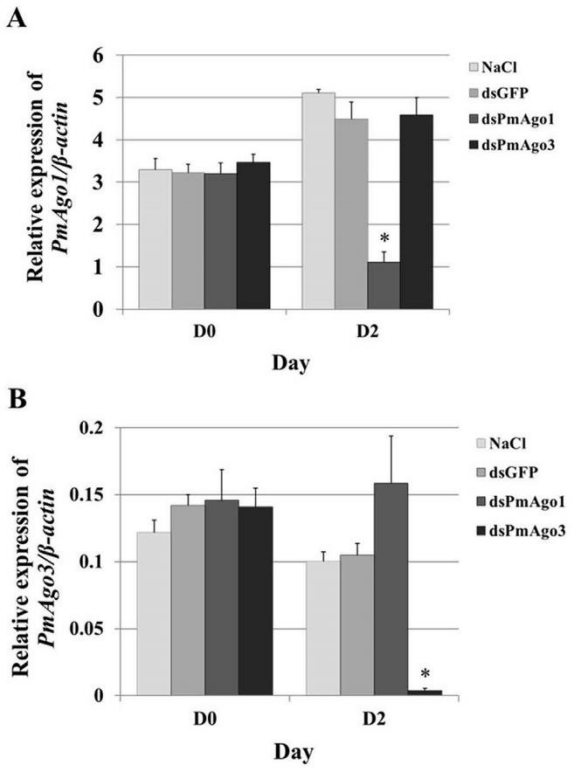

Fig. 2. Suppression of PmAgo1 and PmAgo3 transcripts by dsRNA *P. Monodon* were injected with 2.5 μg g−1 shrimp b.w. of either PmAgo1-dsRNA (dsPmAgo1) or PmAgo3-dsRNA (dsPmAgo3). The expression of PmAgos in the hemolymph was determined by multiplex RT-PCR at 2 days post-injection comparing with that in shrimp injected with NaCl and GFP-dsRNA as the control groups. The levels of PmAgo1 and PmAgo3 transcripts in the hemolymph of shrimp in each group were analyzed by agarose gel electrophoresis together with the internal control β-actin transcript. The histograms show the relative expression of PmAgo1 (A) and PmAgo3 (B) normalized with that of β-actin as measured by Scion image analysis program. Each bar represents mean ± SEM (n = 5). Asterisks (*) indicate the significant difference ($p < 0.05$) between PmAgo1-dsRNA or PmAgo3-dsRNA injection groups and the control groups at each time point.

Effect of PmAgo1 and PmAgo3 knockdown on viral infection in shrimp

To investigate the function of PmAgo1 and PmAgo3 on virus infection, viral replication and shrimp mortality after YHV or WSSV challenge in PmAgo-knockdown shrimp were determined compared with that in the control groups (NaCl or GFP-dsRNA injcetion). The expression of PmAgo1 and PmAgo3 was knocked down by the injection of specific dsRNA two days before YHV challenge. The YHV-hel transcript could be detected in the hemolymph of both control groups at 48 h post-YHV injection (hpi), but not in the hemolymph of PmAgo1-knockdown shrimp (Fig. 4A). In addition, the control shrimp that had been injected with NaCl or GFP-dsRNA prior to YHV challenge started to die after 84 hpi, and the cumulative mortality reached 100% at 108 hpi, whereas the mortality of PmAgo1-knockdown shrimp was observed after 120 h post-YHV challenge and reached 100% at 138 hpi (Fig. 4B). Similarly, barely

detectable level of YHV-hel and delayed cumulative mortality rate upon YHV challenge was also observed in PmAgo3-knockdown shrimp when compared with the control groups (Fig. 5A and B). The detection of YHV-hel gene in the gill tissue from all dead shrimp confirmed that the shrimp were infected with the virus (Figs. 4C and 5C).

Since WSSV is one of major viruses that cause high mortality in the shrimp, the role of PmAgo1 and PmAgo3 in WSSV infection was also investigated. The result showed that the levels of WSSV vp28 transcript as well as WSSV genomic DNA in PmAgo1-knockdown shrimp infected with WSSV was comparable to that in both control groups that were injected with either NaCl or GFP-dsRNA prior to viral challenge (Fig. 6A and B). In addition, the cumulative mortality rate of the shrimp in all groups was not different; shrimp started to die after 36 h, and all were dead by 48 h (Fig. 6C). By contrast, lower levels of WSSV vp28 transcript, notably with undetectable level in two out of five shrimp, and lower amounts of viral DNA genome in the pleopod were detected in PmAgo3-knockdown shrimp at 36 h post-WSSV infection compared with that in both control groups (Fig. 6A and B). Moreover, the delay in the cumulative mortality rate in PmAgo3-knockdown shrimp was observed upon WSSV challenge when compared to the control groups (Fig. 6C). The WSSV vp28 transcript could be detected in gill tissue from dead shrimp in all groups confirming that the shrimp died of WSSV infection (Fig. 6D).

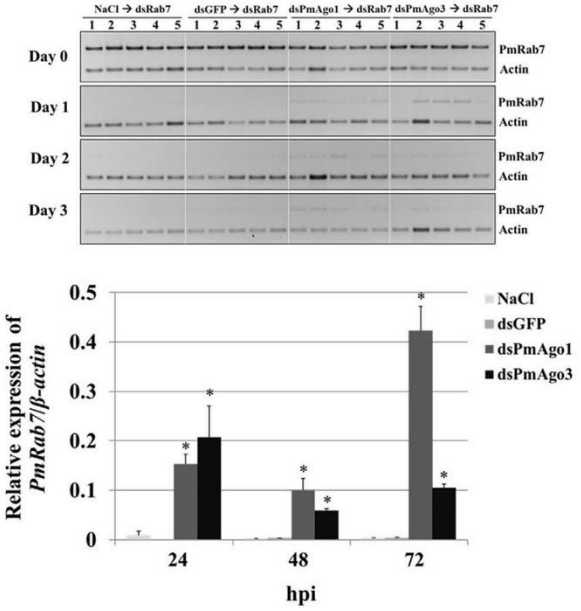

Fig. 3. Impairment of PmRab7 silencing by Rab7-dsRNA in PmAgo1-and PmAgo3-knockdown shrimp. The expression of PmAgo1 and PmAgo3 was suppressed by the injection of PmAgo1-or PmAgo3-dsRNA at 2.5 μg g−1 b.w., whereas NaCl and GFP-dsRNA injection were used as the controls. Two days following the dsRNA injection, shrimp in each group were subsequently injected with PmRab7-dsRNA (0.6 μg g−1 shrimp b.w.), and the expression of PmRab7 in the hemolymph was determined at 0, 24, 48 and 72 h post-PmRab7-dsRNA injection (upper panel). β-actin was detected as an internal control. Numbers represent individual shrimp. The histograms (lower panel) show the relative expression of PmRab7 normalized with that of β-actin as measured by Scion image analysis program. Each bar represents mean ± SEM ($n = 5$). Asterisks (*) indicate the significant difference ($p < 0.05$) between PmAgo1-dsRNA (dsPmAgo1) or PmAgo3-dsRNA (dsPmAgo3) injection groups and the control groups at each time point.

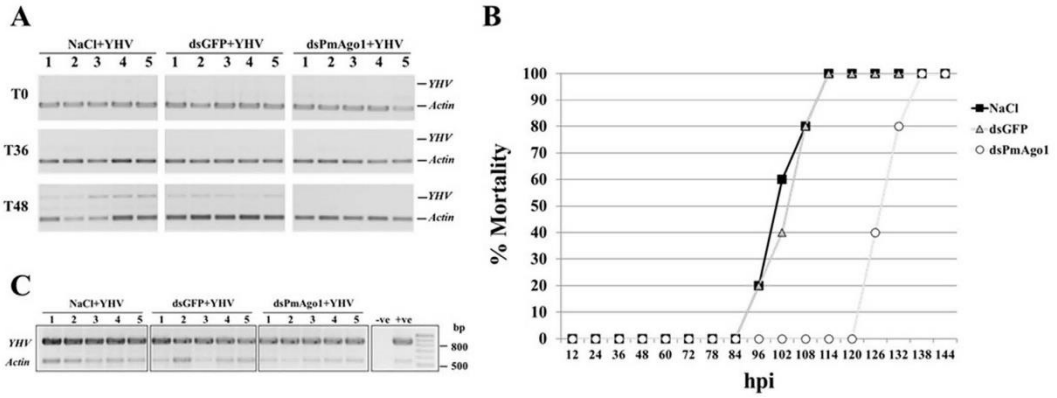

Fig. 4. Effect of PmAgo1 knockdown on YHV replication and cumulative mortality in shrimp upon YHV infection Suppression of PmAgo1 expression was carried out by PmAgo1-dsRNA injection with NaCl and GFP-dsRNA injection as controls. On day 2 after injected with dsRNA, shrimp were subsequently challenged with YHV, and the expression of YHV helicase gene (YHV-hel) in the hemolymph of PmAgo1-knockdown shrimp (dsPmAgo1+YHV) and the control shrimp (NaCl + YHV, dsGFP + YHV) was detected by multiplex RT-PCR compared with that of β-actin at 0, 36 and 48 h post YHV infection (n=5 at each time point) (A). Mortality of individual shrimp in each group was also recorded, and presented as cumulative percent mortality (B). Virus infection in the shrimp was verified by detection of YHVhel mRNA in gill tissue from dead shrimp in all groups (C).

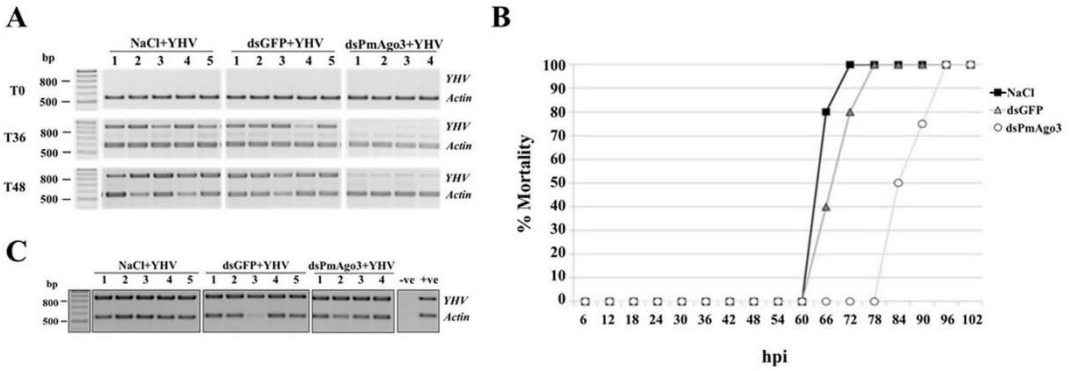

Fig. 5. Effect of PmAgo3 knockdown on YHV replication and cumulative mortality in shrimp upon YHV infection Suppression of PmAgo3 expression was carried out by PmAgo3-dsRNA injection with NaCl and GFP-dsRNA injection as controls. The PmAgo3-knockdown shrimp were infected with YHV (dsPmAgo3+YHV), and the expression of YHV-hel gene in the hemolymph was detected by multiplex RT-PCR compared with that of control shrimp (NaCl + YHV, dsGFP + YHV) at 0, 36 and 48 h post YHV infection (n = 5 at each time point) (A). β-actin transcript was determined as internal control. Mortality of individual shrimp in each group was also recorded, and presented as cumulative percent mortality (B). Expression of YHV-hel mRNA in gill tissue from dead shrimp was examined to confirm virus infection in the shrimp (C).

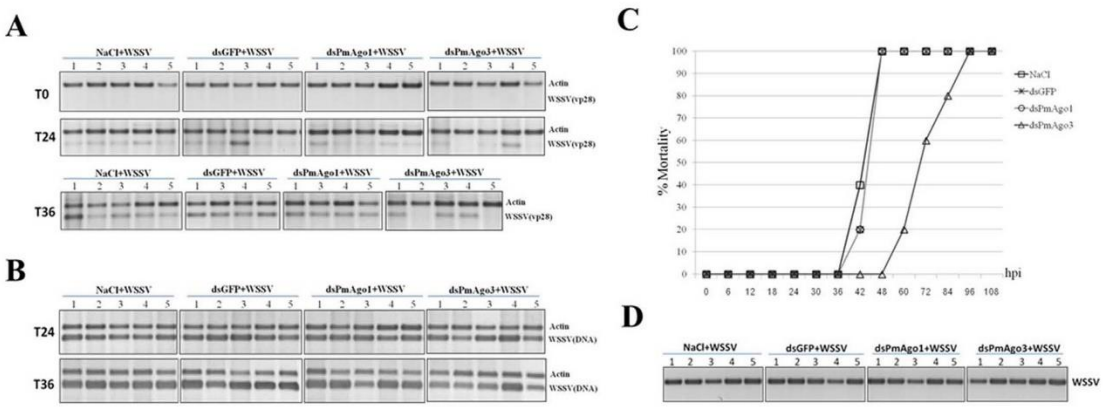

Fig. 6. WSSV replication and shrimp mortality upon WSSV infection in PmAgo1- and PmAgo3-knockdown P. monodon. P. monodon were injected with either 2.5 μg g−1 shrimp of PmAgo1-dsRNA, PmAgo3-dsRNA, GFP-dsRNA or 150mM NaCl (n=5 in each group) 2 days prior to WSSV challenge. WSSV replication in PmAgo1-knockdown shrimp (dsPmAgo1+WSSV), PmAgo3-knockdown shrimp (dsPmAgo3+WSSV) comparing with control shrimp (NaCl + WSSV and dsGFP + WSSV) was determined by both RT-PCR detection of WSSV Vp28 mRNA (A) and PCR amplification of WSSV genomic DNA (B) at 0, 24 and 36 h post WSSV infection. β-actin transcript was determined as an internal control. Mortality of individual shrimp in each group was also recorded, and presented as cumulative percent mortality (C). WSSV infection in all dead shrimp was confirmed by RT-PCR of WSSV-vp28 mRNA in the gill tissue (D).

Discussion

Four types of Argonaute protein were previously identified in *P. monodon*. They are all classified as the Ago subfamily. Nevertheless, the mechanism underlying the Ago-related antiviral immunity in shrimp remains largely unknown. In this study, functional significance of PmAgo1 and PmAgo3 on YHV and WSSV replication and their role in dsRNA-mediated post-transcriptional gene silencing were characterized.

Expression of key proteins in the effective innate antiviral RNAi mechanism was usually stimulated by exogenous RNAs (Choudhary et al., 2007; Garbutt and Reynolds, 2012; Phetrungnapha et al., 2013; Yang et al., 2014). Injection of dsRNA could induce expression of dicer-2 and argonaute-2 in tobacco hornworm (Garbutt and Reynolds, 2012). In Neurospora crassa, the induction of dicer (DCL-2) and argonaute (QDE-2) expression by dsRNA resulted in an increase in the efficiency of dsRNA-mediated RNAi pathway (Choudhary et al., 2007). These evidences suggested that dicer-2 and argonaute-2 are involved in dsRNAmediated gene silencing pathway. Up-regulation of the expression of genes encoding core RNAi proteins e.g. Dcr2, Ago2 and Ago3 and associated components such as TRBP, TSN and Mov-10 upon dsRNA challenge were also demonstrated in penaeid shrimps (Li et al., 2013; Phetrungnapha et al., 2012, 2013, 2015; Yang et al., 2013, 2014). In addition, suppression of HsAgo2 by HsAgo2-siRNA in Human Embryonic Kidney 293 cells (HEK-293) impeded the efficiency of RNAi mechanism to knock-down histone deacetylase 2 (HDAC2) by specific HDAC2-siRNA (Naoghare et al., 2011). Similarly, silencing of PmAgo1 and PmAgo3 expression by specific dsRNAs in this study reduced the efficiency of PmRab7 mRNA suppression by PmRab7-dsRNA, indicating the involvement of PmAgo1 and PmAgo3 in dsRNA-mediated gene silencing process. These results strongly supported the study of Dechklar et al. (2008) where repression of Ago1

reduced the competency of 5HTdsRNA in suppressing 5HT gene in P. monodon's Oka cells. In addition, the knockdown of PmTSN or MjTRBP expression by specific dsRNA in shrimp also impaired the efficiency of dsRNA/ siRNA mediated gene silencing (Phetrungnapha et al., 2012; Wang et al., 2012).

Previous reports on the Argonaute-interacting proteins in shrimp revealed that argonaute-2 of L. vannamei and M. japonicus bound to dicer-2 and TRBP1, respectively. These Ago2 complexes played a role in dsRNA/ siRNA-mediated sequence-specific RNAi process while argonaute-1 primarily functioned in a miRNA pathway (Chen et al., 2011b; Huang and Zhang, 2013). However, the interacting proteins and small RNAs associated with either PmAgo1 or PmAgo3 need to be identified to confirm the precise mechanism of each PmAgo in the RNAi pathway. Previous studies in other species demonstrated that the responsive expression of Ago transcripts upon virus infection enhanced the effective RNAi antiviral defense (Sun et al., 2009; Várallyay et al., 2010). For instance, the increased expression of NbAgo1 mRNA in Cymbidun ringspot virus (CymRSV) infected Nicotiana benthamiana and the accumulation of argonaute-1 protein enhanced the RNAi antiviral activity by reducing the levels of CymRSV accumulation in the plant (Várallyay et al., 2010). In addition, high levels of MjAgo1A and MjAgo1B transcript were accumulated upon WSSV infection in M. japonicus (Huang and Zhang, 2012). Similarly, our result showed that the increased levels of PmAgo1 expression was noticed in the haemolymph of YHV-infected shrimp. This phenomenon was also observed in YHV-infected as well as WSSV-infected lymphoid organ (Unajak et al., 2006) indicating a possible involvement of PmAgo1 during viral infection. Our investigation on the expression of PmAgo3 in WSSV challenge shrimp revealed that PmAgo3 was gradually up-regulated in WSSV infected shrimp. The significant difference of PmAgo3 expression was observed after 12 hpi when compared to its expression level at 0 hpi (Fig. S3). These results demonstrated that WSSV infection in shrimp could activate the expression of both PmAgo1 and PmAgo3 mRNA. Up-regulation of argonaute 2 (GrAgo2) transcripts was exhibited in grass carp reovirus-infected rare minnow Gobiocypris rarus (Su et al., 2009). Likewise, the infection of tomato yellow leaf curl virus in tomato, Solanum lycopersicum induced the expression of dicers and Agos (Bai et al., 2012). In P. monodon, Yang et al., 2014 demonstrated that PmAgo2 mRNA expression was escalated by WSSV challenge while the expression of PmAgo3 and PmAgo4 was not altered in YHV infected shrimp (Leebonoi et al., 2014; Phetrungnapha et al., 2013). In addition, virus infection in Penaeid shrimps could also evoke other RNAi components such as LvDicer-1, LvDrosha and FcTRBP (Huang et al., 2012; Wang et al., 2009; Yoa et al., 2010). Nonetheless, the responsive expression of PmAgos upon viral challenge may not necessarily specify PmAgos' function in antiviral defense. Whether or not PmAgos take part in the response to viral infection in the shrimp was therefore further characterized in this study.

The function of Argonaute proteins in RNAi-mediated antiviral defense in invertebrates was generally demonstrated by an increase in susceptibility to viruses in Ago-knockdown animals (Huang and Zhang, 2012). For instance, the hypersensitivity to Drosophila C virus infection and high viral RNA accumulation were presented in DmAgo2 mutant drosophila comparing to wild type and DmAgo1 mutant flies (Van et al., 2006). A significant increase of viral loads was also observed in the shrimp, in which the expression of RNAi machinery e.g. Ago1, dicer-1, TRBP and Mov10 had

been knocked down (Huang and Zhang, 2012; Phetrungnapha et al., 2015; Su et al., 2008; Wang et al., 2012). Therefore, the functional significance of PmAgo1 and PmAgo3 in RNAi upon viral infection were investigated by determining the level of viral transcript and cumulative mortality in PmAgos-suppressed shrimp comparing to the control groups.

In general, once the hosts are infected by RNA viruses, the dsRNA replicative intermediates of the viruses are recognized by Dicer and cleaved into viral-derived siRNAs (viRNAs). The complex between viRNAs and Ago proteins in the RISC subsequently trigger the activity of RNA silencing-mediated antiviral immunity (Molnar et al., 2005; Pantaleo et al., 2007; Parameswaran et al., 2010; Weng et al., 2015). However, some viruses could express viRNAs that interfered with host gene expression and promoted viral infection (Adkar-purushothama et al., 2015; Wang et al., 2016). For example, the expression of two callose synthase genes in tomato plant was down-regulated by siRNA derived from potato spindle tuber viroid leading to the accumulation of viroids and the severity of disease (Adkar-purushothama et al., 2015). Likewise, siRNAs derived from Cucumber mosaic virus (CMV) Y satellite RNA (Y-sat) could decrease the expression chlI gene in the chlorophyll synthesis pathway, and enhanced the yellowing symptom in tobacco plants (Smith et al., 2011). Our results revealed that inhibition of YHV replication and delay mortality were noticeably observed in PmAgo1- and PmAgo3-knockdown shrimp when compared with that in both control groups (injection with either NaCl or GFPdsRNA prior to viral challenge). These evidences suggest that the positive single-stranded YHV might produce viRNAs that were subsequently loaded into either PmAgo1 or PmAgo3 RISC to regulate cellular gene expression of shrimp, and accounted for promoting viral replication and disease severity. However, the gene required for YHV replication, whose expression was affected by YHV-derived small RNA in the shrimp needs to be further identified.

In addition to RNA viruses, a number of DNA viruses could also produce viral-derived small RNAs. For example, viRNAs derived from shrimp DNA virus, WSSV were reported in Penaeid shrimps (Huang and Zhang, 2013), and they required shrimp Ago2 protein for the effective function in response to WSSV infection (Yang et al., 2014). Our results also showed that the replication of WSSV in P. monodon was suppressed in PmAgo3-knockdown shrimp, but not in PmAgo1-knockdown shrimp suggesting that PmAgo3 might play an important role in both DNA and RNA virus replication in the shrimp. The preference for each Ago protein in response to RNA and DNA viruses is not surprising as it has been demonstrated that Arabidopsis Ago1 and Ago2 played a major role in the anti-RNA viral response (Dzianott et al., 2012; Garcia-Ruiz et al., 2015; Jaubert et al., 2011; Wang et al., 2011), while Ago4 functions in an antiviral activity against several RNA (Bhattacharjee et al., 2009; Hamera et al., 2012) and DNA viruses (Raja et al., 2008, 2014). Nevertheless, what defines these preferential antiviral activities in shrimp is still elusive.

In conclusion, the function of PmAgo1 and PmAgo3 during viral infection in P. monodon was reported in this study. The elevated PmAgo1 expression in the hemolymph upon YHV challenge suggests its association with shrimp response to viral infection. Suppression of PmAgos by specific dsRNA indicated that PmAgo1 was preferentially required for YHV replication, whereas PmAgo3 has more extensive effect on the replication of both YHV and WSSV. Our findings expand an

understanding in Argonaute-associated RNA silencing mechanism and host response during viral infection in Penaeid shrimps.

References

1. Adkar-purushothama, C.R., Brosseau, C., Giguère, T., Sano, T., Moffett, P., Perreault, J.P., 2015. Small RNA derived from the virulence modulation region of the Potato spindle tuber viroid silences callose synthase genes of tomato plants. Plant Cell 27, 2178–2194.

2. Aliyari, R., Wu, Q., Li, H.W., Wang, X.H., Li, F., Green, L.D., Han, C.S., Li, W.X., Ding, S.W., 2008. Mechanism of induction and suppression of antiviral immunity directed by virus-derived small RNAs in Drosophila. Cell Host Microbe 4, 387–397.

3. Assavalapsakul, W., Smith, D.R., Panyim, S., 2003. Propagation of infectious yellow head virus particles prior to cytopathic effect in primary lymphoid cell cultures of Penaeus monodon. Dis. Aquat. Org. 55, 253–258.

4. Attasart, P., Kaewkhaw, R., Chimwai, C., Kongphom, U., Namramoon, O., Panyim, S., 2009. Inhibition of white spot syndrome virus replication in Penaeus monodon by combined silencing of viral rr2 and shrimp PmRab7. Virus Res. 145, 127–133.

5. Bai, M., Yang, G.S., Chen, W.T., Mao, Z.C., Kang, H.X., Chen, G.H., Yang, Y.H., Xie, Y.B., 2012. Genome-wide identification of Dicer-like, Argonaute and RNA-dependent RNA polymerase gene families and their expression analyses in response to viral infection and abiotic stresses in Solanum lycopersicum. Gene 501, 52–62.

6. Bhattacharjee, S., Zamora, A., Azhar, M.T., Sacco, M.A., Lambert, L.H., Moffett, P., 2009. Virus resistance induced by NB-LRR proteins involves Argonaute4-dependent translational control. Plant J. 58, 940–951.

7. Borregaard, N., Elsbach, P., Ganz, T., Garred, P., Svejgaard, A., 2000. Innate immunity: from plants to humans. Immunol. Today 21, 68–70.

8. Chen, P.Y., Meister, G., 2005. MicroRNA-guided posttranscriptional gene regulation. Biol. Chem. 386, 1205–1218.

9. Chen, S., Chahar, H.S., Abraham, S., Wu, H., Pierson, T.C., Wang, X.A., Manjunath, N., 2011a. Ago-2-mediated slicer activity is essential for anti-flaviviral efficacy of RNAi. PLoS One 6, e27551.

10. Chen, Y.H., Jia, X.T., Zhao, L., Li, C.Z., Zhang, S., Chen, Y.G., Weng, S.P., He, J.G., 2011b.

11. Identification and functional characterization of Dicer2 and five single VWC domain proteins of *Litopenaeus vannamei*. Dev. Comp. Immunol. 35, 661–671.

12. Choudhary, S., Lee, H.C., Maiti, M., He, Q., Cheng, P., Liu, Q., Liu, Y., 2007. A doublestranded-RNA response program important for RNA interference efficiency. Mol. Cell Biol. 27, 3995–4005.

13. Dechklar, M., Udomkit, A., Panyim, S., 2008. Characterization of Argonaute cDNA from *Penaeus monodon* and implication of its role in RNA interference. Biochem. Biophys. Res. Commun. 367, 768–774.

14. Dzianott, A., Sztuba-Solinska, J., Bujarski, J.J., 2012. Mutations in the antiviral RNAi defense pathway modify Brome mosaic virus RNA recombinant profiles. Mol. Plant Microbe Interact. 25, 97–106.

15. Garbutt, J. S., Reynolds, S. E., 2012. Induction of RNA interference genes by doublestranded RNA; implications for susceptibility to RNA interference. Insect Biochem. Mol. Biol. 42, 621–628.

16. Garcia-Ruiz, H., Carbonell, A., Hoyer, J.S., Fahlgren, N., Gilbert, K.B., Takeda, A., Giampetruzzi, A., Garcia Ruiz, M. T., McGinn, M. G., Lowery, N., Martinez Baladejo, M. T., Carrington, J. C., 2015. Roles and programming of Arabidopsis ARGONAUTE proteins during turnip mosaic virus infection. PLoS Pathog. 11, e1004755.

17. Hamera, S., Song, X., Su, L., Chen, X., Fang, R., 2012. Cucumber mosaic virus suppressor 2b binds to AGO4-related small RNAs and impairs AGO4 activities. Plant J. 69, 104–115.

18. Hammond, S. M., Bernstein, E., Beach, D., Hannon, G. J., 2000. An RNA-directed nuclease mediates post- transcriptional gene silencing in Drosophila cells. Nature 404, 293–296.

19. Hock, J., Meister, G., 2008. The Argonaute protein family. Genome Biol. 9, 210.

20. Hoffmann, J. A., Kafatos, F. C., Janeway, C. ,A. ,, Ezekowitz, R. A., 1999. Phylogenetic perspectives in innate immunity. Science 284, 1313–1318.

21. Huang, T., Xu, D., Zhang, X., 2012. Characterization of shrimp Drosha in virus infection. Fish Shellfish Immunol. 33, 575–581.

22. Huang, T., Zhang, X., 2012. Contribution of the argonaute- 1 isoforms to invertebrate antiviral defense. PLoS One 7, e50581.

23. Huang, T., Zhang, X., 2013. Host defense against DNA virus infection in shrimp is mediated by the siRNA pathway. Eur. J. Immunol. 43, 137–146.

24. Janowski, B.A., Huffman, K.E., Schwartz, J.C., Ram, R., Nordsell, R., Shames, D.S., Minna, J.D., Corey, D.R., 2006. Involvement of AGO1 and AGO2 in mammalian transcriptional silencing. Nat. Struct. Mol. Biol. 13, 787–792.

25. Jaubert, M. J., Bhattacharjee, S., Mello, A. F., Perry, K. L., Moffett, P., 2011. AGO2 mediates RNA silencing anti- viral defenses against Potato virus X in Arabidopsis. Plant Physiol. 156, 1556–1564.

26. Kalmykova, A.I., Klenov, M.S., Gvozdev, V.A., 2005. Argonaute protein PIWI controls mobilization of retrotransposons in the Drosophila male germline. Nucleic Acids Res. 33, 2052–2059.

27. Kiriakidou, M., Tan, G.S., Lamprinaki, S., De Planell-Saguer, M., Nelson, P.T., Mourelatos, Z., 2007. An mRNA m(7)G cap binding- like motif within human Ago2 represses translation. Cell 129, 1141–1151.

28. Kuramochi-Miyagawa, S., Kimura, T., Ijiri, T.W., Isobe, T., Asada, N., Fujita, Y., Ikawa, M., Iwai, N., Okabe, M., Deng, W., Lin, H., Matsuda, Y., Nakano, T., 2004. Mili, a mammalian member of piwi family gene, is essential for spermatogenesis. Development 131, 839–849.

29. Kwak, P. B., Tomari, Y., 2012. The N domain of Argonaute drives duplex unwinding during RISC assembly. Nat. Struct. Mol. Biol. 19, 145–151.

30. Labreuche, Y., Veloso, A., de la Vega, E., Gross, P. S., Chapman, R. W., Browdy, C. L., Warr, G. W., 2010. Non- specific activation of antiviral immunity and induction of RNA interference may engage the same pathway in the Pacific white leg shrimp Litopenaeus vannamei. Dev. Comp. Immunol. 34, 1209–1218.

31. Leebonoi, W., Sukthaworn, S., Panyim, S., Udomkit, A., 2014. A novel gonad-specific Argonaute 4 serves as a defense against transposons in the black tiger shrimp *Penaeus monodon*. Fish Shellfish Immunol. 42, 280–288.

32. Lingel, A., Simon, B., Izaurralde, E., Sattler, M., 2003. Structure and nucleic-acid binding of the Drosophila Argonaute 2 PAZ domain. Nature 426, 465–469.

33. Li, X., Yang, L., Liang, S., Fu, M., Huang, J., Jiang, S., 2013. Identification and expression analysis of Dicer2 in black tiger shrimp (Penaeus monodon) responses to immune challenges. Fish Shellfish Immunol. 35, 1–8.

34. Ma, J.B., Ye, K., Patel, D.J., 2004. Structural basis for overhang-specific small interfering RNA recognition by the PAZ domain. Nature 429, 318–322.

35. Meister, G., Landthaler, M., Patkaniowska, A., Dorsett, Y., Teng, G., Tuschi, T., 2004. Human Argonaute2 mediates RNA cleavage targeted by miRNAs and siRNAs. Mol. Cell. 15, 185–197.

36. Miyoshi, K., Tsukumo, H., Nagami, T., Siomi, H., Siomi, M.C., 2005. Slicer function of Drosophila Argonautes and its involvement in RISC formation. Genes Dev. 19, 2837–2848.

37. Molnar, A., Csorba, T., Lakatos, L., Varallyay, E., Lacomme, C., Burgyan, J., 2005. Plant virus-derived small interfering RNAs originate predominantly from highly structured single-stranded viral RNAs. J. Virol. 79, 7812–7818.

38. Naoghare, P.K., Tak, Y.K., Kim, M.J., Han, E., Song, J.M., 2011. Knock-down of argonaute 2 (AGO2) induces apoptosis in myeloid leukaemia cells and inhibits siRNA-mediated silencing of transfected Oncogenes in HEK-293 cells. Basic Clin. Pharmacol. Toxicol. 109, 274–282.

39. Ongvarrasopone, C., Chanasakulniyom, M., Sritunyalucksana, K., Panyim, S., 2008. Suppression of PmRab7 by dsRNA inhibits WSSV or YHV infection in shrimp. Mar. Biotechnol. 10, 374–381.

40. Ongvarrasopone, C., Roshorm, Y., Panyim, S., 2007. A simple and cost effective method to generate dsRNA for RNAi studies in invertebrates. Sci. Asia 33, 35–39.

41. Pantaleo, V., Szittya, G., Burgyán, J., 2007. Molecular bases of viral RNA targeting by viral small interfering RNA-programmed RISC. J. Virol. 81, 3797–3806.

42. Parameswaran, P., Sklan, E., Wilkins, C., Burgon, T., Samuel, M.A., Lu, R., Ansel, K.M., Heissmeyer, V., Einav, S., Jackson, W., Doukas, T., Paranjape, S., Polacek, C., dos Santos, F.B., Jalili, R., Babrzadeh, F., Gharizadeh, B., Grimm, D., Kay, M., Koike, S., Sarnow, P., Ronaghi, M., Ding, S.W., Harris, E., Chow, M., Diamond, M.S., Kirkegaard, K., Glenn, J.S., Fire, A.Z., 2010. Six RNA viruses and forty-one hosts: viral small RNAs and modulation of small RNA repertoires in vertebrate and invertebrate systems. PLoS Pathog. 6, e1000764.

43. Phetrungnapha, A., Ho, T., Udomkit, A., Pamyim, S., Ongvarrasopone, C., 2013.

44. Molecular cloning and functional characterization of Argonaute-3 gene from *Penaeus monodon*. Fish Shellfish Immunol. 35, 874–882.

45. Phetrungnapha, A., Kondo, H., Hirono, I., Panyim, S., Ongvarrasopone, C., 2015.

46. Molecular cloning and characterization of Mj-MOV10, a putative RNA helicase involved in RNAi of Kuruma shrimp. Fish Shellfish Immunol. 44, 241–247.

47. Phetrungnapha, A. , Panyim, S. , Ongvarrasopone, C. , 2012. A Tudor staphylococcal nuclease from Penaeus monodon: cDNA cloning and its involvement in RNA interference. Fish Shellfish Immunol. 31, 373–380.

48. Posiri, P., Ongvarrasopone, C., Panyim, S., 2013. A simple one-step method for producing dsRNA from E. coli to inhibit shrimp virus replication. J. Virol. Methods 188, 64–69.

49. Raja, P., Jackel, J.N., Li, S., Heard, I.M., Bisaro, D.M., 2014. Arabidopsis double-stranded RNA binding protein DRB3 participates in methylation-mediated defense against geminiviruses. J. Virol. 88, 2611–2622.

50. Raja, P., Sanville, B.C., Buchmann, R.C., Bisaro, D.M., 2008. Viral genome methylation as an epigenetic defense against geminiviruses. J. Virol. 82, 8997–9007.

51. Robalino, J., Browdy, C.L., Prior, S., Metz, A., Parnell, P., Gross, P., Warr, G., 2004. Induction of antiviral immunity by double-stranded RNA in a marine invertebrate. J. Virol. 78, 10442–10448.

52. Smith, N.A., Eamens, A.L., Wang, M.B., 2011. Viral small interfering RNAs target host genes to mediate disease symptoms in plants. PLoS Pathog. 7, e1002022.

53. Song, J.J., Smith, S.K., Hannon, G.J., Joshua-Tor, L., 2004. Crystal structure of Argonaute and its implications for RISC slicer activity. Science 305, 1434–1437.

54. Su, J., Oanh, D.T., Lyons, R.E., Leeton, L., Van Hulten, M.C., Tan, S.H., Song, L., Rajendran, K.V., Walker, P.J., 2008. A key gene of the RNA interference pathway in the black tiger shrimp, Penaeus monodon: identification and functional characterization of Dicer-1. Fish Shellfish Immunol. 24, 223–233.

55. Su, J., Zhu, Z., Wang, Y., Jang, S., 2009. Isolation and characterization of Argonaute2: a key gene of the RNA interference pathway in the rare minnow, Gobiocypris rarus. Fish Shellfish Immunol. 29, 164–170.

56. Sun, Q., Choi, G.H., Nuss, D.L., 2009. A single Argonaute gene is required for induction of RNA silencing antiviral defense and promotes viral RNA recombination. Proc. Natl. Acad. Sci. U.S.A. 106, 17927–17932.

57. Till, S., Lejeune, E., Thermann, R., Bortfeld, M., Hothorn, M., Enderle, D., Heinrich, C., Hentze, M.W., Ladurner, A.G., 2007. A conserved motif in Argonaute-interacting proteins mediates functional interactions through the Argonaute PIWI domain. Nat. Struct. Mol. Biol. 14, 897–903.

58. Unajak, S., Boonsaeng, V., Jitrapakdee, S., 2006. Isolation and characterization of cDNA encoding Argonaute, a component of RNA silencing in shrimp (*Penaeus monodon*). Comp. Biochem. Physiol. B Biochem. Mol. Biol. 145, 179–187.

59. Van Rij, R.P., Saleh, M.C., Berry, B., Foo, C., Houk, A., Antoniewski, C., Andino, R., 2006. The RNA silencing endonuclease Argonaute 2 mediates specific antiviral immunity in Drosophila melanogaster. Genes Dev. 20, 2985–2995.

60. Várallyay, É., Válóczi, A., Ágyi, Á., Burgyán, J., Havelda, Z., 2010. Plant virus-mediated induction of miR168 is associated with repression of argonaute1 accumulation. EMBO J. 29, 3507–3519.

61. Wang, J., Tang, Y., Yang, Y., Ma, N., Ling, X., Kan, J., He, Z., Zhang, B., 2016. Cotton leaf curl multan virus-derived viral small RNAs can target cotton genes to promote viral infection. Front. Plant Sci. 7, 1162.

62. Wang, S., Chen, A.J., Shi, L.J., Zhao, X.F., Wang, J.X., 2012. TRBP and eIF6 homologue in Marsupenaeus japonicus play crucial roles in antiviral response. PLoS One 7, e30057.

63. Wang, S., Liu, N., Chen, A.J., Zhao, X.F., Wang, J.X., 2009. TRBP homolog interacts with eukaryotic initiation factor 6 (eIF6) in Fenneropenaeus chinensis. J. Immunol. 182, 5250–5258.

64. Wang, X.B., Jovel, J., Udomporn, P., Wang, Y., Wu, Q., Li, W.X., Gasciolli, V., Vaucheret, H., Ding, S.W., 2011. The 21-nucleotide, but not 22-nucleotide, viral secondary small interfering RNAs direct potent antiviral defense by two cooperative Argonautes in Arabidopsis thaliana. Plant Cell 23, 1625–1638.

65. Wang, X.H., Aliyari, R., Li, W.X., Li, H.W., Kim, K., Carthew, R., Atkinson, P., Ding, S.W., 2006. RNA interference directs innate immunity against viruses in adult Drosophila. Science 312, 452–454.

66. Wang, Y., Sheng, G., Juranek, S., Tuschl, T., Patel, D.J., 2008. Structure of the guidestrand-containing argonaute silencing complex. Nature 456, 209–213.

67. Weng, K.F., Hsieh, P.T., Huang, H.I., Shih, S.R., 2015. Mammalian RNA virus-derived small RNA: biogenesis and functional activity. Microb. Infect. 17, 557–563.

68. Yang, L., Li, X., Huang, J., Zhou, F., Su, T., Jiang, S., 2013. Isolation and characterization of homologous TRBP cDNA for RNA interference in Penaeus monodon. Fish Shellfish Immunol. 34, 704–711.

69. Yang, L., Li, X., Jiang, S., Qiu, L., Zhou, F., Liu, W., Jiang, S., 2014. Characterization of Argonaute2 gene from black tiger shrimp (Penaeus monodon) and its responses to immune challenges. Fish Shellfish Immunol. 36, 261–269.

70. Yao, X., Wang, L., Song, L., Zhang, H., Dong, C., Zhang, Y., Qiu, L., Shi, Y., Zhao, J., Bi, Y., 2010. A Dicer-1 gene from white shrimp Litopenaeus vannamei: expression pattern in the processes of immune response and larval development. Fish Shellfish Immunol. 29, 565–570.

71. Yigit, E., Batista, P.J., Bei, Y., Pang, K.M., Chen, C.C., Tolia, N.H., Joshua-Tor, L., Mitani, S., Simard, M.J., Mello, C.C., 2006. Analysis of the C. elegans Argonaute family reveals that distinct Argonautes act sequentially during RNAi. Cell 127, 747–757.

72. Yodmuang, S., Tirasophon, W., Roshorm, Y., Chinnirunvong, W., Panyim, S., 2006. YHVprotease dsRNA inhibits YHV replication in Penaeus monodon and prevents mortality. Biochem. Biophys. Res. Commun. 341, 351–356.

73. Zambon, R.A., Vakharia, V.N., Wu, L.P., 2006. RNAi is an antiviral immune response against a dsRNA virus in Drosophila melanogaster. Cell Microbiol. 8, 880–889.

PmEEA1, the early endosomal protein is employed by YHV for successful infection in *Penaeus monodon*

Yellow head disease (YHD) is an infectious disease of *Penaeus monodon* which is caused by the yellow head virus (YHV). YHV infection invariably leads to 100% shrimp mortality within 3-5 days. Currently, an effective method to prevent or cure shrimp from YHV infection has not been elucidated. Therefore, the molecular mechanism underlying YHV infection should be examined. In this study, early endosome antigen 1 (EEA1) protein that was involved in the tethering step of the vesicle and early endosome fusion was investigated during YHV infection. The open reading frame of *P. monodon* EEA1 (PmEEA1) was cloned and sequenced (3,000 bp). It encoded a putative protein of 999 amino acids and contained the zinc finger C_2H_2 domain signature at the N-terminus and the FYVE domain at the C-terminus. Suppression of PmEEA1 by specific dsRNA in shrimp showed inhibition of YHV replication after 48 hours post YHV injection (hpi). On the other hand, shrimp received only NaCl without any dsRNA showed high YHV levels at approximately one hundred thousand times at 24 hpi and 48 hpi. Moreover, silencing of PmEEA1 by specific dsRNA followed by YHV challenge demonstrated a delay in shrimp mortality from 60 hpi to 168 hpi when compared to the control. These results indicated that YHV required PmEEA1 for trafficking within the infected cells, strongly suggesting that PmEEA1 may be a potential target to control and prevent YHV infection in *P. monodon*.

Introduction

YHD outbreaks have been reported since 1990 as epizootic events in the eastern, central and southern parts of Thailand, and resulted in shrimp production loss worldwide. A causative agent of this disease is the Yellow head virus (YHV) (1). YHV is a positive-sense single stranded RNA virus that is classified into genus *Okavirus*, family *Roniviridae*, in the order *Nidovirales* (2, 3) and is closely related to gill-associated virus (GAV) from Australia particularly in terms of the nucleotide and amino acid sequences, histological, and morphological observations (4, 5). YHV is approximately 50-60 × 190-200 nm in size, with enveloped bacilliform surrounded by prominent peplomers or spikes (6). The genome of the virus is approximately 27 kb in length and consists of ORF1a, ORF1b, ORF2 and ORF3. The enveloped glycoprotein, gp116, which is involved in the entry process of YHV into the cells is encoded from ORF3 (7).

Currently, it is believed that the major route of YHV entry into the cells of *Penaeus monodon* is by clathrin-mediated endocytosis via clathrin heavy chain and AP17 protein (8, 9). The clathrin-coated vesicle containing YHV requires a small GTPase Rab5 protein to traffic it from the plasma membrane towards the first sorting station, the early endosome. *P. monodon* Rab5 was identified and showed to colocalize with YHV particles (10, 11). At the early endosomal compartment, Rab5 protein binds to the Rab5 effector protein, the early endosome antigen 1 (EEA1), to promote the fusion between the vesicular and early endosomal membranes, causing the cargo proteins including the virus to be transported inside of the early endosome (12).

Rab5 effector EEA1 works with SNAREs (Soluble NSF (N-Ethylmaleimide-Sensitive Factor) Attachment Protein Receptors) complex which consists of

synaptobrevin, syntaxin and two SNAP-25 proteins. This interaction helps to promote the transported vesicle-endosome membrane tethering and fusion (12). EEA1 location is associated with the early endosome and showed colocalization with Rab5 protein (13). The EEA1 structure is a long parallel coiled coil homodimer that contains C_2H_2 zinc finger (ZF) domain at the N-terminus and FYVE domain at the C-terminus (14). Interactions between the N-terminal ZF domain of EEA1 with Rab5 protein and the SNAREs complexes facilitate the docking and fusion processes. Furthermore, the fusion step of the vesicle and the early endosome requires phosphatidylinositol-4-5-bisphosphate 3-kinase (PI(3)K) activity whereby the C-terminal FYVE domain of EEA1 can bind directly to the product of PI(3)K, phosphatidylinositol-3-phosphate (PtdIns3P). Taken together, the specific binding of Rab5-GTP bound form, together with PI(3)K activity are needed in the vesicle-early endosome membrane fusion (15-18). Furthermore, EEA1 has been shown to colocalize with Semliki forest virus (SFV) (19) and hepatitis C virus (HCV) (20). Our previous study found that YHV utilized clathrin heavy chain, Rab5 and Rab7 proteins to get into the shrimp cells (9, 11, 21). It is thus possible that YHV also requires Rab5 effector early endosome antigen 1 (EEA1) protein during infection. Therefore, in this study, the roles of EEA1 during YHV infection and shrimp mortality in *P. monodon* was investigated.

Materials and methods

The black tiger shrimp

Penaeus monodon or the black tiger shrimps were obtained from Choochai farm in Chonburi province and also from the Shrimp Genetic Improvement Center (SGIC, BIOTEC) in Surat Thani province, Thailand. Shrimps were acclimatized for at least 2 days and maintained in large containers with oxygenated sea water at 10-30 ppt salinity before used. They were fed with commercial feed every day. The water was changed every 2 days.

Cloning of the full-length PmEEA1

Coding region of EEA1 from *Marsupenaeus japonicus* kindly provided by Dr. Hidehiro Kondo, Tokyo University of Marine Science and Technology, Japan was used to design specific primers to amplify a region of PmEEA1. First, total RNA from ovary was extracted using Tri Reagent (Molecular Research Center) and cDNA was synthesized using Improm-II reverse transcriptase (Promega) according to the manufacturer's protocol. The full-length open reading frame of EEA1 was amplified using Q5 DNA polymerase (New England Biolabs) wtih cdEEA1-F and cdEEA1-R primers (Table 1), with an expected size of approximately 3,000 bp. The PCR condition was: denaturation at 98°C for 30 sec, then 35 cycles of 98°C for 10 sec, 55°C for 20 sec, and 72°C for 3 min. The PCR product was purified and cloned into pGEMT-easy vector and sequenced using T7, SP6, EEA1-Fseq, EEA1-Rseq and asEEA1-R2 primers (Table 1) by First Base Co, Ltd. (Malaysia).

PmEEA1 Nucleotide and protein sequence analysis

The nucleotide sequence of PmEEA1 was confirmed and analyzed by BLASTN program using search under nucleotide database. Predictions of molecular weight and isoelectric point (pI) of the protein were performed by Expert Protein Analysis System (www.expasy.org). Conserved motifs of the deduced amino acids were scanned using

ScanProsite tool (http://prosite.expasy.org/scanprosite). EEA1 protein sequences from several organisms were obtained from GenBank database. Phylogenetic analysis was performed using Phylogeny.fr with "A la Carte" mode (http://www.phylogeny.fr) based on neighbor-joining method and 1000 replicates of bootstrap with distance methods (22, 23).

Table 1 Primer sequences used in this study

Name	**Sequence (5'–> 3')**	**Purposes**
cdEEA1-F	ATGTCAGAGAGAGGAATG	Amplification of full-length cDNA coding region of PmEEA1
cdEEA1-R	TCACATTTTTGAAGTGAG	
T7	TAATACGACTCACTATAGGG	Sequencing of PmEEA1 nucleotides
SP6	ATTTAGGTGACACTATAG	
EEA1-Fseq	GCAGGGTTGAAGGAAGAGATG	
EEA1-Rseq	CCCTTAGCAGCTTCTCTCTCC	
PRT	CCGGAATTCAAGCTTCTAGAGGATCCTT TTTTTTTTTTTTT	The first strand cDNA synthesis
sEEA1-F1	*Xba*I GCTCTAGAACAAAATGAAGCCAAGCAGC	Construction of the recombinant plasmid expressing dsRNA-Cter targeting PmEEA1 mRNA
lEEA1-R1	*Eco*RI GGAATTCTAGCAACCTCAGCCTCCAG	
asEEA1-F2	*Xho*I CCGCTCGAGACAAAATGAAGCCAAGCAGC	
asEEA1-R2	*Eco*RI GGAATTCGGCATCAATTTCAAGCTGG	
nSLEEA1-F1	*Xba*I GCTCTAGAGGGCTTCTTGTGTCCAAC	Construction of the recombinant plasmid expressing dsRNA-Nter targeting PmEEA1 mRNA
nSLEEA1-R1	*Kpn*I GGGGTACCACCTTTTCAGCTTGTAGGG	
nASEEA1-F2	*Eco*RI GGAATTCGGGCTTCTTGTGTCCAAC	
nASEEA1-R2	*Kpn*I GGGGTACCCGCAAGGAACTGTTCAAC	
PmEEA1-F	AGCTTGAAATTGATGCCCAGAAG	Detection of PmEEA1 mRNA level
PmEEA1-R	TTGTTGCAGCTGTGGCAATTTAG	
PmActin-F	GACTCGTACGTGGGCGACGAGG	Detection of PmActin mRNA level
PmActin-R1	AGCAGCGGTGGTCATCTCCTGCTC	
qYHV-F	ATCATCAGCTCACAGGCAAGTTCC	Detection of YHV mRNA level by realtime PCR
qYHV-R	GGGTCTAAATGGAGCTGGAAGACC	
EF-1α-F	GAACTGCTGACCAAGATCGACAGG	Detection of EF-1α mRNA level by realtime PCR
EF-1α-R	GAGCATACTGTTGGAAGGTCTCCA	

Construction of two dsRNAs targeting PmEEA1 mRNA

Recombinant plasmid containing stem-loop of dsRNA of PmEEA1 was constructed in pET-17b (Novagen) vectors. Two plasmids containing dsRNA-Cter and dsRNA-Nter whose targets were close to the stop and start codons of *PmEEA1* gene, respectively, were constructed. Sense-loop regions of the dsRNAs located near stop and start codons were amplified from the first-strand cDNA using specific primers, sEEA1-

F1 and lEEA1-R1 for dsRNA-Cter, and nSLEEA1-F1 and nSLEEA1-R1 for dsRNA-Nter (Table 1). In addition, antisense regions were amplified using asEEA1-F2 and asEEA1-R2 for dsRNA-Cter, and nASEEA1-F2 and nASEEA1-R2 for dsRNA-Nter (Table 1). All PCR fragments were gel-purified and verified by restriction enzyme digestion. The purified fragments of the sense-loop and antisense of the Cter region were digested with *Eco*RI and ligated together using T4 DNA ligase (NEB). Then, the sense fragment was digested by *Xba*I whereas the antisense fragment was cut by *Xho*I. The ligated fragment of the sense and antisense of PmEEA1 was cloned into pET-17b to obtain pET-17b-dsRNA-Cter. In addition, the PCR fragment of sense-loop of the Nter region was cloned into pGEM-3Zf+ at *Xba*I and *Kpn*I sites and then the antisense fragment of the Nter region was subsequently cloned into *Kpn*I and *Eco*RI site of this recombinant plasmid. Then, the sense-loop and antisense fragments of the Nter region in pGEM-3Zf+ was cut and subcloned into pET-17b vector to construct recombinant plasmid named pET-17b-dsRNA-Nter. Both of the recombinant plasmids were used for dsRNA production by *in vivo* bacterial expression.

Production of dsRNAs by in vivo bacterial expression

The recombinant plasmids, pET-17b-dsRNA-Cter and –Nter, were transformed into a RNase III mutant HT115 *E. coli* strain. DsRNAs expression were induced by 0.1 mM IPTG. Then, they were extracted by using ethanol method (24, 25). The quality of the dsRNAs were characterized by ribonuclease digestion assay using RNase A and RNase III digestions. Concentration of dsRNA was estimated visually using agarose gel electrophoresis by comparing the target band intensity to that of the 100 bp DNA marker.

Yellow head virus (YHV) preparation

YHV stock was prepared using the hemolymph of YHV-infected moribund black tiger shrimp. The hemolymph was drawn and mixed with anticoagulant (AC-1) solution (27 mM Sodium citrate, 34.33 mM NaCl, 104.5 mM Glucose, 198.17 mM EDTA, pH 7.0), at ratio 1:1, and centrifuged at 20,000 ×g for 20 minute at 4 °C to remove hemocyte debris. YHV was separated from the hemolymph by ultracentrifugation at 100,000 ×g for 1 h. YHV contained pellet was then dissolved with 150 mM NaCl and stored at -80 °C until used. The viral titer that caused 100% mortality within 3-4 days was used in this study. For confirmation of YHV infection, total RNA was extracted from the YHV-infected hemolymph that used to prepare the YHV stock and RT-PCR was performed to detect the level of YHV. In addition, the pellet obtained after ultracentrifugation of the hemolymph was dissolved with 150 mM NaCl and injected into shrimp. After 3-4 days of YHV injection, YHV levels can be detected in all dead shrimp, suggesting that the pellet contained YHV.

Injection of P. monodon with dsRNAs

The efficiency of dsRNA-Cter and dsRNA-Nter were examined by injection of dsRNAs into shrimp hemocoel. Shrimps were injected with 2.5 µg. g^{-1} shrimp of dsRNA-Cter, -Nter, C+Nter or unrelated dsRNA-GFP dissolved in 150 mM NaCl. Injection of 150 mM NaCl was used as control. After 24 h post dsRNA injection, gills of the individual shrimp were collected for total RNA extraction. Suppression effect of dsRNAs was analyzed by reverse-transcription PCR (RT-PCR) to determine PmEEA1 mRNA level.

Study of the knock down effect by dsRNAs upon YHV infection and shrimp mortality assay

In order to investigate the silencing effect of PmEEA1 upon YHV infection, shrimp were injected with 2.5 µg. g^{-1} shrimp of the combination of dsRNA-C and dsRNA-Nter (1.25 µg. g^{-1} shrimp each) or unrelated dsRNA-GFP, followed by YHV challenged after 24 h post dsRNA injection. For each group, 5 shrimp were used. Twenty-four and forty-eight hours post YHV injection (hpi), gills of individual shrimp were collected and analyzed for PmEEA1 and YHV levels. To determine whether YHV levels could be detected at 60, 72, 84, and 96 hpi, gills from the living shrimp were collected. Moreover, shrimp mortality was also recorded every 12 h post YHV injection (hpi) for 144 hpi. Three replicates of the experiment were performed. Gills from the dead shrimp were also collected to determine YHV and PmEEA1 levels.

Total RNA extraction and RT-PCR analysis

Total RNA from gill tissue was isolated using Tri Reagent® (Molecular Research Center) following the manufacturer's protocol. Two microgram of the total RNA was used to produce first-strand cDNA using Improm-II™ reverse transcriptase (Promega) with PRT primer (Table 1). PCR products were amplified by using Taq DNA polymerase (New England Biolabs). Multiplex PCR of PmEEA1 (PmEEA1-F and PmEEA1-R1 primers, and PmActin (PmActin-F and PmActin-R1) (Table 1) were amplified under this condition: 95°C for 5 min, then 30 cycles of 95°C for 30 s, 61°C for 30 s, and 68°C for 45 s, followed by 68°C for 7 min. YHV mRNA level was amplified using primers, YHV(hel)-F and YHV(hel)-R (Table 1). The multiplex PCR condition for YHV and PmActin was performed according to this condition: 95 °C for 5 min; 25 cycles of 95 °C for 30 s, 55°C for 30 s, and 72 °C for 45 s; followed by 72 °C for 7 min. The PCR products were analyzed on 1.5% agarose gel. The intensity of each band was quantitated using Scion Image program. Relative mRNA transcript levels of PmEEA1 was normalized with PmActin intensity and recorded as arbitrary unit.

Detection of YHV mRNA levels by quantitative real time PCR (qPCR)

For qPCR analysis, cDNA template was diluted at 1:4 and mixed with qPCR reaction using KAPA™ SYBR® Fast qPCR master mix (2X) ABI Prism™ (KAPA Biosystems) following manufacturer's protocol. The qPCR was analyzed using Mastercycler RealPlex4 (Eppendorf). qYHV-F and qYHV-R primers (Table 1) were used to amplify YHV mRNA. For internal control, EF1-α, was used (EF1α-F and EF1α-R primers) (Table 1). The qPCR condition was as followed: 95°C for 3 min; 40 cycles of 95°C for 5 s, 60°C for 30 s. The cycle threshold (C_t) values of YHV and EF1-α were compared and calculated using $2^{-\Delta\Delta C_T}$ method (26).

Statistical analysis

The relative transcription levels of PmEEA1 and YHV that were normalized with PmActin or EF1α were presented as mean ± SD. In addition, cumulative percent shrimp mortality was plotted as mean ± SD. A significant difference of the experiment groups was examined by analysis of variance (ANOVA). A probability *(P)* value less than 0.05 was accepted as significant difference.

Results

Cloning and sequence analysis of PmEEA1 coding region

The full-length sequence of PmEEA1 is 3,000 bp, including the stop codon (TGA), thus encoded a protein of 999 amino acids (GenBank accession number MK775551; Supplementary Fig.1). The predicted molecular weight and pI of PmEEA1 protein are 112.6 kDa and 5.04, respectively. Sequence analysis revealed that PmEEA1 protein contains conserved domain of EEA1 which are Zinc finger C_2H_2 type domain at the amino acids 43-64 and 73-94, and the FYVE domain at the amino acids 938-996. These domains are conserved in both invertebrates and vertebrates including CeEEA1, DrEEA1, HsEEA1, LaEEA1, LpEEA1, and RnEEA1 (Fig. 1 and Table 2). Phylogenetic tree analysis revealed that PmEEA1 was closely related to the invertebrate group (Fig. 2).

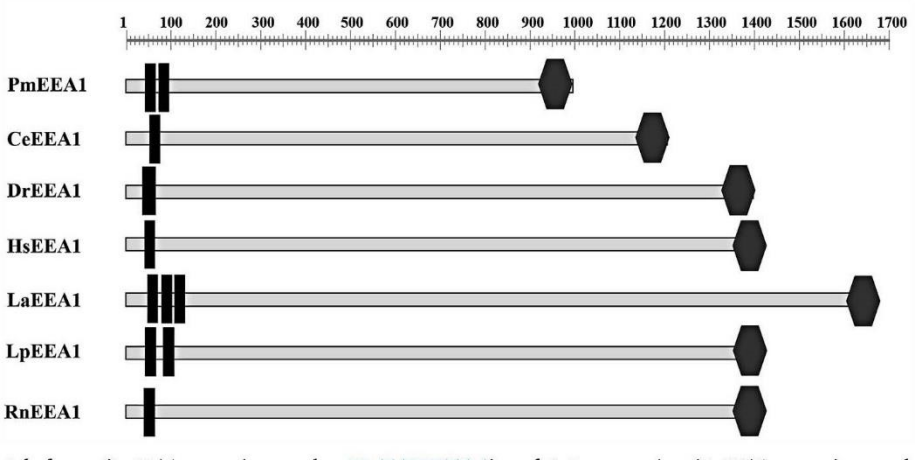

Fig. 1. The nucleotide and deduced amino acid sequences of *Penaeus monodon* Early endosome antigen 1 (PmEEA1). The coding region of PmEEA1 is 3,000 bp encoding the protein of 999 amino acids. Start and stop codons are in bold letters; the dash represents the stop codon. The nucleotide sequences were deposited in the GenBank database under the accession number MK_775551.

Table 2 Early endosome antigen 1 (EEA1) proteins used for multiple sequence alignment and phylogenetic analysis.

Abbreviations	Species	Accession number
AcEEA1	*Aplysia californica*	XP_005095892.2
BaEEA1	*Balaenoptera acutorostrata scammoni*	XP_007166165.1
BgEEA1	*Biomphalaria glabrata*	XP_013093515.1
CeEEA1	*Caenorhabditis elegans*	NP_001024127.1
DrEEA1	*Danio rerio*	XP_003200485.1
FhEEA1	*Fundulus heteroclitus*	XP_012731526.1
HsEEA1	*Homo sapiens*	NP_003557.2
LaEEA1	*Lingula anatina*	XP_013419201.1
LpEEA1	*Limulus polyphemus*	XP_013777228.1
NgEEA1	*Nannospalax galili*	XP_008822059.1
ObEEA1	*Octopus bimaculoides*	XP_014782058.1
PmEEA1	*Penaeus monodon*	MK_775551
TcEEA1	*Tupaia chinensis*	ELW_61492.1
TrEEA1	*Takifugu rubripes*	XP_003967354.1
RnEEA1	*Rattus norvegicus*	NP_001101556.1
XtEEA1	*Xenopus tropicalis*	XP_002935361.1

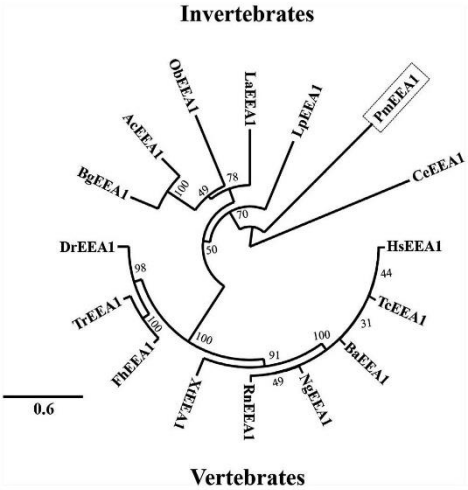

Fig. 2. Phylogenetic analysis of EEA1 protein. The phylogenetic tree was reconstructed using the Neighbor-joining method based on the full amino acid sequences of EEA1 with bootstrap value of 1,000. Organisms used for the tree reconstruction were *Aplysia californica* (AcEEA1), *Balaenoptera acutorostrata scammoni* (BaEEA1), *Biomphalaria glabrata* (BgEEA1), *Caenorhabditis elegans* (CeEEA1), *Danio rerio* (DrEEA1), *Fundulus heteroclitus* (FhEEA1), *Homo sapiens* (HsEEA1), *Lingula anatine* (LaEEA1), *Limulus Polyphemus* (LpEEA1), *Nannospalax galili* (NgEEA1), *Octopus bimaculoides* (ObEEA1), *Penaeus monodon* (PmEEA1), *Tupaia chinensis* (TcEEA1), *Takifugu rubripes* (TrEEA1), *Rattus norvegicus* (RnEEA1), *and Xenopus tropicalis* (XtEEA1).

Silencing of PmEEA1 mRNA levels by two dsRNAs

Two dsRNAs, dsRNA-Cter and dsRNA-Nter, targeting the PmEEA1 mRNA and dsRNA-GFP that used as unrelated dsRNA control could be cleaved by RNase III but not by RNase A, suggesting that they were of good quality. The expected sizes of these dsRNAs were approximately 400 bp (Supplementary Fig. 2).-The effectiveness of dsRNA-Cter and dsRNA-Nter on silencing of PmEEA1 mRNA were investigated. Shrimp were injected with dsRNAs targeting PmEEA1 or unrelated dsRNA-GFP for 24 hours. NaCl injection was employed as an experimental control. The result found that shrimp received either dsRNA-Cter or dsRNA-Nter showed a significant reduction of PmEEEA1 mRNA levels at 81% and 76%, respectively. Moreover, in shrimp injected with dsRNA-Cter and dsRNA-Nter (dsRNA-C+Nter), the level of PmEEA1 mRNA could hardly be detected (91% suppression). Interestingly, PmEEA1 mRNA level could be silenced at about 33% in dsRNA-GFP injected shrimp (Fig. 3).

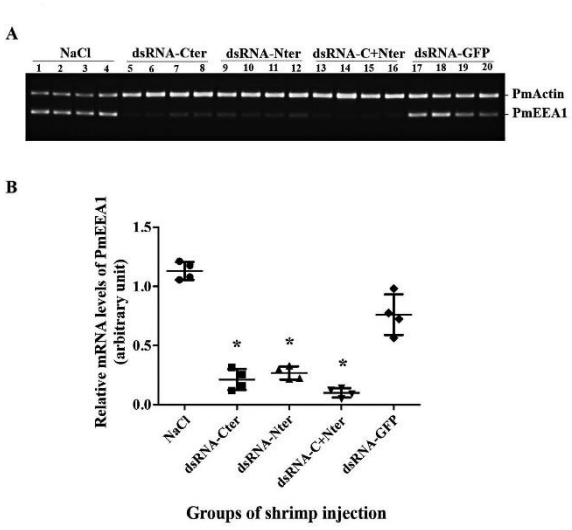

Fig. 3. Effectiveness of two types of dsRNAs targeting PmEEA1 mRNA. A representative gel of RT-PCR products was presented as expression levels of PmEEA1 and PmActin of shrimp injected with NaCl control (lanes 1-4), each dsRNA targeting PmEEA1 which are dsRNA-Cter (lanes 5-8) and dsRNA-Nter (lanes 9-12), the combination between dsRNA-Cter and -Nter (dsRNA-C+Nter) (lanes 13-16) and unrelated dsRNA-GFP (lanes 17-20) at 2.5 $\mu g.g^{-1}$ shrimp at 24 h post dsRNA injection (n=4) (A). The relative mRNA expression levels of PmEEA1 normalized with PmActin are shown as mean ± SD (n= 4) (B). (*) Statistically significant difference between dsRNA injected shrimp as compared to NaCl injected group ($P < 0.05$).

Knockdown effect of PmEEA1 reduced YHV replication levels

The role of PmEEA1 on YHV level was next investigated during YHV replication. The combination dsRNA-C+Nter was used to silence PmEEA1 mRNA. Shrimp received the dsRNA after 24 h were challenged with YHV. After 24 and 48 hours post YHV injection (hpi), the level of PmEEA1 and YHV mRNAs were determined from the gills. Injected shrimp with dsRNA-C+Nter following YHV challenge showed significant reduction of PmEEA1 at 24 and 48 hpi about 82% and 78% when compared to NaCl→YHV control group, respectively. Moreover, shrimp injected with unrelated dsRNA-GFP → YHV showed no difference in PmEEA1 mRNA levels at both 24 and 48 hpi when compared to the control (Fig. 4A).

The level of YHV mRNAs were determined by real time PCR and expressed as mean ± SD of the fold change of YHV mRNA levels compared to the NaCl injected group at 24 hpi. At 24 hpi, the fold change of YHV mRNA level in the PmEEA1 knock down group injected with dsRNA-C+Nter showed no significant difference when compared to the control groups injected with NaCl or dsRNA-GFP. At 48 hpi, the fold change of the YHV level increased more than 100,000 and 25,000 times for NaCl- and dsRNA-GFP- injected groups, respectively. However, the fold change of the YHV level at 48 hpi (1.28 ± 1.31 fold) remained at very low level and showed no significant difference when compared at 24 hpi (1.16 ± 0.53 fold) of the PmEEA1 knock down group (Fig. 4B). In addition, the expression of YHV mRNA levels were detected in the gills collected from the living shrimp between 48-96 hpi. The results showed that knockdown of PmEEA1 resulted in complete inhibition of YHV mRNA levels at 48 hpi. The expression of YHV mRNA levels can be detected at very low levels at 60 hpi and increased from 72-96 hpi in living shrimp. High levels of YHV mRNA could be detected in both control groups between 48-72 hpi. All shrimp in the control groups died at 72 hpi. These results suggested that knockdown of PmEEA1 restricted the YHV in the early compartment of the endosome. YHV levels could be detected but not high enough to cause shrimp dead between 60-96 hpi. Therefore, shrimp mortality was delayed in the dsRNA-C+Nter injected group (Supplementary Fig. 4).

Silencing of PmEEA1in YHV-infected shrimp decreased shrimp mortality

The shrimp mortality was further observed to investigate the involvement of PmEEA1 on YHV infection. There were 10-15 shrimp per group and the experiments were performed three times. Shrimp received dsRNA-C+Nter followed by YHV challenge showed a significant delay in shrimp mortality as observed in 60 hpi to 168 hpi when compared to NaCl → YHV and unrelated dsRNA-GFP → YHV groups (*P* value = 0.05). At 60 hpi, no shrimp in dsRNA-C+Nter → YHV group died whereas shrimp in the control groups of NaCl → YHV and unrelated dsRNA-GFP → YHV had 80% and 50% shrimp mortality, respectively. In addition, at 84 hpi, shrimp in both control groups showed 100% mortality while the dsRNA-C+Nter → YHV group demonstrated only 40% mortality (Fig. 5A). In addition, expression of YHV can be detected in all dead shrimp (Fig. 5B).

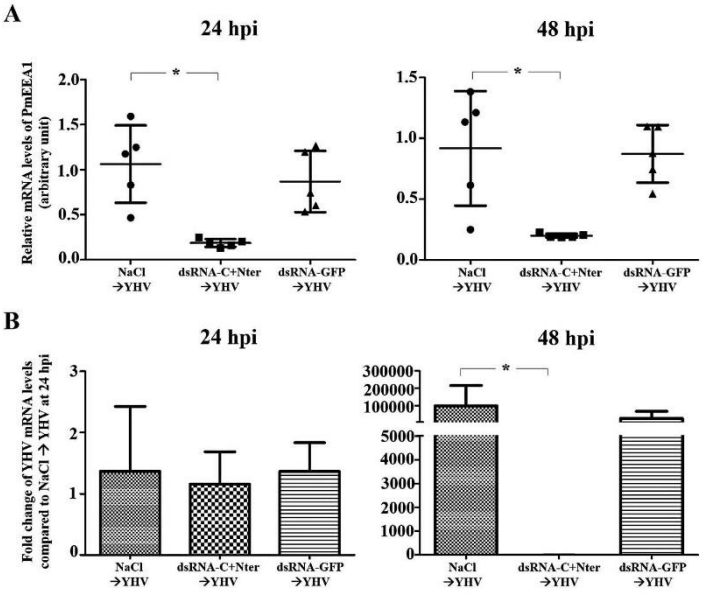

Fig. 4. Effect of PmEEA1 depletion during YHV infection. Shrimp were injected with NaCl alone, dsRNA-C+Nter, and dsRNA-GFP at 2.5 $\mu g.g^{-1}$ shrimp for 24 h followed by YHV challenge and detection at 24 and 48 hpi from gill tissues (n=5). The relative mRNA levels of PmEEA1 normalized with PmActin are presented as dot graphs of arbitrary unit of mean ± SD (A). Bar graphs represent the quantitative RT-PCR of fold change of YHV mRNA levels compared to NaCl → YHV at 24 hpi. The result was demonstrated as mean ± SD (B). Asterisks indicate significant differences between experimental group and the control group ($P < 0.05$).

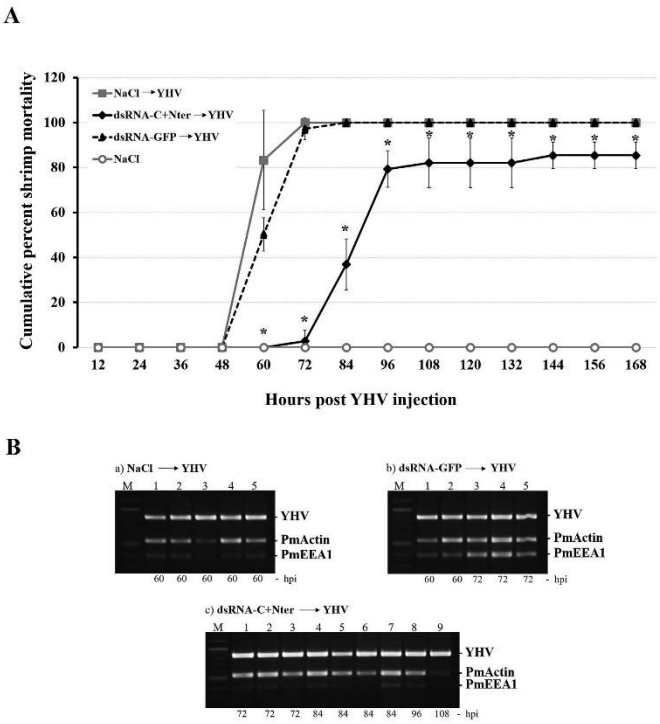

Fig. 5 Silencing of PmEEA1 by the combination dsRNA-C+Nter on YHV infection delayed shrimp mortality. (A) The cumulative percent mortality of shrimp injected with NaCl, dsRNA targeting PmEEA1 (dsRNA-C+Nter), or unrelated dsRNA-GFP at 2.5 $\mu g.g^{-1}$ shrimp followed by YHV injection were observed. Dead shrimp were recorded every 12 hpi. The graph was plotted as mean ± SD from three replicates per group (n=12-15 shrimp per group). Asterisks represents statistically significant difference between NaCl → YHV and dsRNA-C+Nter → YHV group ($P < 0.05$). (B) A representative gel of RT-PCR products of YHV and PmEEA1 mRNA levels from gill of the dead shrimp in the 3 groups. PmActin was used as an internal control. PmAcin expression level is low in the dead shrimp samples that showed high levels of YHV expression. This result was also demonstrated in the previous studies (9, 15). The number on the bottom of each lane represents the time (hours of post YHV challenge, hpi) that the shrimp die.

Discussion

Clathrin-mediated endocytosis is the major route of YHV penetration inside the shrimp host cell (8, 9). After internalization, YHV requires a small GTPase Rab5 protein to regulate the transportation from plasma membrane to early endosome. Colocalization between YHV and *Penaeus monodon* Rab5 (PmRab5) was observed in the hemocytes from 10 min to 3 h post YHV infection (11). Rab5 proteins on vesicle membrane are tethered with Rab5 effector early endosome antigen 1 (EEA1) that appeared on the surface of the early endosome to promote the fusion of the two membrane (12, 17, 18). Previously under transmission electron microscopy, it was found that YHV particles are inside the early endosomes of shrimp cells (27).. PmEEA1 protein contains 999 amino acids, while other species including CeEEA1, DrEEA1, HsEEA1, LaEEA1, LpEEA1, and RnEEA1 have more than 1,200 amino acids (Fig. 1). Although the size of the protein from different species present a wide range of sizes, but they all showed signature characteristics of EEA1, two Zinc finger C_2H_2 domains and FYVE domain of N- and C-terminal sites (14). Moreover, the function of EEA1

during YHV infection in *P. monodon* was examined. Two dsRNAs targeting N- and C-terminus of PmEEA1 were produced and used to knockdown PmEEA1 transcripts. A combination of two dsRNAs were used to improve the inhibition of YHV infection in shrimp (28). Since, dsRNA targeting C-terminus of PmEEA1 region (the first construction) was located near 3' end of the open reading frame (dsRNA-Cter). This dsRNA was first injection into shrimp resulting in inhibition of PmEEA1 mRNA levels only 50-80% compared to the control (data not shown). Local protein factors involving in termination of protein synthesis may cause the positional effect that interrupts the accessibility of RISC-siRNA complex to the local target (29). After obtaining the full-length coding region of PmEEA1, another dsRNA targeting PmEEA1 mRNA was constructed. This dsRNA was located on near the 5' end of the open reading frame (dsRNA-Nter). The result demonstrated that injection of the combined two types of dsRNA targeting PmEEA1 could silence the mRNA levels more than using only one type of the dsRNA (Fig. 3). This is probably due to a variety of siRNA population generated from the combined two dsRNAs. It could increase the efficiency of siRNA to bind to the mRNA target. The siRNA could bind with the secondary structure of mRNA as stem and loop structure better than the hairpin structure (30, 31).

After testing the effectiveness of the dsRNA, the role of PmEEA1 during YHV infection was investigated. Shrimp that were injected with NaCl → YHV at 48 hpi showed increased YHV replication at about 100,000 times when compared to 24 hpi. On the other hand, injected shrimp with dsRNA targeting PmEEA1 (using the combination between dsRNA-Cter and –Nter (dsRNA-C+Nter)) followed by YHV challenge demonstrated no significant difference of YHV levels at 24 and 48 hpi (Fig. 4B). In addition, dsRNA-C+Nter → YHV group showed a delay in shrimp mortality when compared to the control NaCl → YHV group (Fig. 5). Injection of dsRNA targeting PmEEA1 alone has no effect on shrimp mortality (Supplementary Fig. 3). Shrimp started dying after receiving dsRNA-C+Nter followed by YHV challenge at 84 to 96 hpi (about 108 to 120 h post dsRNA injection) is probably caused by the loss of the effectiveness of its dsRNA and the increasing number of virus progenies. An increasing levels of YHV expression could be detected between 60-96 hpi in gills collected from the living shrimp. However, it did not cause shrimp die (Supplementary Fig. 4). High levels of YHV expression could be detected in all dead shrimp samples (Fig. 5B). Longevity of dsRNA inside the shrimp cells is about five days (120 h) after dsRNA injection and YHV challenge (32). Therefore, to improve the effectiveness of dsRNA-C+Nter targeting PmEEA1 during YHV infection, multiple injections of dsRNA every 72 h may be performed in order to reduce shrimp mortality. Based on this study, silencing of PmEEA1 which is not lethal is possibly used as an alternative approach to prevent YHV replication. Taken together, this study demonstrated the crucial role of PmEEA1 during YHV transportation inside the cells.

References

1. Boonyaratpalin S, Supamattaya K, Kasornchandra J, Direkbusaracom S, Aekpanithanpong U, Chantanachooklin C. Non-occluded baculo-like virus, the causative agent of yellow head disease in the black tiger shrimp (*Penaeus monodon*). Fish Pathol. 1993;28(3):103-9.

2. Mayo MA. A summary of taxonomic changes recently approved by ICTV. Arch Virol. 2002;147:1655-6.

3. Walker PJ, Bonami JR, Boonsaeng V, Chang PS, Cowley JA, Enjuanes L, Flegel TW, Lightner DV, Loh PC, Snijder EJ, Tang K. Virus taxonomy: classification and nomenclature of viruses: eighth report of the international committee on the taxonomy of viruses. Elsevier. 2005:975-9.

4. Cowley JA, Dimmock CM, Wongteerasupaya C, Boonsaeng V, Panyim S, Walker PJ. Yellow head virus from Thailand and gill-associated virus from Australia are closely related but distinct prawn viruses. Dis Aquat Org. 1999;36(2):153-7.

5. Spann KM, Donaldson RA, Cowley JA, Walker PJ. Differences in the susceptibility of some penaeid prawn species to gill-associated virus (GAV) infection. Dis Aquat Org. 2000;42:221-5.

6. Nadala ECB, Tapay LM, Cao S, Loh PC. Yellow-head virus: a rhabdovirus-like pathogen of penaeid shrimp. Dis Aquat Org. 1997;31:141-6.

7. Sittidilokratna N, Dangtip S, Cowley JA, Walker PJ. RNA transcription analysis and completion of the genome sequence of yellow head nidovirus. Virus Res. 2008;136(1-2):157-65.

8. Jatuyosporn T, Supungul P, Tassanakajon A, Krusong K. The essential role of clathrin-mediated endocytosis in yellow head virus propagation in the black tiger shrimp *Penaeus monodon*. Dev Comp Immunol. 2014;44:100–10.

9. Posiri P, Kondo H, Hirono I, Panyim S, Ongvarrasopone C. Successful yellow head virus infection of *Penaeus monodon* requires clathrin heavy chain. Aquaculture. 2015;435:480–7.

10. Chavrier P, Parton RG, Hauri HP, Simons K, Zerial M. Localization of low molecular weight GTP binding proteins to exocytic and endocytic compartments. Cell. 1990;62: 317-29.

11. Posiri P, Panyim S, Ongvarrasopone C. Rab5, an early endosomal protein required for yellow head virus infection of *Penaeus monodon*. Aquaculture 2016;459:43-53.

12. Christoforidis S, McBride HM, Burgoyne RD, Zerial M. The Rab5 effector EEA1 is a core component of endosome docking. Nature. 1999;397(6720):621-5.

13. Mu FT, Callaghan JM, Steele-Mortimer O, Stenmark H, Parton RG, Campbell PL, McCluskey J, Yeo JP, Tock EP, Toh BH. EEA1, an early endosome-associated protein. EEA1 is a conserved alpha-helical peripheral membrane protein flanked by cysteine "fingers" and contains a calmodulin-binding IQ motif. J Biol Chem. 1995;270(22):13503-11.

14. Callaghan JSA, Gaullier JM, Toh BH, Stenmark H. The endosome fusion regulator early-endosomal autoantigen 1 (EEA1) is a dimer. Biochem J. 1999;338:539-43.

15. Simonsen A, Lippé R, Christoforidis S, Gaullier JM, Brech A, Callaghan J, Toh BH, Murphy C, Zerial M, Stenmark H. EEA1 links PI(3)K function to Rab5 regulation of endosome fusion. Nature. 1998;394(6692):494-8.

16. Callaghan J, Nixon S, Bucci C, Toh BH, Stenmark H. Direct interaction of EEA1 with Rab5b. Eur J Biochem. 1999;265(1):361-6.

17. Lawe DC, Patki V, Heller-Harrison R, Lambright D, Corvera S. The FYVE domain of early endosome antigen 1 is required for both phosphatidylinositol 3-phosphate and Rab5 binding. J Biol Chem. 2000;275(5):3699–705.

18. Merithew E, Stone C, Eathiraj S, Lambright DG. Determinants of Rab5 interaction with the N terminus of early endosome antigen 1. J Biol Chem. 2003;278(10):8494-500.

19. Vonderheit A, Helenius A. Rab7 associates with early endosomes to mediate sorting and transport of semliki forest virus to late endosomes. PLoS Biol. 2005;3(7):1225-38.

20. Lai CK, Jeng KS, Machida K, Lai MM. Hepatitis C virus egress and release depend on endosomal trafficking of core protein. J Virol. 2010;84(21):11590-8.

21. Ongvarrasopone C, Chanasakulniyom M, Sritunyalucksana K, Panyim S. Suppression of PmRab7 by dsRNA inhibits WSSV or YHV infection in shrimp. Mar Biotechnol. 2008;10(4):374-81.

22. Dereeper A, Guignon V, Blanc G, Audic S, Buffet S, Chevenet F, Dufayard JF, Guindon S, Lefort V, Lescot M, Claverie JM, Gascuel O. Phylogeny.fr: robust phylogenetic analysis for the non-specialist. Nucleic Acids Res 2008;36:465-9.

23. Dereeper A, Audic S, Claverie J-M, Blanc G. BLAST-EXPLORER helps you building datasets for phylogenetic analysis. BMC Evol Biol. 2010;12:10:8.

24. Ongvarrasopone C. Roshorm Y, Panyim S. A simple and cost effective method to generate dsRNA for RNAi studies in invertebrates. ScienceAsia. 2007;33:35-9.

25. Posiri P, Ongvarrasopone C, Panyim S. A simple one-step method for producing dsRNA from *E. coli* to inhibit shrimp virus replication. J Virol Methods. 2013;188:64-9.

26. Livak KJ, Schmittgen TD. Analysis of relative gene expression data using real-time quantitative PCR and the $2^{-\Delta\Delta C_T}$ method. Methods. 2001;25:402–8

27. Duangsuwan P, Tinikul Y, Withyachumnarnkul B, Chotwiwatthanakun C, Sobhon P. Cellular targets and pathways of yellow head virus infection in lymphoid organ of *Penaeus monodon* as studied by transmission electron microscopy. Songklanakarin J Sci Technol. 2011;33(2):121-7.

28. Posiri P, Ongvarrasopone C, Panyim S. Improved preventive and curative effects of YHV infection in *Penaeus monodon* by a combination of two double stranded RNAs. Aquaculture 2011;314:34-8.

29. Holen T, Amarzguioui M, Wiiger MT, Babaie E, Prydz H. Positional effects of short interfering RNAs targeting the human coagulation trigger tissue factor. Nucleic Acids Res. 2002;30(8):1757-66.

30. Luo KQ, Chang DC. The gene-silencing efficiency of siRNA is strongly dependent on the local structure of mRNA at the targeted region. Biochem Biophys Res Commun. 2004;318(1):303-10.

31. Pascut D, Bedogni G, Tiribelli C. Silencing efficacy prediction: a retrospective study on target mRNA features. Biosci Rep. 2015;35(2) e00185.

32. Yodmuang S, Tirasophon W, Roshorm Y, Chinnirunvong W, Panyim S. YHV-protease dsRNA inhibits YHV replication in *Penaeus monodon* and prevents mortality. Biochem Biophys Res Commun 2006;341(2):351-6.

Identification and expression of white spot syndrome virus-encoded microRNAs in infected *Penaeus monodon*

White spot syndrome virus (WSSV) is the most devastating DNA virus that causes shrimp mortality worldwide. To better understand WSSV and *Penaeus monodon* interactions, WSSV-encoded microRNAs (wsv-miRs) were identified by small RNA cloning and next-generation sequencing. Ten wsv-miRs were identified and their expressions can be detected in WSSV-infected tissues only. These wsv-miRs and their flanking sequences can spontaneously form hairpin structure as predicted by Mfold. The expression profiles of 6 wsv-miRs increased dependent on time course of WSSV infection and slightly decreased after 48 hours post WSSV challenge. The highest expression was wsv-miR-9 followed by miR-13 and -15. Computational prediction of the candidate targets of wsv-miRs revealed possible functions of wsv-miRs in the controlling of apoptosis, transcription and signaling. This finding provided insights into WSSV-host interaction.

Introduction

White spot syndrome virus (WSSV) is a serious causative agent of white spot disease in cultivated shrimp worldwide. Infection of WSSV leads to 100% shrimp mortality within a few days. In addition, this virus showed the highest infection rate in Thailand (Khawsak et al., 2008). WSSV is classified in the *Whispovirus* of the *Nimaviridae* family (Jehle et al., 2006). It has a double-stranded DNA genome of approximately 300 kb, is packed with the nucleocapsid proteins and is surrounded by Envelope proteins such as VP28, VP26 and VP19. Currently, genome sequences of 4 WSSV isolates from the pandemic areas were sequenced including China (WSSV-Ch: AF332093), Taiwan (WSSV-Tw, AF440570), Thailand (WSSV-Th: AF369029) and Korea (WSSV-Kr: JX515788) (Chai et al., 2013). Several strategies are used to control WSSV infection such as environmental control, herbal treatment, recombinant vaccination and RNA interference (RNAi) approach (Sánchez-Paz, 2010). However, effective method to prevent and cure WSSV infection remains limited due to the lack of understanding about WSSV pathogenesis and viral-host interaction. Insights in these areas will drive the therapeutic strategy.

Invertebrates lack adaptive immunity nevertheless they adapt to use the RNAi pathway as a specific immunity. RNAi mechanism plays crucial roles in the regulation of gene expression and antiviral defense by the use of small interference RNA (siRNA) or micro RNA (miRNA). MiRNA is a non-coding single-stranded RNA (ssRNA) of about ~22 nucleotides (nt) in length, which function as regulatory small RNA in the RNAi mechanism. MiRNA is also believed to be involved in post-transcriptional gene regulation in many eukaryotic processes such as development, cell differentiation, apoptosis, and immune response (Dong et al., 2013). The miRNA is transcribed from the genome into a non-perfect matched primary-miRNA (pri-miRNA) and is then cleaved as a precursor-miRNA (pre-miRNA) by Drosha and its cofactor, Pasha (Denli et al., 2004; Gregory et al., 2004). The pre-miRNA is exported to the cytoplasm and is cleaved by Dicer and its partner, Loqs, to become a ~22 bp miRNA duplex (Park et al., 2011; Saito et al., 2005). The miRNA is preferentially selected based on the 5´-end thermostability associated with an argonaute protein (AGO) in an RNA-induced

silencing complex (RISC) to become a mature miRNA (Khvorova et al., 2003; Schwarz et al., 2003). For siRNA processing, the perfectly matched dsRNA is the substrate and is directly cleaved by Dicer into a siRNA duplex. The mature miRNA guides the RISC to target mRNA by using complementary base-pairing with the 3´-untranslated region (UTR) of mRNA. Any imperfect match with their target (Pasquinelli, 2012) will result in translational inhibition; whereas, perfectly matched causes mRNA degradation at post-transcriptional levels (Bartel, 2004; Kim et al., 2009).

Recently, a number of miRNAs are found to be encoded by DNA viruses (Grundhoff and Sullivan, 2011) and at least 530 viral-encoded miRNAs are deposited in the miRBase 22 (Kozomara and Griffiths-Jones, 2014) (www.mirbase.org). Virus that can encode miRNA usually has a DNA genome, can invade into the nucleus of the host cell, has long term or persistent infection, and can switch between the lytic and latent stages of viral life cycle. Upon viral infection, host cells will encode miRNAs that function in the immune system to protect against the invading viruses. On the other hand, the virus can encode its own miRNAs by using host miRNA machineries and uses them to escape the host defense and also to remodel host gene expression to support the viral life cycle. For example, Epstein-Barr virus (EBV) encodes miR-BART5 which targeted PUMA mRNA to prevent the infected cell from undergoing apoptosis and also to promote latent infection (Choy et al., 2008). Simian virus 40 (SV40) encodes miR-S1 from the late transcripts, which cleaved an antisense transcript that encoded T-antigen, which resulted in infected cells becoming less susceptible to cytotoxic T-cell mediated lysis (Sullivan et al., 2005). Additionally, some viruses also encode miRNAs to control the viral genes itself. For examples, Herpes Simplex Virus 1 and 2 express miR-H2-3p from latency associated transcript (LAT) from its own antisense direction of an immediate early protein, ICP0. MiR-H2-3p is targeted to the viral coding gene and resulted in the switching of virus to the latency stage (Jurak et al., 2010; Tang et al., 2009; Umbach et al., 2008). An insect virus, *Heliothis virescens* ascovirus (HvAC), encodes miR-1 from the major capsid protein gene (MCP) which directly degrades its own DNA polymerase I transcript and thus, regulates its replication (Hussain et al., 2008).

To gain more insights into WSSV pathogenesis and viral-host interaction, this study aimed to identify the WSSV-encoded miRNAs from WSSV-Th during the late stage of viral infection. The results identified 14 candidate WSSV-encoded miRNAs by using next generation Illumina Solexa sequencing. Six of the candidate miRNAs were specifically expressed in viral-infected cells and its expression were up-regulated. *In silico* analysis identified potential cellular- and viral-gene targets of these candidate WSSV-miRNAs.

Materials and methods

Shrimp culture and WSSV stock

Healthy *P. monodon*, size about 10 g, were purchased from commercial shrimp farms in Nakhon Pathom, Thailand. Shrimps were reared in tanks containing 20 liters of continuously aerated saltwater at 10 ppt salinity and maintained at temperature of 28 $^{\circ}$C. They were acclimatized a day before WSSV injection and fed with commercial feed every day.

WSSV-Th isolate stock was kindly provided by Dr. Sritunyalucksana, BIOTEC. The viral titer (10^6 virions μl^{-1}) was determined by real-time PCR (Sritunyalucksana et

al., 2006) and maintained at -80 °C until used. For WSSV lysate, it was prepared according to the method of Natividad et al., (2007) (Natividad et al., 2007). Briefly, WSSV-infected gill tissue was homogenized in 10% w/v TNE buffer (50 mM Tris, 100 mM NaCl, 1 mM EDTA, pH 7.4) and the tissue debris was removed by centrifugation at 3000×g for 15 min at 4 °C. The supernatant was filtered through a 0.45 μm membrane (Millipore) and stored at -80 °C until use.

Sample preparation and RNA extraction

WSSV-infected or uninfected shrimp (control) were intramuscularly injected with 50 μl of diluted purified-WSSV (~10^6 copies) or 150 mM NaCl (control) using tuberculin syringe needle, respectively. After 48 hours post challenge, gill tissues were collected and total RNAs were extracted by using TRIzol Reagent® (Molecular Research Center, Inc.) according to the manufacture's protocol. The quantity and integrity of the total RNAs were determined by Nanodrop spectrophotometer (Thermo Scientific, Wilmington, DE) and RNA agarose gel electrophoresis in Tris-EDTA-acetate (TAE) buffer, respectively.

Detection of WSSV infection

WSSV infection was confirmed by using reverse transcription PCR (RT-PCR) to amplify viral protein 28 mRNA (*vp28)* (Attasart et al., 2009). Two micrograms of total RNAs were used as templates for complementary DNA (cDNA) synthesis by using reverse transcriptase (ImProm-II™ Reverse Transcriptase, Promega) and PRT primer (Table 1). Elongation factor 1-alpha (EF1α) was used as an internal control gene to normalize for the relative expression of *vp28* mRNA. Stable expression of EF1α can be observed under WSSV (Dhar et al., 2009), YHV and PstDNV infection. Condition of PCR was as followed: 94 °C for 5 min followed by 25 cycles of 94 °C for 30 s, 55 °C for 30 s, 72 °C for 30 s and continued with 72 °C for 7 min to complete the extension. The PCR products of WSSV-VP28 (407 bp) and *EF1α* (140 bp) were separated on 2% agarose gel electrophoresis.

Construction and sequencing of small RNA libraries

Total RNAs from WSSV-infected and WSSV-free tissues were submitted to Beijing Genome Institute (BGI), China, to construct the small RNAs libraries. Briefly, small RNAs ranged from 18-30 nt were purified by polyacrylamide gel electrophoresis before ligation with the 3′ and 5′ adaptors for Solexa sequencing. RT-PCR approach was used to convert the ligation products to DNA and amplified it. The amplicons were used as templates for cluster generation and directly sequenced by Illumina's Solexa sequencer.

Bioinformatics analysis of small RNAs

Raw small RNAs sequencing data were cleaned by eliminating fragments with sizes shorter than 18 nt, low quality reads, sequences with poly-A and adaptor contamination. Total cleaned reads were blasted against microRNA database (miRbase version 17) to identify the conserved miRNA that matched to mature RNAs in other species. The unannotated sequences were aligned using Rfam 10.1 and GenBank database to get rid of other small RNAs (rRNA, tRNA, snRNAs, and repeat associated RNAs). To identify novel candidate miRNAs derived from shrimp or WSSV, the

remaining sequences were blasted against Express Sequence Tag (EST) database of *P. monodon* from the Marine Genomics Project (www.marinegenomics.org) and WSSV genome Thai isolate from GenBank database (accession no. AF369029), respectively. Sequences that perfectly matched to viral genome and not to shrimp's EST were considered for further analysis. To investigate the candidate miRNAs ability to form hairpin structure, flanking sequence of about ~100 nt from each side of the viral genome were used in Mfold prediction with minimum free energy (MFE) less than -20 kcal/mol. The stem-loop structures were analyzed by MIREAP using the following criteria: mature miRNA length 20-24 nt, precursor miRNA has minimum 14 paired and minimum free energy <-18 kcal/mol, to predict the candidate WSSV-encoded miRNAs.

Table 1 Sequence of primers used in this study

Primers	Sequence 5′→3′	Purposes
VP28-F	CCGCTCGAGACTCTTTCGGTCGTGTCGGCC	PCR detection of WSSV *vp28*
VP28-R	GGCACCATCTGCATACCAGTG	
YHV-F	CAAGGACCACCTGGTACCGGTAAGAC	PCR detection of YHV
YHV-R	GCGGAAACGACTGACGGCTACATTCAC	
PstDNV-F*	TCCAACACTTAGTCAAAACCAA	PCR detection of PstDNV
PstDNV-R*	TGTCTGCTACGATGATTATCCA	
EF1α-F	GAACTGCTGACCAAGATCGACAGG	PCR of shrimp's *Ef1α*
EF1α-R	GAGCATACTGTTGGAAGGTCTCCA	
PRT	CCGGAATTCAAGCTTCTAGAGGATCCTTTTTTTTTTTTTTT	Reverse transcription (RT)
SRT-4-5p	GTTGGCTCTGGTGCAGGGTCCGAGGTATTCGCACCAGAGC CAACcatggt	Stem-loop RT of wsv-miR-4-5p
SRT-4-3p	GTTGGCTCTGGTGCAGGGTCCGAGGTATTCGCACCAGAGC CAACttcagg	Stem-loop RT of wsv-miR-4-3p
SRT-5	GTTGGCTCTGGTGCAGGGTCCGAGGTATTCGCACCAGAGC CAACagcaca	Stem-loop RT of wsv-miR-5
SRT-6	GTTGGCTCTGGTGCAGGGTCCGAGGTATTCGCACCAGAGC CAACttagcc	Stem-loop RT of wsv-miR-6
SRT-7-5p	GTTGGCTCTGGTGCAGGGTCCGAGGTATTCGCACCAGAGC CAACagaata	Stem-loop RT of wsv-miR-7-5p
SRT-7-3p	GTTGGCTCTGGTGCAGGGTCCGAGGTATTCGCACCAGAGC CAACgacagc	Stem-loop RT of wsv-miR-7-3p
SRT-8	GTTGGCTCTGGTGCAGGGTCCGAGGTATTCGCACCAGAGC CAACttggcc	Stem-loop RT of wsv-miR-8
SRT-9	GTTGGCTCTGGTGCAGGGTCCGAGGTATTCGCACCAGAGC CAACaggaag	Stem-loop RT of wsv-miR-9
SRT-10	GTTGGCTCTGGTGCAGGGTCCGAGGTATTCGCACCAGAGC CAACtttctt	Stem-loop RT of wsv-miR-10
SRT-11	GTTGGCTCTGGTGCAGGGTCCGAGGTATTCGCACCAGAGC CAACccagcc	Stem-loop RT of wsv-miR-11
SRT-12	GTTGGCTCTGGTGCAGGGTCCGAGGTATTCGCACCAGAGC CAACcgcatc	Stem-loop RT of wsv-miR-12
SRT-13	GTTGGCTCTGGTGCAGGGTCCGAGGTATTCGCACCAGAGC CAACaatgtg	Stem-loop RT of wsv-miR-13
SRT-14	GTTGGCTCTGGTGCAGGGTCCGAGGTATTCGCACCAGAGC CAACgcacga	Stem-loop RT of wsv-miR-14
SRT-15	GTTGGCTCTGGTGCAGGGTCCGAGGTATTCGCACCAGAGC CAACtctcca	Stem-loop RT of wsv-miR-15
SRT-let7	GTTGGCTCTGGTGCAGGGTCCGAGGTATTCGCACCAGAGC CAACaacta	Stem-loop RT of shrimp's let7
SRT-U6	GTTGGCTCTGGTGCAGGGTCCGAGGTATTCGCACCAGAGC CAACaaaatgtggaac	Stem-loop RT of shrimp's U6
SF-4-5p	CGCCGCCAGGGAAGAAATAG	PCR of wsv-miR-4-5p
SF-4-3p	CGCCGCTGGAGCATATGTATTC	PCR of wsv-miR-4-3p
SF-5	GCGTTACCCTTTTCGGTTGGC	PCR of wsv-miR-5
SF-6	CGCCGGTTCGGTTCTTCAAAGA	PCR of wsv-miR-6
SF-7-5p	GCGCTCAGTAGTGTTGTTGCC	PCR of wsv-miR-7-5p
SF-7-3p	CGCCGGCCGCGAAATAATAATAAT	PCR of wsv-miR-7-3p
SF-8	GATTATTGGACCGCTGGGTCG	PCR of wsv-miR-8
SF-9	GCCGCAGCCTAAAAATCTCCC	PCR of wsv-miR-9
SF-10	GCCGATCTTCTGGGTTTGGCT	PCR of wsv-miR-10
SF-11	TTATGACTTGGTGCGGCGGG	PCR of wsv-miR-11
SF-12	GCGCCGCTTTTTCCAACACAGAA	PCR of wsv-miR-12
SF-13	GCCGCCAGTCATATCCGTGAT	PCR of wsv-miR-13
SF-14	GCCGTCCAATGTCTTGAAGCTG	PCR of wsv-miR-14
SF-15	CGCCGCAATATTGTCACCGATGT	PCR of wsv-miR-15
SF-let7	GCCGCtGAGGTAGTAGGTTGTA	PCR of shrimp's let7
SF-U6	ACAGAGAAGATTAGCATGGCCCCT	PCR of shrimp's U6
SR	GTGCAGGGTCCGAGGTATT	PCR of every wsv-miR, let-7 and U6

* PstDNV-F and PstDNV-R primers correspond to IHHNV309-F and IHHNV309-R in Kathy et al., 2007.
The small characters are nucleotides, specifically designed for each wsv-miRNA.
SRT primers are used for stem-loop reverse transcription of each wsv-miRNA.
SF primers are employed for PCR detection of each wsv-miRNA.
SR primer is a universal primer used for PCR detection of all wsv-miRNAs and shrimp's let-7 and U6.

Stem-loop RT-PCR for validation of candidate miRNAs

Total RNAs from WSSV-infected and uninfected gill tissues at 48 h were extracted and used in the confirmation of WSSV infection by PCR before miRNA validation. Stem-loop primers used to generate cDNA were designed according to Chen (Chen et al., 2005). The primer contained an insertion of the universal sequence binding site of the reverse primer in the stem as described (Varkonyi-Gasic and Hellens, 2010). To set the RT reaction, 250 ng of the total RNA of each sample was mixed with 0.5 µl of 1 µM of stem-loop primers (SRT primers, Table 1) before denaturation at 65°C for 5 min and quickly cooled on ice. Pre-denatured RNA was mixed with the reaction buffer containing 1X First-strand cDNA buffer, 250 nM of each dATP, dCTP, dGTP and dTTP, 10 mM DTT, 4 unit of RNaseOUT, 25 unit of SuperScript® III RT (Invitrogen) and adjusted to the final volume with sterilized RNase-free water to 10 µl. Reactions were incubated at 16°C for 30 min, followed by pulsed RT of 60 cycles at 30°C for 30 s, 42°C for 30 s and 50°C for 1 s and terminated by incubation at 85°C for 5 min. PCR reaction was performed in a total volume of 20 µl; the reaction contained 2 µl of cDNA, 1X *Taq* buffer with $[NH_4]_2SO_4$ (Fermentas), 2.5 mM $MgCl_2$, 0.5 mM dNTPs, 50 nM of specific forward primer (SF) and universal reverse primer (SR) and 1 unit of Taq DNA polymerase. The PCR condition was as followed: 95°C for 3 min followed by 35 cycles of 95°C for 10 s, 60°C for 20 s and cool downed at 20°C. The expected products of sizes approximately 62-65 bp were analyzed on 15% non-denaturing polyacrylamide gel electrophoresis.

Profiling of WSSV-encoded miRNAs expression

To prepare WSSV-infected tissues at various time points, shrimps were challenged with WSSV lysate that resulted in shrimp death within 3 days. Gill tissues were collected at 3, 6, 9, 18, 24, 36 and 48 h. At the same time, an uninfected gill tissue injected with 150 mM NaCl was taken at 48 h and used as the control. Three shrimps were used for each time point. Then, total RNAs were extracted and WSSV detection was performed as described above. The expression of the candidate miRNAs were detected by stem-loop RT-PCR. The relative expression levels of the wsv-miRs were determined by semi-quantitative RT-PCR. The intensity of the PCR products was measured using Scion Image 4.0 program and normalized against U6 small nuclear RNA (snRNA) expression.

Detection of WSSV-encoded miRNAs from other virus infections

To ensure that WSSV-encoded miRNAs identified in this study are specifically derived from the WSSV genome not due to the host immune response against the viral challenge, investigation of the wsv-miRNA expression was performed under various pathogen challenges. Viruses containing the DNA genome such as WSSV or *Penaeus stylirostris* Densovirus (PstDNV, previously name infectious hypodermal and haematopoietic necrosis virus or IHHNV) and the RNA genome such as yellow head virus (YHV) were used in this study. Shrimp were separately injected with 150 mM NaCl solution, WSSV, YHV or IHHNV lysate. The dose of WSSV and YHV that lead to complete mortality within 3 days, IHHNV lysate dilution at 10^{-1} were employed. Based on the high expression level of WSSV-encoded miRNAs at 36 h, viral infected gill tissues were collected at this time. For non-lethal virus as PstDNV, an infected tissue was taken at 72 h which was a time with successful infection of PstDNV (Ho et

al., 2011). RT-PCR with specific primers; YHV-F and YHV-R primers (Kongprajug et al., 2017), PstDNV-F and PstDNV-R (formerly called IHHNV309F and IHHNV309R primers, respectively (Kathy et al., 2007) were used for YHV and PstDNVdetections, respectively. *EF1α* was useded as an internal control. After confirmation of viral infections, expressions of WSSV-encoded miRNAs were detected by stem-loop RT-PCR and the nuclease free water was used as the negative control of PCR reactions.

Target prediction of the WSSV-encoded miRNAs

To identify potential targets of the candidate miRNAs, miRanda 1.0 webserver was employed (www.microrna.org). The miRanda scores are based on sequence complementarity between miRNA and their target was >90, the free energy of miRNA:mRNA duplex was <-20 kcal/mol, and a perfect match seed region at the 5´ of miRNA. Due to the lack of the complete genome sequence database for *Penaeus monodon* and other shrimp species, the dataset of identified miRNAs in this study and the EST of *P. monodon* or WSSV-Th genome were used as input. The potential limitation in miRNA target prediction is the EST database which does not equivalent to 3´-UTR of the mRNA target. For viral target genes, WSSV genome sequence was used which may encounter with the problem of short 3´-UTR of some WSSV genes and of polycistronic (encode more than 1 gene per mRNA). The target genes that fit with the above criteria were identified by BLASTn against shrimp's EST and nucleotide database or translated into protein using BLASTp against protein database in NCBI.

Results

Solexa sequencing and bioinformatics analysis of the small RNA libraries

In order to identify WSSV-encoded miRNAs, gill tissues from WSSV-infected and non-infected (control) shrimp were used in small RNAs library construction and were sequenced by NGS. The length distribution of raw sequence reads was similar between both small RNA libraries at 18-23 nt (Fig. 1), which are the ideal size of miRNA. A total of 16,257,357 and 16,513,781 raw sequence reads were obtained from control and WSSV-infected library, respectively. After removal of the low quality reads, approximately 15 million clean reads were obtained from each library and 96% of the sequences were shared between the two libraries. Only a few unique sequences were found in the control (0.34%) and WSSV-infected (3.53%) libraries. The repeated sequences and other small RNAs (rRNA, tRNA, snRNA and snoRNA) were removed after analysis with Rfam10.1 and GenBank database. The remaining sequences were compared against miRBase17 to identify known and conserved miRNAs (Table 2). After alignment of the unannotated sequences with expressed sequence tag (EST) of *P. monodon* and the genome of WSSV-Th isolate, the flanking regions of the matching sequences were used for secondary structure prediction of precursor miRNAs by Mfold and analyzed by MIREAP. The results showed that 17 miRNAs were obtained from WSSV-infected library; however, three of them matched with shrimp's EST, pmo-miR-1, -2 and -3. Therefore, 14 candidate miRNAs (wsv-miR-4 to -15) remained that were encoded from WSSV. Notably, the candidate miRNAs, wsv-miR-4 and wsv-miR-7 were predicted to be derived from the 5´- and 3´-arms of pre-miRNAs (wsv-miR-4-5p, wsv-miR-4-3p, wsv-miR-7-5p and wsv-miR-7-3p) (Table 3).

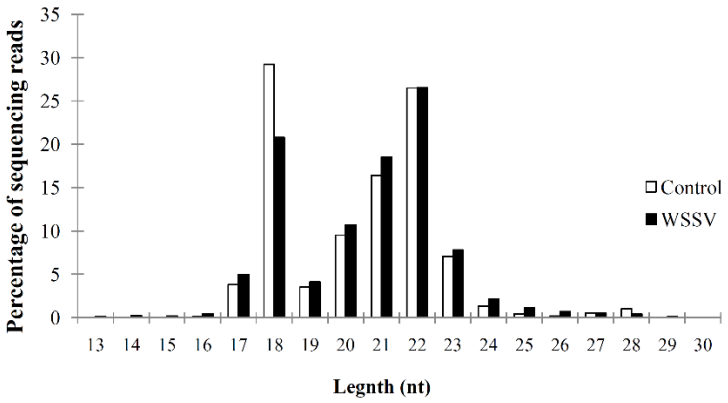

Fig. 1 Length distribution of small RNAs from control (□) and WSSV-infected libraries (■). The highest frequency was around 18-23 nt.

Table 2
Classification of cleaned small RNA sequencing reads.

Small RNAs	Number of reads			
	Control		WSSV-infected	
	Unique[a]	Total reads	Unique	Total reads
Total reads		16,257,357		16,513,781
High_quality		16,219,800		16,467,059
Clean_reads	99,105	15,466,517	343,476	15,158,589
Conserved miRNAs	21,980	14,868,766	52,893	13,448,697
Other small RNAs	14,052	50,739	30,248	250,671
- rRNA	9355	20,542	15,732	121,737
- snoRNA	1184	1513	8214	27,693
- snRNA	237	365	1090	2881
- tRNA	3276	28,319	5212	98,360
Unannotate[b]	63,073	547,012	260,335	1,459,221
Matched shrimp's EST	588	2314	1841	27,880
Matched WSSV-Th genome	122	882	39,195	369,354

[a] They are type of sequence.
[b] Do not match with any-RNA.

Table 3 Sequence and genomic position of the candidate miRNAs

miRNA	Location	strand	Sequence 5′→3′	No. of read	Length (nt)
wsv-mir-4-5p	55069-55088	+	cagggaagaaauagaccaug	12	20
wsv-mir-4-3p	55123-55144		uggagcauauguauucccugaa	2	22
wsv-mir-5	66621-66642	+	acccuuuucgguuggcugugcu	5	22
wsv-mir-6	155594-155615	+	uucgguucuucaaagaggcuaa	5	22
wsv-mir-7-5p	188534-188555	+	caguaguguuguugccuauucu	9	22
wsv-mir-7-3p	188578-188597		gaaauaauaauaaugcuguc	1	20
wsv-mir-8	28262-28282	-	uggaccgcugggucgggccaa	21	21
wsv-mir-9	38575-38596	-	agccuaaaaaucucccuuccu	11	22
wsv-mir-10	58933-58954	-	ucuucuggguuuggcuaagaaa	13	22
wsv-mir-11	90678-90699	-	gacuuggugcggcgggggcugg	11	22
wsv-mir-12	186737-186758	-	uuuuuccaacacagaagaugcg	6	22
wsv-mir-13	209404-209425	-	cagucauauccgugaucacauu	12	22
wsv-mir-14	276164-276186	-	ccaaugucuugaagcugucgugc	7	22
wsv-mir-15	288685-288707	-	aauauugucaccgauguuggaga	6	23

Characterization of candidate WSSV-encoded pre-miRNA

Secondary structure of WSSV pre-miRNAs were predicted using Mfold (Fig. 2). All the flanking sequences of each candidate WSSV-encoded miRNA could form stem-loop structure with the minimum free energy (MFE) ranging from -18.3 to -27 kcal/mol. Hairpin structure of WSSV pre-miRNAs showed characteristics of internal mismatches with bulges in the stem and the terminal loop.

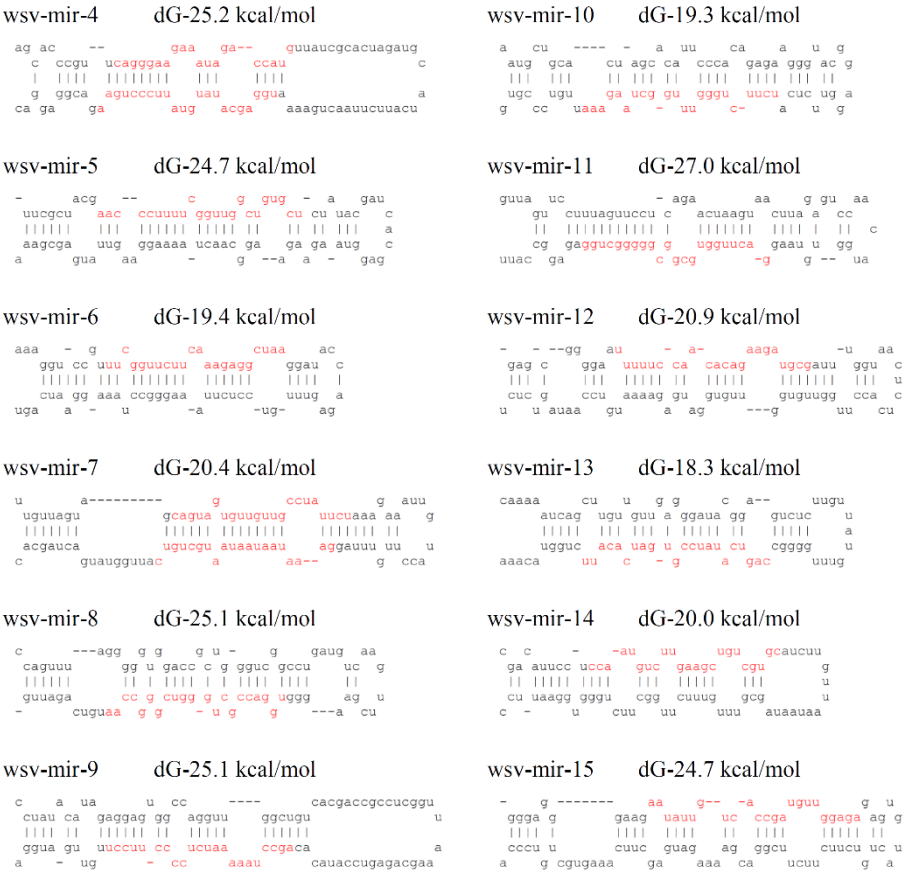

Fig. 2 Secondary structures of the 12 candidate WSSV-encoded pre-miRNAs. The minimum free energy (MFE) was predicted by Mfold program. Red nucleotides indicate mature sequences of miRNAs.

Mapping of WSSV-encoded miRNAs on WSSV genome

All 12 candidate WSSV-encoded pre-miRNAs were distributed along the WSSV genome. The nucleotides sequences and the genomic position of the candidate wsv-miRs are shown as a schematic diagram (Fig. 3). Candidate wsv-miRs were classified into 4 groups according to the transcriptional direction and location. In the first group, the candidate wsv-miRs (wsv-miR-4, -5, -6 and -7) were located on the sense strand and were encoded in the same direction as the open reading frame (ORFs) of WSSV. The second and third groups were embedded in the antisense strand of the viral genome and were either encoded in the opposite (wsv-miR-8, -9, -12, -13 and -14) or in the same transcriptional orientation with viral ORFs (wsv-miR-10 and -15). The last group which contained only a single candidate, wsv-miR-11, was located in the overlapping sequence between ORF63 and 64 in an antisense direction. Notably,

wsv-mir-9 was found located in the antisense strand of the putative WSSV DNA polymerase (ORF27).

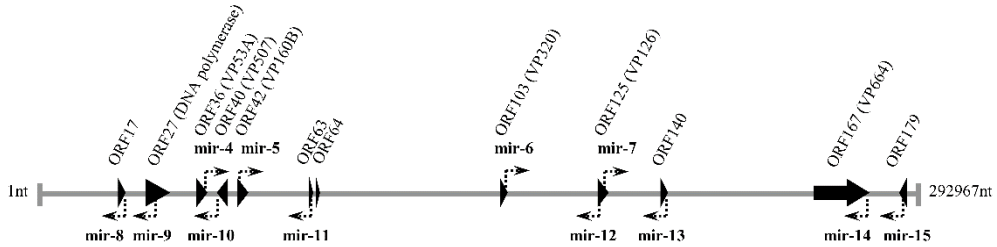

Fig. 3 A schematic diagram of the locations of the candidate WSSV-encoded miRNAs on WSSV genome (GenBank accession number: AF369029). ORFs of WSSV and candidate miRNAs were represented as big and small arrows with the transcriptional direction, respectively.

Validation of the candidate WSSV-encoded miRNAs expression

To verify whether the candidate miRNAs were specifically expressed in WSSV-infected tissue, stem-loop RT-PCR technique was performed. Total RNA samples that were used to construct the small RNA libraries were employed as templates. In addition, other sample set which was the control- and WSSV infected- gill samples obtained from different set of shrimp was used to ascertain that the amplification signals of wsv-miRNAs in the WSSV-infected gill tissues were not the artifact. The results showed that most of candidate wsv-miRs can be detected only from WSSV-infected tissues, except for wsv-miR-7-5p, -7-3p, -8 and -11. The same results were obtained from these two independent experiments. MicroRNA let-7 which was used as a positive control was found in all samples (Fig. 4).

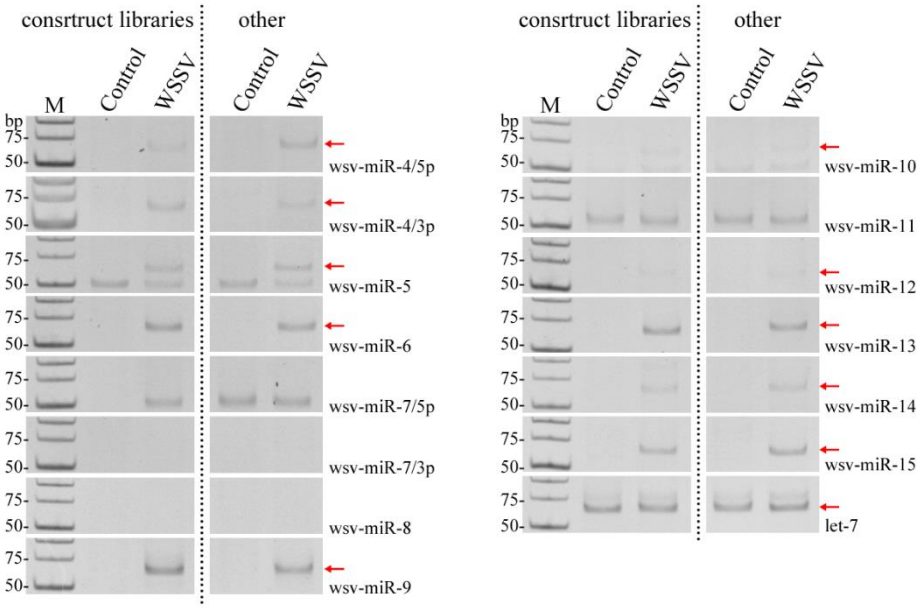

Fig. 4 Validation of the 14 candidate WSSV-encoded miRNAs by stem-loop RT-PCR. The sample that was used to construct the small RNAs libraries (set 1) was compared to the other sample set (set 2). The expressed miRNAs was about 62 bp (red arrow). M is ultra low range DNA ladder.

WSSV-encoded miRNAs specifically expressed in shrimp challenging with WSSV but not with YHV and PstDNV.

The RT-PCR results confirmed WSSV, YHV and PstDNV replication in the viral challenged shrimp and the individual shrimp was infected with a single virus (Fig. 5A). After performing of SRT-PCR, ten validated wsv-miRs could be detected from WSSV- but not YHV- and PstDNV- infected shrimp. Supporting to the validation of the wsv-miRs expression, wsv-miR-7-5p, -7-3p, -8, and -11 could not be detected (Fig. 5B). These results implied that viral encoded-miRNAs in this study were specifically expressed by WSSV and they were not inducible miRNAs that derived from the immune response to RNA and DNA virus infections.

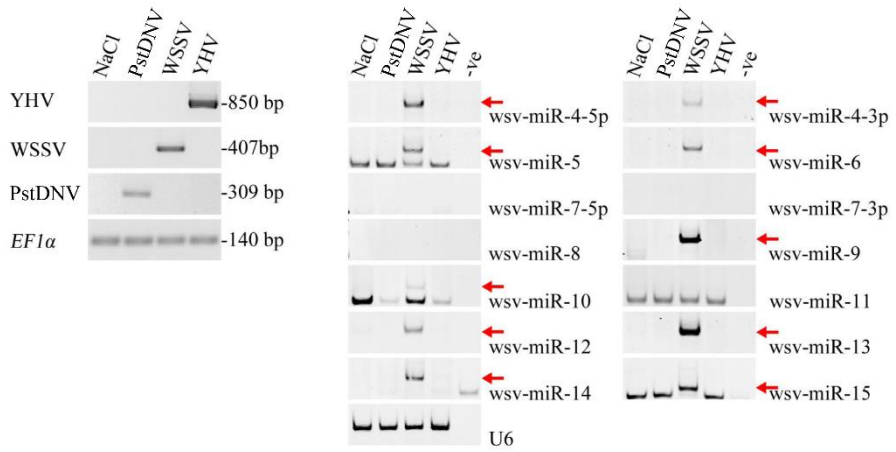

Fig. 5 WSSV-encoded miRNAs specifically expressed in shrimp challenging with WSSV but not with YHV and PstDNV. (A) RT-PCR confirmation of the infectivity of the individual shrimp infected with PstDNV, WSSV or YHV. (B) Expressions of ten WSSV-encoded miRNAs were specifically detected from WSSV infected shrimp (red arrow).

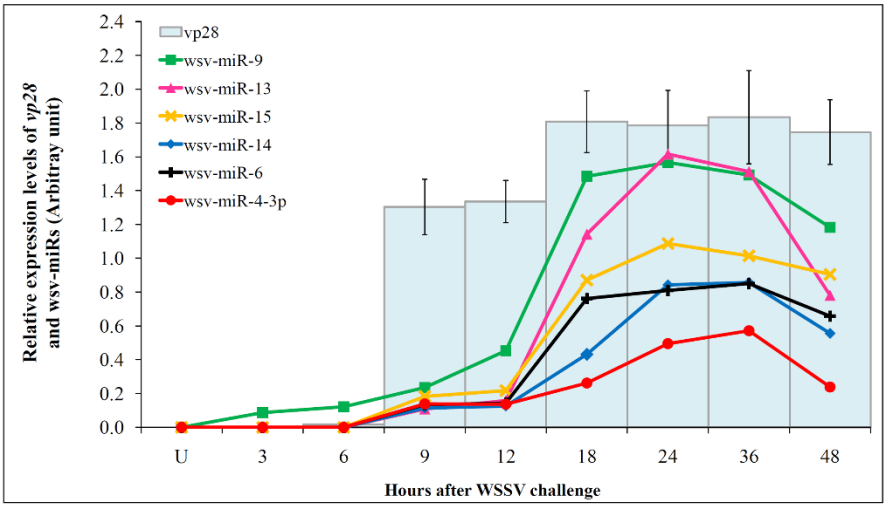

Fig. 6 Expression profiles of wsv-miRs at each time point of WSSV-infection. Uninfected shrimp is marked with U. Semi-quantitative expression of 6 wsv-miRs (color lines) and *vp28* (blue bars) were normalized with U6 snRNA and *EF1α*, respectively. The result is shown as means from 3 shrimps at each time point.

Profiling of wsv-miRNA expressions depend on time course of WSSV infection

To investigate the expression profiles of wsv-miRs, the expression levels of wsv-miRs from control and WSSV-infected shrimp at several time points were determined by stem-loop RT-PCR. Six wsv-miRs (wsv-miR-4-3p, -6, -9, -13, -14 and -15) were found to be expressed at different levels and were up-regulated depending on the time course of WSSV infection. Expressions of most wsv-miRs were increased after 12 or 18 hpi and were slightly decreased at 48 hpi. The expression of U6 snRNA in all samples was relatively constant. Detection of *vp28* mRNA confirmed WSSV infection with early at 9 hpi. A representative gel from three sets of experiments is shown in Fig. 6 with the expression level of *vp28* (blue bars). After normalization, wsv-miR-9 showed the highest expression level among all candidate miRNAs, followed by wsv-miR-13 and -15.

Computational prediction of miRNA targets

Potential targets screening was performed using miRanda software. EST database of *P. monodon* was used for cellular target prediction. After blast search, potential cellular targets were identified and were classified into innate-immune related genes, transporter proteins, proteins involved in translation, and structural proteins (Table 4). The wsv-miR-10 and -13 were predicted to target to just one mRNA which was hemocyanin (HcVn) and *F. chinensis* double WAP domain-containing protein, respectively. Some wsv-miRNAs (miR-4-3p, -5, -6, -14 and -15) were predicted to recognize several mRNA targets for example; wsv-miR-6 was predicted to recognize either anti-lipopolysaccharide factor or cyclophilin. Cellular genes such as anti-lipopolysaccharide factor and elongation factor 1-alpha of *P. monodon* may be recognized by multiple miRNAs. For example, elongation factor 1-alpha of *P. monodon* may be the candidate target of wsv-miR-5, -14, and -15. For viral genes (Table 5), potential targets were distributed on the viral genome encoding either non-structural (helicase, ribonucleotide reductase large subunit (RR1)) or structural proteins (such asVP53A, VP664).

Table 4 Cellular target prediction of wsv-miRNAs

wsv-miRs	Potential cellular target genes
	Innate-immune related
wsv-miR-4-3p, -5, -10	*P. monodon* hemocyanin (HcVn) mRNA
wsv-miR-6, -15	*P. monodon* anti-lipopolysaccharide factor
wsv-miR-5	*P. monodon* masquerade-like serine proteinase-like protein 3
wsv-miR-4-3p, -13, -14	*F. chinensis* double WAP domain-containing protein
	Transporter proteins
wsv-miR-15	*P. monodon* putative ligand-gated ion channel-like protein
wsv-miR-15	*P. monodon* NADH dehydrogenase subunit F-like protein
	Protein translation
wsv-miR-5, -14, -15	*P. monodon* elongation factor-1 alpha
wsv-miR-5	*L. vannamei* ribosomal protein L8
	Structural and other proteins
wsv-miR-15	*P. monodon* cathepsin D
wsv-miR-6	*F. paulensis* cyclophilin

Table 5 Viral target prediction of wsv-miRNAs

wsv-miRs	Potential viral target genes
wsv-miR-4-5p	ORF105, ORF110, ORF154 VP53A, VP15, VP57, VP664, VP544, VP136B ICP11
wsv-miR-4-3p	ORF89, ORF135, ORF142, ORF169, ORF14, ORF38 VP53A, VP300, VP664 TK-TMK, Helicase
wsv-miR-5	ORF18, ORF19, ORF42, ORF43, ORF56, ORF89, ORF96, ORF121, ORF122, ORF125, ORF12, ORF14, ORF25, ORF38, ORF53, ORF82, ORF83, ORF104, ORF108 VP357, VP507, VP387, VP53C P-collagen, CBP, STF[a], class1 cytokine receptor, Helicase, dUTPase, RR1 repeat4
wsv-miR-6	ORF5, ORF73, ORF89, ORF97, ORF47 VP53A, VP320, VP544 STK
wsv-miR-9	ORF121
wsv-miR-10	ORF4, ORF43, ORF63, ORF65, ORF97, ORF122, ORF123, ORF138, ORF67, ORF82, ORF154 VP53B, VP664 P-collagen, E3, AAP-1, STK repeat4, repeat8, repeat7
wsv-miR-12	ORF37, ORF90 VP664
wsv-miR-13	ORF55, ORF3, ORF33, ORF116, ORF159, ORF166 VP38A, VP136B TK-TMK, RR1
wsv-miR-14	ORF4, ORF17, ORF19, ORF49, ORF175, ORF33, ORF111, ORF179 VP53A, VP51A, VP664, VP26 class1 cytokine receptor, RR1
wsv-miR-15	ORF26, ORF136, ORF85, ORF154 VP216, VP136B PK1

TK-TMK: Chimeric Thymidine/Thymidylate kinase, CBP: CREB-binding protein, STF: SOX-transcription factor, RR1: Ribonucleotide reductase I, STK: Putative Serine/Threonine protein kinase, E3: E3 ubiquitin ligase, AAP-1: Anti-apoptotic protein 1, PK1: Protein kinase 1
Marks, 2005; Li et al., 2007[a]; He et al., 2006[b]

Discussion

Several miRNAs have been identified from various organisms and these are conserved in metazoans, including aquatic invertebrates such as *M. japonicus* (Huang et al., 2012; Ruan et al., 2011), *P. monodon* (Kaewkascholkul et al., 2016), *L. vannamei* (Sun et al., 2016) and *F. chinensis* (Li et al., 2017). After viral-encoded miRNAs were first found in the Epstein-Barr virus (EBV) (Pfeffer et al., 2004), a number of viral-encoded miRNAs were identified from other DNA and some RNA viruses (Klase et al., 2013). Here, NGS and small RNAs cloning were used to identify WSSV-encoded miRNAs in *P. monodon*. Fourteen candidate viral-encoded miRNAs were predicted to derive from 12 precursors which can spontaneously form hairpin structure (MFE <-20 kcal/mol) (Fu et al., 2011). Using stem-loop RT-PCR approach, ten candidate wsv-miRs were validated. Most of them could not be detected by northern blot. This might be due to the very low expression level of wsv- miRs which might be *below* the *detection limit* of this method. This was not unexpected as other studies also

failed to detect viral encoded miRNAs such as HSV-1-5p and MuHV-M1-1, by northern blot (Diebel et al., 2010; Tang et al., 2008).

Different from the eukaryote, the viral-derived miRNAs are less conserved in sequence except for the closely related viruses such as HSV-1 and HSV-2 that show high sequence similarity (Umbach and Cullen, 2009). Novel candidate miRNAs in this study do not appear to share high sequence homology against viral miRNAs in miRNA database. In addition, the number and sequence of our wsv-miRNAs were different from the previously identified 101 WSSV-miRNAs from WSSV-Cn isolate (Huang et al., 2014; Liu et al., 2016). This may be because of the different in viral isolate (WSSV-Th vs WSSV-Cn), stage of WSSV infection (48 h vs 6-24 h), shrimp tissues (gill vs lymphoid) and methods to identify miRNAs (NGS vs microarray). Nonetheless, the stem-loop sequences of pre-miRNAs in this study were conserved among the four WSSV isolates. WSSV-Th genome sequence differs greatly from that of WSSV-Cn isolate as WSSV-Th has a big deletion of 12 kb (Marks et al., 2004). Two WSSV-Cn miRNAs, WSSV-miR197 and -miR201 can be found to be located in the deleted region of WSSV-Th (He and Zhang, 2012). Therefore these miRNAs could not be identified in this study. This suggested that neither WSSV-miR197 nor -miR201 are necessary for WSSV-Th. Moreover, one of our wsv-miRs, wsv-miR-5, showed sequence overlaps with WSSV-miR12 of the previous study (He and Zhang, 2012). The location of WSSV-miR12 is embedded in the wsv-miR-5 precursor, suggesting that they might be conserved in the genomic location similar to the miR-1 of some members in the polyomavirus family: SV-40, JCV and BKV (Lagatie et al., 2013). This study also identified wsv-miRs from the gill tissue in the late stage of WSSV infection at 48 h whereas most of the previously identified WSSV-encoded miRNAs from other study are at the early stage of WSSV infection (He and Zhang, 2012). Some WSSV-miRs were expressed in specific tissues such as hemocyte-specific expression of WSSV-miR-129 and -162 and lymphoid organ-specific expression of WSSV-miR-N30 (Huang et al., 2014). In addition, differences in miRNA expression levels can be observed in lymphoid organ and stomach of WSSV-infected *F. chinensis* (Liu et al., 2016).

WSSV miRNA expression profile showed that 6 wsv-miRs increased upon viral infection at 12-18 h after *vp28*, a viral late gene, expression, suggesting that these wsv-miRs might function at the late stage of viral infection. The viral-encoded miRNA that controls late stage or lytic life cycle of virus is usually up-regulated after late protein expression (Tang et al., 2009). For example, HvAv encoded miR-1 form a major capsid protein (MCP) gene whose expression was increased during the late stage of HvAv infection and targeted its own *DNA polymerase I* mRNA, resulting in the inhibition of viral replication (Hussain et al., 2008). Among wsv-miRs, the expression level of wsv-miR-9 was highest, followed by wsv-miR-13 and -15, when compared to other wsv-miRs at the same time point. MicroRNA-mediated translational inhibition requires an imperfect binding between miRNA and their target at the ratio of at least 1:1 (tenOever, 2013). Therefore, high expression levels of certain wsv-miRs suggested the abundance of that mRNA targets or that the virus is attempting to quickly suppress the target mRNA. The decreased wsv-miRs expression at 48 h might be caused by WSSV infection that can induce apoptosis after 24 hpi in haematopoietic and gill tissue (Wongprasert et al., 2003).

The potential cellular and viral gene targets were screened by computational prediction. As the complete shrimp genome sequence is not available, this study picked

up potential cellular targets from EST of *P. monodon*. Some potential target genes, such as NADH dehydrogenase and elongation factor 1 have been shown to be down-regulated during WSSV-challenged (Wongpanya et al., 2007; Wu et al., 2007). This study used the WSSV genome sequence instead of the WSSV 3´-UTR (Huang et al., 2012) for viral target prediction because some viral mRNAs have an initial ribosome entry site (IRES) and share a poly-A tail (Han and Zhang, 2006; Kang et al., 2013; Kang et al., 2009). Wsv-miRs could target many non-structural genes such as DNA polymerase, anti-apoptotic protein 1 and dUTPase, suggesting that WSSV might use wsv-miRs to control its expression through various mechanisms such as transcription, apoptosis and signaling pathway. Some targets may be recognized by multiple miRNAs, such as the elongation factor 1-alpha and hemocyanin of *P. monodon* or the DNA polymerase and VP664 genes of WSSV. Such event was demonstrated in Kaposi sarcoma-associated herpesvirus (KSHV) as it encoded multiple miRNAs targeting to THBS1 or MAF mRNA (Hansen et al., 2010; Samols et al., 2007). In contrast, the result showed some candidate targets such as wsv-miR-4-3p that recognized *P. monodon* hemocyanin and VP35A. Similarly, WSSV-miR-66, miR-68 (He et al., 2014) and miR-32 (He et al., 2017) each of which binds to two WSSV mRNAs. In addition, this was also demonstrated in *M. japonicus* that encoded *Mj*-miR-12 (Shu and Zhang, 2017) and miR-965 (Shu et al., 2016) to control both shrimp and WSSV genes for down regulation of the virus. Furthermore, wsv-miRs were targeted to WSSV-related sequences such as helicase and putative serine/threonine protein kinase (Huang et al., 2011), suggesting that this wsv-miRs can target either virus or host gene.

Accumulation of wsv-miRNAs in this study and others suggested that WSSV has a lot of miRNAs when compared to other viruses in the miRBase database. The results also suggested that several wsv-miRNAs that were expressed in the late stages of WSSV infection could crosstalk between the host and the virus. Identification of wsv-miRs and their targets revealed the complexity of miRNA-mediated WSSV-host interaction. This knowledge will provide insights into the understanding of WSSV-host interaction and pathogenesis. Understanding of the roles of wsv-miRNAs and their expression pattern during WSSV infection may have potential applicability in applying miRNAs as valuable diagnostic and/or prognostic biomarkers for screening of virus infection and determination of the severity of the disease. Wsv-miRs and their targets may serve as potential therapeutic targets in miRNA-based vaccine development to effectively prevent and control the WSSV infection in shrimp.

References

1. Attasart, P., et al., 2009. Inhibition of white spot syndrome virus replication in *Penaeus monodon* by combined silencing of viral rr2 and shrimp PmRab7. Virus Res. 145, 127-133.

2. Bartel, D.P., 2004. MicroRNAs: Genomics, Biogenesis, Mechanism, and Function. Cell. 116, 281-297.

3. Chai, C.Y., et al., 2013. Analysis of the complete nucleotide sequence of a white spot syndrome virus isolated from pacific white shrimp. J.Microbiol.. 51, 695-699.

4. Chen, C., et al., 2005. Real-time quantification of microRNAs by stem–loop RT–PCR. Nucleic Acids Res. 33, e179.

5. Choy, E.Y.-W., et al., 2008. An Epstein-Barr virus–encoded microRNA targets PUMA to promote host cell survival. The Journal of Experimental Medicine. 205, 2551-2560.

6. Denli, A.M., et al., 2004. Processing of primary microRNAs by the Microprocessor complex. Nature. 432, 231-235.

7. Dhar, A.K., et al., 2009. Validation of reference genes for quantitative measurement of immune gene expression in shrimp. Mol. Immunol. 46, 1688-1695.

8. Diebel, K.W., Smith, A.L., van Dyk, L.F., 2010. Mature and functional viral miRNAs transcribed from novel RNA polymerase III promoters. RNA. 16, 170-185.

9. Dong, H., et al., 2013. MicroRNA: Function, Detection, and Bioanalysis. Chemical Reviews. 113, 6207-6233.

10. Fu, Y., et al., 2011. Identification and differential expression of microRNAs during metamorphosis of the Japanese Flounder (*Paralichthys olivaceus*). PLoS ONE. 6, e22957.

11. Gregory, R.I., et al., 2004. The Microprocessor complex mediates the genesis of microRNAs. Nature. 432, 235-240.

12. Grundhoff, A., Sullivan, C.S., 2011. Virus-encoded microRNAs. Virology. 411, 325-343.

13. Han, F., Zhang, X., 2006. Internal initiation of mRNA translation in insect cell mediated by an internal ribosome entry site (IRES) from shrimp white spot syndrome virus (WSSV). Biochem. Biophys. Res. Commun. 344, 893-899.

14. Hansen, A., et al., 2010. KSHV-encoded miRNAs target MAF to induce endothelial cell reprogramming. Genes Dev. 24, 195-205.

15. He, F., Fenner, B.J., Godwin, A.K., Kwang, J., 2006. White spot syndrome virus open reading frame 222 encodes a viral E3 ligase and mediates degradation of a host tumor suppressor via ubiquitination. J. Virol. 80, 3884-3892.

16. He, Y., Zhang, X., 2012. Comprehensive characterization of viral miRNAs involved in white spot syndrome virus (WSSV) infection. RNA Biol. 9, 1019-1029.

17. He, Y., Yang, K., Zhang, X., 2014. Viral microRNAs targeting virus genes promote virus infection in shrimp *in vivo*. J. Virol. 88, 1104-12.

18. He, Y., Ma, T., Zhang, X., 2017. The mechanism of synchronous precise regulation of two shrimp white spot syndrome virus targets by a viral microRNA. Front.Immunol. 8.

19. Ho, T., Yasri, P., Panyim, S., Udomkit, A., 2011. Double-stranded RNA confers both preventive and therapeutic effects against *Penaeus stylirostris* densovirus (*Pst*DNV) in *Litopenaeus vannamei*. Virus Res. 155, 131-136.

20. Huang, S.-W., et al., 2011. Fosmid library end sequencing reveals a rarely known genome structure of marine shrimp *Penaeus monodon*. BMC Genomics. 12, 242.

21. Huang, T., Xu, D., Zhang, X., 2012. Characterization of host microRNAs that respond to DNA virus infection in a crustacean. BMC Genomics. 13, 159.

22. Huang, T., Cui, Y., Zhang, X., 2014. Involvement of viral microRNA in the regulation of antiviral apoptosis in shrimp. J. Virol. 88, 2544-54.

23. Hussain, M., Taft, R.J., Asgari, S., 2008. An insect virus-encoded microRNA regulates viral replication. J. Virol. 82, 9164-9170.

24. Jehle, J.A., et al., 2006. On the classification and nomenclature of baculoviruses: A proposal for revision. Arch. Virol. 151, 1257-1266.

25. Jurak, I., et al., 2010. Numerous conserved and divergent microRNAs expressed by Herpes simplex viruses 1 and 2. J. Virol. 84, 4659-4672.

26. Kaewkascholkul, N., et al., 2016. Shrimp miRNAs regulate innate immune response against white spot syndrome virus infection. Dev. Comp. Immunol. 60, 191-201.

27. Kang, S.-T., et al., 2013. The DNA virus WSSV uses an internal ribosome entry site (IRES) for translation of the highly expressed non-structural protein ICP35. J. Virol.

28. Kang, S.-T., et al., 2009. Polycistronic mRNAs and internal ribosome entry site elements (IRES) are widely used by White spot syndrome virus (WSSV) structural protein genes. Virology. 387, 353-363.

29. Kathy, F.J.T., Solangel, A.N., Donald, V.L., 2007. PCR assay for discriminating between infectious hypodermal and hematopoietic necrosis virus (IHHNV) and virus-related sequences in the genome of *Penaeus monodon*. Dis. Aquat. Org. 74, 165-170.

30. Khawsak, P., Deesukon, W., Chaivisuthangkura, P., Sukhumsirichart, W., 2008. Multiplex RT-PCR assay for simultaneous detection of six viruses of penaeid shrimp. Mol. Cell. Probes. 22, 177-183.

31. Khvorova, A., Reynolds, A., Jayasena, S., 2003. Functional siRNAs and miRNAs exhibit strand bias. Cell. 115, 209 - 216.

32. Kim, V.N., Han, J., Siomi, M.C., 2009. Biogenesis of small RNAs in animals. Nat. Rev. Mol. Cell Biol. 10, 126-139.

33. Klase, Z.A., Sampey, G.C., Kashanchi, F., 2013. Retrovirus infected cells contain viral microRNAs. Retrovirology. 10, 15.

34. Kongprajug, A., Panyim, S., Ongvarrasopone, C., 2017. Suppression of PmRab11 inhibits YHV infection in *Penaeus monodon*. Fish Shellfish Immunol. 66, 433-444.

35. Kozomara, A., Griffiths-Jones, S., 2014. miRBase: annotating high confidence microRNAs using deep sequencing data. Nucleic Acids Res. 42, D68-D73.

36. Lagatie, O., Tritsmans, L., Stuyver, L.J., 2013. The miRNA world of polyomaviruses. Virology Journal. 10, 268.

37. Li, X., et al., 2017. The identification of microRNAs involved in the response of Chinese shrimp *Fenneropenaeus chinensis* to white spot syndrome virus infection. Fish Shellfish Immunol. 68, 220-231.

38. Li, Z., et al., 2007. Shotgun identification of the structural proteome of shrimp white spot syndrome virus and iTRAQ differentiation of envelope and nucleocapsid subproteomes. Molecular & Cellular Proteomics. 6, 1609-1620.

39. Liu, C., et al., 2016. Virus-derived small RNAs in the penaeid shrimp *Fenneropenaeus chinensis* during acute infection of the DNA virus WSSV. Scientific Reports. 6, 28678.

40. Marks, H., 2005. Genomics and transcriptomics of white spot syndrome virus. Ph.D. thesis. Department of Plant Sciences, Wageningen University, The Netherlands.

41. Marks, H., Goldbach, R.W., Vlak, J.M., van Hulten, M.C.W., 2004. Genetic variation among isolates of white spot syndrome virus. Arch. Virol. 149, 673-697.

42. Natividad, K.D.T., et al., 2007. White spot syndrome virus (WSSV) inactivation in *Penaeus japonicus* using purified monoclonal antibody targeting viral envelope protein. Aquaculture. 269, 54-62.

43. Park, J.-E., et al., 2011. Dicer recognizes the 5' end of RNA for efficient and accurate processing. Nature. 475, 201-205.

44. Pasquinelli, A.E., 2012. MicroRNAs and their targets: recognition, regulation and an emerging reciprocal relationship. Nat. Rev. Genet. 13, 271-282.

45. Pfeffer, S., et al., 2004. Identification of virus-encoded microRNAs. Science. 304, 734-736.

46. Ruan, L., et al., 2011. Isolation and identification of novel microRNAs from *Marsupenaeus japonicus*. Fish Shellfish Immunol. 31, 334-340.

47. Saito, K., Ishizuka, A., Siomi, H., Siomi, M.C., 2005. Processing of pre-microRNAs by the Dicer-1–Loquacious complex in *Drosophila* cells. PLoS Biol. 3, e235.

48. Samols, M.A., et al., 2007. Identification of cellular genes targeted by KSHV-encoded microRNAs. PLoS Pathog. 3, e65.

49. Sánchez-Paz, A., 2010. White spot syndrome virus: an overview on an emergent concern. Vet. Res. 41, 43.

50. Schwarz, D., et al., 2003. Asymmetry in the assembly of the RNAi enzyme complex. Cell. 115, 199 - 208.

51. Shu, L., Zhang, X., 2017. Shrimp miR-12 suppresses white spot syndrome virus Infection by synchronously triggering antiviral phagocytosis and apoptosis pathways. Front. Immunol. 8, 855.

52. Shu, L., Li, C., Zhang, X., 2016. The role of shrimp miR-965 in virus infection. Fish Shellfish Immunol. 54, 427-434.

53. Sritunyalucksana, K., et al., 2006. Comparison of PCR testing methods for white spot syndrome virus (WSSV) infections in penaeid shrimp. Aquaculture. 255, 95-104.

54. Sullivan, C.S., et al., 2005. SV40-encoded microRNAs regulate viral gene expression and reduce susceptibility to cytotoxic T cells. Nature. 435, 682-686.

55. Sun, X., Liu, Q.-h., Yang, B., Huang, J., 2016. Differential expression of microRNAs of *Litopenaeus vannamei* in response to different virulence WSSV infection. Fish Shellfish Immunol. 58, 18-23.

56. Tang, S., Patel, A., Krause, P.R., 2009. Novel less-abundant viral microRNAs encoded by Herpes Simplex Virus 2 latency-associated transcript and their roles in regulating ICP34.5 and ICP0 mRNAs. J. Virol. 83, 1433-1442.

57. Tang, S., et al., 2008. An acutely and latently expressed herpes simplex virus 2 viral microRNA inhibits expression of ICP34.5, a viral neurovirulence factor. Proc. Natl. Acad. Sci. 105, 10931-10936.

58. tenOever, B.R., 2013. RNA viruses and the host microRNA machinery. Nat Rev Micro. 11, 169-180.

59. Umbach, J.L., Cullen, B.R., 2009. The role of RNAi and microRNAs in animal virus replication and antiviral immunity. Genes Dev. 23, 1151-1164.

60. Umbach, J.L., et al., 2008. MicroRNAs expressed by herpes simplex virus 1 during latent infection regulate viral mRNAs. Nature. 454, 780-783.

61. Varkonyi-Gasic, E., Hellens, R., 2010. qRT-PCR of Small RNAs, Plant Epigenetics:Methods in Molecular Biology, Humana Press. pp. 109-122.

62. Wongpanya, R., et al., 2007. Analysis of gene expression in haemocytes of shrimp *Penaeus monodon* challenged with white spot syndrome virus by cDNA microarray. ScienceAsia. 33, 161-164.

63. Wongprasert, K., et al., 2003. Time-course and levels of apoptosis in various tissues of black tiger shrimp *Penaeus monodon* infected with white-spot syndrome virus. Dis. Aquat. Org. 55, 3-10.

64. Wu, J., et al., 2007. White spot syndrome virus proteins and differentially expressed host proteins identified in shrimp epithelium by shotgun proteomics and cleavable isotope-coded affinity tag. J. Virol. 81, 11681-11689.

Functional characterization of a cDNA encoding Piwi protein in *Penaeus monodon* and its potential roles in controlling transposon expression and spermatogenesis

Piwi proteins comprise a subfamily of Argonaute that plays a major role in germline development by association with a distinct class of small RNAs called Piwi interacting RNA (piRNA). Although the functions of Piwi in the development of germline cells as well as transposon regulation were reported in a number of mammalians and insects, developmental expression and function of Piwi subfamily in crustaceans is poorly known. This study is aimed at cloning and characterization of a Piwi cDNA in the black tiger shrimp, *Penaeus monodon*. The cDNA encoding a Piwi protein of *P. monodon* (PmPiwi1) was obtained by rapid amplification of cDNA ends (RACE). The PmPiwi1 coding cDNA contains 2811nt encoding a putative protein of 936 amino acids, and was specifically expressed in testis and ovary, suggesting its possible function in gametogenesis. RNAi experiment showed that suppression of PmPiwi1 expression led to a significant up-regulation of retrotransposon gypsy2 and DNA element transposon mariner in shrimp testis. Investigation of the function of PmPiwi1 in spermatogenesis by sperm count showed significantly lower number of sperms in the spermatophore sac of PmPiwi1-knockdown shrimp compared with that in the control shrimp. Our study thus reported for the first time the cDNA encoding a Piwi protein in the shrimp P. monodon. Its roles in controlling transposons and spermatogenesis as implied by the results in this study will be important for understanding sperm development and could be useful for the improvement of reproduction in male shrimp in the future.

Introduction

Argonaute is a central protein component of an RNA-induced silencing complex (RISC) in a small RNA-mediated gene silencing pathway called RNA interference (RNAi). Argonaute protein family is characterized by the presence of two major conserved domains: the PAZ domain that binds specifically to small non-coding RNAs, and the PIWI domain that forms a catalytic triad Asp-Asp-His (DDH) required for the cleavage of a target mRNA that is complementarily bound to the small RNA (Carmell et al., 2002; Niraj and Leemor, 2006; Olina et al., 2018; Peters and Meister, 2007). Phylogenetic analysis classifies proteins in the Argonaute family into Ago and Piwi subfamilies. The Ago subfamily is ubiquitously expressed and normally functions in association with small interfering RNAs (siRNAs) and/or micro RNAs (miRNAs). In contrast to the Ago subfamily, Piwi proteins exhibit a germline-specific expression pattern and bind to adistinct class of small RNA called PIWI interacting RNAs or piRNAs in germline cells (Carmell et al., 2002; Peters and Meister, 2007; Seto et al., 2007; Sheu-Gruttadauria and MacRae, 2017).

Piwi proteins and their small RNA partners, piRNAs are implicated in transcriptional gene expression, post-transcriptional gene regulation and transposon silencing that are important during germline development, particularly in spermatogenesis and oogenesis (Akkouche et al., 2017; Marie et al., 2017; Vagin et al., 2006). Loss of piwi causes defects in germ cell development in diverse organisms (Houwing et al., 2007; Ma et al., 2017a). Piwi is most studied in Drosophila, whose

genome codes for three Piwi members; Piwi, Aubergine (Aub) and Argonaute 3 (Ago3). Both Aub and Ago3 are cytoplasmic proteins that are restrictedly expressed in the germline granules called a nuage (Huang et al., 2014; Macdonald, 2001; Nagao et al., 2010). Aub-deficient flies displayed male sterility and maternal effect lethality (Ma et al. 2017b; Sahin et al., 2016; Schmidt et al., 1999). By contrast, Drosophila's Piwi seems to be predominantly expressed in the nucleus and is necessary for self-renewing division of germline stem cells in both males and females (Coxetal., 1998, 2000; Gonzalezetal.,2015). The depletion of Piwi led to infertility and axis specification defects in the developing egg chambers (Cox et al., 1998). In the mouse, Mus musculus, three members of Piwi have been identified namely Miwi, Mili and Miwi2. Miwi and Mili are expressed in both testis and oocyte. They are involved in meiotic regulation of spermatogenesis and oocyte development (Ding et al., 2013; Kabayama et al., 2017; Kuramochi-Miyagawa et al., 2001; Kuramochi-Miyagawa et al., 2004). On the other hand, Miwi2 is expressed in both germ cells and somatic cells, and is essential for maintaining germ-line stem cells (Carmell et al., 2007; Wasserman et al.,2017). Similarly, the two Piwiproteins ofzebrafish,Ziwiand Zili, are essential for germ line maintenance. Ziwi is abundantly expressed during both mitotic and early meiotic stages of germ cell differentiation, while Zili is involved in germ cell differentiation similar to the mouse Miwi2 (Houwing et al., 2007; Saskia Houwing, 2008). Like in other organisms, the expression of two Piwi proteins in the silkworm Bombyx mori, Siwi and BmAgo3, was found in germline cells. Both of them are abundantly expressed in testes and ovaries indicating that they might be involved in spermatogenesis and oogenesis in B. Mori (Kawaoka et al., 2008). Similarly, the regulation of spermatogenesis and oogenesis in the honey bee, Apis mellifera is regulated by two piwilike genes, Am-aub and Am-ago3 (Liao et al., 2010). Recently, genes encoding three crustacean Piwi proteins have been first identified in the crab *Portunus trituberculatus*. All of *P. trituberculatus'* piwi genes were expressed in adult testis, thus suggesting their functions during spermiogenesis (Xiang et al., 2014).

Recent studies have shown that piRNAs are central players in transposon silencing, which is particularly important for germ cell differentiation and genome maintenance during germline developmental process (Chambeyron etal., 2008; De Fazioetal., 2011; Teixeira et al., 2017). The piRNAs are primarily derived from transposons and other repeated elements by a proposed ping-pong model that involves the three Piwi proteins in *Drosophila* (Saitoetal., 2006; Wang and Elgin, 2011; Wang et al., 2015; Webster et al., 2015). The Piwi proteins are important for controlling transposon mobilization in germ cells. For examples, loss-of-miwi,-mili and -miwi2 mice exhibited transposon activation in germline that consequently resulted in germ cells deficiency (Carmell et al., 2007;Kabayama et al., 2017). In *Drosophila*, Piwi controlled expression and mobilization of retrotransposons. Mutationof piwi deregulates retrotransposon expression in the germline that finally led to embryonic defects (Akkouche et al., 2017; Kalmykova et al., 2005; Teixeira et al., 2017). Although Piwi proteins have been extensively studied in diverse organisms, but Piwi in crustacean is less known. To help fulfill our knowledge in the control of gonad development in this large subphylum of arthropods, we cloned and characterized a cDNA encoding a member of Piwi proteins from the black tiger shrimp, *Penaeus monodon.* The expression of PmPiwi during gonad developmental stage, its function in

controlling transposon expression and regulating spermatogenesis in the male germline of *P. monodon* were also investigated.

Materials and methods

Penaeus monodon samples

P. monodon were kindly provided by Shrimp Genetic Improvement Center, Surat Thani, Thailand. Male shrimps at three different maturation stages were used in this study: adolescent or immature shrimp about 4months old or approximately 20g bodyweight (bw) were defined as those forming spermatophores without sperm inside; sub-adult male shrimp were about 6months of age with approximately 40g bw; and adult male shrimp were over 10months old. Female shrimp were divided into five reproductive maturation stages based on histochemical staining with hematoxylin and eosin according to Tan-Fermin and Pudadera (1989). The experiments involving animals were carried out in accordance with animal and use protocol of the Mahidol UniversityInstitute Animal Care and Use Committee.

Cloning of a full-length Piwi cDNA of P. monodon (PmPiwi1)

Total RNA was extracted from the testis of P. monodon by TriSolution Plus Reagent (GMbiolab) as described in the manufacturer's protocol. Approximately 2μg of total RNA were used for cDNA synthesis by incubating with 0.5μM of oligo dT primer in a volume of 5μl followed by incubating at 70°C for 5min and cooling on ice for 5min. Then, the mixture containing 5× Improm pt II™ reaction buffer, 3mM MgCl2, 0.5mM each dNTP, and 1μl of Impromt II™ reverse transcriptase (Promega) was added, and the reaction was continued at 42°C for 60min, then at 70°C for 15min. One microliter of the cDNA was used as a template for amplification of the partial Piwi cDNA with specific primers PIWI-F4 and PIWI-R4 (Table 1) at 95°C for 5min followed by 35cycles of 95°C for 30s, 57°C for 30s, and 68°C for 30s.

The 3′ end of PmPiwi1 cDNA were obtained from the oligo-dTprimed first strand cDNA by 3′ RACE. The first amplification was performed with 3RACE1 primer designed from the partial Piwi cDNA obtained above and oligo-dT reverse primer. Subsequently, the nested PCR was performed using3′ inner primer 3RACE2 and PM1primer. The PCR profile for 3' RACE was as follows; initial denaturation at 95°C for 5min, annealing at 55°C for 30s and extension at 68°C for 2min 30s for 35cycles using Taq DNA polymerase (NEB® Inc.).

For 5′ RACE, the first strand cDNA was synthesized using specific reverse primerof PmPiwi1 (5RACE-R1), followed by tailing of poly A at its 3′ end using terminal deoxynucleotidyl transferase (Promega). The5′ cDNA of PmPiwi1 was obtained by three rounds of 5' RACE using the following temperature profile: initial denaturation at 95°C for 5min, annealing at 55°C for 30s and extension at 68°C for 2min 30s for 35cycles using Taq DNA polymerase (NEB® Inc.). Schematic diagrams of 3′ and 5′ RACE amplification are shown in Fig. 1, and all primers together with their nucleotide sequences are shown in Table 1.

The entire coding region of PmPiwi1 was obtained by amplification with coding-Fand coding-R primers using Expand High Fidelity enzyme (Roche) in a 25μl reaction containing 1× Expand High Fidelity buffer with MgSO4, 0.352mM dNTP and 0.3μM each primer. The amplification was carried out using the following temperature profile; denaturation at 94°C for 10s, annealing at 50°C for 30s and extension at 68°C

for 2min for 10cycles, followed by the second round of amplification with 25cycles of denaturation at 94°C for 15s, annealing at 50°C for 30s and extension at 68°C for 2min 20s. All the primers used and their nucleotide sequences are listed in Table 1. The amplified fragments were purified and cloned into pGEM®-T easy (Promega). The nucleotide sequences were determined by automated DNA sequencing (1st BASE DNA Sequencing Services, Singapore) and analyzed by Blast program (http://www.ncbi.nlm.nih.gov/blast).

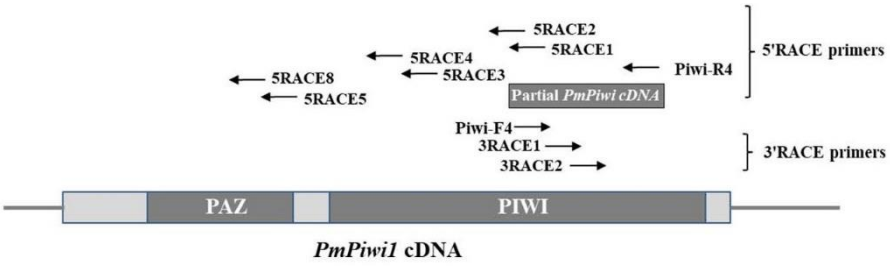

Fig. 1. A schematic diagram for 3′ and 5’ RACE of PmPiwi1 cDNA amplification.
Specific primers were designed from the partial Piwi cDNA sequence. A diagram represents the structure of PmPiwi1 cDNA and primers for cloning.

Table 1
Primers used in this study and their nucleotide sequences.

Primer name	Primer sequence (5′ to 3′)	Experiment
oligo dT	CCGGAATTCAAGCTTCTAGAGGATCCTTTTTTTTTTTTTTTT	Cloning, mRNA expression and detection of PmPiwi1 knockdown
PM1	CCGGAATTCAAGCTTCTAGAGGATCC	
Actin-F	GACTCGTACGTGGGCGACGAG	
Actin-R	AGCAGCGGTGGTCATCTCCTGCTC	
Piwi-F4	TACCGCGACGGCGTGAGCGAG	
Piwi-R4	CAAAAGCTAGTTTATGTGCAT	
5RACE1	TAACGAGCGTGATGCCGTCGTG	
5RACE2	CGAGTCGAAGTGCTGGAAGA	
5RACE3	AATACCGATCCTCACGCTGG	
5RACE4	ATGGAGCGTGTGACTTGTCG3	
5RACE5	GAGGATCCATTGACATTCCTGAC	
5RACE8	GCCAGATCTCTAGCTTGTGC	
Piwi1-3RACE1	GATCAGCACCAGGATCTT	
Piwi1-3RACE2	TGGCCTCAAGATCTCACTCC	
Coding-F1	ATGAAGGTGATATTCAGGAAGCG	
Coding-F2	ATGGATGGGGACCCAACTCC	
Coding-R	TCAGAGGAAGAAGAGCTTGTCA	
Sense-*Xba*I-F	GCTCTAGACCACGTGATTAAGGCTCTGG	dsRNA-PmPiwi1 synthesis
Sense-*Hind*III-R	CCCAAGCTTGGATCCATTGACATTCCTGAC	
dsPAZ-anti-*Xho*I-F	CCGCTCGAGCCACGTGATTAAGGCTCTGG	
dsPAZ-anti-Hind-R	CCCAAGCTTTGTCATGTAGCATAGCTCTGG	
MarinerF	CGGTTGGGAGAATAGGCAAATCA	Transposable elements expression
MarinerR	CCTTACAAACTGACGTTGATGGC	
GyPemo1bF	CTACAGCACCAACAACGTCCAA	
GyPemo1bR	CGTTTCCTCAAGCTGTATGAGGTG	
GyPemo2F	GATGCCTCAAACCTCGGGCT	
GyPemo2R	AGTGACGGAGGGCCCATGTG	
EF1αF	GAACTGCTGACCAAGATCGACAGG	
EF1αR	GAGCATACTGTTGGAGGTCTCCA	

Determination of PmPiwi1 expression in P. monodon

Adult male and female P. monodon (approximately 100g bw) were used for tissue distribution determination. Several tissues such as brain, gill, hepatopancreas, heart lymphoid, throracic ganglia, testis, vas deferens, spermatophore and ovary were dissected and sliced into small pieces. About 100mg of each tissue were homogenized in Trisolution Plus Reagent (GMbiolab), Approximately 2μg of total RNA from each tissue were used for cDNA synthesis with oligo dT as described above. The PmPiwi1 mRNA expression was determined by cDNA amplification with Coding-F1 and 5RACE-R5 primers by Taq DNA polymerase (NEB® Inc.) in a 25μl PCR reaction

using the PCR profile as previously described for the amplification of PmPiwi1 coding cDNA. Actin was used as an internal control. All primers were shown in Table 1.

The mRNA expression levels of PmPiwi1 in the ovary and testis at different developmental stages were determined by real-time PCR using KAPA SYBR® FAST qPCR kit (Kapa Biosystems) according to the manufacturer's protocol. The fluorescent signal was detected by Eppendorf Realplex (Eppendorf) machine. Relative expression level of PmPiwi1 was compared with that of the reference gene (elongation factor 1 alpha: Ef1α), and the data was analyzed by $2^{-\Delta\Delta CT}$ method.

Double-stranded RNA preparation

The recombinant plasmid harboring the PAZ domain region of PmPiwi1 cDNA was used as a template for PmPiwi1 dsRNA production. The dsRNA was synthesized as a stem-loop precursor in Escherichia coli expression system. The template of the sense (stem) strand was amplified with sense-Xba IeF and sense-Hind III-R primers, whereas the anti-sense (stem-loop) strand template was amplified with anti-Xho IeF and anti-Hind -R primers. The reaction was performed by 30cycles of denaturation at 95°C for 2min, annealing at 55°C for 30min and extension at 72°C for 1min using Pfu DNA polymerase (Thermo scientific). The sense and anti-sense template fragments were sequentially cloned into pET17b vector at the restriction sites corresponding to their termini. The pET17b vector harboring PmPiwi1 dsRNA template was expressed in E. coli strain HT115 with 0.4mM IPTG induction at 37°C for 4h. The PmPiwi1 dsRNA was extracted by TriSolution Plus Reagent with the addition of 5ng RNaseA to digest host single strand RNA and the loop region of the stem-loop dsRNA precursor. The quality of dsRNA was determined by RNase digestion assay with RNaseA and RNaseIII.

In vivo silencing of PmPiwi1

In order to investigate the function of PmPiwi1, its expression was first suppressed by dsRNA-mediated silencing. To demonstrate the potency of dsRNA to knockdown PmPiwi1 expression in the shrimp, male *P. monodon* approximately 50g bw (approximately 8months old) were injected with PmPiwi1-dsRNA (dsPiwi1) at 2.5μg·g−1 shrimp bw in a volume of 100μl. Shrimp injected with 150mM NaCl were used as a control group. The shrimp were injected twice on day 0 and day 7. Testes were collected on day14 after the first injection to determine silencing effect of dsRNA by detecting transcript levels of PmPiwi1 in the testis by RT-PCR with specific primers as shown in Table 1.

Effect of PmPiwi1 silencing on transposon expression level

The consequence of PmPiwi1 silencing on transposon expression was determined in the testis of PmPiwi1-silenced shrimp on day 14 after the first dsRNA injection. Three types of transposon elements i.e. two LTRretrotransposons; gypsy1 (Accession no. HF548819), gypsy2 (Accession no. HF548820.1) and DNA element transposon mariner (partially cloned in our laboratory, unpublished data) were examined. The expression level of each transposon was determined by real-time PCR with specific primers for each element as shown in Table 1 using KAPA SYBR® FAST qPCR kit (Kapa Biosystems) according to the manufacturer's protocol. The fluorescent signal was detected by Eppendorf Realplex (Eppendorf) machine. All samples were

analyzed in duplicate. Ef1α was used as reference gene, and the data was analyzed by $2^{-\Delta\Delta CT}$ method.

Determination of sperm numbers in PmPiwi1-silenced shrimp

According to Jiang et al. (2009), spermatophores and sperms in male P. monodon were first detected at 157days of age or about 21.7g bw. To ensure the formation of spermatophore, adult male shrimp approximately 11months old was used to determine the function PmPiwi1 in spermatogenesis. The shrimp were divided into 2 groups; the first group was injected with GFP-dsRNA (dsGFP) as a control group, and the second group was injected with dsPiwi1 (n=4 each). The dsRNA was injected at a dose of $2.5\mu g \cdot g^{-1}$ shrimp bw into the hemocoel at the base of the fifth pleopod. Previous study reported that spermatogenesis was related to molting cycle in P. monodon, and the newly formed spermatophores could be observed around day 3 after molt. Therefore, to investigate the function of PmPiwi1, male shrimps were injected on day 3 after molting (molting stage C-D0), and tissues (testes and spermatophores) were collected on day 3 after the next molt. One of the two spermatophores (theleftone) was collected andhomogenizedin1mlof Ca2+-free seawater (370mM NaCl, 15mM KCl, 8.5mM H3BO3, 4.75mM NaOH, 20mM MgSO4.7H2O, pH7.4) at 4°C. Then, 25μl of sperm suspension were mixed with 0.4% trypan blue and incubated at room temperature for 5min. After that, 15μl of the mixture were dropped on a hemacytometer, and the number of sperms were counted under light microscope. Data were analyzed using SPSS program. Differences between groups was analyzed by t-test at $P < .05$ as statistical significance. All experiments were repeated in triplicate.

Results

Cloning and characterization of Piwi1 cDNA in P. monodon

The full-length nucleotide sequence of PmPiwi1 cDNA was obtained by RACE strategy. The combined PmPiwi1 cDNA fragment is 2988bp in length with a 66bp 5′UTR, a putative 2811bp coding region and a 111bp 3′ UTR (GenBank accession no. MH279567). The continuous reading frame of PmPiwi1 was verified by RT-PCR. The deduced amino acid sequence of PmPiwi1 contains 936 residues with a predicted molecular weight of 105.31kDa and a theoretical isoelectric point of 9.36. Identification of conserved domains by ScanProsite program (prosite.expazy.org/scanprosite) revealed that PmPiwi1 contains the signature PAZ and PIWI domains of the Argonaute family (Supplementary Fig. S1). The predicted catalytic residues Asp-Asp-His (DDH) were also present at the C-terminal PIWI domain of PmPiwi1 similar to other members of the Argonaute family.

Comparison of similarity among PmPiwi1 and their homologues in other species shows that most of the similarities lay in the conserved PAZ and PIWI domains. Phylogenetic tree analysis revealed that PmPiwi1 was classified into the PIWI subfamily of Argonaute proteins and clustered in the same group as insect Ago3 with the closet relatedness to Piwi1 of the crab P. trituberculatus (Fig. 2).

Expression of PmPiwi1 in P. monodon

The expression of PmPiwi1 mRNA in *P. monodon* tissues was determined by RT-PCR. High levels of PmPiwi1 transcript were detected in the testis and, at a lower level, in the ovary but was not detected in other tissues (Fig. 3A). In order to investigate

further whether or not the expression of PmPiwi1 in the ovary changes upon ovarian development, the levels of PmPiwi1 transcript in the ovary at different developmental stages were determined by real-time PCR. The result in Fig. 3B showed that the expression levels of PmPiwi1were not significantly different throughout ovarian development from stage 0 to stage IV. In male shrimp, the expression levels of PmPiwi1 in the testis was rather constant from immature to adult shrimp (Fig. 3C).

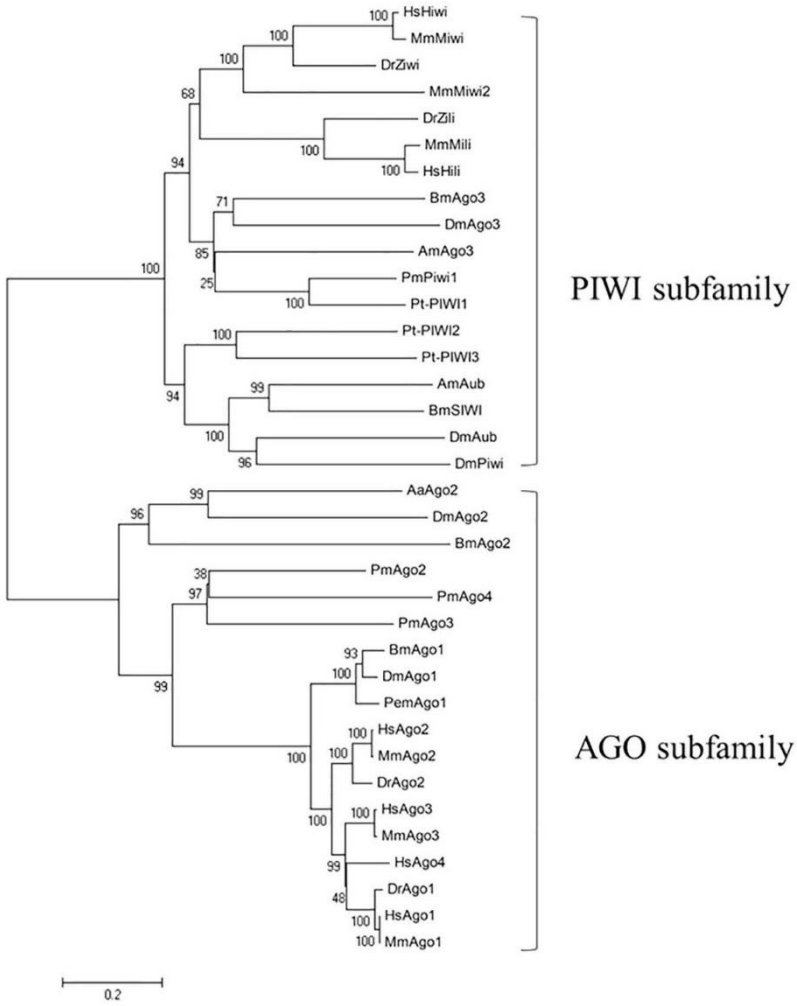

Fig. 2. Phylogenetic relationship among Piwi and Argonaute proteins. Phylogenetic tree was constructed by Mega4 Program using the neighbor-joining distance analysis. The amino acid sequences analyzed include Piwi and Argonaute proteins of *P. monodon*: PemAgo1 (ABG66640.1), PmAgo2 (AHB63227.1), PmAgo3 (AGC95229.1), PmAgo4 (AIE15914.1), PmPiwi1 (MH279567); B. mori: SIWI (AB372006), BmAgo1 (BAF73719.1) BmAgo2, (BAD91160.2), BmAgo3 (AB372007); D. melanogaster: DmPiwi (AAF53043.1), DmAub (AG18944.1), DmAgo1 (AAF58314.1), DmAgo2 (AAF49620.2), DmAgo3 (ABO27430.1); Aedes aegypti: AaAgo2 (ACR56327.1); A. mellifera: AmAub (GQ444142), AmAgo3 (GQ444137); P. trituberculatus: Pt-PIW1 (KC203335), Pt-PIWI2 (KC203336), Pt-PIWI3 (KC203337); D. rerio: Ziwi (NP899181.1), Zili (NP001073668.2), DrAgo1 (AFU66007.1), DrAgo2 (AFU66008.1); M. musculus: Miwi (AAL3104.1), Mili (BAA93706.1), Miwi2 (AAN75583.1), MmAgo1 (NP_700452.2), MmAgo2 (NP_694818.3), MmAgo3 (NP_700451.2); Homo sapiens: HsAgo1 (NP_036331.1), HsAgo2 (NP_036286.2), HsAgo3 (NP_079128.2), HsAgo4 (NP_060099.2), HsHiwi (AAC97371.2), HsHili (NP_001129193.1). Bootstrap values from 1000 replicates are indicated at the nodes.

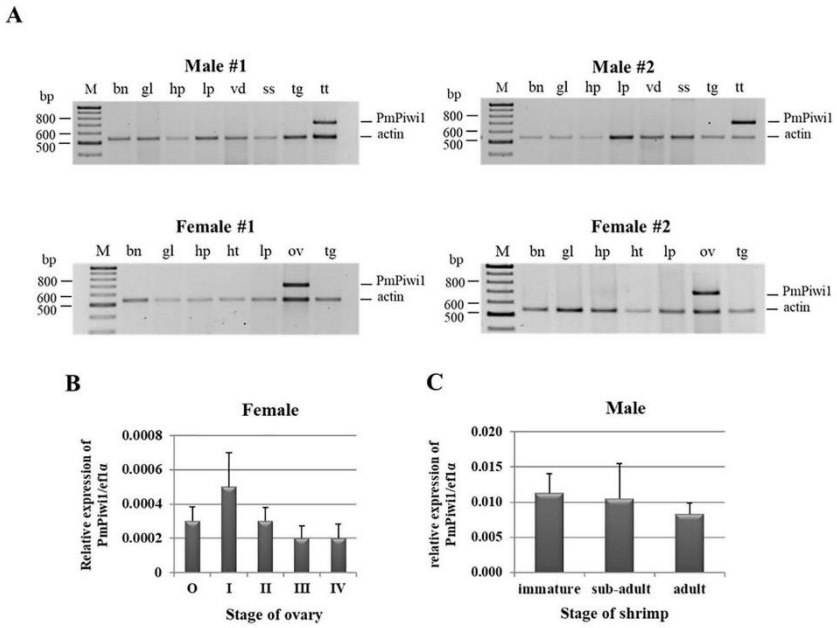

Fig. 3. Expression profile of PmPiwi1 in *P. monodon*. A) Tissue distribution of PmPiwi1 expression in P. monodon. The mRNA transcript levels of PmPiwi1 in eyestalk ganglia (Es), brain (Bn), gill (Gl), haemolymph (Hl), hepatopancreas (Hp), lymphoid organ (Lp), throracic ganglia (Tg), testis (Tt), sperm duct or vas deferens (Vd), spermatophore sac (Ss) and ovary (Ov) were detected by semi-quantitative RT-PCR. The level of actin transcript (550 bp) was also detected as an internal control. The pictures show the inverted images of ethidium bromide stained agarose gels of PmPiwi1 transcript in two male and two female shrimp. B) The expression levels of PmPiw1 in shrimp ovaries at different stages of ovarian development i.e. undeveloped stage (stage O), pre-developed stage (stage I), early-developed stage (stage II), late developed stage (stage III) and mature stage (stage IV) were determined by real-time PCR (n=4 each). Expression levels of PmPiwi1 relative to that of EF1α were analyzed by 2-ΔΔCt method and presented as mean ± SEM. C) The expression levels of PmPiwi1 in the testis of adolescent or immature, sub-adult and adult *P. monodon* (n=4 each) were determined by RT-PCR and analyzed as mentioned above.

Function of PmPiwi1 in transposon suppression

The efficiency of PmPiwi1 silencing by specific dsRNA was investigated in the testis of *P.monodon*. The injection with double dosages of dsPiwi1 at 2.5μg·g^{-1} bw on day 0 and day 7 showed the highest suppression of PmPiwi1, approximately 96%, at 14days post-injection (dpi.) (Fig. 4A). The expression of other Agos of *P. monodon* was not affected by dsPiwi1 (Fig. 4B), indicating the specificity of dsPiwi1 to knockdown its target transcript. To determine the influence of PmPiwi1 silencing on transposon expression in shrimp testis, the expression of PmPiwi1 was suppressed by dsPiwi1 for 14days as described above. The transcript levels of three types of transposons including two gypsy-like elements and a marinerlike element in PmPiwi1-knockdown shrimp were determined by realtime PCR. The results showed that the expression level of gypsy1 was slightly increased, while gypsy2 and mariner-like elements were significantly up-regulated in PmPiwi1-knockdown shrimp when compared with the control (Fig. 5).

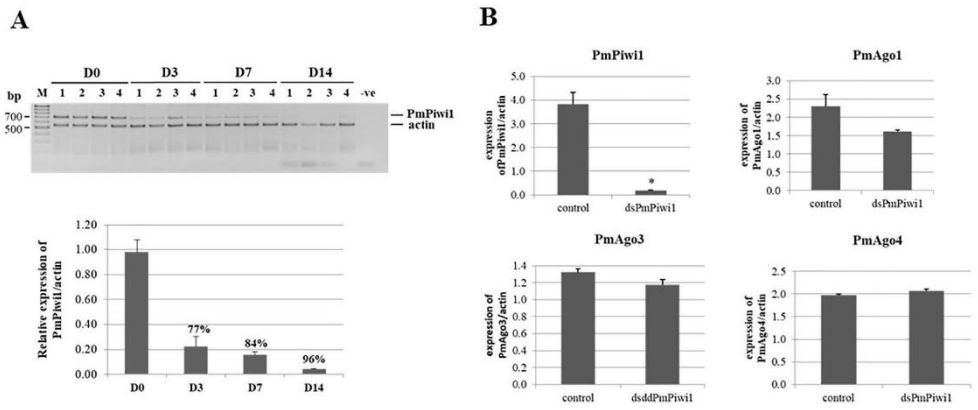

Fig. 4. Efficiency of PmPiwi1 suppression by dsPiwi1. A) The PmPiwi1 transcript levels in the testis of dsPiwi1-injected P. monodon at 14 dpi were determined by RT-PCR comparing to that of the control (NaCl injected shrimp). Actin transcript was amplified as an internal control. The intensity of each band of PmPiwi1 and actin transcripts on the ethidium bromide-stained agarose gel (upper panel) was determined by Scion-Image program and used for the calculation of the relative expression levels of PmPiwi1 and actin as shown in bar graph (lower panel). B) Specificity of PmPiwi1 suppression by dsPiwi1 is demonstrated by determination of the expression levels of PmAgo1, PmAgo3 and PmAgo4 cDNAs in dsPiwi1-injected shrimp compared with the control. An asterisk indicates statistical difference between groups as determined by Turkey's test of independent sample t-test from SPSS program ($p < .05$).

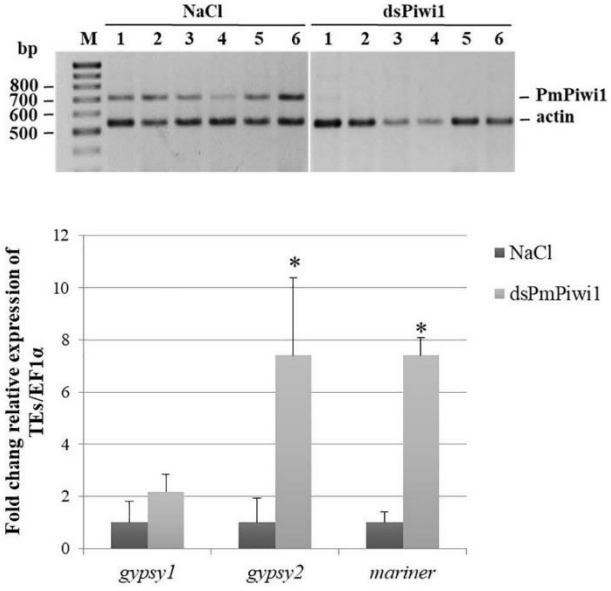

Fig. 5. Transposon expression in the testis of PmPiwi1-knockdown *P. monodon*. The expression of PmPiwi1 in the testis of *P. monodon* was suppressed by the injection of dsPiwi1 as determined by RT-PCR compared to that of the control (NaCl injected shrimp). Actin transcript was amplified as an internal control (upper panel). The expression levels of three types of transposons (gypsy1, gypsy2 and mariner-like elements) in the testis of PmPiwi1-knockdown shrimp and the control (NaCl-injected shrimp) were determined by real-time PCR (lower panel). Expression level of each transposon relative to that of Ef1α was analyzed by $2^{-\Delta\Delta Ct}$ method and shown as mean ± SEM ($n=6$). Asterisk indicates statistical difference between the PmPiwi1-knockdown and NaCl-injected groups as analyzed by t-test from SPSS program ($p < .05$).

Effect of PmPiwi1-knockdown on spermatogenesis in P. monodon

To investigate the function of PmPiwi1 in sperm production, male shrimp were injected withdsPiwi1at 2. 5μg·g− 1 bwonday3aftermolt, and the testes and spermatophores were collected on day 3 after the next molting. The efficiencies of PmPiwi1 knockdown in this experiment (Fig. 6A) were comparable to the previous experiment. The numbers of sperm deposited in the spermatophores of PmPiwi1-knockdown shrimp were significantly reduced when compared with that in the dsGFP-injected and the control group (Fig.6B). Moreover, the spermatophores of PmPiwi1-knockdown shrimp were apparently smaller than that of the control groups (Fig. 6C).

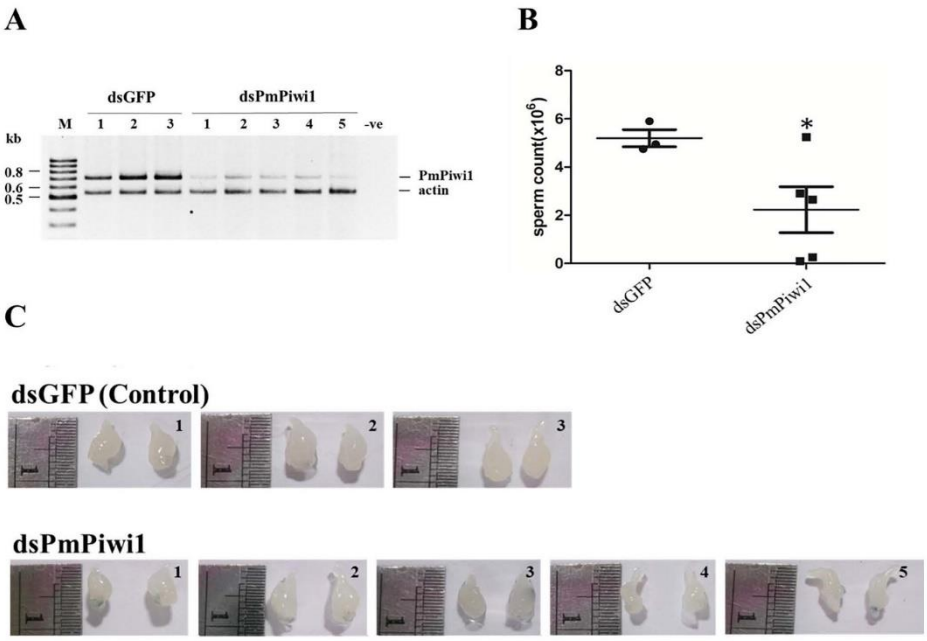

Fig. 6. Numbers of sperms in PmPiwi1-knockdown *P. monodon*. DsPiwi1 was injected into male P. monodon at 2.5 μg.g−1 bw on day 3 after molt, and the testes and spermatophores were collected on day 3 after the next molt. Shrimp injected with dsGFP were used as a control group. A) The efficiency of dsPiwi1 to knockdown PmPiwi1expression in the testis was determined by RT-PCR compared to the control shrimp. B) The numbers of sperms in the spermatophore of PmPiwi1-knockdown and the control shrimp were counted using the hemacytometer under microscope. Asterisk indicates statistical difference of sperm numbers between both groups as determined by One-way ANOVA from SPSS program ($\rho < 0.05$). C) Morphology of spermatophore of the PmPiwi1-knockdown shrimp (dsPmPiwi1) and dsGFP-injected shrimp (control) was compared.

Discussion

A cDNA encoding Piwi protein in the black tiger shrimp, *P. monodon* was identified and characterized. The alignment of the deduced amino acid sequences revealed that PmPiwi1 contained the conserved PAZ and PIWI domains, which are signature of the Argonaute family. Similarly to the PAZ domain of the Ago subfamily that forms a specific binding module for the 2-nt 3′ overhang of small RNAs generated by RNase III-like enzyme such as Dicer, the PAZ domain of the PIWI subfamily forms a binding pocket that anchors the exonuclease-trimmed 3′ end of piRNAs (Matsumoto et al., 2016). The PIWI domain has similar fold to RNaseH with the catalytic triad DDH that is essential for slicing activity of the Ago subfamily (Niraj and Leemor, 2006; Olina et al., 2018; Peters and Meister, 2007). In Drosophila, all three members of the PIWI

subfamily (Ago3, Aub and Piwi) also possess the conserved DDH residues in their PIWI domain. Whereas the nuclease catalytic triad of Ago3 and Aub was essential for the piRNA biogenesis pathway via the ping-pong cycle, it did not seem to be required for the function of Drosophila's Piwi in repressing transcription of its targets (Rozhkov et al., 2013). The PIWI domain of PmPiwi1 also contained the conserved DDH residues, indicating that PmPiwi1 could form a nuclease catalytic triad, possibly for cleavage of the substrate RNA complementary to the bound piRNAs.

One feature that distinguishes Piwi proteins from the Ago subfamily proteins is the presence of putative asymmetric dimethylated arginine residues (arginine-glycine/RG, arginine-alanine/RA) or symmetrically dimethylated arginine (sDMA) composing of arginine flanked by glycine (GRG) or alanine (GRA or ARG) repeats at the N-terminal region (Kirino et al., 2009; Vagin et al., 2009). Arginine methylation is an important post-transcriptional modification that mediates protein-protein interaction. Piwi proteins were reported to associate with multiple members of the Tudor protein family through sDMA methylation, which are necessary for piRNA function in transposon silencing and gametogenesis in both flies and mice (Kirino et al., 2010; Mathioudakis et al., 2012; Nishida et al., 2009; Vagin et al., 2009). The deduced PmPiwi1possesses multi-arginine methylation sites at the N-terminus, suggesting the potential to form heterodimeric complex with Tudor proteins and play role in the operation of piRNA pathway during germline development of the shrimp.

The restricted gonad expression of PmPiwi1 conforms to the expression and the role in germline development, a conserved function of Piwi proteins across species. Different types of Piwi may display distinct expression profiles during sperm development suggesting that they have diverse functions in different phases of spermatogenesis. For example, in the murine Mus musculus, Miwi2 was restricted expressed only in the testis (Carmell et al., 2007) whereas Miwi and Mili were detected in both testis and oocyte (Deng, 2002; Ding et al., 2013; Kabayama et al., 2017). Miwi is expressed from meiotic spermatocytes to elongating spermatids (Deng, 2002), whereas Mili is expressed from 3 dpp mitotically arrested prenatal germline stem cell to round spermatids (Kuramochi-Miyagawa et al., 2004; Unhavaithaya et al., 2009). Miwi-deficient mice show spermatogenesis arrest at early spermiogenic stage while Mili-deficient mice are terminally blocked at zygotene or early pachytene stages of meiotic prophase I (Beyret and Lin, 2011; Deng, 2002; Grivna et al., 2006; Kuramochi-Miyagawa et al., 2004). Miwi2 is detected from day 15.5 dpc to 3 dpp in mitotically arrested prenatal germline stem cells (Aravin et al.; Aravin et al., 2008). Miwi2 was also found in Sertoli cells, which are somatic supporting cells within seminiferous tubules (Carmell et al., 2007). Miwi2 mutants not only displayed a meiotic progression defect inearly prophaseof meiosis I but also seemed to affect mitotic germ cell maintenance (Wasserman et al., 2017). In addition, Miwi and Mili proteins were detected in mouse oocyte, implicating that it may also function in oocyte development (Ding et al., 2013; Kabayama et al., 2017). The function of Piwi was also required for germline stem cell maintenance and differentiation in Drosophila. The piwi mutant female showed ovarioles that are deficient in germline cells, whereas piwi mutant testis contained much fewer bundles of mature sperm. A novel group of pumilio mutations affects the asymmetric division of germline stem cells in the Drosophila ovary (Lin and Spradling, 1997). A mutation in aubergine, one of Drosophila's piwi genes also affected the mitotic cycle during oogenesis and led to loss of germline cells. Cutoff and

aubergine mutations result in retrotransposon upregulation and checkpoint activation in Drosophila (Chen et al., 2007).

In *P. monodon*, the significant decrease in the number of sperms in spermatophore of PmPiwi1-knockdown shrimp compared with that in the control shrimp indicated the function of PmPiwi1 during spermatogenesis. Recent report in the crab, P. trituberculatus, showed the expression of three piwi genes at different stages of spermtid and mature spermatozoon suggesting their roles in spermiogenesis (Xiang et al., 2014). Since PmPiwi1 transcript was detected in the testis but not in vas deferens and spermatophore, PmPiwi1 might be directly involved in meiotic regulation in spermatogenesis but not in sperm differentiation or sperm maturation. Although the gonad-specific expression of PmPiwi1 suggests its function in both sperm and oocyte development, the detail at which steps PmPiwi1 play a role in gametogenesis control in the shrimp remains tobe elucidated. Moreover, other Piwi proteinsin P. monodon that participate in piRNA biogenesis and reproductive regulation still await identification.

Piwi proteins have important function in the control of transposon in animal germline. Piwi knockout resulted in transposon activation, which led to germline defects. For example, derepression and up-regulation of endogenous retrotransposon copia was found in loss-of-Piwi Drosophila testes. Similarly, Drosophila Piwi mutant caused accumulation of mdg1 transcripts at the apical tip of testes where Piwi protein was not detected (Brennecke et al., 2007; Kalmykova et al., 2005). In the zebrafish, Zili mutant resulted in up-regulation of both retrotransposons and DNA transposable element (Saskia Houwing, 2008). The increased expression levels of gypsy LTR-retrotransposons and DNA element mariner in the PmPiwi1-knockdown testis of P. monodon in this study suggested the function of PmPiwi1 in the control of transposable elements in shrimp testis. Another member of Argonaute proteins, namely PmAgo4, that is highly expressed in P. monodon's germline was also demonstrated to regulate transposable elements in shrimp testis (Leebonoi et al., 2015). Whether or not PmPiwi1 works in cooperation with PmAgo4 to protect shrimp germ cells from deleterious effects of excessive movement of transposable elements during gamete development needs further investigation. In addition, piRNA biogenesis and transposable elements activation in Drosophila and mice are known to be regulated bythree members of Piwi proteins (Brennecke et al., 2007; Manakov et al., 2015; Rozhkov et al., 2013; Saito et al., 2006). Three types of Piwi transcripts were also identified in the crab, P. trituberculatus (Xiang et al., 2014). Therefore, identification of additional members of Piwi in *P. monodon* still awaits exploration.

In conclusion, a novel cDNA encoding PmPiwi1 in P. monodon was identified. Its gonad-specific expression was correlated with potential roles in sperm production and regulation of transposable elements in shrimp testis. The possibility that PmPiwi1 functions together with PmAgo4 and other Piwi members to maintain integrity of shrimp germ cells from transposition effects as has been demonstrated in anumber of organisms needs to be elucidated.

Supplementary data to this article can be found online at https://doi.org/10.1016/j.cbpa.2018.11.022.

References

1. Akkouche, A., et al., 2017. Piwi is required during Drosophila embryogenesis to license dual-strand piRNA clusters for transposon repression in adult ovaries. Mol. Cell 66 (3), 411–419.
2. Aravin, A.A., et al., 2008. A piRNA pathway primed by individual transposons is linked to de novo DNA methylation in mice. Mol. Cell 31 (6), 785–799.
3. Beyret, E., Lin, H., 2011. Pinpointing the expression of piRNAs and function of the PIWI protein subfamily during spermatogenesis in the mouse. Dev. Biol. 355 (2), 215–226.
4. Brennecke, J., et al., 2007. Discrete small RNA-generating loci as master regulators of transposon activity in Drosophila. Cell 128 (6), 1089–1103.
5. Carmell, M.A., Xuan, Z., Zhang, M.Q., Hannon, G.J., 2002. The Argonaute family: tentacles that reach into RNAi, developmental control, stem cell maintenance, and tumorigenesis. Genes Dev. 16 (21), 2733–2742.
6. Carmell, M.A., et al., 2007. MIWI2 is essential for spermatogenesis and repression of transposons in the mouse male germline. Dev. Cell 12 (4), 503–514.
7. Chambeyron, S., et al., 2008. piRNA-mediated nuclear accumulation of retrotransposon transcripts in the Drosophila female germline. Proc. Natl. Acad. Sci. U. S. A. 105 (39), 14964–14969.
8. Chen, Y., Pane, A., Schupbach, T., 2007. Cutoff and aubergine mutations result in retrotransposon upregulation and checkpoint activation in Drosophila. Curr. Biol. 17 (7), 637–642.
9. Cox, D.N., Chao, A., Lin, H., 2000. piwi encodes a nucleoplasmic factor whose activity modulates the number and division rate of germline stem cells. Development 127, 503–514.
10. Cox, D.N., et al., 1998. A novel class of evolutionarily conserved genes defined by piwi are essential for stem cell self-renewal. Genes Dev. 12 (23), 3715–3727.
11. De Fazio, S., et al., 2011. The endonuclease activity of Mili fuels piRNA amplification that silences LINE1 elements. Nature 480 (7376), 259–263.
12. Deng, W., Lin, H., 2002. miwi, a Murine homolog of piwi, encodes a cytoplasmic protein essential for spermatogenesis. Dev. Cell 2, 819–830.
13. Ding, X., Guan, H., Li, H., 2013. Characterization of a piRNA binding protein Miwi in mouse oocytes. Theriogenology 79 (4), 610–615.
14. Gonzalez, J., Qi, H., Liu, N., Lin, H., 2015. Piwi is a key regulator of both somatic and germline stem cells in the Drosophila testis. Cell Rep. 12 (1), 150–161.
15. Grivna, S.T., Pyhtila, B., Lin, H., 2006. MIWI associates with translational machinery and PIWI-interacting RNAs (piRNAs) in regulating spermatogenesis. Proc. Natl. Acad. Sci. U. S. A. 103 (36), 13415.
16. Houwing, Saskia, Berezikov, Eugene, Ketting, R.F., 2008. Zili is required for germ cell differentiation and meiosis in zebrafish. EMBO J. 27, 2702–2711.
17. Houwing, S., et al., 2007. A role for Piwi and piRNAs in germ cell maintenance and transposon silencing in Zebrafish. Cell 129 (1), 69–82.
18. Huang, H., et al., 2014. AGO3 Slicer activity regulates mitochondria–nuage localization of Armitage and piRNA amplification. J. Cell Biol. 206 (2), 217–230.
19. Jiang, S.-G., et al., 2009. Observations of reproductive development and maturation of male *Penaeus monodon* reared in tidal and earthen ponds. Aquaculture 292 (1–2), 121–128.

20. Kabayama, Y., et al., 2017. Roles of MIWI, MILI and PLD6 in small RNA regulation in mouse growing oocytes. Nucleic Acids Res. 45 (9), 5387–5398.

21. Kalmykova, A.I., Klenov, M.S., Gvozdev, V.A., 2005. Argonaute protein PIWI controls mobilization of retrotransposons in the Drosophila male germline. Nucleic Acids Res. 33 (6), 2052–2059.

22. Kawaoka, S., Minami, K., Katsuma, S., Mita, K., Shimada, T., 2008. Developmentally synchronized expression of two Bombyx mori Piwi subfamily genes, SIWI and BmAGO3 in germ-line cells. Biochem. Biophys. Res. Commun. 367 (4), 755–760.

23. Kirino, Y., et al., 2009. Arginine methylation of Piwi proteins catalysed by dPRMT5 is required for Ago3 and Aub stability. Nat. Cell Biol. 11 (5), 652–658.

24. Kirino, Y., et al., 2010. Arginine methylation of Aubergine mediates Tudor binding and germ plasm localization. RNA 16 (1), 70–78.

25. Kuramochi-Miyagawa, S., et al., 2001. Two mouse piwi-related genes; miwi and mili. Mech. Dev. 108, 121–133.

26. Kuramochi-Miyagawa, S., et al., 2004. Mili, a mammalian member of piwi family gene, is essential for spermatogenesis. Development 131 (4), 839–849.

27. Leebonoi, W., Sukthaworn, S., Panyim, S., Udomkit, A., 2015. A novel gonad-specific Argonaute 4 serves as a defense against transposons in the black tiger shrimp *Penaeus monodon*. Fish Shellfish Immunol 42 (2), 280–288.

28. Liao, Z., Jia, Q., Li, F., Han, Z., 2010. Identification of two piwi genes and their expression profile in honeybee, Apis mellifera. Arch. Insect Biochem. Physiol. 74 (2), 91–102.

29. Lin, H., Spradling, A.C., 1997. A novel group of pumilio mutations affects the asymmetric division of germline stem cells in the Drosophila ovary. Development 124 (12), 2463.

30. Ma, X., et al., 2017a. Piwi1 is essential for gametogenesis in mollusk Chlamys farreri. PeerJ 23 (5).

31. Ma, X., et al., 2017b. Aubergine controls germline stem cell self-renewal and progeny differentiation via distinct mechanisms. Dev. Cell 41 (2), 157–169.e5.

32. MacDonald, P.M., Harris, A.N., 2001. aubergine encodes a Drosophila polar granule component required for pole cell formation and related to elF2C. Development 128, 2823–2832.

33. Manakov, Sergei, A., 2015. MIWI2 and MILI have differential effects on piRNA biogenesis and DNA methylation. Cell Reports 12 (8), 1234–1243.

34. Marie, P.P., Ronsseray, S., Boivin, A., 2017. From embryo to adult: piRNA-mediated silencing throughout germline development in Drosophila. G3 7 (2), 505–516.

35. Mathioudakis, N., et al., 2012. The multiple Tudor domain-containing protein TDRD1 is a molecular scaffold for mouse Piwi proteins and piRNA biogenesis factors. RNA 18 (11), 2056–2072.

36. Matsumoto, N., et al., 2016. Crystal structure of silkworm PIWI-clade Argonaute Siwi bound to piRNA. Cell 167 (2), 484–497 (e9).

37. Nagao, A., et al., 2010. Biogenesis pathways of piRNAs loaded onto AGO3 in the Drosophila testis. RNA 16 (12), 2503–2515.

38. Niraj, H.T., Leemor, J.-T., 2006. Slicer and the Argonautes. Nat. Chem. Biol. 3 (1), 36–43.

39. Nishida, K.M., et al., 2009. Functional involvement of Tudor and dPRMT5 in the piRNA processing pathway in Drosophila germlines. EMBO J. 28 (24), 3820–3831.

40. Olina, A.V., Kulbachinskiy, A.V., Aravin, A.A., Esyunina, D.M., 2018. Argonaute proteins and mechanisms of RNA interference in eukaryotes and prokaryotes. Biochem. Mosc. 83 (5), 483–497.

41. Peters, L., Meister, G., 2007. Argonaute proteins: mediators of RNA silencing. Mol. Cell 26 (5), 611–623.

42. Rozhkov, N.V., Hammell, M., Hannon, G.J., 2013. Multiple roles for Piwi in silencing Drosophila transposons. Genes Dev. 27 (4), 400–412.

43. Sahin, H.B., et al., 2016. Novel mutants of the aubergine gene. Fly 10 (2), 81–90.

44. Saito, K., et al., 2006. Specific association of Piwi with rasiRNAs derived from retrotransposon and heterochromatic regions in the Drosophila genome. Genes Dev. 20 (16), 2214–2222.

45. Schmidt, A., et al., 1999. Genetic and molecular characterization of sting, a gene involved in crystal formation and meiotic drive in the male germ line of Drosophila melanogaster. Genetics 151, 749–760.

46. Seto, A.G., Kingston, R.E., Lau, N.C., 2007. The coming of age for Piwi proteins. Mol. Cell 26 (5), 603–609.

47. Sheu-Gruttadauria, J., MacRae, I.J., 2017. Structural foundations of RNA silencing by Argonaute. J. Mol. Biol. 429 (17), 2619–2639.

48. Tan-Fermin, J.D., Pudadera, R.A., 1989. Ovarian maturation stages of the wild giant tiger prawn, Penaeus monodon Fabricius. Aquaculture 77 (2–3), 229–242.

49. Teixeira, F.K., et al., 2017. piRNA-mediated regulation of transposon alternative splicing in the soma and germ line. Nature 552 (7684), 268–272.

50. Unhavaithaya, Y., et al., 2009. MILI, a PIWI-interacting RNA-binding protein, is required for germ line stem cell self-renewal and appears to positively regulate translation. J. Biol. Chem. 284 (10), 6507–6519.

51. Vagin, V.V., et al., 2006. A distinct small RNA pathway silences selfish genetic elements in the germline. Science 313 (5785), 320–324.

52. Vagin, V.V., et al., 2009. Proteomic analysis of murine Piwi proteins reveals a role for arginine methylation in specifying interaction with Tudor family members. Genes Dev. 23 (15), 1749–1762.

53. Wang, S.H., Elgin, S.C., 2011. Drosophila Piwi functions downstream of piRNA production mediating a chromatin-based transposon silencing mechanism in female germ line. Proc. Natl. Acad. Sci. U. S. A. 108 (52), 21164–21169.

54. Wang, W., et al., 2015. Slicing and binding by Ago3 or Aub trigger Piwi-bound piRNA production by distinct mechanisms. Mol. Cell 59 (5), 819–830.

55. Wasserman, G.A., et al., 2017. Expression of Piwi protein MIWI2 defines a distinct population of multiciliated cells. J. Clin. Invest. 127 (10), 3866–3876.

56. Webster, A., et al., 2015. Aub and Ago3 are recruited to nuage through two mechanisms to form a Ping-Pong complex assembled by Krimper. Mol. Cell 59 (4), 564–575.

57. Xiang, D.F., Zhu, J.Q., Hou, C.C., Yang, W.X., 2014. Identification and expression pattern analysis of Piwi genes during the spermiogenesis of Portunus trituberculatus. Gene 534 (2), 240–248.

Regulation of vitellogenin gene expression under the negative modulator, gonad-inhibiting hormone in *Penaeus monodon*

Vitellogenesis is a principal process during ovarian maturation in crustaceans. This process is negatively regulated by gonad-inhibiting hormone (GIH), a neuronal peptide hormone from eyestalks. However, the detailed mechanism through which GIH regulates Vg expression is still ambiguous. In this study, suppression subtractive hybridization (SSH) under specific GIH-knockdown condition was utilized to determine the expression of genes in the ovary that may act downstream of GIH to control vitellogenin synthesis in Penaeus monodon. The total of 102 and 82 positive clones of up-regulated and down-regulated genes in GIH-knockdown shrimp were identified from the forward and reverse SSH libraries, respectively. Determination of the expression profiles of these reproduction-related genes during ovarian development revealed that the expression of calreticulin (CALR) was significantly reduced in vitellogenic ovary suggesting its role in vitellogenesis. Suppression of CALR by specific dsRNA showed elevated vitellogenin (Vg) transcript level in the ovary at day 7 post-dsRNA injection. Since CALR can bind to steroid hormone receptors and prevents the binding of the receptor to its responsive element to regulate gene expression, it is possible that CALR is an inhibitory mediator of vitellogenin synthesis via steroidal pathway. Our results posted a possible novel pathway of GIH signaling that might interfere the steroid signaling cascade to mediate Vg synthesis in the shrimp.

Introduction

Vitellogenesis is essential for ovarian maturation in crustaceans. This process can be divided into two phases: the synthesis of a yolk precursor, vitellogenin (Vg) and the accumulation of a yolk protein or vitellin (Vn) into oocytes. In the black tiger shrimp Penaeaus monodon, Vg is synthesized in both the ovary and hepatopancreas like in other penaeid shrimps (Tiu et al., 2006). Following its synthesis, the Vg precursor is proteolytically cleaved into smaller subunits by enzymes of the subtilisin family in the hemolymph. The processed Vg is subsequently deposited into developing oocytes before undergoing further biochemical modifications into vitellin that is a major source of nutrient during embryogenesis (Tiu et al., 2008; Wilder et al., 2010). Vitellogenesis in crustaceans is negatively influenced by a gonad-inhibiting hormone (GIH), which is well characterized in a number of crustaceans (Yang and Rao, 2001; Edomi et al., 2002; Treerattrakool et al., 2008; Chen et al., 2014). GIH is a member of type II crustacean hyperglycemic hormone family that is synthesized and stored in the X-organ-sinus gland complex in the eyestalks. The mature peptide of GIH consists of 78–83 amino acid residues with the predicted molecular weight of 8–9 KDa (Treerattrakool et al., 2008; Webster et al., 2012). Detection of GIH peptide in the hemolymph revealed high levels of GIH during immature stage before rapidly declined in later stages of ovarian maturation cycle (de Kleijn et al., 1998; Okumura et al., 2007; Urtgam et al., 2015). Oppositely, Vg levels in the hemolymph as well as Vg mRNA levels in both hepatopancreas and ovary were almost undetectable at the immature stage, then sharply increased in vitellogenic stage and maintained at relatively high levels throughout the rest of ovarian maturation cycle (Longyant et al., 2003; Kang et al., 2014).

Recent studies demonstrated that, ovarian maturation in P. monodon could be induced when the GIH expression was suppressed by a specific double-stranded RNA (Treerattrakool et al., 2011), and neutralization of GIH peptide by monoclonal antibody against the recombinant GIH (Treerattrakool et al., 2014) also gave rise to ovarian maturation. These results suggest that GIH retards ovarian maturation via inhibition of Vg expression. However, the detailed mechanism through which GIH regulates Vg expression is not well studied.

In order to understand the molecular basis underlying vitellogenesis regulation in the shrimp, we investigated differential gene expression in the ovary of P. monodon under GIH silencing by suppression subtractive hybridization. The expression pattern during ovarian maturation of calreticulin (CALR), one of the genes that were significantly downregulated upon GIH deprivation, and its possible involvement in the control of Vg expression were determined. The understanding of the control mechanism of vitellogenesis via GIH-mediated pathway will be useful for hormonal manipulation methods to achieve efficient improvement of shrimp reproductive performance in the future.

Materials and methods

Shrimp sample

Immature and previtellogenic female shrimp were kindly provided by the Shrimp Genetic Improvement Center, Suratthani, Thailand. Vitellogenic shrimp were caught from the Andaman sea in the southern part of Thailand. The shrimp were acclimatized in 30 ppt sea water at 28 °C at the aquaculture unit, Institute of Molecular Biosciences, Mahidol University until used.

Silencing of PmGIH using dsRNA interference

To investigate the differential ovarian gene expression under specific GIH-knock down condition in female shrimp, the GIH-specific double-stranded RNA (GIH-dsRNA) was synthesized in Escherichia coli as described earlier (Treerattrakool et al., 2008). Previtellogenic female shrimp (approximately 85–120 g) were injected with 0.3 μg. g− 1 shrimp bodyweight (bw.) at the base of eyestalks. Shrimp injected with GFPdsRNA were used as the control group (n = 3). The shrimp were cultured in 30 ppt sea water at 28 °C for 5 days. Then, the expression of GIH in the eyestalk and Vg in the ovary of the shrimp in each group were determined by RT-PCR.

Detection of transcript levels by RT-PCR

Shrimp eyestalk ganglia and ovaries were freshly dissected and homogenized in TRI-Reagent® (Molecular Research Center). The RNA was extracted according to the manufacturer's protocol, and analyzed by NanoDropTM 1000 Spectrophotometer and 2% agarose gel electrophoresis.

The first strand cDNA was synthesized from 1.5 μg of total RNA sample with PRT-oligo-dT12 primer, and reverse transcriptase using the following condition: 25 °C for 5 min, 42 °C for 60 min, and 70 °C for 15 min. The suppression of GIH transcript in the eyestalk ganglia was determined by PCR in a 25 μl-reaction containing 1 μl of the first strand cDNA, 0.5 μM each of GIH1-F and 3UTR-PmGIHR1 primers, 0.5 mM of dNTPs, 1× Taq buffer, and 1.25 U of Taq DNA polymerase (New England BioLab). The PCR reaction was subjected to the following temperature profile: 94 °C for 2 min;

35 cycles of 94 °C for 15 s; 55 °C for 15 s; 68 °C for 2 min, and a final extension at 72 °C for 3 min. The transcript of Vg gene in the ovary of GIH-dsRNA treated shrimp and GFP-dsRNA treated shrimp was also determined by RT-PCR using the above condition except that Vg-F1 and Vg-R1 primers were used instead. The actin transcript was amplified as an internal control using PmActin-F and PmActin-R primers with 21 cycles of 94 °C for 30 s, 55 °C for 30 s and 74 °C for 1 min followed by 74 °C for 7 min. The amplicons of GIH, Vg, and actin with the expected sizes of 360, 380 and 550 bp, respectively were analyzed by 1.5% agarose gel electrophoresis.

Construction of suppression subtractive hybridization (SSH) library

dsRNA-mediated GIH silencing, changes in gene expression in the ovary of the GIH-knockdown shrimp were determined by suppression subtractive hybridization (SSH). One milligram of total RNA from three individual shrimp in either GIH-dsRNA or GFP-dsRNA treated group were pooled, and poly A+ RNA was isolated using poly A+ Spin™ mRNA isolation kit (New England Biolabs) according to manufacturer's protocol. Then, 1.5 μg of the poly A+ RNA from each group were used to construct forward and reverse cDNA libraries using a PCR-select™ cDNA subtraction kit (Clonetech). Briefly, the cDNA synthesized from the poly A+ RNA of the GFP-dsRNA treated and GIH-dsRNA treated shrimps were digested with Rsa I to generate the blunt-ended cDNA fragments. In order to obtain the genes that were up-regulated upon GIH-knockdown condition, the Rsa I-digested cDNA from GFP-dsRNA treated shrimp was used as a driver, while the Rsa I-digested cDNA from GIH-dsRNA treated shrimp was ligated to adaptors and used as the tester. After hybridization and amplification as mentioned in the manufacturer's protocol, this library was referred to as a forward library. Vice versa, the reverse library was constructed by using the Rsa Idigested cDNA from GIH-dsRNA treated shrimp as a driver and the Rsa I-digested cDNA from GFP-dsRNA treated shrimp as a tester to determine the genes that were down-regulated upon GIH-knockdown condition. The efficiency of SSH was analyzed using actin gene amplification.

The subtracted mixture was nested amplified, cloned into the pGEM-T Easy vector (Promega), and introduced into E. coli strain DH5α by transformation. All the transformants were selected on X-gal/IPTG agar plates and screened by EcoR I digestion. The nucleotide sequences of the subtracted libraries were determined by automated DNA sequencing at 1st BASE Laboratories Sdn Bhd, Malaysia.

Analysis of cDNA from SSH libraries by bioinformatics

The cDNA fragments obtained from subtractive libraries were analyzed and processed by removing the unwanted vector and primer sequences using the Bio-Edit program and NCBI VecScreen. Homologs of known sequences were searched by the blastn and blastx programs against NCBI GenBank database (http://www.ncbi.nlm.nih.gov/BLAST) for clone annotation. The significant matches were accepted at E-values lower than $1 \times 10{-}7$.

Validation of the expression of responsive genes upon GIH suppression

The expression of the genes of interest from forward and reverse SSH libraries were verified by quantitative reverse transcription PCR (RT-qPCR). The dilution of 1:5 of cDNA from the ovary of either GIHdsRNA-injected shrimp or GFP-dsRNA-

injected shrimp were used in the amplification of gene transcripts with 0.2 pmol of each gene specific primer, (Table 1) using KAPA SYBR® FAST qPCR kit (KAPABIOSYSTEMS, USA) according to the manufacture's protocol. The reactions were subjected to ABI® Prism 7500 with the following temperature profile; 95 °C for 3 min then 40 cycles of 95 °C for 5 s and 60 °C for 30 s. The EF-1α gene was amplified with 0.1 pmol of each gene- specific primer, and used as an internal control. The melting curve of the amplification products was analyzed by subsequent dissociation process at 95 °C for 15 s, followed by annealing at 60 °C for 15 s, then gradually increased for 10 s each at 0.2 °C increment to 95 °C (Fig. A.1). The amplification of each gene was done in triplicate. The amount of relative gene transcript levels was calculated using $2^{-\Delta\Delta Ct}$ method according to Livak and Schmittgen (2001). The efficiency of each primer pair was analyzed by the standard curve generated in triplicate with 5 different cDNA concentrations prepared by 2- fold serial dilution. The relative expression was calculated using a mathematic model of Pfaffl (2001).

Table 1
Primers use in this study.

Primer	Sequences (5′-3′)	size	Usage
PRT	CCGGAATTCAAGCTTCTAGAGGATCCTTTTTTTTTTTTTTT		cDNA synthesis
GIH1-F	GTGGTGGGAGCGCAGCTTAGCT	360	GIH gene silencing and Vg expression
3UTR-PmGIHR1	TCT CCCCCCTGCGCTAGGATCCCG		
Vg-F1	CTAAGGCAATTATCACTGCTGCT	380	
Vg-R1	AAGCTTGGCAATGTATTCCTTTT		
PmActin-F	GACTCGTACGTCGGGCGACGAGG	550	
PmActin-R	AGCAGCGGTGGTCATCACCTGCTC		
TSP-F	GGCAGCACTGCTTTGGCATGA	114	The genes obtained by SSH and validation
TSP-R	ACCCTGGTACAAGTAGAACCTAATGG		
Per1-F	GCTTGGTGGCGTGTTGCAG	160	
Per1-R	GGCCTGGACACAAGTTATCAGGG		
qVg-F	TCCATCTGCAGCACCAATCTTCGC	174	
qVgR	GCAACAGCCTTCATTCTGATGCCA		
CALR-F	CCAGACTGGACAGGATGCCC	187	
CALR-R	GGTATGGCGACTCTCCGTGC		
Sap-F	CGTCCCTTTCCAACAGGTGC	236	
Sap-R	GGAGAGCATCCAGCTTGGAC		
ANT-F	CGAGCGAAGTCAAGGGGGTAG	177	
ANT-R	CCGATATTTCCCCACCCAGGC		
EF1α-F	GAACTGCTGACCAAGATCGACAGG	140	
EF1α-R	GAGCATACTGTTGGAAGGTCTCCA		
PmCALR-F	ATGAAGACCTGGGTTTTTCTTGCC	1221	CALR-dsRNA construction and CALR gene silencing
PmCALR-R	TTACAGCTCGTCATGTTCAAGATCATTATCAAG		
SL-NCALR F-*Xba*I	GCTCTAGACGACAGCCCAGATTGGGAG	511	
SL-NCALR R-*Bam*HI	CGGGATCCCTCGAGTTCACCAGACTGAGC		
ST-NCALR F-*Xho*I	CGCTCGAGCGACAGCCCAGATTGGGAG	431	
ST-NCALR R-*Bam*HI	CGGGATCCGATGGGAAAATACGTCATCCTTGC		
3CALR-F	GGGTGAATGGAAGCCTAAGCAG		

Relative quantification of gene expression levels in the ovary during ovarian maturation

Ovarian maturation was divided into four stages as determined by ovarian size and color, gonado- somatic index (GSI) as well as by histochemical staining with hematoxylin and eosin based on Tan- Fermin and Pudadera (1989). Ovary from the shrimp at each stage of ovarian development (n = 3–5) was dissected for total RNA isolation by Tri Reagent® (Molecular Research Center). Approximately 1.5 μg of the total RNA was subjected to reverse transcription reaction with oligo- dT primer as described in 2.3. The cDNA from shrimp at each ovarian maturation stage was used for amplification of the selected genes by RT-qPCR as described in 2.6.

Production of calreticulin specific double-stranded RNA (CALRdsRNA)

Calreticulin (PmCALR) is probably involved in the regulation of Vg synthesis because its expression was down-regulated under GIHknockdown condition. The RNA interference (RNAi) gene silencing was chosen as an approach to investigate the function of PmCALR in this study. The PmCALR cDNA was amplified from shrimp

ovary using specific primers designed from the ORF of PmCALR (Visudtiphole et al., 2010) in a reaction containing 1 μl of first-stranded cDNA from shrimp ovary, 0.3 mM of dNTPs, 1× long range buffer, 1.75 mM MgCl2, 0.5 μM PmCALR-F primer, 0.5 μM PmCALR-R primer and 1.25 U KAPA Long-Range DNA polymerase in a total volume of 25 μl. The PCR reaction was carried out with the following temperature profile: 94 °C for 2 min; then 35 cycles of 94 °C for 15 s; 55 °C for 15 s; 68 °C for 2 min, and a final extension at 72 °C for 3 min.

After verification of the nucleotide sequence, the plasmid harboring PmCALR cDNA was used as a template to design specific dsRNA targeting the N-terminal domain, and produced in a bacterial expression system. Briefly, a DNA template for the 511 bp stem-loop template of dsRNA was amplified with primers SL-NCALR F-Xba I, and SL-NCALR RBamH I, while the DNA template for the 431 bp stem of dsRNA was amplified with primers ST-NCALR F-EcoR I and ST-NCALR R-BamH I. The stem-loop fragment was first cloned into pET17b vector at Xba I and BamH I sites, following by the stem fragment at EcoR I and BamH I site. Then, the recombinant NCALR-pET17b expression cassette was used to transform E. coli strain DH5α. After verification of the nucleotide sequence, the plasmid of the correct clone was transformed to E. coli strain HT115. The expression of a stem-loop CALR-dsRNA was carried out by 0.4 mM IPTG induction in 2XYT medium for 4 h at 37 °C with shaking. The stem-loop CALR-dsRNA was extracted by Tri-solution and dissolved in 150 mM NaCl and stored at −30 °C until used. The concentration and purity of the dsRNA was determined by agarose gel electrophoresis. The quality of the dsRNA was verified by RNAse digestion assay.

In vivo silencing of CALR

To investigate the role of CALR in regulating Vg gene, the expression of Vg was determined upon CALR-knockdown in P. monodon. Vitellogenic female shrimp (approximately 250 g) were divided into two groups; shrimp injected with GFP-dsRNA as a negative control and shrimp injected with CALR-dsRNA at $2.5\ \mu g.g^{-1}$ body weight of shrimp (bw) ($n = 5$). The expression level of CALR and Vg in the ovary of shrimp in each group were determined on day 7 after injection by semiquantitative RT-PCR. The CALR transcript was amplified using multiplex PCR reaction containing 0.5 μM of 3CALR-F and CALR-R primers, 0.1 μM actin-F and actin-R primers with 25 cycles of 94 °C for 30 s, 55 °C for 30 s and 74 °C for 1 min followed by 74 °C for 7 min. The transcript levels of Vg in the ovary of both groups were also determined by semi-quantitative RT-PCR using Vg-F1 and Vg-R1 primers as previously mentioned.

Statistical analysis

All statistical analyses were performed using SPSS 18.0 Software. The statistically significant differences among treatments ($p < .05$) was analyzed by One-way ANOVA and Student's t-test. Before the comparison, Kolmogorov–Smirnov and Levene's test were used to test the normality and homogeneity of variances, respectively.

Results

Differential gene expression in the ovary of P. monodon under GIHknockdown condition

In order to identify genes that may play roles in vitellogenesis, changes in global gene expression in the ovary of GIH-knockdown shrimp were determined by SSH. SSH libraries were constructed from a pool of ovary cDNA of three individual GIH-dsRNA-injected P. monodon in which the expression levels of Vg was confirmed to be up-regulated (Fig. 1).

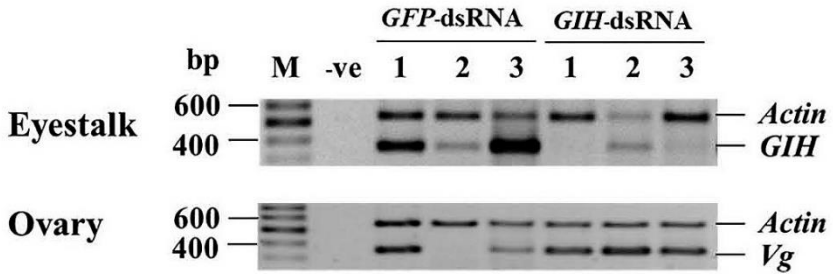

Fig. 1. Silencing of PmGIH by dsRNA. Previtellogenic P. monodon (approximately 85–120 g) were injected with GIH-dsRNA and a negative control GFPdsRNA at 0.3 μg.g−1 shrimp b.w. at the basal of eyestalk. On day 5 post-injection, the eyestalk and ovary were collected and processed for RT-PCR analysis of PmGIH and Vg expression, respectively. The expression of actin was used as an internal control. The amplification products were analyzed on 1.5% agarose gel along with the 100 bp ladder DNA size marker (M). The number above each lane represents individual shrimp in each group; −ve is a negative control of PCR.

The efficiency of SSH was shown by the successful subtraction of the actin transcript (Fig. A.2). After nucleotide sequence determination and processing by removing the unwanted vector and primer sequences, 102 and 82 high-quality sequences were obtained from the forward and reverse subtraction libraries, respectively. The homology search against the GenBank database by blastn and blastx programs at NCBI revealed that 63 cDNA sequences from the forward library (representing genes that were up-regulated upon GIH-knockdown) were annotated to 37 different known genes, and 39 were hypothetical or unknown genes. Whereas the reverse library contained 45 down-regulated sequence that could be annotated to 32 different genes, and the remaining 37 cDNA sequences were hypothetical or unknown genes (Fig. 2).

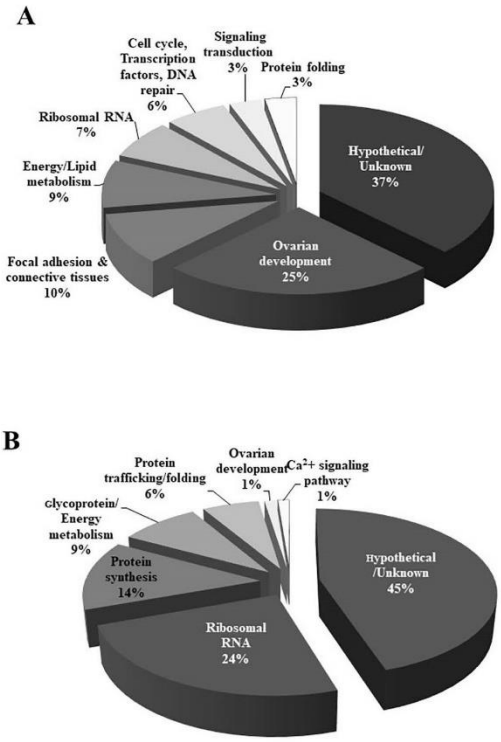

Fig. 2. Percentage of genes identified from SSH libraries according to the functional annotation. A total of 102 and 82 sequences of clones from forward (A) and reverse (B) SSH libraries, respectively, were annotated and categorized into each functional group of genes using BLAST analysis at NCBI.

Verification of reproduction-related genes under GIH deprivation

The genes that were up-regulated upon GIH-knockdown were categorized based on their functions as shown in Table 2. These include ribosomal RNA genes, hypothetical and unknown genes, genes encoding proteins in several pathways such as ovarian development, focal adhesion, energy/lipid metabolism, signaling transduction pathway, cell cycle/transcription factor/DNA repair, and protein folding. The RTqPCR analysis of three ovarian development related genes namely peritrophine I (Per I), thrombospondin II (TSP II), and Vg with the efficiency of 97.7%, 98.0% and 99.9%, respectively confirmed their upregulated expression under GIH-suppressed condition (Fig. 3).

The 32 down-regulated genes upon GIH-knockdown from the reverse library were categorized into ribosomal RNA genes, hypothetical and unknown genes, and genes that are involved in ovarian development, energy/lipid metabolism, calcium signaling pathway, protein trafficking/protein folding, and protein synthesis (Table 3). The validation of expression levels of genes involving in reproductive system i.e. calreticulin (CALR) and energy metabolism such as saposin (Sap), and Adenine nucleotide translocate (ANT) with RT-qPCR efficiency of 98.4%, 99.0% and 99.8%, respectively revealed the reduced expression levels under GIH-suppressed condition (Fig. 3).

Table 2
Candidate genes from the forward SSH library that were up-regulated upon GIH-knockdown.

Highest homology	Accession no	*E*-value	Closet species	Assigned accession no	No of clones
Ovarian development					
Ovarian peritrophin I	AF510331.1	0	*Penaeus monodon*	MN639222–25	4
Ovarian peritrophin II	AF510332.1	$1.00E^{-85}$	*Penaeus monodon*	MN639226	1
Ovarian peritrophin III	EF153270.1	$4.00E^{-98}$	*Penaeus monodon*	MN639227–32	6
Peritrophin-44-like isoform X1	XP_027222433.1	$3.00E^{-44}$	*Litopenaeus vannamei*	MN639233	1
Thrombospondin II	AGI56293.1	0	*Penaeus monodon*	MN639234–44	11
Vitellogenin	DQ288843.1	0	*Penaeus monodon*	MN639245	2
Polehole-like protein	ACV60547.1	$2.00E^{-91}$	*Penaeus monodon*	MN639246	1
Focal adhesion					
Connectin	XM_027363872.1	0	*Litopenaeus vannamei*	MN639247	2
Paxillin	NG_029820.1	$3.00E^{-50}$	*Homo sapiens*	MN639248	1
Myosin light chain kinase var. x1	XR_003475463.1	$2.00E^{-107}$	*Litopenaeus vannamei*	MN639249	1
Myosin light chain kinase var. x5	XM_027353508.1	$2.00E^{-73}$	*Litopenaeus vannamei*	MN639250	1
Actin1	AF100986.1	$5.00E^{-149}$	*Penaeus monodon*	MN639251	2
Actin2	AF100987.1	$4.00E^{-104}$	*Penaeus monodon*	MN639252	1
Tubulin	AEI88096.1	$2.00E^{-73}$	*Scylla paramamosain*	MN639253–4	2
Energy/Lipid metabolism					
Glutaryl-CoA dehydrogenase	XM_027376212.1	$3.00E^{-99}$	*Litopenaeus vannamei*	MN639255	1
GAPDH	MG787341.1	$8.00E^{-146}$	*Litopenaeus vannamei*	MN639256	1
Glycogen phosphorylase	MK721970.1	0	*Litopenaeus vannamei*	MN639257	1
Cytochrome c oxidase IV	JQ828862.1	$9.00E^{-99}$	*Litopenaeus vannamei*	MN639258	1
Nitric oxide synthase	GQ429217.1	0	*Litopenaeus vannamei*	MN639259	1
Thioredoxin reductase 2	AAF21431.1	$2.00E^{-116}$	*Homo sapiens*	MN639260	1
Glutamine synthetase	AMD09631.1	$6.00E^{-94}$	*Penaeus monodon*	MN639261	2
NADH dehydrogenase 1 alpha subunit 11-like	XP_027210098.1	$2.00E^{-42}$	*Litopenaeus vannamei*	MN639262	1
Signaling transduction pathway					
Serum deprivation response	NM_004657.5	$5.00E^{-27}$	*Homo sapiens*	MN639263	1
Calpain-1-like	XM_027378586.1	0	*Litopenaeus vannamei*	MN639264	1
Arrestin	XM_027382709.1	0	*Litopenaeus vannamei*	MN639265	1
Cell cycle, Transcription factors, DNA repair					
CDK5 regulatory subunit associated 1	XM_027382438.1	0	*Litopenaeus vannamei*	MN639266	1
Origin recognition complex subunit 3	XM_027380864.1	$3.00E^{-111}$	*Litopenaeus vannamei*	MN639267	1
Ku protein	XP_012363148.1	$2.00E^{-59}$	*Nomascus leucogenys*	MN639268	2
Protein bicaudal C homolog 1 isoform X5	ROT69835.1	$7.00E^{-44}$	*Litopenaeus vannamei*	MN639269	1
Protein folding					
Ubiquitin-conjugating enzyme E2	KR106186.1	$3.00E^{-110}$	*Penaeus monodon*	MN639270	1
Ubiquitin/ribosomal S27 fusion protein	KR106186.1	$4.00E^{-107}$	*Penaeus monodon*	MN639271	1
Cold shock Y-box protein	XM_027378572.1	$7.00E^{-38}$	*Litopenaeus vannamei*	MN639272	1
Ribosomal genes				MN639273–77	7
Hypothetical & unknown genes					39

Table 3
Candidate genes from the reverse SSH library that were down-regulated upon GIH-knockdown.

Highest homology	Accession no	*E*-value	Closet species	Assigned accession no	No of clones
Ovarian development					
QM protein	ROT74357.1	$2.00E^{-67}$	*Litopenaeus vannamei*	MN639286	1
Energy/Lipid metabolism					
Saposin	ADK94870.1	$1.00E^{-157}$	*Penaeus monodon*	MN639287	1
Transketolase	XP_623196.3	$3.00E^{-169}$	*Apis mellifera*	MN639288	1
Glyceraldehyde-3-phosphate-dehydrogenase	AWH12534.1	$4.00E^{-128}$	*Litopenaeus vannamei*	MN639289	1
Adenine nucleotide translocase	AFK93891.1	$9.00E^{-153}$	*Penaeus monodon*	MN639290	1
Metallothionein	ADQ28316.1	$8.00E^{-19}$	*Penaeus monodon*	MN639291–2	2
NADH dehydrogenese	XP_027237828.1	$1.00E^{-105}$	*Litopenaeus vannamei*	MN639293	1
Ca^{2+} signaling pathway					
Calreticulin	ADO00927.1	$1.00E^{-179}$	*Penaeus monodon*	MN639294	1
Protein trafficking/ Protein folding					
Rab GDP dissociation inhibitor alpha-like	XP_018016172.1	$6.00E^{-19}$	*Hyalella azteca*	MN639295–6	2
Coatomer subunit delta-like isoform X2	XP_018026409.1	$2.00E^{-51}$	*Hyalella azteca*	MN639297	1
Prefoldin subunit 6	XM_027379965.1	$9.00E^{-81}$	*Litopenaeus vannamei*	MN639298	2
Protein synthesis					
Elongation factor 1α	MG775229.1	$1.00E^{-107}$	*Penaeus monodon*	MN639299	1
Elongation factor 2	ABR01223.1	$1.00E^{-113}$	*Penaeus monodon*	MN639300	1
Eukaryotic translation initiation factor 3	AEI88048.1	$2.00E^{-92}$	*Scylla paramamosain*	MN639301	1
Arginine kinase	C7E3T4.1	$2.00E^{-131}$	*Penaeus monodon*	MN639302–4	4
Beta-actin	ACZ60616.1	$1.00E^{-106}$	*Panulirus argus*	MN639305	2
nm23 protein	AFL02665.1	$4.00E^{-27}$	*Penaeus monodon*	MN639306	1
Nucleolar protein 58	XP_027208389.1	$5.00E^{-131}$	*Litopenaeus vannamei*	MN639307	1
Ribosomal genes				MN639308–22	20
Hypothetical& unknown gene					37

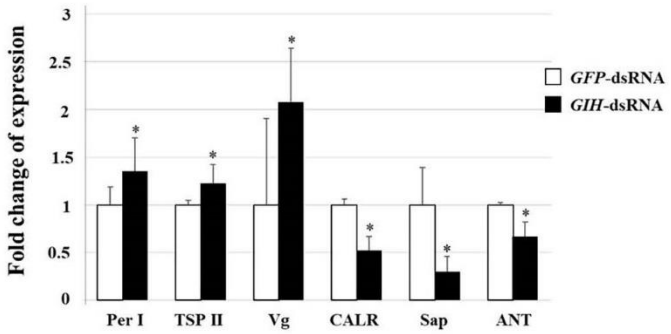

Fig. 3. Verification of the expression of selected genes from SSH libraries in the ovary of GIH-knockdown *P. monodon*. The cDNA from GIH-dsRNA-injected shrimp were analyzed for the transcription level of genes from the forward library (peritrophine I, Per I; thrombospondin II, TSP II; vitellogenin, Vg) and genes from the reverse library (calreticulin, CALR; saposin, Sap; Adenine nucleotide translocate, ANT). The expression levels of each gene were calculated relatively to that of the control shrimp injected with GFP-dsRNA. The results from three independent experiments were present as mean ± SEM (n = 3). Asterisks indicates statistically significant differences from the control at $P < .05$.

Expression of reproduction-related genes at different ovarian developmental stages in P. monodon

In order to investigate whether the genes that were expressed responsively to GIH-knockdown have function in ovarian development or not, the relative expression of six candidate genes during different stages of ovarian development in the shrimp was determined by RTqPCR The result showed that all of the genes from the forward library i. e. Per I, TSP II and Vg exhibited similar expression profile during ovarian development. Their expression levels were elevated from previltellogenic stage through late-vitellogenic stage, and declined when the ovary entered the ripe stage (Fig. 4A-C). By contrast, the candidate genes from the reverse library (CALR, Sap, and ANT) were highly expressed in the pre-vitellogenic stage and decreased to the lowest levels at early-vitellogenic or late-vitellogenic stages before rising again when the ovary entered the ripe stage (Fig. 4D-F). The ovarian developmentrelated patterns of the expression of these up- or down-regulated genes are consistent with their relative expression in the GIH-knockdown shrimp, and suggests the importance of these gene products in earlyvitellogenic development of the ovary.

Functional study of PmCALR in regulating the expression of Vg gene

The possible function of PmCALR in regulating the expression of Vg gene was studied by RNA interference experiment. The CALR-dsRNA was produced in the E. coli expression system, and verified by RNase digestion assay (Fig. A.3). The result in Fig. 5 showed that injection of the CALR-dsRNA at $2.5\ \mu g.g^{-1}$ shrimp bw could suppress the expression level of PmCALR by approximately 54% on day 7 after dsRNA injection, and the Vg expression level in the ovary of CALR-knockdown shrimp was increased by approximately 2.7-fold when compared with that in GFP-dsRNA treated group. This result suggests that PmCALR possibly controls vitellogenesis by inhibiting Vg gene expression in the ovary.

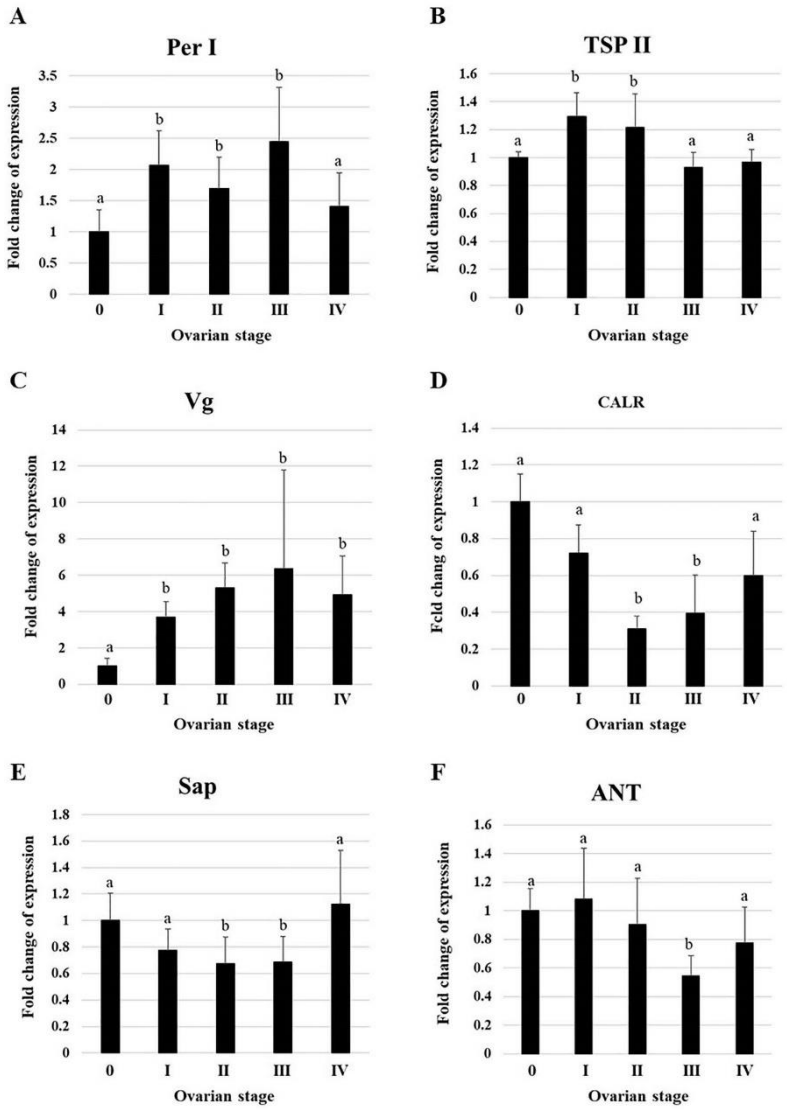

Fig. 4. Expression of candidate genes in the ovary of female *P. monodon* during ovarian development. The expression levels of six selected genes; Per I (A), TSP II (B), Vg (C), CALR (D), Sap (E), and ANT (F) in the ovary of female P. monodon at the immature stage (0), previtellogenic stage (I), early vitellogenic stage (II), late vitellogenic stage (III) and ripe stage (IV) were determined by RT-qPCR. The amounts of gene transcripts in relation to that of EF1-α were analyzed by $2^{-\Delta\Delta Ct}$ method. The expression level of each gene at each ovarian stage was calculated relatively to that of the shrimp at stage 0. The results from three independent experiments were presented as mean ± SEM (n = 3–5). Different letter indicates statistically significant differences from the control at $P < .05$.

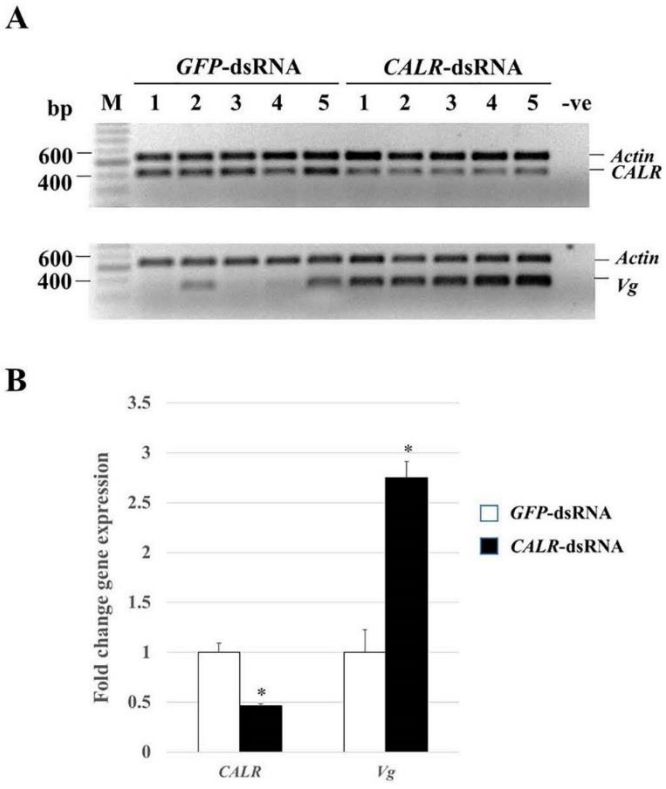

Fig. 5. Determination of CALR and Vg transcript in the ovary of CALR-dsRNAinjected vitellogenic female *P. monodon*. (A) The expression of CALR and Vg in the ovary of CALR-dsRNA-injected vitellogenic female P. monodon was determined by RT-PCR compared to the expression of CALR in GFP-dsRNA treated control shrimp on day 7 after dsRNA injection. The number above each lane represents individual shrimp in each group. (B) The relative amounts of CALR and Vg transcripts to the actin transcript in individual shrimp were quantitated by Scion-image program. The data of the relative expression of CALR and Vg was presented as bar graphs comparing between that of the CALR-dsRNA-injected shrimp and the control shrimp injected with GFP-dsRNA. Asterisks indicate statistically significant difference from the control ($P < .05$).

Discussion

Ovarian maturation in shrimp is reliant on successful vitellogenesis, which is known to be mediated by an eyestalk peptide hormone GIH. Eyestalk ablation destroys the synthesis and storage site of GIH, and thus is a powerful technique that has been widely used in the hatcheries to induce ovarian maturation of the female broodstock. Although eyestalk ablation gives predictable and reliable shrimp production, it also has adverse effects on the broodstock (Benzie, 1998; Racotta et al., 2003; Sainz-Hernández et al., 2008). We have shown previously that suppression of GIH expression by specific double-stranded RNA (GIHdsRNA) could induce the expression level of Vg gene as well as the successful maturation of shrimp ovary. (Treerattrakool et al., 2008; Treerattrakool et al., 2011). Since GIH-dsRNA provided specific suppression on GIH gene, the dsRNA-mediated GIH suppression was therefore used in this study to determine genes in the ovary that may act downstream of GIH to regulate Vg gene expression.

With the use of suppression subtractive hybridization (SSH), 102 up-regulated and 82 down-regulated sequences in the ovary upon GIH suppression were obtained

from the forward library and reverse library, respectively. Gene annotation revealed that ovarian development-related genes were found in both libraries. Among these, Per I, TSP II and Vg genes were validated to be up-regulated under GIH suppressed condition. In addition, the high expression levels throughout vitellogenic stages suggest that these genes are required for ovarian development in the shrimp. These dynamic expression profiles are consistent with previous reports (Khayat et al., 2001; Yamano et al., 2004; Urtgam et al., 2015).

A majority of negatively regulated genes under GIH deprivation in the reverse library includes Sap, which codes for a lysosomal lipid-degrading enzyme (Kishimoto et al., 1992) and a gene involving in ATP synthesis, ANT (Liu et al., 2016). The verification of expression levels revealed the up-regulation of these two genes during ovarian development in female shrimp. This event suggests the reservation of energy for yolk lipoprotein synthesis in the maturating ovary.

One of the interesting genes is a gene in the calcium signaling cascade, calreticulin (CALR). CALR is a multifunctional endoplasmic reticulum (ER) luminal resident protein that plays roles in Ca2+homeostasis, molecular chaperoning, and stress responses (Michalak et al., 1999; Dey and Matsunami, 2011; Jeffery et al., 2011). It is located mainly in the ER lumen and the nuclear envelope (Roderick et al., 1997; Michalak et al., 2009). CALR is a major Ca2+ binding protein in the lumen of the ER. CALR deficient cells have substantially reduced capacity of ER Ca2+ storage and impaired agonist-induced Ca2+ release as well as delayed store-operated Ca2+ entry (Nakamura et al., 2001; Wang et al., 2017).

In this study, CALR expression was significantly down-regulated upon GIH-knockdown. The expression of CALR during ovarian maturation was declined in early vitellogenic stage, corresponding to the expression pattern of GIH that was previously reported (Urtgam et al., 2015). Further study of a possible function of CALR in the regulation of Vg gene in P. monodon by CALR-specific dsRNA revealed an elevated Vg expression level in the ovary of CALR-knockdown shrimp. This result suggest that Vg regulation is a calreticulin-dependent process.

The Vg synthesis in insects such as Drosophila melanogaster and Aedes aegypti was reported to be controlled by the activation of the heterodimer of ecdysone-ultraspiracle nuclear receptor by ecdysteroids that enables the direct binding of the heterodimeric receptor to its responsive element on the regulatory region of Vg gene in insect adipose tissue (Antoniewski et al., 1996; Martin et al., 2001). In crustacean, several clusters of heat shock factor binding site (HSE), and estrogen responsive element were identified within the 5′-upstream region (5'UPS) of MeVg2 gene of the shrimp Metapenaeus ensis. The expression of MeVg2 was negatively regulated by the heat shock cognate 70 (Hsc70) through the formation of a repression complex with heat shock factor (Chan et al., 2014). Moreover, the study of Wu, 2008 demonstrated that another molecular chaperone Hsp90 could be induced by estradiol -17β in the immature M. ensis, suggesting that Vg expression in shrimp is probably regulated by estrogen-related hormone similar to that in vertebrates. In addition, previous studies by Nagaraju et al., 2011 and Gong et al., 2015 indicated that ecdysone receptor (EcR) and retinoid X receptor (RxR) could promote ovarian development in the crabs Scylla paramamosain and Carcinus maenas, respectively.

Calreticulin can bind to the DNA binding motif (KXGFFKR) of a steroid nuclear protein receptor, and prevents the binding of the receptor to its responsive

element to regulate gene expression in vertebrate (Dedhar et al., 1994). Taken together, our present study suggests that calreticulin is a potential mediator of Vg synthesis in P. monodon, possibly by interfering the binding of steroid nuclear receptor to its binding site on Vg 5' UPS. Further investigation on the regulatory sequences of the Vg gene and the effect of CALR-steroid receptor complex on the regulation of Vg expression will help unravel the molecular mechanism modulating vitellogenin synthesis via GIH mediated pathway in shrimp ovary.

Conclusion

This study utilized suppression subtractive hybridization technique to determine genes in the ovary of P. monodon whose expression was altered under specific-dsRNA mediated GIH suppression. The expression of calreticulin (CALR) gene was significantly down-regulated in response to GIH suppression. Silencing of CALR led to the elevated Vg expression in shrimp ovary. Since CALR can bind to a steroid receptor, and prevents the binding of the receptor to its responsive element to regulate gene expression, it is possible that CALR is an inhibitory mediator of Vg synthesis via the steroidal pathway. Further studies on the influence of this mechanism on ovarian development will shed light on the molecular mechanism of reproductive modulation in female shrimp.

References

1. Antoniewski, C., Mugat, B., Delbac, F., Lepesant, J.A., 1996. Direct repeats bind the EcR/ USP receptor and mediate ecdysteroid responses in Drosophila melanogaster. Mol. Cell. Biol. 16, 2977–2986.
2. Benzie, J., 1998. Penaeid genetics and biotechnology. Aquaculture. 164, 23–47.
3. Chan, S.F., Guo, J., Chu, K.H., Sun, C.B., 2014. The shrimp heat shock cognate70 functions as a negative regulator in vitellogenin gene expression. Biol. Reprod. 91, 1–11.
4. Chen, T., Zhang, L.P., Wong, N.K., Zhong, M., Ren, C.H., Hu, C.Q., 2014. Pacific white shrimp (Litopenaeus vannamei) vitellogenesis-inhibiting hormone (VIH) is predominantly expressed in the brain and negatively regulates hepatopancreatic vitellogenin (VTG) gene expression. Biol. Reprod. 47, 1–10.
5. Dedhar, S., Rennie, P.S., Shago, M., Hagesteijn, C.Y.L., Yang, H., Filmus, J., et al., 1994. Inhibit of nuclear hormone receptor activity by calreticulin. Nature. 367, 480–483.
6. Dey, S., Matsunami, H., 2011. Calreticulin chaperones regulate functional expression of vomeronasal type 2 pheromone receptors. Proc. Natl. Acad. Sci. U. S. A. 108, 16651–16656.
7. Edomi, P., Azzoni, E., Mettulio, R., Pandolfelli, N., Ferrero, E.A., Giulianini, P.G., 2002. Gonad-inhibiting hormone of the Norway lobster (Nephrops norvegicus): cDNA cloning, expression, recombinant protein production, and immunolocalization. Gene. 284, 93–102.
8. Gong, J., Ye, H., Xie, Y., Yang, Y., Huang, H., Li, S., Zeng, C., 2015. Ecdysone receptor in the mud crab Scylla paramamosain: a possible role in promoting ovarian development. J. Endocrinol. 224, 273–287.
9. Jeffery, E., Peters, L.R., Raghavan, M., 2011. The polypeptide binding conformation of calreti culin facilitates its cell-surface expression under conditions of endoplasmic reticulum stress. J. Biol. Chem. 286, 2402–2415.

10. Kang, B.J., Okutsu, T., Tsutsui, N., Shinji, J., Bae, S.H., Wilde, M.N., 2014. Dynamics of vitellogenin and vitellogenesis-inhibiting hormone levels in adult and subadult whiteleg shrimp, *Litopenaeus vannamei*: relation to molting and eyestalk ablation. Biol. Reprod. 90 (12), 1–10.

11. Khayat, M., Babin, P.J., Funkenstein, B., Sammar, M., Nagasawa, H., Tietz, A., Lubzen, E., 2001. Molecular characterization and high expression during oocyte development of a shrimp ovarian cortical rod protein homologous to insect intestinal peritrophins. Biol. Reprod. 64, 1090–1099.

12. Kishimoto, Y., Hiraiwa, M., O'Brien, J.S., 1992. Saposins: structure, function, distribution, and molecular genetics. J. Lipid Res. 33, 1255–1267.

13. de Kleijn, D.P.V., Janssen, K.P., Waddy, S.L., Hegeman, R., Lai, W.Y., Martens, G.J., Van Herp, F., 1998. Expression of the crustacean hyperglycemic hormones and the gonadinhibiting hormone during the reproductive cycle of the female American lobster Homarus americanus. J. Endocrinol. 156, 291–298.

14. Liu, Q.N., Chai, X.Y., Tu, J., Xin, Z.Z., Li, C.F., Jiang, S.H., Zhou, C.J., Tang, B.P., 2016. An adenine nucleotide translocase (ANT) gene from Apostichopus japonicus; molecular cloning and expression analysis in response to lipopolysaccharide (LPS) challenge and thermal stress. Fish Shellfish Immun. 49, 16–23.

15. Livak, K.J., Schmittgen, T.D., 2001. Analysis of relative gene expression data using realtime quantitative PCR and the $2^{-\Delta\Delta C(T)}$ method. Methods. 25, 402–408.

16. Longyant, S., Sithigorngul, P., Sithigorngul, W., Chaivisuthangkura, P., Thampalerd, N., 2003. The effect of eyestalk extract on vitellogenin levels in the haemolymph of the giant tiger prawn Penaeus monodon. Sci. Asia 29, 371–381.

17. Martin, D., Wang, S.F., Alexamder, S., Raikhel, A.S., 2001. The vitellogenin gene of the mosquito Aedes aegypti is a direct target of ecdysteroid receptor. Mol. Cell. Endocrinol. 173, 75–86.

18. Michalak, M., Corbett, E.F., Mesaeli, N., Nakamura, K., Opas, M., 1999. Calreticulin: one protein, one gene, many functions. Biochem. J. 344, 281–292.

19. Michalak, M., Groenendyk, J., Szabo, E., Gold, L.I., Opas, M., 2009. Calreticulin, a multiprocess calcium-buffering chaperone of the endoplasmic reticulum. Biochem. J. 417, 651–666.

20. Nagaraju, G.P.C., Rajitha, B., Borst, D.W., 2011. Molecular cloning and sequence of retinoid X receptor in the green crab Carcinus maenas: a possible role in female reproduction. J. Endocrinol. 210, 379–390.

21. Nakamura, K., Zuppini, A., Arnaudeau, S., Lynch, J., Ahsan, I., Krause, R., et al., 2001. Functional specialization of calreticulin domains. J. Cell Biol. 154, 961–972.

22. Okumura, T., Yamano, K., Sakiyama, K., 2007. Vitellogenin gene expression and hemolymph vitellogenin during vitellogenesis, final maturation, and oviposition in female kuruma prawn, Marsupenaeus japonicus. Comp. Biochem. Phys. A. 147A, 1028–1037.

23. Pfaffl, M.W., 2001. A new mathematical model for relative quantification in real-time RTPCR. Nucleic Acids Res. 29 (e), 45.

24. Racotta, L.S., Palacios, E., Ibarra, A.M., 2003. Shrimp larval quality in relation to broodstock condition. Aquaculture. 227, 107–130.

25. Roderick, H.L., Campbell, A.K., Llewellyn, D.H., 1997. Nuclear localisation of calreticulin in vivo is enhanced by its interaction with glucocorticoid receptors. FEBS Lett. 405, 181–185.

26. Sainz-Hernández, J.C., Racotta, L.S., Dumas, S., Hernández-López, J., 2008. Effect of unilateral and bilateral eyestalk ablation in Litopenaeus vannamei male and female on several metabolic and immunologic variables. Aquaculture. 283, 188–193.

27. Tan-Fermin, J.D., Pudadera, R.A., 1989. Ovarian maturation stages of the wild giant tiger prawn, Penaeus monodon Fabricius. Aquaculture. 77, 229–242.

28. Tiu, S.H.K., Hui, J.H.L., Mak, A.S.C., He, J.-G., Chan, S.-M., 2006. Equal contribution of hepatopancreas and ovary to the production of vitellogenin (PmVg1) transcripts in the tiger shrimp, *Penaeus monodon*. Aquaculture. 254, 666–674.

29. Tiu, S.H.K., Benzie, J., Chan, S.M., 2008. From hepatopancreas to ovary: molecular characterization of a shrimp vitellogenin receptor involved in the processing of vitellogenin. Biol. Reprod. 79, 66–74.

30. Treerattrakool, S., Panyim, S., Chan, S.M., Withyachumnarnkul, B., Udomkit, A., 2008. Molecular characterization of gonad-inhibiting hormone of Penaeus monodon and elucidation of its inhibitory role in vitellogenin expression by RNA interference. FEBS J. 275, 970–980.

31. Treerattrakool, S., Panyim, S., Udomkit, A., 2011. Induction of ovarian maturation and spawning in Penaeus monodon broodstock by double-stranded RNA. Mar. Biotechnol. 13, 163–169.

32. Treerattrakool, S., Boonchoy, C., Urtgam, S., Panyim, S., Udomkit, A., 2014. Functional characterization of recombinant gonad-inhibiting hormone (GIH) and implication of antibody neutralization on induction of ovarian maturation in marine shrimp. Aquaculture. 428–429, 166–173.

33. Urtgam, S., Treerattrakool, S., Roytrakul, S., Wongtripop, S., Prommoon, J., Panyim, S., Udomkit, A., 2015. Correlation between gonad-inhibiting hormone and vitellogenin during ovarian maturation in the domesticated Penaeus monodon. Aquaculture. 437, 1–9.

34. Visudtiphole, V., Watthanasurorot, A., Klinbunga, S., Menasveta, P., Kirtikara, K., 2010. Molecular characterization of Calreticulin: a biomarker for temperature stress responses of the giant tiger shrimp Penaeus monodon. Aquaculture. 308, S100–S108.

35. Wang, W.-A., Liu, W.-X., Durnaoglu, S., Lee, S.-K., Lian, J., Lehner, R., Ahnn, J., Luis, B., Agellon, L.B., Michalak, M., 2017. Loss of calreticulin uncovers a critical role for calcium in regulating cellular lipid homeostasis. Sci. Rep. 7, 5941.

36. Webster, S.G., Keller, R., Dircksen, H., 2012. The CHH-superfamily of multifunctional peptide hormones controlling crustacean metabolism, osmoregulation, moulting, and reproduction. Gen. Comp. Endocrinol. 175, 217–233.

37. Wilder, M.N., Okamura, T., Tsutsui, N., 2010. Reproductive mechanisms in crustacean focusing on selected prawn species: Vitellogenin structure, processing and synthetic control. Aqua. BioSci. Monogra. 3, 73–110.

38. Wu, L,T., Chu, K.H., 2008. Characterization of heat shock protein 90 in the shrimp Metapenaeus ensis: evidence for its role in the regulation of vitellogenin synthesis. Mol. Reprod. Dev. 75, 952–959.

39. Yamano, K., Qiu, G.F., Unuma, T., 2004. Molecular cloning and ovarian expression profiles of thrombospondin, a major component of cortical rods in mature oocytes of penaeid shrimp, Marsupenaeus japonicas. Biol. Reprod. 70, 1670–1678.

40. Yang, W.J., Rao, K.R., 2001. Cloning of precursors for two MIH/VIH-related peptides in the prawn, Macrobrachium rosenbergii. Biochem. Biophys. Res. Commun. 289, 407–413.

An ATP synthase beta subunit is required for internalization of dsRNA into shrimp cells

Extracellular dsRNA is an important modulator in innate immunity in both vertebrates and invertebrates. In shrimp, extracellular dsRNA can trigger RNAi pathway and serves as antiviral defense mechanism. However, the mechanism of dsRNA internalization into the cells has not yet known in shrimp cells. This study identified candidate cell surface proteins from shrimp hepatopancreatic cells that could interact with dsRNA by a ligand blot assay. Among the candidate proteins, a cell surface beta subunit of ATP synthase was shown to be capable of internalizing dsRNA into shrimp hepatopancreatic cells that could rapidly occur in just one minute upon dsRNA challenge. Colocalization between dsRNA and ATP synthase beta subunit implied correlation between dsRNA and ATP synthase beta subunit during dsRNA internalization. Furthermore, dsRNA showed colocalization with endocytic proteins, Rab5 and Rab7 indicating that dsRNA was internalized via the receptor-mediated endocytosis. For the above evidences as well as the reduction of dsRNA internalization by angiostatin and antibodies against ATP synthase beta subunit, we propose that dsRNA interact with ATP synthase via a nucleotide binding site in the beta subunit prior to internalize dsRNA into cells.

Introduction

Cellular uptake of nucleic acids such as siRNA, mRNA or dsRNA has been widely studied in various cell types and organisms for its important role as new therapeutic strategies in both medical and agricultural aspects [1-6]. Although a large number of evidences indicate that the internalization pathway of dsDNA and dsRNA are likely to share endocytic pathway in animal cells [3, 7, 8], diverse routes of entry have also been demonstrated including other endocytic pathways and channel protein-mediated internalization [2-4, 9-12]. Pattern recognition receptors have been shown to be involved in nucleic acid recognition and internalization in order to trigger host defense mechanisms [13].

Extracellular dsRNA could be produced in viral-infected cells and released into extracellular space during cell lysis via various mechanisms [14, 15]. Cell lysis can occur not only by viral infection that causes bursting of the infected cells, but the host cells themselves also have their own mechanisms to induce cell lysis at early infection, which is actively triggered by many viruses [15-17]. Extracellular dsRNA is an important modulator for antiviral innate immunity in multicellular organisms. In mammalian cells, extracellular dsRNA is recognized and internalized by a scavenger receptor [7]. The internalized dsRNA is transported to endosome and subsequently detected by TLR3 in the endosome. In addition, cytoplasmic sensors such as MDA-5 or RIG-I play a role in dsRNA detection in the cytosol [7]. These sensor proteins activate downstream proteins such as TRIF, IRF NF-kB and eventually induce type I interferon production in response to dsRNA or viral infection [18, 19]. Whereas in invertebrates, internalization of extracellular dsRNA into cytoplasm is recognized by a transactivation response RNA binding protein (TRBP), which is an initial protein to recruit Dicer and Argonaute proteins to form a multi-component complex known as RISC [20, 21] and ultimately lead to viral mRNA degradation. To trigger cellular

antiviral response, the extracellular dsRNA must be internalized into the cells through the membrane bound proteins.

The mechanism of dsRNA internalization involves recognition through an interaction with cell surface proteins prior to internalization via endocytic proteins and eventually released to the cytosol to activate the RNAi pathway. Although RNAi screening in human, *Drosophila S2* cells and *C. elegans* showed that scavenger receptors and endocytic proteins are involved in dsRNA internalization, there seems to be no direct linkage between scavenger receptors and RNAi activity [3,10]. A class A scavenger receptor in mammals has been proved to internalize dsRNA via a clathrin-mediated endocytic pathway similar to the dsRNA internalization by the Class C scavenger receptor in *Drosophila* [3, 7, 10]. Both class A and class C scavenger receptors showed high specificity to dsRNA and preferred to internalize long dsRNA rather than siRNA [3, 7]. Knockdown of scavenger receptor exhibited the reduction of dsRNA internalization, which confirms that scavenger receptor could recognize and internalize dsRNA into the cells to trigger antiviral defense mechanism [7, 10].

In shrimp, it has been shown that a SID-1 homologue is involved in dsRNA internalization subsequent to dsRNA injection into shrimp, suggesting that systemic RNAi in shrimp might involve SID-1 [22]. However, the upregulation of SID-1 expression level in response to long dsRNA injection occurred only in gills and muscles, but not in the hepatopancreas. This probably suggests an alternative pathway of dsRNA internalization from gastric juice environment in the hepatopancreas [22]. This organ functions for both absorbtion of nutrients and innate immunity which exhibits high endocytosis activity [23]. Feeding shrimp with long dsRNA targeting endogenous or exogenous genes could also lead to mRNA target suppression suggested that hepatopancreatic cells could internalize dsRNA into cells [24].

Here we describe the identification of a candidate dsRNA-interacting protein on the membrane of shrimp hepatopancreatic cells using dsRNA ligand blotting. The candidate cell surface protein was proven for its ability to internalize dsRNA into the primary-cultured hepatopancreatic cells, and trigger RNAi pathway. This gives a better understanding on the mechanism of dsRNA internalization which could lead to the development of dsRNA delivery system to get higher efficiency of target gene suppression by RNAi technique in the shrimp.

Materials and methods

Membrane proteins extraction

Membrane proteins from hepatopancreas of the pacific white shrimp *Litopenaeus vannamei* was extracted for binding assay according to previous methods with adaptations [41,42]. All steps were carried out at 4 ºC. Briefly, hepatopancreas from 15 shrimp, approximately 2 g body weight were dissected and minced in either buffer M (150 mM NaCl, 10 mM Tris-HCl pH 7.5, 2 mM MgCl2, 1 mM EDTA, 0.2% Triton-X, 1 mM PMSF, 1 mM Benzamidine and 1X cocktail inhibitor) or buffer W (150 mM NaCl, 10 mM Tris-HCl pH 7.5, 2 mM MgCl2, 10 mM HEPES, 1 mM EDTA, 1 mM PMSF, 1 mM Benzamidine and 1X cocktail inhibitor). The hepatopancreatic cells were then dissociated by gently pipetting and filtrated through 120 μm mess. The cells were washed one time with the same buffers and centrifuged at 600g for 5 min. The cell pellet was then homogenized in each buffer by homogenizer. The homogenized cells were centrifuged at 600g for 5 min to remove cell debris, and the supernatant was

centrifuged at 12,000g for 10 min in order to sediment cellular organelles. The final membrane protein fraction was obtained by centrifugation of the supernatant at 100,000g for 60 min and used for binding assay.

Ligand blot assay between shrimp hepatopancreatic membrane proteins and labeled dsHSD

To identify potential dsRNA binding proteins from membrane protein fraction of shrimp hepatopancreas, ligand blot assays was performed as described previously with adaptations [43]. Briefly, 25 or 50 μg of the membrane protein extract were separated on 12.5% SDS gel and blotted onto nitrocellulose membrane as described above. The blotted proteins were denatured on the membrane in 8 M Urea and slowly renatured by incubation in 10 stepwise dilutions of urea in Tris-buffered saline (1X TBS: 50 mM Tris-Cl, pH 7.5, 150 mM NaCl) (Urea:TBS 2:3 v/v), for 10 min each. Thereafter, the membrane was rinsed in TBS and blocked in blocking solution (25 mM NaCl, 10 mM MgCl2, 10 mM Hepes, pH 8, 0.1 mM EDTA, 1 mM dithiothreitol, 5% (w/v) skimmed milk) for 1 h at room temperature or 4 ºC for overnight. The binding assay between the immobilized proteins and fluorescein-UTP labeled dsHSD was carried out in a binding buffer containing 50 mM NaCl, 10 mM MgCl2, 10 mM Hepes, pH 8, 0.1 mM EDTA, 1 mM dithiothreitol, 2.5% skim milk plus 500 ng/ml labeled dsHSD. The interaction between the fluorescein-labeled dsHSD and its potential binding protein was subsequently detected and visualized by rabbit anti-fluorescein polyclonal antibody and HRP-conjugated goat anti-rabbit IgG using Immobilon Western chemiluminescent HRP substrate under Azure Imager C300 (Azure Biosystems). The band in duplicated SDS gel corresponding to the visualized bands on the nitrocellulose membrane were cut for mass spectrometry analysis, and the proteins were identified against NCBI database with Mascot software (Matrix Science) using and carbamidomethyl and Oxidation M as parameters.

Primary cell culture of shrimp hepatopancreas

To establish the primary cell culture from hepatopancreas, five shrimp of approximately 2 g were anesthetized on ice. The shrimp outer surfaces were cleaned with 75% ethanol. Thereafter, hepatopancreas were immediately dissected and kept on ice in washing medium (1X L15 medium, 15% bovine serum supplemented with 100 mg/ml pen-strep and 50 μg/ml gentamycin). The tissues were washed 4 times in the washing medium and minced on ice. The minced hepatopancreas were then transferred into a sterile place and washed for another 4 times in washing medium. Small pieces of hepatopancreas were then transferred into working medium (1X L15 medium, 15% bovine serum, 15% shrimp meat extract supplemented with 100 mg/ml pen-strep and 50 μg/ml gentamycin) and gently pipette to dissociate the cell until homogeneous in the medium. The dissociated cells were filtrated through 60 mess sieve and centrifuged with 500g for 5 min at 4 ºC. The cells were then seeded into 8-well chamber slide and incubated at 28 ºC for 15 h.

Optimization of dsRNA internalization by hepatopancreatic cells

To achieve the optimal condition for dsRNA uptake, hepatopancreatic cells were prepared as mentioned above and seeded into an 8-well chamber slide for 15 h to obtain about 60% confluence. The attached cells were washed 3 times with the culture

medium. The cells were incubated with 10 μg fluorescein-UTP labeled dsHSD for 1, 5, and 10 min in 1X working medium. Thereafter, the cells were washed and fixed with 4% formaldehyde. The fixed cells were washed three times with 1X PBS prior to permeabilized with 1/1000 (v/v) cold acetone and washed three time with 1X PBS. The cells were then blocked with 1% BSA in 1X PBS for 1 h followed by incubation with 1:200 rabbit anti-fluorescein polyclonal antibody in 1X PBS containing 1% BSA. Thereafter, the cells were washed three times with 1X PBS and were incubated with 1:1000 FITC-conjugated goat anti-rabbit IgG. The images were captured using LSM800 confocal microscope.

Investigation of specificity of dsHSD internalization

In order to investigate whether dsRNA internalization route is specific for only dsRNA, shrimp hepatopancreatic cells were blocked with unlabeled dsHSD, dsRab7 or plasmid DNA at 100 and 500 μg/ml in working medium for 10 min. The cells were then added with 10 μg/ml of fluorescein-UTP labeled dsHSD for 1 min and fix with 4% formaldehyde for 10 min following by washing for three time. The cells were then permeabilized with cold acetone and washed as mentioned above. The detection was performed using rabbit anti-fluorescein antibody and observed under confocal microscopy as mentioned above.

Colocalization between the labeled dsHSD and cell surface ATP synthase beta subunit on shrimp hepatopancreatic cells

In order to demonstrate cell surface colocalization between labeled dsHSD and cell surfaced ATP synthase beta subunit at plasma membrane, live cell staining technique was utilized. Briefly, shrimp primary hepatopancreatic cells were washed and pre-chilled on ice for 15 min prior to challenging with 100 μg/ml labeled dsHSD for 2.5 min in working medium. The cells were then quickly washed with 1X PBS followed by incubating with 1:150 mouse anti-human ATP synthase beta subunit monoclonal antibody and 1:150 rabbit anti-fluorescein polyclonal antibody for 20 min on ice. Thereafter, the primary antibodies were removed and 1:300 Alexa Flour® 647 goat anti-mouse IgG and FITC-conjugated goat anti-rabbit IgG secondary antibodies were added and further incubated for 20 min on ice. The cells were then washed with 1XPBS and fixed with 1% formaldehyde for 10 min. After washing for three times, the fixed cells were blocked with 1% BSA in 1X PBS for 1 h. The cells were then stained with 1:1000 Phalloidin for 1 h following incubation with DAPI for nuclear staining at 10 μg/ml for 10 min. The chamber slide was dried and prepared for confocal microscopy.

In addition, the dynamic of dsRNA internalization via cell surface ATP synthase beta subunit was determined by the time course study of colocalization in both non-permeabilized and permeabilized cells. Shrimp hepatopancreatic cells were challenged with 100 μg/ml labeled dsHSD in working medium at room temperature for 1, 2.5, 5 or 10 min. The medium was then removed, and the cells were then fixed with 1% formaldehyde for 10 min. After washing for three times, total colocalization signals either at the cell surface or inside the cell were detected by permeabilizing the fixed cells with 1/1000 (v/v) acetone. After permeabilization, the cells were washed for three times prior to block with 1% BSA in 1X PBS for 1 h. The ATP synthase beta subunit and the labeled-dsHSD were detected as described above. Colocalization at the cell

surface was determined in non-permeabilized cells without acetone treatment. The cells were then incubated with DAPI for nuclear staining at 10 μg/ml for 10 min. The chamber slide was dried and prepared for confocal microscopy as mentioned above.

Colocalization between the labeled dsHSD and Rab5 or Rab7

To investigate whether dsHSD is internalized via endocytic pathway, the endocytic proteins Rab5 and Rab7 were used as marker proteins for colocalization analysis. Briefly, shrimp hepatopancreatic cells were washed three times with cold 1X PBS before incubating with 30 μg/ml labeled dsHSD in working medium at room temperature for 15 min. The cells were washed two times and fixed, then permeabilized and washed following the protocol as previously mentioned. The permeabilized cells were subsequently blocked with 1% BSA in 1X PBS for 1 h prior to incubate with 1:100 rabbit anti-Rab5 or anti-Rab7 polyclonal antibody for 1 h. After washing three times with 1X PBS, 5 min each, 1:3000 Alexa Flour® 594 goat anti-rabbit IgG were added and further incubated for 1 h. Thereafter, the cells were washed again three times, and the fluorescence signal was visualized under SR-LDSM confocal microscope.

Investigation of dsHSD internalization pathway in shrimp hepatopancreatic cells

Shrimp hepatopancreatic cells were prepared and seeded at 28 ºC for 15 h. The cells were then washed three times with the culture medium prior to incubating with 15 and 30 μM chlopromazine for 1 hr or with 800 nM bafilomycin A for 30 min in the culture medium. The inactivated cells were then challenged with 10 μg/ml fluorescein-UTP labeled dsHSD in working medium for 1 min. The medium was removed and the cells were washed twice with 1X PBS following fixation with 4% formaldehyde for 10 min. The fixed cells were washed with 1X PBS for three times, 5 min each and were blocked with 1% BSA in 1XPBS for 1 h. Thereafter, the signals from labeled dsHSD were amplified by 1:200 rabbit anti-fluorescein polyclonal antibody for 1 h. After washing, the cells were detected by 1:100 FITC-conjugated goat anti-rabbit IgG. The cells were washed again for three times, 5 min each before incubating with DAPI (10 μg/ml) for 10 min. The slide was dried and mounted with mounting medium prior to visualization with SR-LDSM confocal microscope.

Interfering of dsHSD internalization using antibody targeting ATP synthase beta subunit or angiostatin

To investigate whether interfering of ATP synthase could reduce dsHSD internalization in hepatopancreatic cells, the cells were incubated with 1.6, 3.2 and 6.5 μg/ml mouse anti-ATP synthase beta subunit monoclonal antibody on ice for 10 min or with 1, 2 and 4 μg/ml angiostatin at room temperature for 30 min. Thereafter, 10 μg/ml of labeled dsHSD was added and further incubated for 1 min. The cells were fixed prior to permeabilized and the detection was performed using antibodies and the signals were observed under confocal microscope as mentioned above.

Investigation of RNAi activity by the internalized dsRNA

To investigate whether the internalized dsRNA could activate RNAi activity, the hepatopancreatic cells were prepared from 18-20 shrimp as mentioned above. The cells were seeded in culture dish and dsRNAs were added immediately at 24 μg/ml and incubated at 28 °C overnight. The cells were then collected and used for RNA extraction

by Tri-reagent according manufacturer's instruction. About 2.5 μg of total RNA were then used as a template for semi- quantitative RT- PCR detection of mRNA corresponding to each dsRNA using actin as an internal control. The PCR product was then visualized using 2 % agarose gel electrophoresis. The primers used for amplification of each gene and their nucleotide sequences were shown in Table 1. For antibody assay, 6.5 μg/ml of mouse anti-human ATP synthase beta subunit monoclonal antibody was added immediately to the resuspension cells, and incubated on ice for 15 min prior to the addition of 24 μg/ml labeled dsHSD and further incubated on ice for 15 min prior to seeding in working medium to the total volume of 5 ml and incubated at 28 °C for 12 h following semi-quantitative RT-PCR technique.

Table 1 Primers for amplification of gene transcript and their nucleotide sequences

Target gene	Nucleotide sequence
Actin	
Forward	5′ GACTCGTACGTGGGCGACGAGG 3′
Reverse	5′ AGCAGCGGTGGTCATCTCCTGCTC 3′
HSD	
Forward	5′ CTCTGCCACGATTCCTGCCC 3′
Reverse	5′ CTTGCTTATTGTGCCTGGGC 3′
Rab7	
Forward	5′ ATGGCATCTCGCAAGAAGATT 3′
Reverse	5′ TTAGCAAGAGCATGCATCCTG 3′

Quantitative colocalization analysis

In order to investigate the degree of colocalization between the labeled dsHSD and cell surface ATP synthase beta subunit in shrimp hepatopancreatic cells, 30 images from three replicates containing approximately 200- 300 cells per time point were selected for analysis using region of interest (ROI) by Coste protocol [36]. The significant colocalization was determined using Pearson's colocalization coefficient (PCC) and Mander's overlapping coefficient (MOC). Only colocalization spots that showed PCC more than 0. 3 were counted. *P*- value for statistically significant colocalization was obtained from each replicate comparing to the negative control. For quantitative intensity analysis, the direct intensity from fluorescein- UTP labeled dsHSD was measured using image analysis accompany with SR- LDSM confocal microscope. The intensity values were averaged and presented as mean±SEM in arbitrary unit.

Results

Specific binding of labeled dsRNA to shrimp hepatopancreatic membrane proteins

To identify dsRNA interacting proteins in shrimp hepatopancreas that potentially act as a dsRNA receptor on the cell surface, membrane protein fractions extracted using buffer M and buffer W were resolved by 12.5% SDS-PAGE. Thereafter, the resolved proteins were transferred onto a nitrocellulose membrane for ligand blot assay. Five specific protein bands corresponding to fluorescein-generated signals (M1, W1, W2, W3 and W4) were selected for mass spectrometry analysis prior to homology search against the NCBI database using Mascot software (Matrix Sciences). The

matched proteins are shown in the **Table 2**. ATP synthase alpha and beta subunits were identified from the bands M1 and W4, respectively. The presence of a putative nucleotide binding sequence in ATP synthase beta subunit suggests that it could be a potential candidate protein for dsRNA internalization in shrimp cells. Thus, the ATP synthase beta subunit was selected for further investigation.

Table 2 Mascot search results for protein bands from ligand blot assay

Bands	Matched proteins (species)	kDa	Amino acid sequences of matched fragments	Coverage (%)	score
M1	ATP synthase α subunit (*L. vannamei*)	11.6	SPEYTSENPLETK IAGLASGLETGETPIAK	2	88
W1	Hsp90 (*P. monodon*)	83.5	LVPNKDDRTLTIIDSGIG MTKADLVNNLGTIAK ALLFLPRRAPFDLFENR LGIHEDSTNR EQVQNSAFVER	9	226
W2	Ribophorin I (*P. monodon*)	68	TIIPASAK IQDDAVELDLRPRFPLFGGWK NLVESHIQDFSLK	6	120
W3	Beta actin (*L. vannamei*)	42.2	AVFPSIVGRPR VAPEEHPVLLTEAPLNPK GYTFTTTAER EITALAPSTMK	13	63
W4	ATP synthase β subunit (*L. vannamei*)	56	IINVIGEPIDER VVDLLAPYSK IGLFGGAGVGR	6	142

The results were analyzed via www.matrixsience.com

Internalization of the dsHSD into hepatopancreatic cells

In order to optimize the condition for dsRNA internalization assay, shrimp primary hepatopancreatic cells were incubated with the fluorescein-UTP labeled dsHSD (dsRNA targeting shrimp hydrogen sulfide dismutase) at various time points. The cells were subsequently fixed and permeabilized prior to detection of the labeled dsHSD using rabbit anti-fluorescein polyclonal antibody. The result of signal amplification using FITC-conjugated goat anti-rabbit secondary antibody showed that the labeled dsHSD was internalized into hepatopancreatic cells, and accumulated in tiny punctate structures within just one minute after incubation. The internalized dsHSD was increasingly accumulated into larger vesicles upon longer incubation times at 5-10 min (Fig. 1A). This evidence indicates the rapid internalization of dsHSD into hepatopancreatic cells in the working medium, which is optimal for further assays. Pretreatment of the cells with various concentrations of the unlabeled dsHSD prior to challenging with the labeled dsHSD showed that the intensity of the signal in the cells decreased significantly compared with the dsHSD-challenged cells without pretreatment (Fig. 1B), suggesting that the internalization of dsRNA occurred in a competitive manner.

In addition, to investigate whether the internalization process is specific only for dsHSD or not, an unlabeled dsRab7 as well as a plasmid DNA was used as competitors for dsHSD internalization. The result in Fig. 1C showed that both competitors could also reduce the signal of the internalized labeled dsHSD at the same extent as the unlabeled dsHSD, which suggests that dsRNA and DNA may share the internalization pathway in shrimp hepatopancreatic cells which is likely to be broadly specific to nucleic acids.

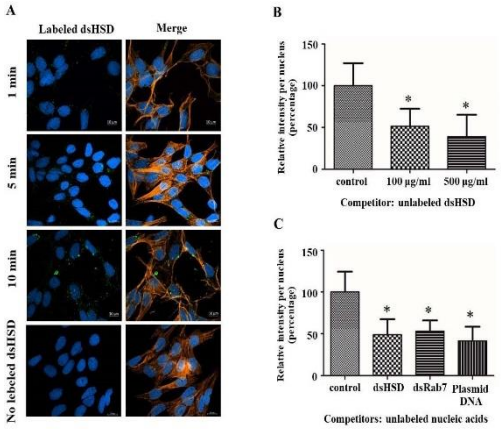

Fig. 1 Internalization of labeled dsHSD into shrimp hepatopancreatic cells Primary hepatopancreatic cells from P. *monodon* were challenged with different concentrations of fluorescein-UTP labeled dsHSD. (A) The signals of dsHSD (green) were shown in the left panels, and the merging between the dsHSD signals and Rhodamine Phalloidin staining of actin (orange) to indicate cell boundary was shown in the right panels. (B) Competitive internalization was performed by the pretreatment with 100 μg/ml and 500 μg/ml of unlabeled dsHSD, and the intensity of dsHSD signals were calculated as a percentage to that of the control cells using image wizard analysis. (C) The competitive internalization was analyzed by using different dsRNA (dsRab7) and plasmid DNA.

Colocalization between fluorescein-UTP labeled dsHSD and ATP synthase beta subunit

To investigate the capability of cell surface ATP synthase beta subunit to internalize dsRNA into hepatopancreatic cells, the colocalization between the cell surface ATP synthase beta subunit and the labeled dsHSD was investigated. Shrimp primary hepatopancreatic cells were incubated on ice with fluorescein-UTP label dsHSD for 2.5 min, then the labeled dsHSD and ATP synthase beta subunit were detected by incubating with their antibodies on ice to prevent endocytosis prior to cell fixation. The result in Fig. 2 showed the colocalization between the signals of dsHSD and the ATP synthase beta subunit on the cell surface. This co-existence therefore implies the potential internalization process of dsHSD via the cell surface ATP synthase beta subunit of the hepatopancreatic cells.

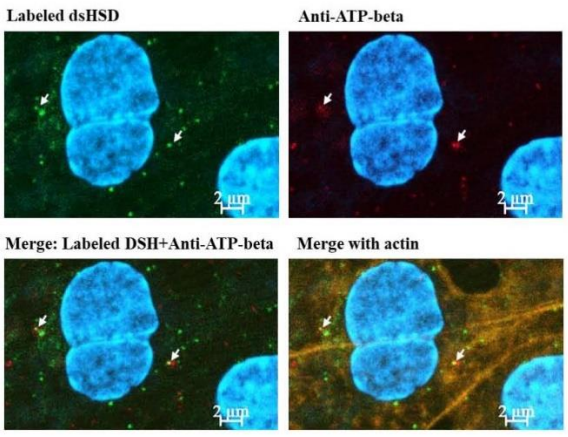

Fig. 2 Colocalization between cell surface fluorescein-UTP-labeled dsHSD and ATP synthase beta subunit Primary cell culture from hepatopancreas were incubated on ice with 10 μg of fluorescein-UTP-labeled dsHSD for 2.5 min followed by detection of the labeled dsHSD (green) and ATP synthase beta subunit (red) on ice. After cell fixation with 1% formaldehyde, the images were captured using LSM800 confocal microscope. The colocalization spots were indicated by white arrows. The cell boundary was indicated using Rhodamine Phalloidin staining (orange).

To determine the dynamic of dsRNA internalization by ATP synthase beta subunit, the colocalization was further performed at different time courses of dsHSD challenge in non-permeabilized as well as in permeabilized cells. At 2.5 min time course, the colocalized signals were observed in both non-permeabilized and permeabilized cells (Fig. 3A). The presence of colocalization signals on the cell surface of non-permeabilized cells confirms that the interaction between the cell surface ATP synthase beta subunit and dsHSD is required for the internalization process. To a lesser extent, the colocalization could also be observed at other time courses from 45 sec to 5 min (Fig. S1) suggesting that ATP synthase beta subunit could internalize dsHSD rapidly after challenging to the cells. Nevertheless, no colocalized signal could be detected at 10-minute time course implying that dsHSD may have been dissociated from ATP synthase beta subunit prior to entering into the trafficking pathway (Fig. S1).

Considering the number and the site of colocalization, most of the colocalized signals were detected intracellularly in permeabilized cells at 45 sec time course while the majority of colocalization at 2.5 and 5 min time course was presented at the cell surface indicating the dynamic of rapid internalization of dsHSD into shrimp hepatopancreatic cells within the first 45 sec (Fig. 3B).

To determine the degree of colocalization and the correlation between the green fluorescence from FITC (dsHSD) and red fluorescence from Alexafluor 647 (ATP synthase beta subunit) at each time course, quantitative colocalization analysis was performed using Costes protocol [36]. According to this analysis, the co-occurrence or overlapping of the two signals was calculated using Mander's overlapping coefficient (MOC) (Fig. 3C). This coefficient reflects true colocalization. When the two signals are overlapping in the same place then the relationship between the two signals was determined by Pearson's colocalization coefficient (PCC) (Fig. 3C). The average MOC, r=0.838 is highest at 2.5 minutes suggesting that the two signals are in the best co-occurrence at this time course generating brighter colocalization signals. The average PCC from each time point are not significantly different from time course 45 sec to 5 min indicating similar correlation at these time courses. At the 10 min time course, colocalization spots were not observed, and the PCC and MOC are close to the negative control implying their dissociation occurred earlier than this time course (Fig. 3C).

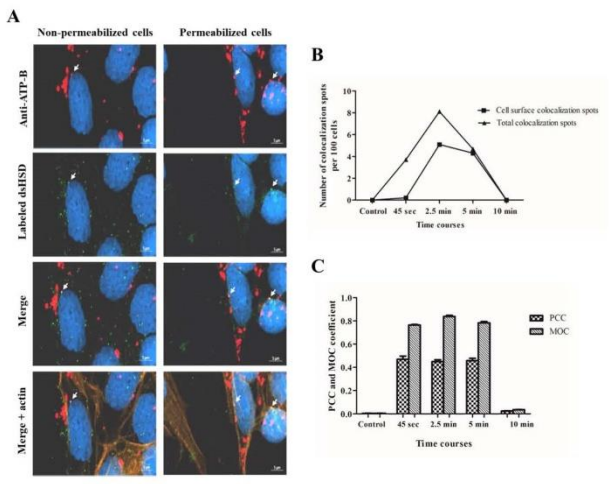

Fig. 3 Time course colocalization between labeled dsHSD and cell surface ATP synthase beta subunit Shrimp primary hepatopancreatic cells were incubated with 10 μg of labeled dsHSD at 2.5 min time course prior to detection of the labeled dsHSD and ATP synthase beta subunit as described in Fig. 2. (A) Colocalization signals (yellow) between ATP synthase beta subunit (red) and dsHSD (green) at 2.5 min in non-permeabilized cells (left panels) and permeabilized cells (right panels). (B) Line graphs comparing total colocalization spots counted from permeabilized cells and cell surface colocalization spots counted from non-permeabilized cells at different time courses. (C) Quantitative colocalization analysis was performed by using Pearson colocalization coefficient (PCC) and Mander colocalization coefficient (MCC) at each time course.

Interfering of ATP synthase beta subunit with monoclonal antibody and angiostatin impeded internalization of dsRNA

The function of ATP synthase beta subunit to internalize dsRNA into cells was further verified by antibody neutralization. We hypothesized that dsHSD interacts with ATP synthase beta subunit via the nucleotide binding site prior to cellular internalization and thus, the antibody designed to target the nucleotide biding site of ATP synthase beta subunit should be able to block the internalization of dsHSD in primary hepatopancreatic cells. The result showed that although significantly different from the control, the mouse anti-ATP synthase beta subunit monoclonal antibody could inhibit the internalization by approximately 25% only (Fig. S2). The binding between the antibody and its target at room temperature presumably induced endocytosis of the antibody into cells resulting in less efficiency of antibody blocking. The antibody blocking was thus further carried out on ice to investigate whether this could inhibit endocytosis and enable effective inhibition of dsHSD internalization. Strikingly, the result showed a significant decrease of dsHSD internalization when the nucleotide binding site of ATP synthase beta subunit was neutralized with either 1.6, 3.2 or 6.5 μg/ml mouse anti-ATP synthase beta subunit monoclonal antibody on ice comparing to the control (Fig. 4A, B). The result indicated that nucleotide binding site plays a key role in dsRNA internalization. Similarly, treatment of shrimp primary hepatopancreatic cells with different concentrations of angiostatin prior to incubation with dsHSD showed a significant reduction of dsHSD internalization in the cells treated with 4 μg/ml angiostatin comparing to the control (Fig. 4C). These results confirmed that dsHSD interacts with ATP synthase beta subunit via the nucleotide binding site prior to internalize into cells.

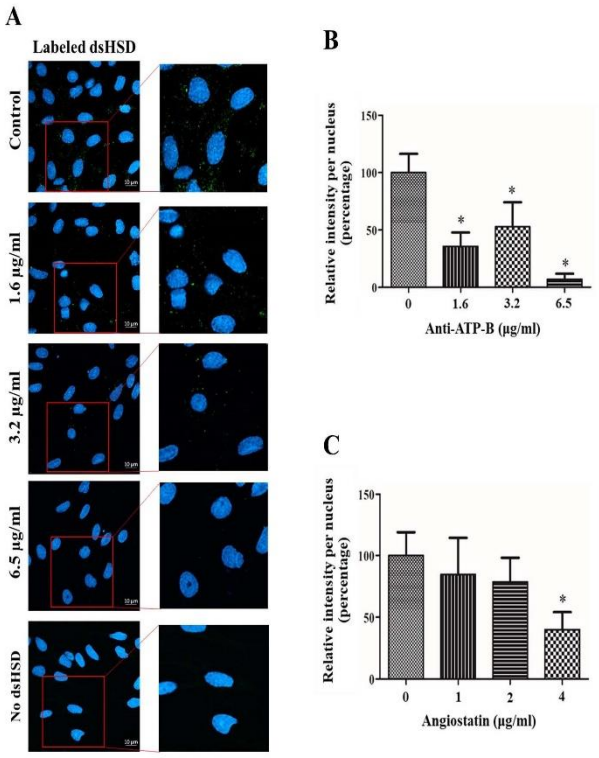

Figure 4 Interference of dsHSD internalization by anti-ATP synthase beta subunit monoclonal antibody and angiostatin (A) Shrimp primary hepatopancreatic cells were challenged with mouse anti-human ATP synthase beta subunit monoclonal antibody on ice prior to challenge with the labeled dsHSD. The signal of dsHSD (green) was detected by rabbit anti-fluorescein-UTP polyclonal antibody, and actin was visualized by Rhodamine Phalloidin staining (orange). The enlargement of the images in square boxes was illustrated in the right panels (B) Quantitative analysis of the signal intensities as a percentage to that of the control cells was performed using image wizard analysis. (C) The cells were challenged with different amounts of an ATP inhibitor, angiostatin prior to dsHSD internalization, and the quantitative analysis was performed.

Pathway of dsHSD internalization into shrimp primary hepatopancreatic cells

To determine whether dsHSD is internalized via receptor-mediated endocytosis which requires interaction with ATP synthase beta subunit, the primary hepatopancreatic cells were treated with endocytic inhibitors chlorpromazine or bafilomycin A prior to incubating with the labeled dsHSD. Chlorpromazine binds effectively to clathrin heavy chains while bafilomycin A inhibits vacuolar ATPase in endosomal-lysosomal acidification, and therefore could reduce endocytosis into the cells. The result demonstrated a significant reduction of the fluorescence intensity of dsHSD in 15 or 30 μM chlorpromazine treated cells (Fig. 5A). Likewise, inhibition by 800 nM bafilomycin A also showed dramatically reduced dsHSD signals as compared to the control (Fig. 5B). In addition, colocalization between dsHSD and either Rab5 or Rab7 (Fig. 5C) confirmed that dsHSD internalization into the cells occurs via the clathrin-mediated endocytosis.

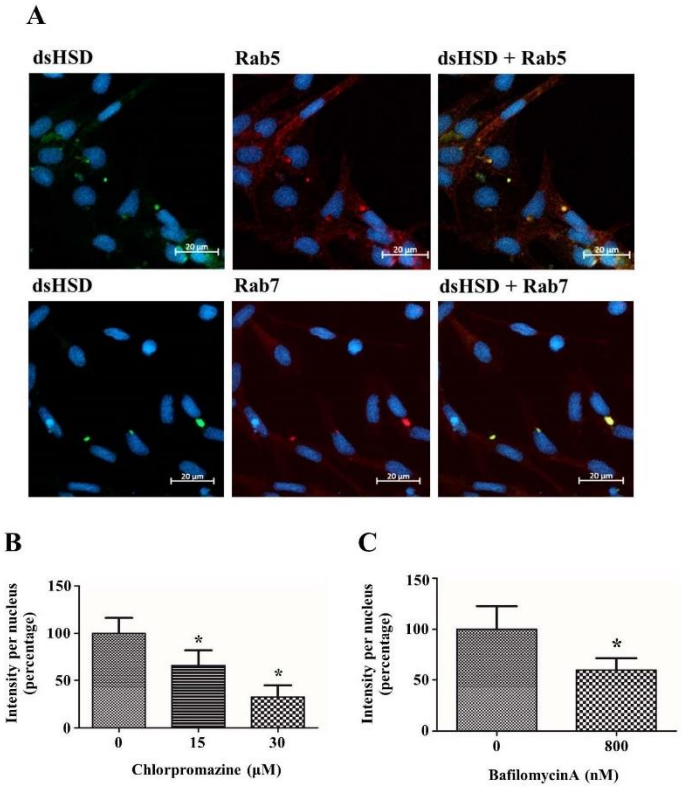

Fig. 5 Pathway of dsRNA internalization Shrimp primary hepatopancreatic cells were treated with endocytic inhibitors before incubating with the labeled dsHSD**.** (A) Colocalization signals in the dsHSD treated cells between the labeled dsHSD (green) and Rab5 (orange; top row) or Rab7 (orange; bottom row) were seen as yellow spots (right panel of both rows). Bar graphs show quantitated intensity of fluorescein-UTP-labeled dsHSD in the cells that were pre-treated with either 15 or 30 μM chlorpromazine (B) or 800 nM bafilomycinA (C) comparing with dsHSD-treated cells that were not pre-treated with endocytic inhibitors as a control

The linkage between ATP synthase beta subunit and RNAi pathway

To demonstrate whether the internalization of dsRNA via ATP synthase beta subunit could activate the RNAi pathway, the expression level of shrimp endogenous genes (HSD and Rab7) in primary hepatopancreatic cells treated with gene-specific

dsRNA was compared with the expression in the cells that was pre-incubated with anti-ATP synthase beta subunit antibody at 4 ºC prior to dsRNA challenge.

Initially, the incubation of primary hepatopancreatic cells with extracellular dsRNA resulted in a reduced expression level of its corresponding gene to around 40-50% of the control level indicating that the internalized dsRNA could activate RNAi pathway to suppress target mRNA expression (Fig. 6A). This knockdown condition was therefore used for further investigation on the involvement of ATP synthase beta subunit in dsRNA-mediated gene silencing pathway.

To investigate whether ATP synthase beta subunit is required for RNAi activation by internalization of dsRNA into cells, the ATP synthase beta subunit on the cell-surface was blocked with anti-ATP synthase beta subunit antibody on ice for 30 min to prevent the antibody endocytosis prior to dsHSD challenge. Analysis of HSD mRNA level by semi-quantitative RT-PCR showed a significant reduction of HSD expression in the dsHSD-treated cells that were not pre-incubated with anti-ATP synthase beta subunit antibody to approximately 25% of HSD expression in control cells. Strikingly, the expression of HSD in the cells that were pre-incubated with anti-ATP synthase beta subunit antibody prior to dsHSD treatment was markedly recovered to about 50% of the control (Fig. 6B). This result indicated that blocking ATP synthase beta subunit with the antibody could reduce dsHSD internalization resulting in impaired HSD suppression by dsHSD, and thus strongly confirmed the role of ATP synthase beta subunit in dsRNA internalization.

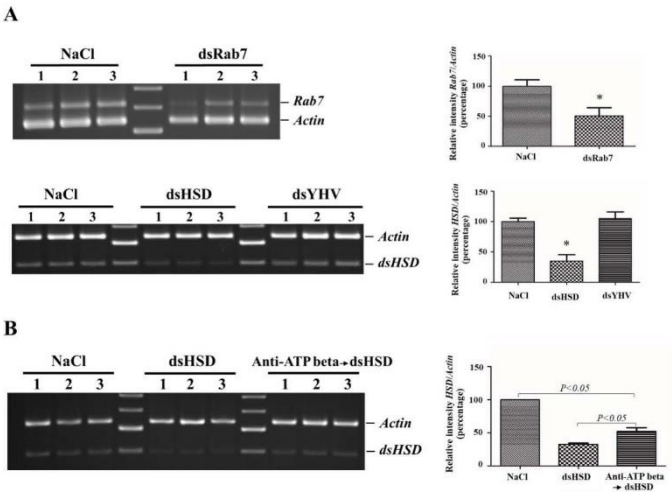

Fig. 6 Functional assay of ATP synthase beta subunit-mediated dsRNA internalization on RNAi activity **(**A**)** Shrimp hepatopancreatic cells were initially challenged with 10 μg/ml of either dsHSD, dsRab7 or dsYHV to investigate whether the cells could show specific knockdown**.** Gene transcript levels were determined by RT-PCR **(**left panels**)**, and the band intensities were calculated by ImageJ program and presented as bar graphs **(**right panels**). (**B**)** The cells were blocked with anti-ATP synthase beta subunit monoclonal antibody at 4 °C prior to challenge with dsHSD**.** Gene transcript levels were determined by RT-PCR comparing between the control and the dsHSD-challenged group either without or with ATP synthase beta subunit blocking by antibody**.** The results were shown as mean±SEM from three independent experiments**.**

Discussion

Endocytic pathway proteins have been identified for years as the proteins that are primarily involved in the internalization of dsRNA by using RNA interference system or drug inhibitors [3]. However, cell surface proteins required for the internalization of dsRNA remain unclear. It has been described that blocking of class A and class C scavenger receptors by specific inhibitors could reduce dsRNA internalization into the cells, but the knockdown of these proteins showed no inhibition of RNAi activity [7,10], which suggests that there might be other pathways for dsRNA internalization. In this study, the cell surface protein that could internalize dsRNA into shrimp hepatopancreatic cells was studied. Membrane proteins that could interact with dsRNA were initially identified using ligand blot assay. In addition to nonionic detergent-containing buffer M that is generally used for membrane protein extraction, buffer W that contains switterionic buffering reagent was also used to maintain stability of the integral membrane proteins [25]. The immobilized proteins on western blot were refolded back to their native form prior to binding with labeled dsHSD to allow proper interactions between them. The bands that could bind with dsHSD were identified by mass spectrometry and analyzed by Mascot matrix science based on the basis that they showed high scores with more than two hits with proteins in the database (data not shown). Interestingly, the alpha and beta subunits of ATP synthase were both identified (Table 2). These subunits contain a nucleotide binding domain and thus, might be able to interact with dsHSD [26]. Although the molecular mass of the proteins identified in the sample does not corresponded to the mutual form of ATP synthase subunits but it is possible that this could be the degraded form of ATP synthase subunits harboring the nucleotide binding domain [27]. ATP synthase beta subunit was selected for investigating the interaction with dsHSD as this subunit is composed of nucleotide binding domain that acts as catalytic site for ATP synthase activity [28] whereas the alpha subunit contains non-catalytic substrate binding site [26].

The primary hepatopancreatic cells could internalize dsHSD in just one minute and showed the intense signal at 5 min indicating rapid and effective internalization similar to the study in *Drosophila* S2 cells and human cell line [3, 7]. To be able to internalize dsHSD into cells, ATP synthase beta subunit must be activated at the cell surface membrane. Many studies in various cell types including shrimp cells showed that the cell surface-expressed ATP synthase beta subunit is capable of activating ATP synthesis [29-34]. The colocalization of ATP synthase beta subunit with the labeled dsHSD suggests the interaction between them prior to dsRNA internalization into the cells. The ATP synthase beta subunit can be in different conformations according to phosphorylation stages of its bound adenine nucleotides. Upon acquiring Pi group, the ADP-bound ATP synthase beta subunit is in a tight stage and will turn into an opened stage when the ATP is produced and released [26]. At this stage, it is possible that ATP synthase beta subunit could provide a binding site for the phosphate group in the nucleotides of dsHSD. This was confirmed by cell surface colocalization using living cell staining, in which the labeled dsHSD was allowed to bind with cell surface ATP synthase beta subunit in culture medium. The punctate appearance of the colocalization signals between the labeled dsHSD and ATP synthase beta subunit was similar to the signal between siRNA and P bodies that also exhibited the tiny colocalization spots [35-37]. The average MOC indicating true colocalization was about 0.8 from 45 sec to 5 min time course of dsHSD internalization, which means that about 80% of signals

from both dsHSD and ATP synthase beta subunit at each colocalization spot were present at the same pixels at the same time [38,39]. Meanwhile, the relationship between the two signals as indicated by the PCC was about 0.48 demonstrating that the chance that the two signals are present together is less than 50%. It was described that the PCC could be even lower as 0.268 while colocalization could still be observed and was also confirmed by FRET method [37].

Most of colocalization spots were observed at 2.5 min time course and have a tendency to reduce after 5 min, while colocalization spot could not be observed at 10 min indicating that the dsRNA internalization into the cells lasts only few minutes. In the event of receptor mediated endocytosis, the ligand must bind to a receptor and forms a cluster of ligand-receptor complex. Clathrin was then recruited to form a clathrin coated pit and released from plasma membrane as clathrin-coated vesicles [40]. This event takes about less than 2.5 min, and this is the chance that the colocalization could be observed prior to internalization, which corresponds to the results obtained in this study. In addition, colocalization between the labeled dsHSD and endocytic proteins Rab5 or Rab7 as well as the interference of dsHSD internalization by endocytic inhibitors, chlorpromazine and bafilomycin A evidently suggests that dsRNA is localized to late endosome after internalization.

The internalization of dsHSD via ATP synthase beta subunit was further confirmed by neutralization assay using anti-ATP synthase beta monoclonal antibody that were designed to bind with the nucleotide binding site of ATP synthase beta subunit and ATP synthase inhibitor angiostatin. The result showed severe inhibition of internalization at about 90% using the antibody and about 50% using angiostatin (Fig. 4), which affirms that the binding between dsHSD and the nucleotide binding site of ATP synthase beta subunit is required for dsHSD internalization. Nevertheless, blocking with antibody and angiostatin did not completely inhibit the internalization of dsHSD indicating that there could be some other pathways for dsRNA internalization.

Whether or not the internalization of dsHSD through ATP synthase beta subunit could activate RNAi pathway was further proven in shrimp hepatopancreatic cell culture. In order to see the clear effect of dsHSD internalization on the suppression of HSD expression, the ATP synthase beta subunit was blocked with the antibody on ice to inhibit endocytosis of the antibody so as to ensure that the antibody could effectively participate in dsHSD uptake as low dsRNA uptake at 4 °C was previously reported [3]. Blocking ATP synthase beta subunit with the antibody showed significant reduction in RNAi activity, as could be seen by a lower degree of suppression of HSD mRNA comparing to the control (Fig. 6B). Thus, this result clearly demonstrated that dsHSD is internalized by ATP synthase beta subunit to activate the RNAi pathway, and eventually suppress the expression of mRNA target.

In conclusion, the mechanism of dsRNA internalization into shrimp cells through the ATP synthase beta subunit was demonstrated. It is likely that dsRNA interacts with the nucleotide binding site of ATP synthase beta subunit prior to internalization into cells, before transported through endocytosis pathway to activate RNAi at the end. However, the mechanism of dsRNA release from endocytic compartments is still unknown. Further investigation should be emphasized on the mechanism of how dsRNA is released into cytosol including other possible pathways of dsRNA internalization that could rapidly activate the RNAi pathway.

References

1. G.V. Limmon, M. Arredouani, K.L. McCann, R.A. Corn Minor, L. Kobzik, F. Imani, Scavenger receptor class-A is a novel cell surface receptor for double-stranded RNA. FASEB J. 22 (2008) 159-167.
2. D. L. McEwan, S. W. Alexandra, P. H. Craig, Uptake of Extracellular Double-Stranded RNA by SID-2. Mol. Cell 47 (5) (2012) 746-754.
3. M.C. Saleh, R. P. van Rij, A. Hekele, A. Gillis , E. Foley, P.H. O'Farrell, R. Andino, The endocytic pathway mediates cell entry of dsRNA to induce RNAi silencing. Nat. Cell Biol. 8 (8) (2006) 793-802.
4. C. Lorenz, M. Fotin-Mleczek, G. Roth, C. Becker, T.C. Dam, W.P.R. Verdurmen, R. Brock, J. Probst, T. Schlake, Protein expression from exogenous mRNA: Uptake by receptor-mediated endocytosis and trafficking via the lysosomal pathway. RNA Biol. 8 (4) (2011) 512 627-636.
5. M.J. Lehmann, G. Sczakiel, Spontaneous uptake of biologically active recombinant DNA by mammalian cells via a selected DNA segment. Gene Ther. 12 (2004) 446.
6. R.L. Juliano, X. Ming, O. Nakagawa, Cellular Uptake and Intracellular Trafficking of Antisense and siRNA Oligonucleotides. Bioconjug. Chem. 23 (2) (2012) 147-157.
7. S. J. DeWitte-Orr, S.E. Collins, C.M.T. Bauer, D.M. Bowdish, K.L. Mossman, An Accessory to the Trinity : SR-As Are Essential Pathogen Sensors of Extracellular dsRNA, Mediating Entry and Leading to Subsequent Type I IFN Responses. PLoS Pathog. 6 (3) (2010) e1000829-e1000829.
8. J.E. Ziello, Y. Huang, I.S. Jovin, Cellular Endocytosis and Gene Delivery. Mol. Med. 16 (5-6) (2010) 222-229.
9. W. Li, K.S. Koutmou, D.J. Leah, M. Li, Systemic RNA Interference Deficiency-1 (SID-1) Extracellular Domain Selectively Binds Long Double-stranded RNA and Is Required for RNA Transport by SID-1. J. Biol. Chem. 290 (31) (2015) 18904-18913.
10. J. Ulvila, M. Parikka, A. Kleino, R. Sormunen, R.A. Ezekowitz, C. Kocks, M. Rämet, Double-stranded RNA Is Internalized by Scavenger Receptor-mediated Endocytosis in Drosophila S2 Cells. J. Biol. Chem. (20) (2006)14370-14375.
11. J.D. Shih, C.P. Hunter, SID-1 is a dsRNA-selective dsRNA-gated channel. RNA 17 (6) (2011) 1057-1065.
12. H. Huvenne, G. Smagghe, Mechanisms of dsRNA uptake in insects and potential of RNAi for pest control: A review. J. Insect Physiol. 56 (3) (2010) 227-235.
13. E. Brencicova, S.S. Diebold, Nucleic acids and endosomal pattern recognition: how to tell friend from foe? Front. Cell. Infect Microbiol. 3 (2013) 37.
14. J. A. Majde, N. Guha-Thakurta, Z. Chen, S. Bredow, J.M. Krueger, Spontaneous release of stable viral double-stranded RNA into the extracellular medium by influenza virus-infected MDCK epithelial cells: implications for the viral acute phase response. Arch. Virol. 143 (12) (1998) 2371-2380.
15. O. Mandelboim, N. Lieberman, M. Lev, L. Paul, T.I. Arnon, Y. Bushkin, D.M. Davis, J.L. Strominger, J.W. Yewdell, A. Porgador, Recognition of haemagglutinins on virus-infected cells by NKp46 activates lysis by human NK cells. Nature 409 (6823) (2001) 1055-1060.
16. H. Jiang, E.J. White, C.I. Ríos-Vicil, J. Xu, C. Gomez-Manzano, J. Fueyo, Human Adenovirus Type 5 Induces Cell Lysis through Autophagy and Autophagy-Triggered Caspase Activity. J.Virol. 85 (10) (2011) 4720-4729.

17. N.J. Topham, E.W. Hewitt, Natural killer cell cytotoxicity: how do they pull the trigger? Immunology 128 (1) (2009) 7-15.
18. T. Kawai, S. Akira, The roles of TLRs, RLRs and NLRs in pathogen recognition Int Immunol. 21:313. Int. Immunol. 21 (4) (2009) 317-337.
19. Kawai, S. Akira, TLR signaling. Cell Death Differ. 13 (5) (2006) 816-825.
20. L. Vuković , H.R. Koh, S. Myong, K. Schulten, Substrate Recognition and Specificity of Double-Stranded RNA Binding Proteins. Biochemistry 53 (21) (2014) 3457-3466.
21. T. Chendrimada, R. Gregory, E. Kumaraswamy, J. Norman, N. Cooch, K. Nishikura, R. Shiekhattar, TRBP recruits the Dicer complex to Ago2 for microRNA processing and gene silencing. Nature 436 (2005) 740-744.
22. K. Maruekawong, W. Tirasophon, S. Panyim, P. Attasart, Involvement of LvSID-1 in dsRNA uptake in Litopenaeus vannamei. Aquaculture 482 (2018) 65-72.
23. T. Rőszer, The invertebrate midintestinal gland (hepatopancreas) is an evolutionary forerunner in the integration of immunity and metabolism. Cell and Tissue Res. 358 (3) (2014) 685-695.
24. P. Sanitt, P. Attasart, S. Panyim, Protection of yellow head virus infection in shrimp by feeding of bacteria expressing dsRNAs. J. Biotechnol. 179 (2014) 26-31.
25. T. Muinao, M. Pal, H.P.D. Boruah, Cytosolic and Transmembrane Protein Extraction Methods of Breast and Ovarian Cancer Cells: A Comparative Study. J. Biomol. Tech. 29 (3) (2018) 71-78.
26. M.A. Bianchet, J. Hullihen, P.L. Pedersen, L.M. Amzel, The 2.8-Å structure of rat liver F1- ATPase: Configuration of a critical intermediate in ATP synthesis/hydrolysis. PNAS 95 (19) (1998) 11065-11070.
27. J.E. Alard, S. Hillion, L. Guillevin, A. Saraux, J.O. Pers, P. Youinou, C. Jamin, Autoantibodies to endothelial cell surface ATP synthase, the endogenous receptor for hsp60, might play a pathogenic role in vasculatides. PloS One 6 (2) (2011) e14654-e14654.
28. S.L. Chi, M.L. Wahl, Y.M. Mowery, S. Shan, S. Mukhopadhyay, S.C. Hilderbrand, D.J. Kenan, B.D. Lipes, C.E. Johnson, M.F. Marusich, R.A. Capaldi, M.W. Dewhirst, S.V. Pizzo, Angiostatin-Like Activity of a Monoclonal Antibody to the Catalytic Subunit of FlFo ATP Synthase. Cancer Res. 67 (10) (2007) 4716.
29. Y. Liang, M.L. Xu, X.W. Wang, X.X. Gao, J.J. Cheng, C. Li, J. Huang, ATP synthesis is active on the cell surface of the shrimp Litopenaeus vannamei and is suppressed by WSSV infection. Virol. J. 12 (2015) 49.
30. T.L. Moser, D.J. Kenan, T.A. Ashley, J.A. Roy, M.D. Goodman, U.K. Misra, D.J. Cheek, S.V. Pizzo, Endothelial cell surface F1Fo ATP synthase is active in ATP synthesis and is inhibited by angiostatin. PNAS 98 (12) (2001) 6656-6661.
31. N. Arakaki, T. Nagao, R. Niki, A. Toyofuku, H. Tanaka, Y. Kuramoto, Y. Emoto, H. Shibata, K. Magota, T. Higuti, Possible Role of Cell Surface H+-ATP Synthase in the Extracellular ATP Synthesis and Proliferation of Human Umbilical Vein Endothelial Cells. Mol. Cancer Res. 1 (13) (2003) 931-939.
32. Z. Ma, M. Cao, Y. Liu, Y. He, Y. Wang, C. Yang, W. Wang, Y. Du, M. Zhou, F. Gao, Mitochondrial F1Fo- ATP synthase translocates to cell surface in hepatocytes and has high activity in tumor-like acidic and hypoxic environment. ACTA BIOCH BIOPH SIN 42 (8) (2010) 530-537.

33. S.L. Chi, S.V. Pizzo, Cell surface F1Fo ATP synthase: A new paradigm? Ann. Med. 38 (6) (2006) 429-438.
34. T. Gorai, H. Goto, T. Noda, T. Watanabe, H. Kozuka-Hata, M. Oyama, R. Takano, G. Neumann, S. Watanabe, Y. Kawaoka, F1Fo-ATPase, F-type proton-translocating ATPase, at the plasma membrane is critical for efficient influenza virus budding. PNAS 109 (12) (2012) 4615-4620.
35. A. Jakymiw, S. Lian, T. Eystathioy, S. Li, M. Satoh, J.C. Hamel, M.J. Fritzler, E.K.L. Chan, Disruption of GW bodies impairs mammalian RNA interference. Nat. Cell Biol. 7 (12) (2005) 1267-1274.
36. A. Jakymiw, K.M. Pauley, S. Li, K. Ikeda, S. Lian, T. Eystathioy, M. Satoh, M. J. Fritzler, E.K.L. Chan, The role of GW/P-bodies in RNA processing and silencing. J.Cell Sci. 120 (8) (2007) 1317-1323.
37. A. Jagannath, M.J.A Wood, Localization of double-stranded small interfering RNA to cytoplasmic processing bodies is Ago2 dependent and results in up-regulation of GW182 and Argonaute-2. Mol. Biol. Cell 20 (1) (2009) 521-529.
38. S.V. Costes, D. Daelemans, E.H. Cho, Z. Dobbin, G. Pavlakis, S. Lockett, Automatic and Quantitative Measurement of Protein-Protein Colocalization in Live Cells. Biophys. J. 86 (6) (2004) 3993-4003.
39. K.W. Dunn, M.M. Kamocka, J.H. McDonald, A practical guide to evaluating colocalization in biological microscopy. Am. J. Physiol.. Cell physiol. 300 (4) (2011) C723-C742. 612
40. O. L. Mooren, B.J. Galletta, J.A. Cooper, Roles for Actin Assembly in Endocytosis. Annu. Rev. Biochem. 81(1) (2012) 661-686.
41. W. Assavalapsakul, D.R. Smith, S. Panyim, Identification and Characterization of a Penaeus monodon Lymphoid Cell-Expressed Receptor for the Yellow Head Virus. J. Virol. 80 (1) (2006) 262-269.
42. Y. Liang, J.J. Cheng, B. Yang, J. Huang, The role of F1 ATP synthase beta subunit in WSSV infection in the shrimp, Litopenaeus vannamei. Virol. J. 7 (2010) 144-144.
43. D. St Johnston, N.H. Brown, J.G. Gall, M. Jantsch, A conserved double-stranded RNA-binding domain. PNAS USA 89 (22) (1992) 10979-10983.

A multi-target dsRNA for simultaneous inhibition of yellow head virus and white spot syndrome virus in shrimp

Outbreaks of diseases caused by yellow head virus (YHV) and white spot syndrome virus (WSSV) infection in shrimp have resulted in economic losses worldwide. dsRNAmediated RNAi has been used to control these viruses, and the best target genes for efficient inhibition of YHV and WSSV are the protease and ribonuleotide reductase small subunit (rr2), respectively. However, one dsRNA can suppress only one virus, and therefore the production of multi-target dsRNA to effectively inhibit both YHV and WSSV is needed. In this study, plasmids pETpro-rr2_one stem and pETpro-rr2_two stems were constructed to produce two different forms of multi-target dsRNA in *E. coli*, which were designed specifically to both YHV protease and WSSV rr2 genes. The potency of each dsRNA in inhibiting YHV and WSSV and reducing shrimp death were investigated in *L. vannamei*. Shrimp were injected with the dsRNAs into the hemolymph before challenge with YHV or WSSV. The results showed that both dsRNAs could inhibit the viruses, however the one stem construct was more effective than the two stems construct when shrimp were infected with WSSV. This study establishes a potential strategy for dual inhibition of YHV and WSSV for further application in shrimp aquaculture.

Introduction

Penaeid shrimp farming is an important aquaculture industry in Thailand, that contributes positively to the Thai economy, and outbreaks of diseases caused by bacteria or viruses cause shrimp production to be dramatically decreased. Yellow head virus (YHV) and white spot syndrome virus (WSSV) are the most devastating pathogens that cause high shrimp mortality (70-100 %) within a very short period of time (3-10 days) after the onset of symptom (Leu et al., 2009; Senapin et al., 2010).
The biological process of RNA interference (RNAi) has been applied to control these diseases (Robalino et al., 2004; Yodmuang et al., 2006; Assavalapsakul et al., 2009; Attasart et al., 2009). This technique requires the introduction of a long double-stranded RNA (dsRNA) that has sequence specificity to a viral gene into shrimp prior to virus challenge, resulting in suppression of that particular virus, as well as reduction of mortality of the infected shrimp. In addition, it has been shown that the best target genes for efficient inhibition of YHV and WSSV are the protease of YHV (Tirasophon et al., 2005) and the ribonuleotide reductase (small subunit; rr2) of WSSV (Attasart et al., 2009).

Outbreaks of YHV and WSSV (either separately or jointly) have frequently been recorded (Flegel et al., 1996; Mohan et al., 1998; Hamano et al., 2017). However, with the sequence specificity required for successful RNAi mediated inhibition of viral replication, one dsRNA can suppress only one virus. Several strategies such as combined shRNAs/dsRNAs (McIntyre et al., 2011; Gou et al., 2007; Hinton and Doran, 2008; Li et al., 2011; Wang et al., 2006; Wu et al., 2005; Song et al., 2008; Ma et al., 2014; Thammasorn et al., 2015) or multi-target shRNA/dsRNA (Chang et al., 2009; Cong et al., 2010; Junn et al., 2010; Gouda et al., 2010) have been developed for simultaneous suppression of multiple targets. However, competition between mixed dsRNAs may reduce the suppression effect (Gouda et al., 2010). Linking multiple

dsRNAs together would enhance RNAi efficacy over that of mixed dsRNAs. Therefore, the establishment of one molecule of dsRNA to simultaneously inhibit both YHV and WSSV is needed.

To knock down multiple genes/ viruses at the same time, four different approaches have been employed so far. Firstly, a mixture of separate expression vectors was used for coexpression of individual shRNA/ dsRNA for simultaneous gene suppression (McIntyre et al., 2011, Li et al., 2011; Thammasorn et al., 2015). Two hairpins against the HIV-1 genes encoding for Tat and Vif were produced from separate plasmid vectors in HEK293a cells (Figure 1 A). Simultaneous suppression of two target genes was observed, but at a reduced levels due to competition of the hairpins for access to the RNAi machinery (McIntyre et al., 2011). Secondly, multiple shRNAs were produced from a vector containing more than one shRNA expression cassette (Ma et al., 2014; Gou et al., 2007; Hinton and Doran, 2008; Li et al., 2011; Wang et al., 2006; Wu et al., 2005; Song et al., 2008). For example, pMultishVP2/2 was developed to generate two shRNAs specific to vp2 of grass carp reovirus (GCRV-JX0901, genotype I) as well as vp2 of HGDRV (Hubei grass carp disease reovirus, genotype III), respectively (Figure 1 B). The construct could suppress GCRVJX0901 and HGDRV vp2 coding genes simultaneously in CIK (*Ctenopharyngodon idellus* kidney) cells (Ma et al., 2014). Thirdly, one shRNA targeting more than one gene was produced from a recombinant plasmid containing one expression cassette (Cong et al., 2010; Gouda et al., 2010). For example, pCWN11 was constructed to express a multitarget shRNA corresponding to the VP1 genes of foot and mouth disease (FMDV) serotype A, Asia I and O (Figure 1 C). This shRNA could effectively inhibit the replication of three serotypes of FMDV in BHK-21 cells and suckling mice (Cong et al., 2010). Finally, a multi-target shRNA was produced based on a single transcript composed of different hairpin domains (Figure 1 D). pAdlox (k) was constructed to produce one single transcript that can fold generating linked multiple shRNAs. Simultaneous knockdown of the Xchromosome-linked inhibitor of apoptosis protein (XIAP), Akt and Bcl-2 effectivelyinhibited adenovirus replication (Junn et al., 2010).

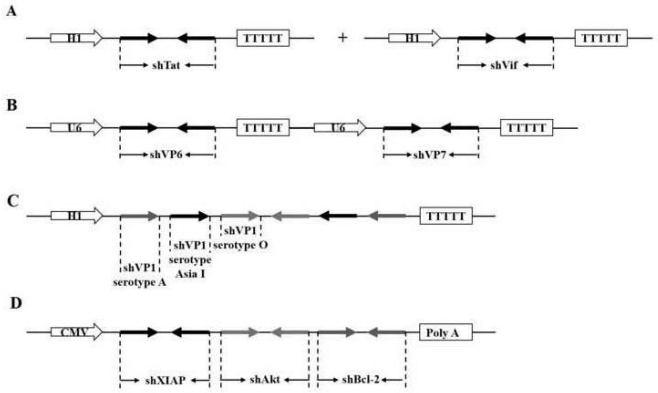

Figure 1. Schematic diagrams for producing shRNAs to suppress multiple target genes

Multiple shRNAs can be synthesized from separate plasmids (A) (McIntyre et al., 2011) or a plasmid containing multiple shRNA expression cassettes (B) (Ma et al., 2014). Multi-targeting shRNA can be produced from a recombinant plasmid containing 1 expression cassette with one inverted repeat of multiple target sequences (C) (Cong et al., 2010) or a recombinant plasmid containing 1 expression cassette with multiple inverted repeats of different target gene sequences (D) (Junn et al., 2010).

In this study, we aimed to produce a long multi-target dsRNA that has two different target genes (YHV protease and WSSV rr2) to minimize competition between two dsRNAs. Two different cloning strategies were employed to produce two forms of stem-loop dsRNA, with one containing one stem and one loop with the second having two stems with their own loops. Their production yield in *E. coli* and dual YHV and WSSV suppression efficacy in shrimp were evaluated.

Materials and methods

Shrimp

Post larva of white leg shrimp (*Litopenaeus vannamei*) were purchased from a farm in Chonburi province. They were reared in a 500 L tank with 10 parts per thousand (ppt) salinity until their bodyweight reached 400 mg.

Viruses

A YHV lysate was kindly provided by Mr. Poohrawind Sanitt. Briefly, the hemolymph of YHV-infected moribund shrimp was drawn and immediately mixed with ACD anticoagulant buffer (85 mM sodium citrate, 62.2 mM citric acid, and 110 mM dextrose, pH 4.9). The solution was centrifuged at 9,000 g for 10 min at 4°C. The crude viral solution was then aliquoted and kept at -80°C until used. The WSSV lysate was prepared from gills of WSSV-infected black tiger shrimp, size about 15-20 g. Fifty milligrams of gill tissue were ground in 500 µl of TN buffer (20 mM Tris-HCL, 400 mM NaCl, pH 7.4). The homogenate was centrifuged at 10,000 g for 10 min at 4°C. The supernatant was transferred to a new 50 ml conical tube and diluted with 150 mM NaCl at 1:10 (v/v). The solution was filtered through a 0.45 µm filter and the virus solution was aliquoted and stored at -80°C until used.

Plasmid construction

In this study, we developed two dsRNA expression plasmids to produce two different forms of dsRNA. One has a single stem-loop (one stem) whereas the other has two stemloop (two stems) structures. The best targets for efficient inhibition of YHV and WSSV are the protease and rr2 genes, respectively. Therefore, these multi-target dsRNAs were designed to contain sequences specific to the YHV protease gene located between 8710-9183 (474 nucleotides) in the YHV genome (Genbank accession no. FJ848675.1) combined with sequences specific to the WSSV rr2 gene located between 146533-146970 (438 nucleotides) in the WSSV genome (Genbank accession no. AF369029.2).

To amplify the YHV protease fragments (sense and anti-sense), RNA extracted from YHV-infected shrimp was converted to cDNA using random primers as described in section 2.9.1. This cDNA was then used as a template for amplification of the protease DNA fragments. DNA extracted from WSSV-infected shrimp was used as a template for rr2 PCR products (both sense and anti-sense) synthesis (using the protocol described in section 2.9.2).

For the one stem dsRNA construct (Figure 2A) the sense fragments of protease (PCR I) and rr2 including loop (PCR II) were amplified using specific primers No.1-2 and No.3-4 (Table 1), respectively. These two fragments were ligated together at the *Hin*d III site before cloning into *Nde* I and *Xho* I digested pET17b. The anti-sense fragments of rr2 (PCR III) and protease (PCR IV) were amplified using primers No.5-

6 and No. 7-8 (Table 1), respectively. The ligated fragment of *Kpn* I digested PCR III and IV was then cloned into the previous vector at the *Nde* I and *Xba* I sites to create the pETpro-rr2_one stem (Figure 2B). Sequence of the construct was confirmed by automated DNA sequencing.

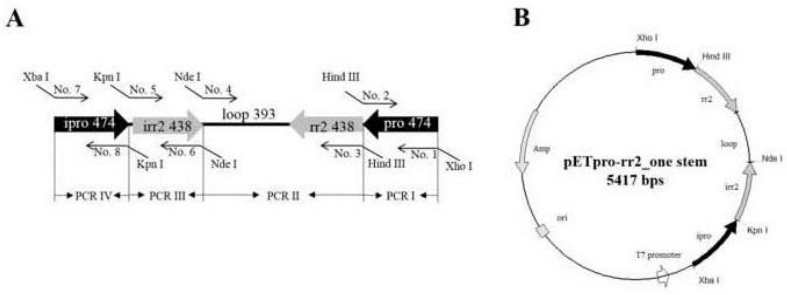

Figure 2. Schematic diagrams for construction of the pETpro-rr2_one stem

(A) The sense fragment of pro-rr2 plus loop was derived from ligation of PCR I and PCR II amplified using primers 1+2 and 3+4, respectively. The anti-sense fragment of pro-rr2 (ipro-irr2) was the ligated product of PCR III (using primers 5+6) and PCR IV (using primers 7+8). The pETpro-rr2_one stem (B) was constructed by cloning inverted repeat of DNA fragments containing YHV protease sequence (pro) (black arrows) linked with WSSV rr2 sequence (rr2) (grey arrows) intervening with one spacer (loop) into pET17b plasmid

Table 1 List of oligonucleotide primers

No	Name	Sequence (5' 3')	Size (bp)	Tm (°C)
1	YHV-*Xho* I-F	GGGGGctcgagTCAGCGGCAAATTCCTCTAC	31	71
2	YHV-*Hin*d III-R	AAAAAaagcttGCCATACCTTGGGTGGAC	29	63
3	rr2-*Hin*d III-F	TTTTTaagcttGGAGCAAGCCAACCAAGTG	30	63
4	rr2-loop-393-*Nde* I-R	TTTTTTTcatatgCAGGCAGGGAAACTGTGAG	32	63
5	irr2-*Kpn* I-F	TTTTTTggtaccGGAGCAAGCCAACCAAGTG	31	66
6	irr2-*Nde* I-R	AAAAAAAcatatgTTCTCCGTAGACGTTGCC	31	62
7	iYHV-*Xba* I-F	GGGGGtctagaTCAGCGGCAAATTCCTCTAC	31	69
8	iYHV-*Kpn* I-R	TTTTTTggtaccGCCATACCTTGGGTGGAC	30	66
9	YHV-loop 124-*Hin*d III-R	CCCCCaagcttGGTCCAGTGTCTCGCAAC	29	72
10	rr2-*Xba* I-F	TTTTTtctagaGGAGCAAGCCAACCAAGTG	30	63
11	rr2-loop-139-*Nde* I-R	GGGGGGGcatatgACAATTAGTTCCGCCAAATCG	34	69
12	Actin-F	ATGGCATCTCGCAAGAAGATT	21	65
13	Actin-R	TTAGCAAGAGCATGCATCCTG	21	65
14	YHV-Hel-F	CAAGGACCACCTGGTACCGGTAAGAC	26	72
15	YHV-Hel-R	GCGGAAACGACTGACGGCTACATTCAC	27	76
16	WSSV-VP28-F	CCGCTCGAGACTCTTTCGGTCGTGTCGGCC	30	84
17	WSSV-VP28-R	GGCACCATCTGCATACCAGTG	21	68

.

For the two stems dsRNA construct (Figure 3A) the sense fragment of the protease with loop (PCR I) and anti-sense fragment of protease (PCR II) were amplified using specific primers No.1-9 and No.1-2 (Table 1), respectively. These two fragments were ligated at the *Hin*d III site and cloned into *Xho* I digested pET17b. Next, the sense fragment of rr2 including loop (PCR III) and the anti-sense fragment of rr2 (PCR IV) were amplified using specific primers No. 10-11 and No. 6-10 (Table 1), respectively. These two PCR products (PCR III and IV) were digested with *Nde* I and ligated together before cloning into the previous vector at *Xba* I site created the pETpro-rr2_two stems (Figure 3B). Sequence of the construct was confirmed by automated DNA sequencing. This pETpro-rr2_two stems was then used to generate the control plasmids (pETrr2 and pETpro) by removing *Xho* I and *Xba* I fragments, respectively. The pETpro was used to produce dsRNA targeted to YHV protease (dspro) while the pETrr2 was used to express dsRNA specific to WSSV rr2 (dsrr2).

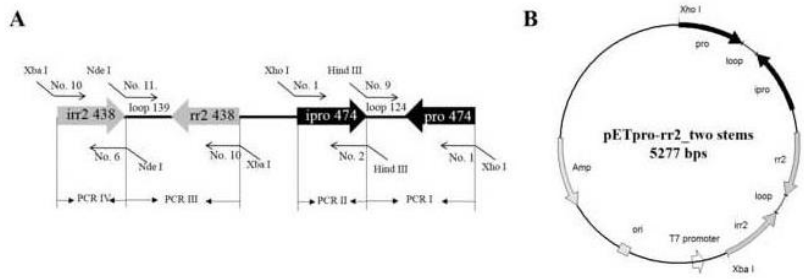

Figure 3. Schematic diagrams for construction of pETpro-rr2_two stems
(A) The inverted repeat of protease was derived from ligation of PCR I and PCR II amplified using primers 1+9 and 1+2, respectively. The inverted repeat of rr2 was the ligated product of PCR III (using primers 10+11) and PCR IV (using primers 6+10). The pETprorr2_two stems (B) was constructed by cloning of two inverted repeats of protease DNA fragment (ipro-loop-pro, black arrows) and rr2 DNA fragments (irr2-loop-rr2, grey arrows) into pET17b plasmid.

Production of dsRNA in E. coli

The recombinant plasmid containing the dsRNA expression cassette of interest was retransformed into *E. coli* HT115 (an RNase III defective strain) bacterial host cells. Then, a single colony of *E. coli* HT115 harboring the recombinant plasmid was grown in 5 ml of 2X YT medium containing 100 µg/ml of ampicillin and 12.5 µg/ml of tetracycline at 37°C overnight. The bacterial starter culture was diluted to 0.5 OD600/15 ml of 2X YT medium containing the same antibiotic as mentioned earlier. The culture was incubated at 37°C until OD600 reached 0.4. Expression of dsRNA was induced by adding 0.4 mM IPTG and incubating at 37°C for 4 hr. Finally, the bacterial cells were harvested by centrifugation at 8,000 g for 5 min at 4°C and the supernatant was discarded and the cells pellets were stored at -20°C until used.

RNA extraction from bacterial cells

Cell pellets were re-suspended in PBS containing 0.1% SDS (at ratio 1 OD600 of cell pellet per 130 µl of solution). Then, 160 µl of RibozolTM reagent (Amresco®) was immediately added, mixed and samples were incubated at room temperature for 5 min. Twenty microliters of chloroform was added and samples were mixed by vortexing before phase separation and RNA precipitation following the manufacturer's

protocol. Finally, total RNA was dissolved in 150 mM NaCl and samples were stored at -20°C until used.

The yield and integrity of each dsRNA (multi-target dsRNAs (one stem and two stems), dspro and dsrr2) in the extracted total RNA was evaluated by RNase A digestion. One microgram of total RNA was mixed with 0.5 ng of RNase A in 1X buffer (10 mM Tris-Cl, 0.1 mM CaCl2 and 2.5 mM MgCl2) before loading. Approximately 100 ng of the digested RNA was analyzed by agarose gel electrophoresis.

Experimental condition and process

Viral suppression analysis

Shrimp with body weight about 400 mg were injected with 20 µl of total RNA (containing 1 µg of dsRNA) 24 hours before challenging with viruses (YHV or WSSV) at dilutions that showed 100% infection within 48 hours. Shrimp were sacrificed 48 hours after viral administration. Their gill tissues were isolated for RNA or DNA extraction for YHV or WSSV detection by RT-PCR or PCR analysis, respectively.

Shrimp mortality analysis

Shrimp were injected with the RNA similar to the previous condition (2.6.1). However, the viral lysates were dilutions that showed 80-90% death of infected shrimp within 5-7 days. Shrimp were cultured in 10 ppt salt water with aeration at 28°C. The cumulative shrimp mortality was recorded every day up to 10 days post infection.

RNA extraction from shrimp tissues

Approximately 10 mg of YHV-infected or mock infected shrimp gill tissue was isolated and ground in 500 µl RibozolTM reagent (Amresco®) and incubated at room temperature for 5 min. Then, 200 µl of chloroform was added and samples subsequently mixed by vortexing for 15 sec. The solution was incubated at room temperature for 5 min before centrifugation at 12,000 g for 15 min at 4°C. The aqueous phase was transferred to a new 1.5 ml microcentrifuge tube. Total RNA was precipitated by mixing with 250 µl isopropanol and subsequent centrifugation at 12,000 g for 10 min at 4°C. The RNA pellet was washed with 70% (v/v) ethanol and air dried before being re-suspended in DEPCtreated water. The RNA solution was stored at -30°C until used.

DNA extraction from shrimp tissues

Approximately 10 mg of gill tissue was isolated from WSSV-infected or mock infected shrimp and ground in 500 µl DNAzol® reagent (Invitrogen). The solution was centrifuged at 10,000 g for 10 min at 4°C. Total DNA was precipitated from the aqueous solution by adding 250 µl of absolute ethanol and storage at room temperature for 5 min. The DNA pellet after centrifugation at 10,000 g for 10 min was washed twice with 500 µl of 70% (v/v) ethanol. The DNA was air dried and re-suspended in sterile distilled water. The dissolved DNA was stored at -20°C until used.

Sample analysis

RT-PCR

Total RNA (1 μg) was used for first strand cDNA synthesis in a mixture containing 2 μM of random primer and sterile DEPC-treated distill water. After heating the mixture at 70°C for 5 min the solution was immediately quick cooled on ice, and the primer was allowed to anneal with mRNA for 5 min. After that, 1X Improm-II™ reaction buffer, 0.5 mM dNTPs, 1 μl of Improm-II™ Reverse transcriptase, and sterile DEPC-treated distill water were added. The mixture was gently mixed and processed at 25°C for 5 min, 42°C for 60 min and 72°C for 15 min to synthesize first strand cDNA. Two microliters of synthesized cDNA were used for PCR amplification.

PCR

To amplify the target DNA fragment, the reaction was performed using either cDNA (2 μl) or total extracted DNA (200 ng) as a template. The components for PCR reaction in a 25 μl total volume contained 0.2 μM of each specific primer, 0.4 mM of dNTPs, 1X PCR buffer (75 mM Tris-HCl, pH 8.8, 20 mM (NH4)2SO4, 0.01% Tween 20) and 1 unit of *Taq* DNA polymerase. The temperature profile for each round of PCR amplification was performed by holding 94°C for 2 min, denaturation at 94°C for 10 sec, annealing at 55°C for 30 sec, and extension at 72°C for 1 min. Then, the temperature was held at 72°C for 5 min. Finally, the PCR product of 25 amplified cycles was analyzed by agarose gel electrophoresis.

Statistical analysis

The statistical analysis of relative level of viral genome normalized by the shrimp's actin was performed by using a one way ANOVA test. The probability (*p*) value of < 0.05 (*), <0.01 (**) or < 0.001 (***) was accepted as statistically significance.

Results

Construction of multi-target dsRNA expression plasmid and dsRNA production in E. coli

In this study, two multi-target dsRNAs (with one stem and two stems) that have the capacity to simultaneously knock down the YHV protease and WSSV rr2 genes were produced from two different recombinant plasmids. The pETpro-rr2_one stem was constructed by cloning inverted repeats of DNA fragments containing YHV protease sequences linked with WSSV rr2 sequences with an intervening one spacer (Figure 2), While pETpro-rr2_two stems was derived from insertion of two inverted repeats, one of protease DNA fragments and another of rr2 DNA fragments (Figure 3). Two different structures of multi-target dsRNA molecules produced from these plasmids were predicted (Figure 4A). The one stem dsRNA contained one long stem (918 bp) with a shared loop. The two stems dsRNA contained two short stems of 474 bp of protease and 438 bp of rr2 with their own loops. After dsRNA production in *E. coli*, total RNA was extracted and the single stranded RNA of the bacteria and the loop regions were

removed by RNase A treatment. The estimated yield of the one stem construct was 8 µg/OD bacterial cells, while 23 µg of dsRNA/OD cells was obtained from the pETpro-rr2_two stems construct. RNase A also digested the single stranded regions from the dsRNAs. As a result, dissociation of dspro from dsrr2 resulted in two dsRNA bands (Figure 4B). The ratio of dspro per dsrr2 of the one stem was 1:1. However, that of the two stems was 1:4, with dsrr2 being present approximately 4 times more than dspro. A possible explanation for this is premature termination of the T7 RNA polymerase before the protease region. Since the position of the inverted repeat of rr2 in pET17pro-rr2_two stems was adjacent to the T7 promoter then the transcribed RNA automatically forms a stem-loop structure that might interfere with transcription of the stem-loop of protease region. The stem-loop of rr2 might represent a pause signal for T7 RNA polymerase transcription, which usually occurs during transcription in *E. coli* (Kang et al., 2019).

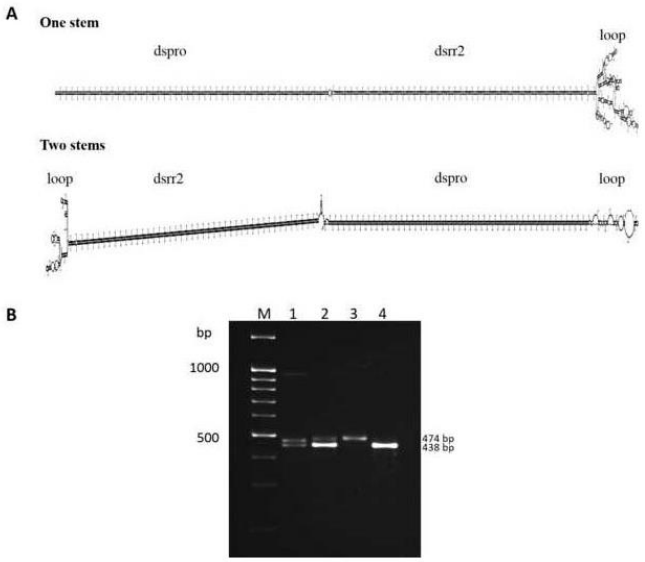

Figure 4. Production of dsRNAs in *E. coli*

(A) The predicted secondary structure of multi-targeting dsRNAs (one stem and two stems). Structures were predicted using free software RNA structure version 5.7 on the webserver (http://rna.urmc.rochester.edu/RNAstructureWeb/Servers/Fold/Fold.html). The region of dsRNA corresponding to YHV protease and WSSV rr2 genes are presented as dspro and dsrr2, respectively. (B) Extracted total RNA was digested with RNase A to remove their structure. Approximately 100 ng of the treated RNA was loaded on 2% agarose gel. The one stem (lane 1) contained two dsRNA bands (dspro and dsrr2 at 1:1 ratio) while the two stems (lane 2) had two dsRNAs of dspro and dsrr2 at a 1:4 ratio. The control dsRNAs; dspro (474 bp) and dsrr2 (438 bp) are presented in lane 3 and 4, respectively.

Viral suppression efficiency of the multi-target dsRNA

YHV suppression

To investigate the inhibitory effect of the multi-target dsRNAs (one stem and two stems) on YHV infection, shrimp were divided into five groups which were separately injected with 150 mM NaCl, one stem, two stems, YHV specific dspro and non-specific dsrr2 24 hr prior YHV challenge. At 48 hours post infection (h.p.i.), the level

of YHV protease mRNA in the treated shrimp was evaluated by RT-PCR. The result showed strong YHV inhibition in shrimp injected with one stem, two stem and dspro when compared with the control shrimp injected with NaCl (no dsRNA) (Figure 5). But partial inhibition of YHV was observed in shrimp injected with the non-specific dsrr2. The results showed that both of the multi-target dsRNAs (one stem and two stems) had a high potency of YHV inhibition comparable to dspro, even though they contained a lower amount of dspro.

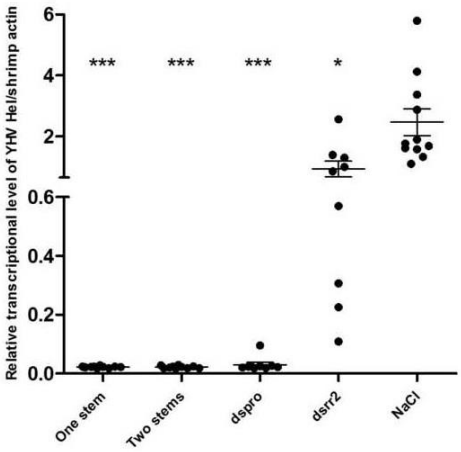

Figure 5. Suppression of YHV replication in shrimp by dsRNAs

Shrimp (400 mg; n = 10) were separately injected with NaCl (control) or total RNA containing 1 µg of each dsRNAs (one stem, two stems, dspro and dsrr2) 24 hrs before YHV administration. After 48 hrs of viral infection, the amount of YHV was determined by RTPCR using YHV helicase specific primers (Table 1) together with shrimp actin primers (for normalization). The relative amount of normalized YHV of each individual shrimp is shown in a dot plot with mean ± SEM. The probability (*p*) value of < 0.05 (*), < 0.01 (**) or < 0.001 (***) was accepted as statistically significance.

WSSV suppression

To investigate the inhibitory effect of the multi-target dsRNAs (one stem and two stems) on WSSV infection, a similar experiment to that described in 3.2.1 was conducted, except that the infecting virus was WSSV. At 48 h.p.i., relative levels of WSSV vp28 DNA were determined by PCR. The results showed no viral inhibition in the non-specific dspro injected shrimp. WSSV was inhibited in the shrimp pre-treated with the dsRNAs containing the specific dsrr2 in which the one stem showed high inhibition potency comparable to the dsrr2 while the two stems dsRNA showed the lowest effect (Figure 6). This result was un-expected, since the two stems construct generated a higher amount of dsrr2 than the one stem construct. In one microgram of dsRNA used for injection the one stem had 500 ng of dspro and 500 ng of dsrr2, while the two stems had 200 ng of dspro and 800 ng of dsrr2. This might be the result of differences in their structures. To test this assumption, both multi-target dsRNAs were treated with RNaseA, to remove their structures, prior shrimp administration. Shrimp were divided into seven groups. The first group was injected with NaCl, which was used as a positive control. The second and third groups were injected with un-treated total

RNAs containing 1 μg of one stem and two stems. The fourth and fifth groups were injected with RNaseA-treated total RNA containing 1 μg of multi-target dsRNAs (one stem-A or two stems-A). The last two groups were injected with 1 μg of the mixed dspro and dsrr2 at ratio 1:1 and 1:4, respectively. At 48 h.p.i., as expected, the mixed dspro:dsrr2 (1:4) gave higher viral suppression than the mixed dsRNAs (1:1) (Figure 7). For untreated multi-target dsRNAs, the one stem still had greater potency in WSSV inhibition than the two stems. In contrast, once their secondary structures had been removed, the two stems-A could inhibit WSSV better than the one stem-A. Moreover, the suppression efficacy of the one stem-A and the two stems-A were comparable to the mixed dspro:dsrr2 at 1:1 and 1:4, respectively, which was correlated with their dsrr2 composition. This indicates that not only the amount of specific dsRNA but the secondary structure of the multi-targeting dsRNA also affects the efficacy of WSSV inhibition in shrimp.

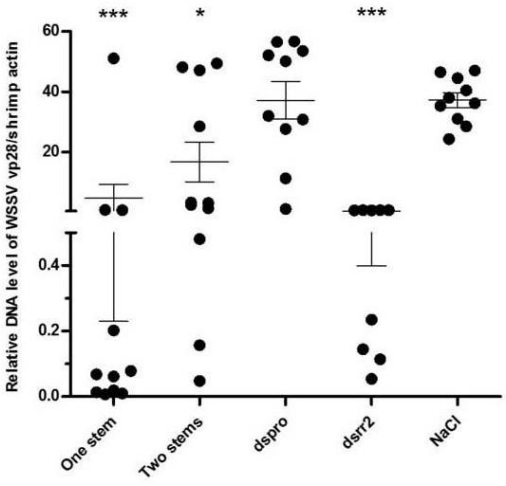

Figure 6. Suppression of WSSV replication in shrimp by dsRNAs

Shrimp (400 mg; n = 10) were separately injected with NaCl (control) or total RNA containing 1 μg of each dsRNAs (one stem, two stems, dspro and dsrr2) 24 hrs before WSSV administration. After 48 hrs of viral infection, the amount of WSSV was determined by PCR using WSSV vp28 specific primers (Table 1) together with shrimp actin primers (for normalization). The relative amount of normalized WSSV of each individual shrimp is shown in a dot plot with mean ± SEM. The probability (*p*) value of < 0.05 (*), < 0.01 (**) or < 0.001 (***) was accepted as statistically significance.

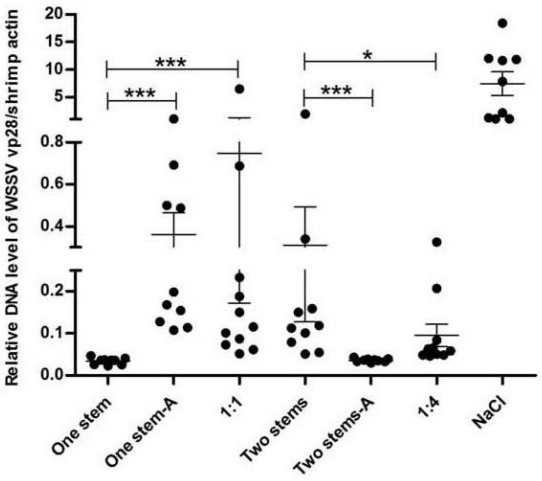

Figure 7. Possible effect of secondary structure of dsRNAs on their potency for WSSV suppression

Shrimp (400 mg; n = 10) were separately injected with total RNA containing 1 μg of dsRNAs; one stem, two stems, mixed dspro and dsrr2 at ratio 1:1 (1:1) and 1:4 (1:4), respectively. To remove the secondary structure of the multi-target dsRNAs, RNase A was used to treated the one stem (one stem-A) and the two stems (two stems-A) before injection into shrimp. The control shrimp were treated with NaCl. At 24 hrs post injection, shrimp were challenged with WSSV. Af 48 hours post viral challenge, the amount of WSSV was determined by PCR using WSSV vp28 specific primers (Table 1) together with shrimp actin primers (for normalization). The relative amount of normalized WSSV of each individual shrimp is shown in a dot plot with mean ± SEM. The probability (*p*) value of < 0.05 (*), <0.01 (**) or < 0.001 (***) was accepted as statistically significance.

The predicted secondary structure of the two stems dsRNA might interfere with the entry of the dsRNA into shrimp cells, or may hinder the binding of the dsRNA with the enzyme Dicer, leading to a reduction in RNAi activity. As Dicer requires open ends for proper substrate (dsRNA) recognition and processing (MacRae et al., 2007; Vermeulen et al., 2005), the two stems dsRNA, which contains only one open end, may not represent a proper substrate for Dicer. This was confirmed by RNase A treatment, as after RNase A digestion, the single-stranded RNA (ssRNA) linking between dspro and dsrr2 as well as the loop spacer were removed. The secondary structure was then altered, resulting in the inhibitory effect of the two stems being recovered.

In this study, the one-stem dsRNA showed a high level of suppression against YHV and WSSV infection, comparable to dspro for YHV and dsrr2 for WSSV, respectively even though it contained only half the amount of each specific dsRNA (Figure 4B). These results demonstrate the ability of longer hairpin RNA structures to improve gene silencing efficiency. This is consistent with previous reports that showed that dsRNA mediated RNAi efficiency was length dependent (Gouda et al., 2010; Miyata et al., 2014). It has also been demonstrated in *Caenorhabditis elegans*, *Diabrotica virgifera* and *Tribolium castaneum* that the efficiency of cellular uptake and/or spreading of longer dsRNA was higher than shorter ones (Bolognesi et al., 2012; Miller et al., 2012; Winston et al., 2002). Recently, an electrophoretic mobility shift assay (EMSAs) showed that a recombinant extracellular domain of *C. elegans* SID-1, a membrane protein required for systemic RNA, bound longer dsRNA more robustly and

effectively than shorter ones (Li et al., 2015). Moreover, when using more than one dsRNA, competition between dsRNAs might occur at several levels such as cellular uptake, transport of the dsRNA, processing of dsRNA or mRNA silencing (Gouda et al., 2010; Miyata et al., 2014; Miller et al., 2009; 2012; Lee et al., 2013). Hence, two dsRNAs linked to each other was created to solve this problem and it showed higher efficacy on gene knockdown than a mixture of two dsRNAs. Therefore, the multi-target dsRNAs (one stem and two stems) established in this study could be beneficial to effectively inhibit YHV and WSSV in shrimp in preference to a mixture of dspro and dsrr2.

Prevention of shrimp mortality by dsRNAs

As the previous experiment demonstrated that total RNA from the one stem construct could inhibit YHV and WSSV replication at 48 h.p.i., whether this viral inhibition could reduce shrimp mortality from these viral infections was investigated. Shrimp were injected with NaCl (positive control), one stem, dspro and dsrr2 before being infected with either YHV or WSSV. Cumulative mortality of the infected shrimp was observed for 10 days. For YHV infection, 90-100% of shrimp without specific dspro (NaCl and dsrr2) died (Figure 8 A). A significant reduction of shrimp death (from 100% to 10%) was observed when shrimp received the specific dspro and the one stem dsRNA. For WSSV, the 100% cumulative mortality was observed in the control shrimp (NaCl) and 70% death was recorded in the non-specific dspro treated shrimp. The cumulative mortality was significantly reduced to 0-10% when shrimp were pre-treated with the specific dsrr2 and the one stem dsRNA (Figure 8 B). These results showed that the one stem dsRNA could effectively protect shrimp from infection by both YHV and WSSV.

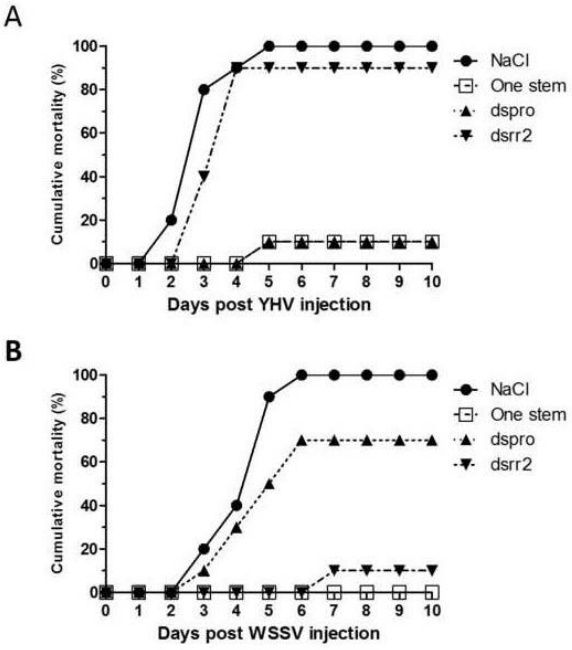

Figure 8. Prevention of shrimp mortality by dsRNAs

Shrimp (400 mg; n = 10) were injected with total RNA containing 1 µg of one stem, dsrr2 and dspro. The control shrimp were treated with NaCl. At 24 hour post injection, shrimp were challenged with either YHV (A) or with WSSV lysate (B). The cumulative percent mortality was recorded every day for 10 days.

The multi-target dsRNAs (one stem and two stems) are the first long dsRNA demonstrating efficient inhibition of both YHV and WSSV in shrimp. This study provides important information essential to design and achieve effective multi-targeting dsRNAs for multiple genes/viruses silencing in shrimp. This also presents a potential dual anti-YHV and WSSV strategy for application in the shrimp farming industry in the future.

References

1. Assavalapsakul, W., Chinnirunvong, W., Panyim, S. 2009. Application of YHVprotease dsRNA for protection and therapeutic treatment against yellow head virus infection in *Litopenaeus vannamei.* Dis. Aquatic Organ. 84(2), 167-71.

2. Attasart, P., Kaewkhaw, R., Chimwai, C., Kongphom, U., Namramoon, O., Panyim, S. 2009. Inhibition of white spot syndrome virus replication in *Penaeus monodon* by combined silencing of viral rr2 and shrimp *Pm*Rab7. Virus Res. 145(1), 127-33.

3. Bolognesi, R., Ramaseshadri, P., Anderson, J., Bachman, P., Clinton, W., Flannagan, R., Ilagan, O., Lawrence, C., Levine, S., Moar, W., Mueller, G., Tan, J., Uffman, J., Wiggins, E., Heck, G., Segers, G. 2012. Characterizing the mechanism of action of double-stranded RNA activity against western corn rootworm (*Diabrotica virgifera virgifera* LeConte). PLoS ONE 7(10), e47534.

4. Chang, C.I., Kang, H.S., Ban, C., Kim, S., Lee, D.K. 2009. Dual-target gene silencing by using long, synthetic siRNA duplexes without triggering antiviral responses. Mol. Cells 27(6), 689-95.

5. Cong, W., Cui, S., Chen, J., Zuo, X., Lu, Y., Yan, W., Zheng, Z. 2010. Construction of a multiple targeting RNAi plasmid that inhibits target gene expression and FMDV replication in BHK-21 cells and suckling mice. Vet. Res. Commun. 34(4), 335-46.

6. Flegel T.W., Boonyaratpalin S., Withyachumnamkul B. 1996. Current status of research on yellow head virus and white spot virus in Thailand. In World aquaculture '96. Book of abstracts. World Aquaculture Society, Baton Rouge, Louisiana. 126-7.

7. Gou, D., Weng, T., Wang, Y., Wang, Z., Zhang, H., Gao, L., Chen, Z., Wang, P., Liu, L. 2007. A novel approach for the construction of multiple shRNA expression vectors. J. Gene Med. 9(9), 751-63.

8. Gouda, K., Matsunaga, Y., Iwasaki, T., Kawano, T. 2010. An altered method of feeding RNAi that knocks down multiple genes simultaneously in the nematode *Caenorhabditis elegans.* Biosci. Biotechnol. Biochem. 74(11), 2361-5.

9. Hamano, K., Maeno, Y., Klomkling, S., Aue-Umneoy, D., Tsutsui, I. 2017. Presence of viral pathogens amongst wild *Penaeus monodon* in Thailand. JARQ. 51(2), 191-7.

10. Hammond, S.M., Caudy, A.A., Hannon, G.J. 2001. Post-transcriptional gene silencing by double-stranded RNA. Nat. Rev. Genet. 2(2), 110-9.

11. Hinton, T.M. and Doran, T.J. 2008. Inhibition of chicken anaemia virus replication using multiple short-hairpin RNAs. Antiviral Res. 80(2), 143-9.

12. Junn, H.J., Kim, J.Y., Seol, D.W. 2010. Effective knockdown of multiple target genes by expressing the single transcript harbouring multi-cistronic shRNAs. Biochem. Biophys. Res. Commun. 396(4), 861-5.

13. Lee, T.Y., Chang, C.I., Lee, D., Hong, S.W., Shin, C., Li, C.J., Kim, S., Haussecker, D., Lee, D. 2013. RNA interference-mediated simultaneous silencing of four genes using cross-shaped RNA. Mol. Cells 35(4), 320-6.

14. Leu, J.H., Yang, F., Zhang, X., Xu, X., Kou, G.H., Lo, C.F. 2009. Whispovirus. Curr. Top. Microbiol. Immunol. 328, 197-227.

15. Li, J., Dai, Y., Liu, S., Guo, H., Wang, T., Ouyang, H., Tu, C. 2011. *In vitro* inhibition of CSFV replication by multiple siRNA expression. Antiviral Res. 91(2), 209-16.

16. Li, W., Koutmou, K.S., Leahy, D.J., Li, M. 2015. Systemic RNA interference deficiency-1 (SID-1) extracellular domain selectively binds long double-stranded RNA and is required for RNA transport by SID-1. J. Biol. Chem. 290(31), 18904-13.

17. Ma, J., Zeng, L., Fan, Y., Zhou, Y., Jiang, N., Chen, Q. 2014. Significant inhibition of two different genotypes of grass carp reovirus *in vitro* using multiple shRNAs expression vectors. Virus Res. 189, 47-55.

18. MacRae, I.J., Zhou, K., Doudna, J.A. 2007. Structural determinants of RNA recognition and cleavage by Dicer. Nat. Struct. Mol. Biol. 14(10), 934-40.

19. McIntyre, G.J., Arndt, A.J., Gillespie, K.M., Mak, W.M., Fanning, G.C. 2011. A comparison of multiple shRNA expression methods for combinatorial RNAi. Genet. Vaccines Ther. 9(1), 9.

20. Miller, R.K., Qadota, H., Stark, T.J., Mercer, K.B., Wortham, T.S., Anyanful, A., Benian, G.M. 2009. CSN-5, a component of the COP9 signalosome complex, regulates the levels of UNC-96 and UNC-98, two components of M-lines in *Caenorhabditis elegans* muscle. Mol. Biol. Cell 20(15), 3608-16.

21. Miller, S.C., Miyata, K., Brown, S.J., Tomoyasu, Y. 2012. Dissecting systemic RNA interference in the red flour beetle Tribolium castaneum: parameters affecting the efficiency of RNAi. PLoS ONE 7(10), e47431.

22. Miyata, K., Ramaseshadri, P., Zhang, Y., Segers, G., Bolognesi, R., Tomoyasu, Y. 2014. Establishing an *in vivo* assay system to identify components involved in environmental RNA interference in the western corn rootworm. PLoS ONE 9(7), e101661.

23. Mohan, C.V., Shankar, K.M., Kulkarni, S., Sudha, P.M. 1998. Histopathology of cultured showing gross signs of yellow head syndrome and white spot syndrome during 1994 Indian epizootics. Dis. Aquatic Organ. 34, 9-12.

24. Robalino, J., Browdy, C.L., Prior, S., Metz, A., Parnell, P., Gross, P., Warr, G. 2004. Induction of antiviral immunity by double-stranded RNA in a marine invertebrate. J Virol. 78(19), 10442-8.

25. Sanitt, P., Attasart, P., Panyim, S. 2014. Protection of yellow head virus infection in shrimp by feeding of bacteria expressing dsRNAs. J. Biotechnol. 179, 26-31.

26. Sanjuktha, M., Stalin Raj, V., Aravindan, K., Alavandi, S.V., Poornima, M., Santiago, T.C. 2012. Comparative efficacy of double-stranded RNAs targeting WSSV structural and nonstructural genes in controlling viral multiplication in *Penaeus monodon*. Arch. Virol. 157(5), 993-8.

27. Senapin, S., Thaowbut, Y., Gangnonngiw, W., Chuchird, N., Sriurairatana, S., Flegel, T.W., 2010. Impact of yellow head virus outbreaks in the white leg shrimp, *Penaeus vannamei* (Boone), in Thailand. J. Fish Dis. 33(5), 421-30.

28. Song, J., Giang, A., Lu, Y., Pang, S., Chiu, R. 2008. Multiple shRNA expressing vector enhances efficiency of gene silencing. BMB Rep. 41(5), 358-62.

29. Thammasorn, T., Sansuriya, P., Meemetta, W., Senapin, S., Jitrakorn, S., Rattanarojpong, T., Saksmerprome, V. 2015. Large-scale production and antiviral efficacy of multi-target double-stranded RNA for the prevention of white spot syndrome virus (WSSV) in shrimp. BMC Biotechnol. 15,110.

30. Tirasophon, W., Roshorm, Y., Panyim, S. 2005. Silencing of yellow head virus replication in penaeid shrimp cells by dsRNA. Biochem. Biophys. Res. Commun. 334(1), 102-7.

31. Tirasophon, W., Yodmuang, S., Chinnirunvong, W., Plongthongkum, N., Panyim, S. 2007. Therapeutic inhibition of yellow head virus multiplication in infected shrimps by YHVprotease dsRNA. Antiviral Res. 74(2), 150-5.

32. Vermeulen, A., Behlen, L., Reynolds, A., Wolfson, A., Marshall, W. S., Karpilow, J., Khvorova, A. 2005. The contributions of dsRNA structure to Dicer specificity and efficiency. RNA 11(5), 674-82.

33. Wang, S., Shi, Z., Liu, W., Jules, J., Feng, X. 2006. Development and validation of vectors containing multiple siRNA expression cassettes for maximizing the efficiency of gene silencing. BMC Biotechnol. 6, 50.

34. Winston, W. M., Molodowitch, C., Hunter, C. P. 2002. Systemic RNAi in *C. elegans* requires the putative transmembrane protein SID-1. Science 295(5564), 2456-9.

35. Wu, K. L., Zhang, X., Zhang, J., Yang, Y., Mu, Y. X., Liu, M., Lu, L., Li, Y., Zhu, Y., Wu, J. 2005. Inhibition of Hepatitis B virus gene expression by single and dual small interfering RNA treatment. Virus Res. 112(1-2), 100-7.

36. Yanofsky, C. 2007. RNA-based regulation of genes of tryptophan synthesis and degradation, in bacteria. RNA 13(8), 1141-54.

37. Yodmuang, S., Tirasophon, W., Roshorm, Y., Chinnirunvong, W., Panyim, S. 2006. YHV-protease dsRNA inhibits YHV replication in *Penaeus monodon* and prevents mortality. Biochem. Biophys. Res. Commun. 341(2), 351-6.

Research Outputs (ทุนวิจัยพื้นฐานเชิงยุทธศาสตร์)

ผลงานตีพิมพ์ในวารสารวิชาการนานาชาติ

1. Involvement of endocytosis in cellular uptake of injected dsRNA into hepatopancreas but not in gill of *Litopenaeus vannamei*. Maruekawong K, Panyim S, Attasart P. Aquaculture 500, 393-397. (2019)

2. Suppression of argonautes compromises viral infection in *Penaeus monodon*. Ho T, Panyim S, Udomkit A. Developmental and Comparative Immunology 90, 130-137. (2019)

3. PmEEA1, the early endosomal protein is employed by YHV for successful infection in *Penaeus monodon*. Posiri P, Thongsuksangcharoen S, Chaysri N, Panyim S, Ongvarrasopone C. Fish and Shellfish Immunology 95, 449-455. (2019)

4. Indentification and expression of white spot syndrome virus- encoded microRNAs in infected *Penaeus monodon*. Nantapojd T, Panyim S, Ongvarrasopone C. Aquaculture 503, 436-445. (2019)

5. Functional characterization of a cDNA encoding Piwi protein in *Penaeus monodon* and its potential roles in controlling transposon expression and spermatogenesis. Sukthaworn S, Panyim S, Udomkit A. Comparative Biochemistry and Physiology -Part A 229, 60-68. (2019)

6. Regulation of vitellogenin gene expression under the negative modulator, gonad-inhibiting hormone in *Penaeus monodon*. Kluebsoongnoen J, Panyim S, Udomkit A. Comparative Biochemistry and Physiology, Part A. 243, 110682. (2020)

ผลงานเตรียมตีพิมพ์ในวารสารวิชาการนานาชาติ

1. An ATP synthase beta subunit is required for internalization of dsRNA into shrimp cells. Fish and Shellfish Immunology. (in-press)

2. A multi-target dsRNA for simultaneous inhibition of yellow head virus and white spot syndrome virus in shrimp. Journal of Biotechnology. (in-press)